

## Supramolecular polymer materials for biomedical applications and diagnostics

Noteborn, W.E.M.

#### Citation

Noteborn, W. E. M. (2017, December 11). Supramolecular polymer materials for biomedical applications and diagnostics. Retrieved from https://hdl.handle.net/1887/55847

Version: Not Applicable (or Unknown)

License: License agreement concerning inclusion of doctoral thesis in the

Institutional Repository of the University of Leiden

Downloaded from: <a href="https://hdl.handle.net/1887/55847">https://hdl.handle.net/1887/55847</a>

Note: To cite this publication please use the final published version (if applicable).

#### Cover Page



## Universiteit Leiden



The handle <a href="http://hdl.handle.net/1887/55847">http://hdl.handle.net/1887/55847</a> holds various files of this Leiden University dissertation

Author: Noteborn, Willem

Title: Supramolecular polymer materials for biomedical applications and diagnostics

Date: 2017-12-11

# Supramolecular polymer materials for biomedical applications and diagnostics

Willem Noteborn

Doctoral Thesis, Leiden University, 2017

Cover Design: Mathieu Noteborn

# Supramolecular polymer materials for biomedical applications and diagnostics

#### Proefschrift

ter verkrijging van

de graad van Doctor aan de Universiteit Leiden,
op gezag van Rector Magnificus prof. mr. C. J. J. M. Stolker
volgens het besluit van het College voor Promoties
te verdedigen op maandag 11 december 2017
klokke 11:15 uur

door

#### Willem Noteborn

Geboren op 24 juni 1988 te Leiden, Nederland

### **Promotiecommissie**

Promotor: Prof. dr. A. Kros

Copromotor: Dr. R. E. Kieltyka

Overige leden:

Prof. dr. H.S. Overkleeft (voorzitter)

Prof. dr. J. Brouwer (secretaris)

Prof. dr. D. Heinrich

Prof. dr. J.H. van Esch

Prof. dr. A. Herrmann

To my friends and family

## **Table of Contents**

Chapter 1 General Introduction	9
Chapter 2 Grafting from a hybrid DNA-dextran graft copolymer by the hybridization chain reaction	49
Chapter 3 Reversible loading of nanoscale elements on a multicomponent supramolecular polymer system using DNA strand displacement	79
Chapter 4 Crosslinker-induced effects on the gelation pathway of a low molecular weight hydrogel	105
Chapter 5 Tuning drug release from a reaction-coupled low molecular weight gelator system by modulating its reaction pathway	143
Chapter 6 Summary and Perspectives	171
Chapter 7 Nederlandse Samenvatting en Perspectieven	177
Curriculum Vitae	185
List of publications	186

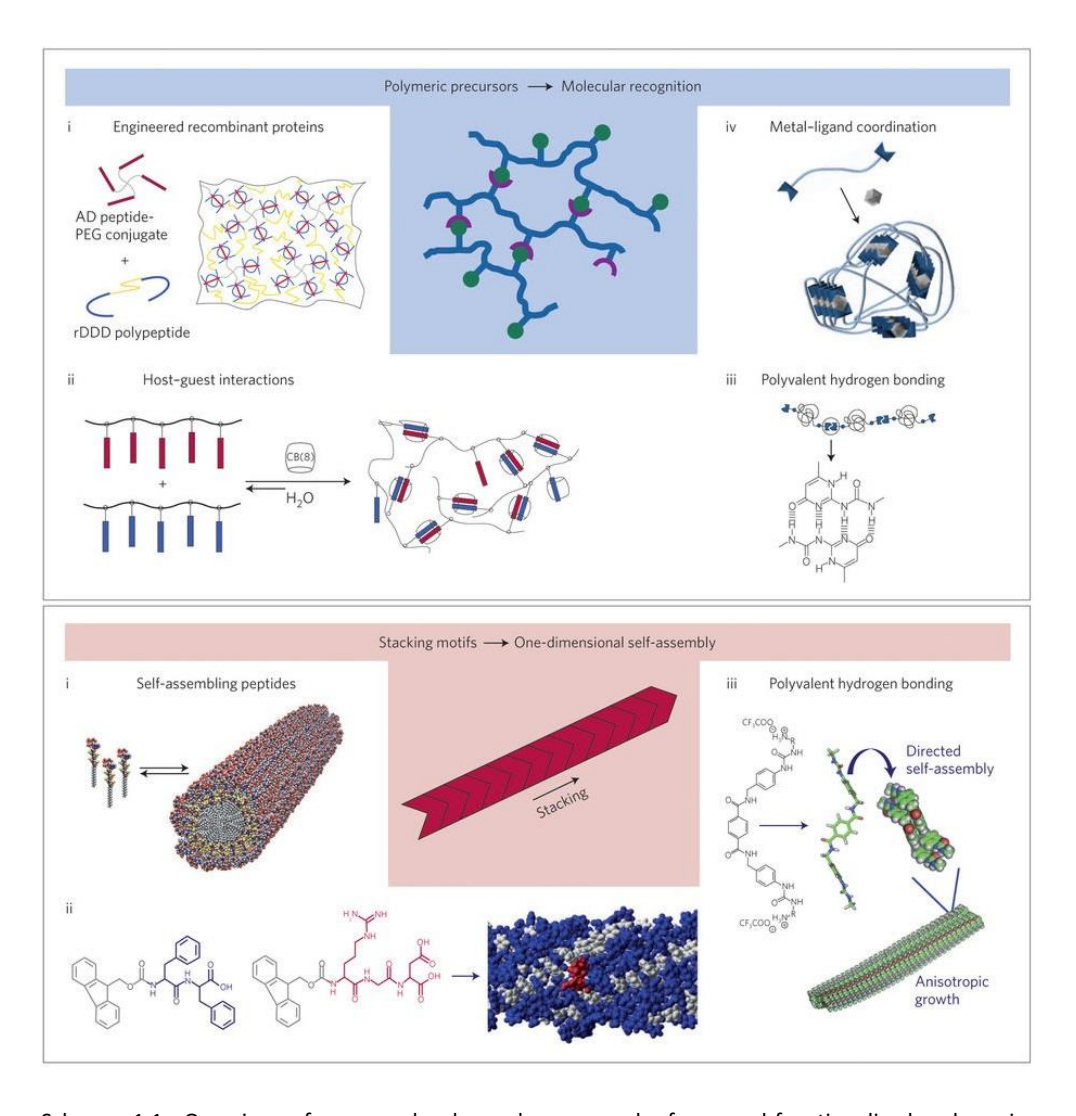
### CHAPTER 1

#### Introduction

#### 1.1 Supramolecular polymers

Self-assembly is ubiquitous in Nature as it is involved in a multitude of processes necessary to sustain life. Cells, one of the most basic units of living organisms, rely on non-covalent assembly to form higher-order structures essential for their function. Proteins self-assemble to form actin filaments and microtubules in the cytoskeleton, lipids organize to form cellular membranes, and a multitude of proteins and small molecules interact to form receptor-ligand pairs. Over the last decades, the fields of polymer science and supramolecular chemistry have been inspired by these biologically self-assembled materials, providing the impetus for the synthesis of rationally designed supramolecular polymers.

Supramolecular polymers are a class of materials that are held together by weak non-covalent interactions such as hydrogen bonding, solvophobicity,  $\pi$ -stacking and ionic interactions.<sup>2</sup> In contrast to their classical covalent polymer counterparts. where monomers are linked together through irreversible bonds, supramolecular monomers typically result in the formation of polymers with a highly tunable and stimuli-responsive nature. Although the individual non-covalent interactions that hold these materials together are weak, their collective nature and directionality can result in materials that can be surprisingly robust, with dynamic characteristics. Because of this unique character, supramolecular materials can be self-healing, modular, tuneable, and potentially biomimetic depending on the choice of monomers used.<sup>3</sup> In terms of structural design, supramolecular polymers can be generally divided in two categories: end-functionalized or grafted polymeric precursors that interact by molecular recognition and stacked monomeric units resulting in the formation of welldefined one-dimensional structures.<sup>4,5</sup> A wide variety of synthons have been made from a broad set of functional groups, some of which are not normally present in nature, thus expanding the supramolecular molecular toolbox. Molecular recognition in these systems has been driven by a wide range of supramolecular units namely peptides, various aspects of nucleic acid chemistry, host-guest interactions, 8 transition metal complexes<sup>9</sup> and hydrogen bonding modules<sup>10</sup> to facilitate the growth of either class of polymer (Scheme 1.1). Supramolecular designs and interaction motifs relevant to the work presented in this thesis will be discussed below.



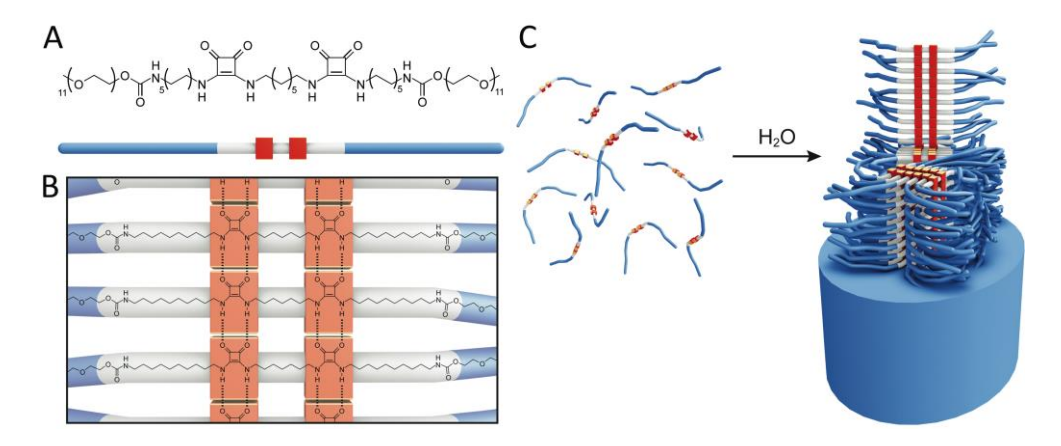
Scheme 1.1. Overview of supramolecular polymers made from end-functionalized polymeric precursors (top) and one-dimensional stacked supramolecular polymers (bottom). Image adapted from reference 3.

The ability of polymers to self-assemble in water opens up the possibility of preparing biomimetic supramolecular polymers, which can provide both useful fundamental knowledge and applied materials for biomedical applications. In aqueous solutions solvophobicity is typically the main driving force for monomer aggregation. The self-assembly can be further driven and tuned by weaker noncovalent interactions such as hydrogen bonding, and  $\pi$ -interactions. Consequently, this requires amphiphiles with molecular designs where the ratios between hydrophobic and hydrophilic domains are well-balanced to promote solubility and

nanophase segregation, while shielding the non-covalent interactions that drive onedimensional self-assembly of the monomer units. Salient examples of such supramolecular polymer materials have involved 2-ureido-4[1H]-pyrimidinone (UPy)<sup>11</sup> and bis-urea units<sup>12</sup> embedded in hydrophobic alkane spacers and surrounded by hydrophilic ethylene glycol oligomers (OEG) or polyethylene glycol (PEG) polymers. Moreover, designs involving peptides with hydrophobic alkane tails which form amphiphiles have also been examined. 13 This same concept has also been applied to make highly hydrophobic hexa-peri-hexabenzocoronene motifs, which typically assemble in organic solvents via  $\pi$ -stacking, water-soluble by shielding the core with twenty-four tetraethylene glycol units. 14 One of the most prominent examples using hydrogen bonding as one of the main directional self-assembly forces concerns a family of molecules based on the 1,3,5-benzene trisamide core (BTA), in which the core provides 3 intermolecular hydrogen bonding units to facilitate the formation of long well-defined fibrillar structures. 15 This supramolecular building block was first designed to assemble in organic solvents and later modified for use in water by exchanging the peripheral alkane chains for charged constituents or poly(ethylene glycol) (PEG) chains. Changing the composition of the three side chains attached to the chiral BTA cores can induce homochirality that imparts a higher level of internal order to the supramolecular polymer, which can be used to both influence and study the thermodynamic parameters of the system. <sup>16</sup> Another C-3 symmetric core that has extensively explored for the formation of hydrogels cyclohexyltrisamide. 17,18 More recently, this trisamide-containing motif was converted into a two component hydrazide-aldehyde system to generate a reaction coupled selfassembling system. 19

Recently, our group has synthesized supramolecular polymers that self-assemble in water from squaramide-based bolaamphiphiles. Squaramides consist of two N-H hydrogen bond donors opposite two carbonyl hydrogen bond acceptors, on a rigid cyclobutene ring. According to Hückel's rule ([4n+2]  $\pi$  electrons, n=0), the squaramide synthons are predicted to be partially aromatic due to the delocalization of the two nitrogen lone pairs into the ring. In the bolaamphiphile monomer, two squaramide synthons are separated by a  $C_7$ -alkane spacer and shielded from the peripheral hydrophilic methoxy-OEG<sub>11</sub> by two  $C_{10}$ -alkane spacers (Scheme 1.2). Upon self-assembly, which occurs due to a combination of hydrophobicity and hydrogen bonding, the squaramide rings show a significant gain in aromatic character which contributes 30% of the total interaction energy by computation. This unique combination of coupling hydrogen bonding to aromatic gain increases the

thermodynamic stability of the resulting supramolecular polymer in comparison to other isosteric synthons such as ureas that cannot exhibit this effect.



Scheme 1.2. Structure of the squaramide-based bolaamphiphile (A), proposed hydrogen bonding interactions between stacked squaramide monomers (B) and their self-assembly in water where hydrogen bonding is parallel to the fiber axis and  $\pi$ -stacking of the squaramide units occurs in lateral direction.(C) Image adapted from reference 20.

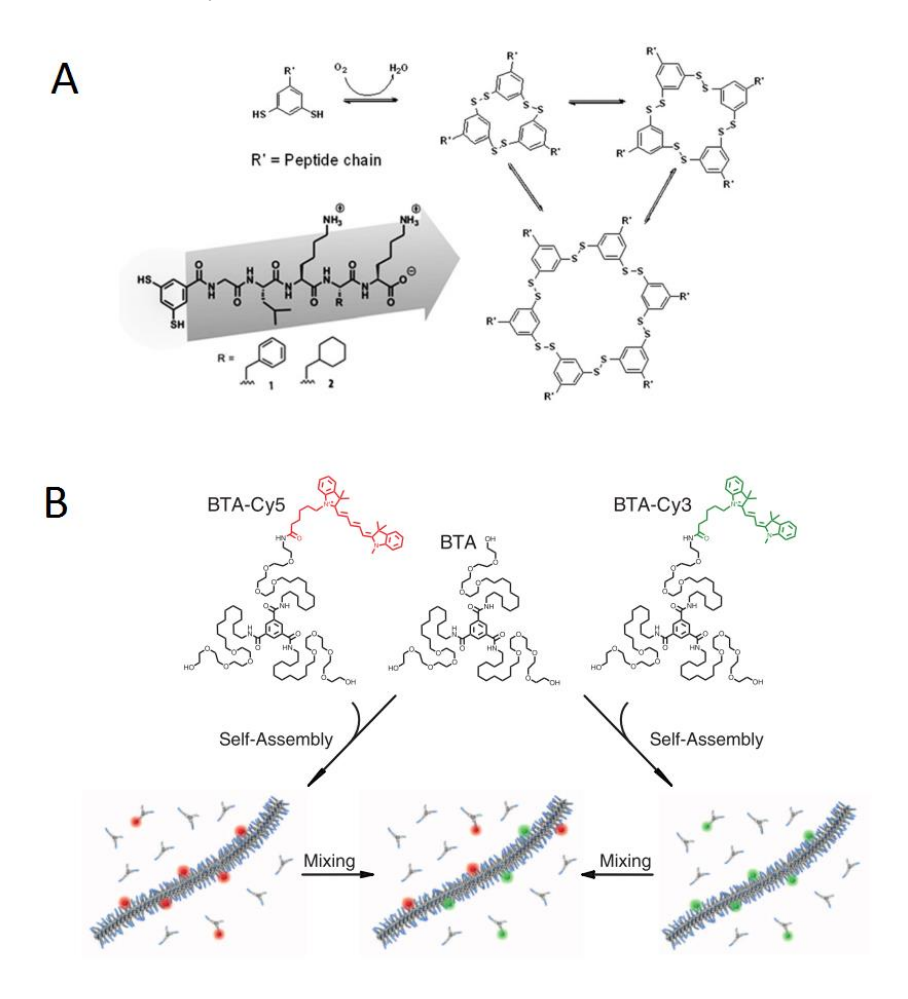
#### 1.2 Functional supramolecular polymers

The creation of novel supramolecular polymers allows for an understanding of their self-assembly principles, but in addition to this they show tremendous potential for use as electronics, <sup>21</sup> sensors, <sup>22</sup> drug delivery platforms <sup>23,24</sup> and biomaterials. <sup>3,25</sup> In general, two strategies can be used to generate functional supramolecular polymers: functional groups can be embedded inside the supramolecular core or functional moieties are tethered to the periphery of the supramolecular polymer. <sup>26</sup> Complex multicomponent mixtures can be readily made by mixing functionalized monomers with their native counterparts, simply by matching their non-covalent binding motifs and using an appropriate processing protocol. In this section, several examples of functional supramolecular polymers and their applications will be discussed.

Supramolecular polymers made from large arene cores like hexa-perihexabenzocoronene can form high aspect ratio tubes in THF, due to the relative solvophobic and solvophilic character of the various domains and  $\pi$ -interactions between the arene cores.<sup>27</sup> After oxidation with NOBF<sub>4</sub> the tubes maintained their shape, but turned from insulating assemblies into conductive tubes that could be deposited between two electrodes with semiconductor properties comparable to inorganic nanotube materials. Mechanical properties can also emerge from monomer self-assembly, with the final aggregate structures affecting the mechanical performance in addition to exhibiting other properties such as self-healing. For example, the Otto group has prepared self-assembling macrocycles that form supramolecular polymers using dynamic covalent chemistry.<sup>28</sup> Thiol-functionalized peptides that can undergo disulfide bond formation provide a dynamic combinatorial library of differently sized macrocyclic monomer structures, in which the macrocycle size can be influenced either by templates or self-recognition. In the self-recognition approach, the most stable population, driven by beta-sheet formation, results in the assembly of fibrous structures and with the consumption of the smaller macrocycles. In both approaches, these building blocks can result in self-replicating supramolecular polymers (Scheme 1.3A).

Other than incorporation of the functional unit inside the supramolecular self-assembly itself, one-dimensional supramolecular polymers can also serve as excellent candidates for tethering functional cargo. Albertazzi *et al.* incorporated Cy3 and Cy5 fluorescent monomers into a BTA supramolecular assembly. <sup>29</sup> By including fluorescently-labeled monomers within the aggregate assembly exchange rates between distinctly labeled fibers were determined by super-resolution stochastic

optical reconstruction microscopy (STORM) (Scheme 1.3B). Moreover, the cationic nature of the fluorescent dyes could also function to electrostatically bind polyanionic single stranded DNAs. Because of the dynamic exchange of monomers in the fibers, the ssDNA strands could template the clustering of the cationic dyefunctionalized monomers. This ability to specifically recruit DNAs to the fiber and their selective elimination by the introduction of a high concentration of monovalent phosphate ions provides a certain level of spatiotemporal control over the DNA distribution on the supramolecular fibers.



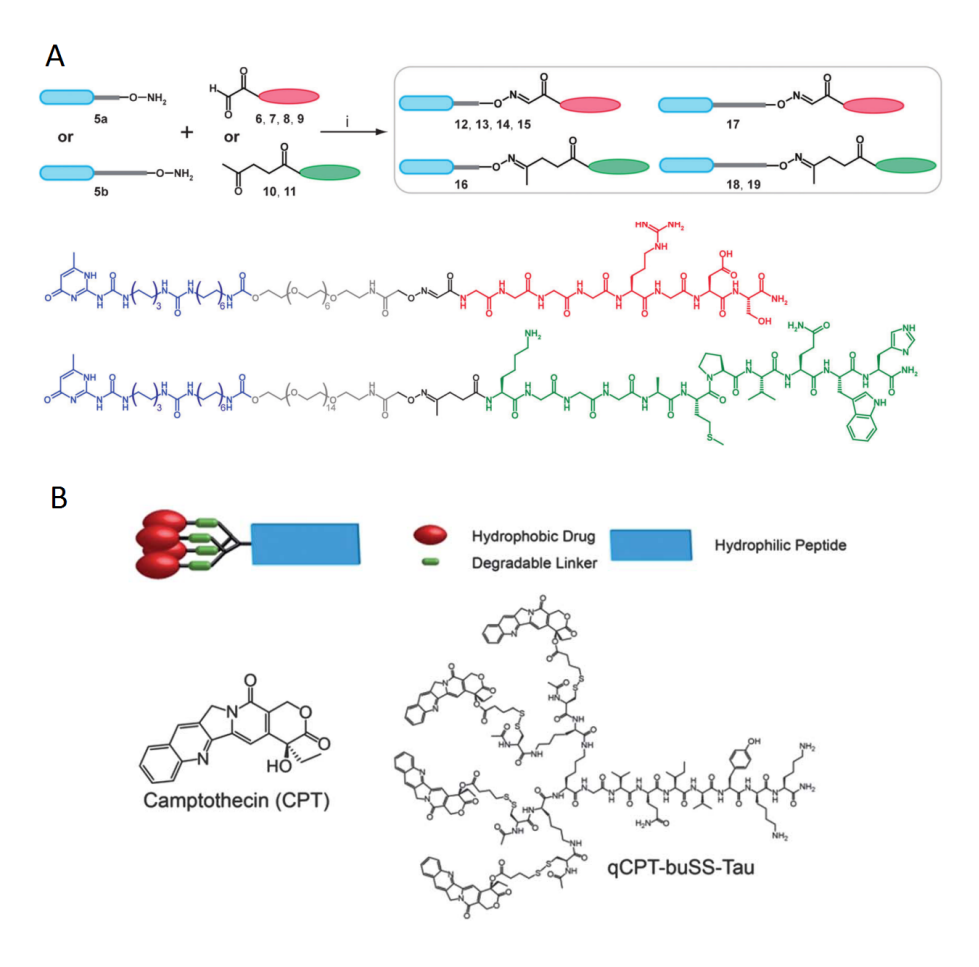
Scheme 1.3. A) Controlling the structure and length of self-synthesizing supramolecular polymers through dynamic covalent chemistry. B) Probing exchange pathways in BTA supramolecular polymers using super-resolution microscopy. Images adapted from references 28 and 29.

An elegant example of loading cargo into supramolecular polymers has been demonstrated by the Häner group. They showed that phosphate-substituted pyrene monomers have the ability to self-assemble into fibrous structures in water based on hydrophobic interactions between the pyrene moieties, with the preferential orientation of the phosphate groups towards the aqueous environment.<sup>31</sup> By extending the pyrene-phosphate monomers with short DNA oligonucleotides, the supramolecular polymer could be loaded with complementary DNA-functionalized gold nanoparticles (AuNPs) using DNA-DNA interactions.<sup>32</sup>

Functional supramolecular polymers have also been used as scaffolds for a range of biomedical techniques, enabling for instance receptor activation and cell signaling. Sulfated saccharides were conjugated to peptide amphiphiles using azidealkyne click chemistry and self-assembled into fibrillar structures through beta sheet formation.<sup>33</sup> The sulfated peptide amphiphiles could bind a range of heparin sulfate binding proteins like bone morphogenetic protein 2 (BMP-2), vascular endothelial growth factor (VEGF) and fibroblast growth factor (FGF). In studies of bone regeneration experiments in a rat animal model system, it was shown that the combination of sulfated peptide amphiphiles and the BMP-2 protein required a hundred-fold less dose compared to administrating BMP-2 exclusively. Kieltyka et al. synthesized bioactive supramolecular UPy-peptide conjugates in a modular approach using an oxime ligation strategy. 34 Both integrin binding RGD and collagen I binding PHSRN peptides were coupled to the supramolecular polymer and self-assembled into fibers using both UPy and urea-based hydrogen bonding motifs within the monomer. Surface coating of the RGD containing polymers and subsequent fibroblast adhesion assays showed comparable actin organization to fibronectin-coated surfaces, while surfaces coated with a scrambled version of the RGD peptide-sequence did not show adhesion and spreading as in the fibronectin control. Thus, both examples highlight the potential of these materials for use in biological domain (Scheme 1.4A).

Supramolecular polymers have also found applications as drug release platforms. Paclitaxel (PTX), a commonly used bulky, hydrophobic, anti-cancer drug, was conjugated to a short peptide using a biodegradable linker to form drug-peptide amphiphiles that self-assembled into filamentous nanostructures. In this way, 41 % of drug loading was achieved (MW fraction of the drug relative to the total conjugate MW), which is more than an order of magnitude larger than for classical drug release systems.<sup>35</sup> After cellular uptake of the nanostructures, the 4-(pyridin-2-yl-disulfanyl)butyrate linker conjugating the drug was cleaved from the peptide due to the high intracellular glutathione (GSH) concentration. PTX released from the

nanostructures showed significant inhibition of MCF-7 breast cancer cells, demonstrating the effectiveness of this supramolecular drug release platform. Using a similar approach, albeit with a smaller drug molecule and thereby not increasing the total percentage of drug loading, the Cui group later synthesized Camptothecin (CPT) functionalized peptide amphiphiles harboring four CPT drugs per supramolecular monomer, further increasing the potential of the drug loading capacity of the supramolecular assemblies(Scheme 1.4B).



Scheme 1.4. A) Modular synthesis of supramolecular RGD (red) and PHSRN (green) peptide-UPy conjugates using an oxime ligation strategy. B) Self-assembly of hydrophobic Camptothecin into discrete supramolecular nanostructures using a degradable linker. Images adapted from references 34 and 36.

#### 1.3 Supramolecular gels

Although there are several ways to classify gelating materials, they can simply be divided into two classes; covalent and supramolecular. Gels can be made from covalent polymer precursors where introduction of chemical covalent crosslinks between polymers and the use of a specific concentration triggers its formation. <sup>37–39</sup> Covalent polymeric gels typically form strong but brittle materials due to the presence of irreversible bonds, but upon surpassing the yield stress of the material there is no way to easily adapt or recover the materials properties. 40,41 Furthermore, they can be susceptible to the trapping of unreacted monomers and the formation of random networks that can detract from their mechanical properties.<sup>42</sup> On the other hand, supramolecular gels self-assemble using non-covalent interactions. 43,44 Here, both the precursors and crosslinking interactions between the self-assembled material can be mediated via non-covalent interactions. 45 Supramolecular gels consist of supramolecular polymer fibers where the complexity and dimensionality of the selfassembly can increase with concentration of the gelator molecule. They form soft ductile materials and the transient non-covalent nature of their self-assembly enables properties such as self-healing. 44,46 Low molecular weight gelators (LMWG) also fall into this class with motifs containing dendritic systems, <sup>47</sup> nucleobases, <sup>48</sup> metallogels, <sup>49</sup> sugars<sup>50</sup> or peptides,<sup>51</sup> in which self-assembled one-dimensional supramolecular polymers physically entangle to form a gel network. 52,53 Depending on the solvent, a volume-spanning three-dimensional organogel or hydrogel network can be constructed. Gels form because the polymeric material, which is typically only present in a low weight percentage (> 5 wt%), entraps solvent molecules in its network and thus, restricts the flow of the solvent to provide a viscoelastic material. Currently, the field is examining how to gain control over bottom-up assembly processes through exploring rational monomer design and methods to reinforce their often mechanically weak structures.

#### 1.4 Stimuli-responsiveness in supramolecular gels

A key advantage of supramolecular gels over traditional covalent polymeric gels is their stimuli-responsive nature, which arises from the non-covalent bonds that hold them together. Consequently, both physical<sup>54</sup> and chemical triggers<sup>55</sup> such as light, heat, pH, enzymes or the introduction of additives<sup>53</sup> can be used to switch supramolecular assemblies from the gel to solution phase or vice versa. Several of these strategies are discussed in detail below.

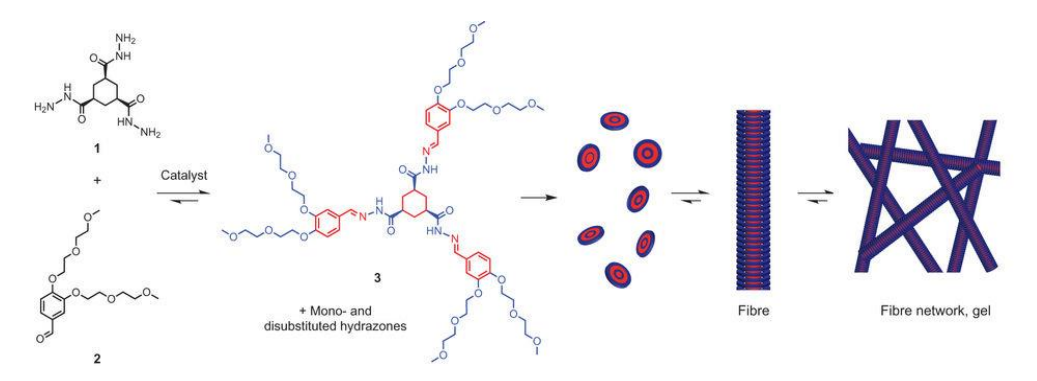
The Stupp group designed and synthesized a light-sensitive peptide amphiphile containing both a photocleavable 2-nitrobenzyl group as well as a fibronectin RGD epitope. 56 Upon photoirradiation at 350 nm, the 2-nitrobenzyl group is cleaved off, allowing the amphiphiles to fold and form β-sheets, which in turn selfassemble into a bioactive hydrogel. The Lee group synthesized penta-p-phenylene rods grafted with oligoethylene dendrimers that form nanofiber solutions at 10 °C. 57 However, upon increasing the temperature to 30 °C these nanofibers self-assemble into a reversible hydrogel network consisting of physically entangled aggregates that result from the dehydration of the oligoethylene dendrimers. Variation of pH is another method to control the formation of one-dimensional aggregates by the reversible protonation/deprotonation of both acidic and basic chemical groups within a given monomer. Adams et al. reported a series of Fmoc-dipeptide based gelators in which sodium salt variants were soluble in water, and upon lowering the pH below their pKa resulted in the formation of their respective acid. 58 The acid form could selfassemble into a wide variety of hydrogels and based on their amino acid sequence they all showed distinct properties. pH-driven self-assembly and disassembly has also been studied using the 1,3,5-trisamide cyclohexane motif.<sup>59</sup> Using the core motif and linking specific amino acid side chains, the van Esch group synthesized a range of stimuli-responsive LMWGs, which could reversibly undergo sol-gel transitions by the addition of acid or base. Interestingly, they found that not only the pKa's of the amino acids influenced pH-responsiveness, but also the strength of intramolecular attractive hydrophobic and hydrogen bonding forces inside the core motif itself.

#### 1.5 Reaction-coupled self-assembly

Many supramolecular assemblies are formed by solvation of preformed monomers and their subsequent self-assembly, often induced by physical stimuli as discussed in the previous section. Another strategy to create supramolecular materials is by using reaction-coupled self-assembly, in which the formation, change, or disruption of a chemical bond initiates the self-assembly process. To achieve this, a wide variety of, for instance, catalytic, bioconjugation and enzymatic reactions is available to drive the formation of hierarchical architectures. 55,60 Catalysis is at the central core of many biological processes, for example, biopolymer fabrication and breakdown, signal transduction and amplification, cytoskeleton formation and regulation of cell movement. The use of organic or bio-catalysis to catalytically control the preparation of the self-assembling monomer allows for additional temporal control by modulating the rate of this process with the potential to affect the resultant materials properties. The use of enzymatic catalysis has been widely demonstrated in the assembly and disassembly of supramolecular hydrogels. <sup>61,62</sup> For example, methyl ester groups have been removed from Fmoc-dipeptide methyl esters using Subtilisin A mediated hydrolysis to trigger their self-assembly.<sup>63</sup> Alternatively, alkaline phosphatase has been used to remove phosphate groups from similar Fmoc-dipeptides to form gelators.<sup>64</sup> However, enzymes can be limited in such systems as they require specific aqueous environments to function properly (e.g. pH, additives, and temperature), are bulky in size, can be very specific to a given substrate and have a limited shelf-life.

Conversely, organic catalysts are not limited by these factors and can be very suitable for wide range of applications. Boekhoven  $\it et al.$  designed a reaction-coupled self-assembling system that can be controlled by acidic catalysis or catalysis by nucleophilic substitution. In Inspired by their previous cyclohexane trisamide motif, they designed a two-component gelator system based on the reaction of a cyclohexane trishydrazide (hydrazide) and benzaldehyde wedge with two oligo(ethylene glycol) chains attached (aldehyde). Both molecules are soluble in water, but only upon formation of the dynamic covalent hydrazone bond between the two components, the gelator is made (Scheme 1.5). The self-assembly in this system is driven by the hydrophobic cyclohexane core, hydrogen bonding of the three hydrazone moieties and  $\pi$ -interactions between the stacked phenyl rings, which are all shielded from the aqueous environment by the six peripheral ethylene glycol chains. The full gelator molecules then self-assemble into one-dimensional fibers that in turn bundle and physically crosslink into an entangled fibrous network. The rate at

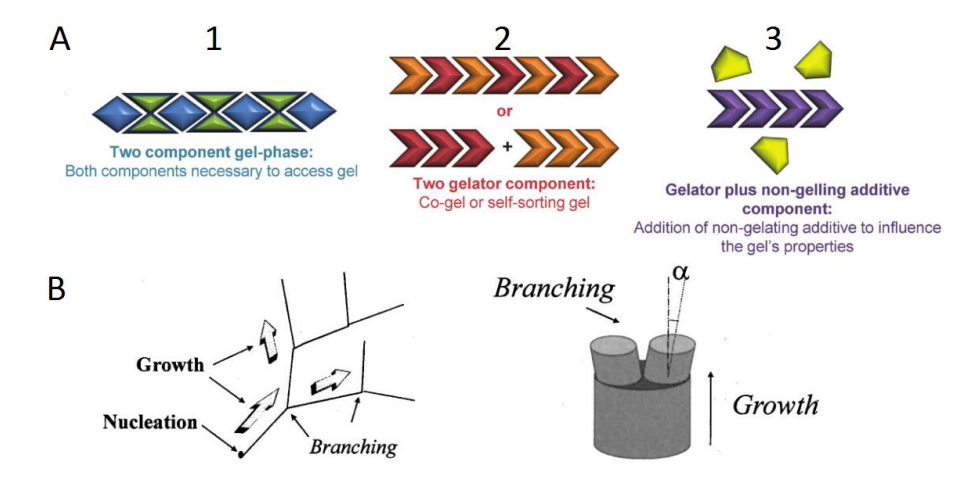
which this gelator forms, and thereby the fibers, highly dictates the mechanical properties of the resulting gel-phase material, highlighting the importance of the catalyst used in this reaction coupled self-assembling system. Uncatalysed hydrogels prepared at neutral pH (pH 7) resulted in weak hydrogels (5 kPa) with thick fiber bundles of up to 1 micron in length and about 5 nm in width. The use of acidic catalysis (pH 5 buffer) resulted in the construction of highly and finely branched network structures and roughly a 10-fold greater storage modulus (≈50 kPa). Finally, addition of a nucleophilic catalyst, aniline, to a pH 7 solution resulted in slightly stronger gels with a storage modulus of 55 kPa. The catalysts were then explored in different presentations such as on surfaces, in membranes, and with light activation to provide spatial control for gel formation.



Scheme 1.5. Catalytic formation of hydrazone gelator 3 from hydrazide 1 and aldehyde 2 leads to assembly into fibers and subsequent gel network formation by physical entanglement. Blue parts: hydrophilic, red parts: hydrophobic groups. *Image adapted from reference 19*.

## 1.6 Multi-component self-assembly to influence the mechanical properties of supramolecular gels

Classically, most LMWG systems consist of a single component that self-assembles into a gel material with its resultant properties being connected to the concentration, solvent and temperature. More recently, multicomponent systems are being explored not only to introduce function into such systems, but also as a facile means to finetune the network properties. 65,66 In general, in terms of molecular design, three possible scenarios exist for constructing multicomponent gelator materials (Scheme 1.6A); 1) all individual components form a gel together where all components are required to work together to form a single network, 2) the components assemble into individual networks by either self-sorting, or via co-assembly. Or lastly, 3) some of the components are responsible for gelation and the others serve as non-gelling additives, which still can influence the outcome of the self-assembled structure.<sup>53</sup> Here these specific additives or components can typically influence the manner of hierarchical assembly of such materials, like the extent of fiber bundling and branching. Variation of the specific multicomponent molecular composition, for instance by changing the ratios of the various components with their various roles, can also be used to affect the outcome of the resulting networks. By modulating these ratios, both the appearance and stability of the network, and also its mechanical properties can be tuned.



Scheme 1.6. A) Three main classes of multicomponent supramolecular gel assembly. B) Graphical representation of nucleation and growth and branching phenomena in supramolecular fiber formation. Images adapted from references 53 and 68.

Most LMWG systems form by a nucleation and growth mechanism, in which a limited number of gelator molecules form a nucleus from which the fiber network of the gel grows (Scheme 1.6B). During the fiber formation process, defects arise that can result in branched junctions in the fibers. These branches heavily contribute to the mechanical properties of the gel-phase material, as they are responsible for the formation of a highly interpenetrating network originating from many nuclei close by. 67,68 However, when comparing this LMWG method of network formation with covalently linked polymer gels, they are still weak. Therefore, methods to improve the mechanical stability of LMWG networks are required, which can be achieved using multi-component self-assembly approaches. A common method to increase the mechanical properties of hydrogels in both covalent and supramolecular polymers is through the introduction of specific crosslinkers. <sup>69–76</sup> These will interact with at least two supramolecular polymers and thereby strengthen their connection, resulting in a stronger material. A rule of thumb in covalent polymer materials is that increasing crosslinker concentrations results in increasingly stronger networks.<sup>77</sup> However, in supramolecular systems, this rule does not necessarily apply. The Sijbesma group has shown that addition of co-assembling flexible homobifunctional polymeric crosslinkers into a urea-based bolaamphiphilic supramolecular fiber network resulted in inefficient crosslinking due to intrafiber back-looping of the flexible crosslinkers into the same fiber. 74 Synthesis of heterobifunctional crosslinkers and co-assembly of two supramolecular polymers, each bearing distinct hydrophobic cores, forced the crosslinkers to interconnect the fibrils resulting in the improvement of mechanical performance of the resulting crosslinked material. Moreover, Kieltyka et al. found that incorporation of a homobifunctional crosslinker in a UPy-based supramolecular hydrogel system only had partially positive effects with increasing concentration.<sup>72</sup> In comparison to the fiber monomers, the bulky crosslinker could not surpass a ratio of 1 wt% to 4 wt% of the crosslinker to gelator monomer, as higher crosslinker concentrations weakened the mechanical properties of the hydrogel. Methods to improve the mechanical properties of supramolecular hydrogels, namely the extent of crosslinking and strategies that target the fibrillar architecture can highly impact the self-assembly process of the native network structure, and thus the outcome of the material. Therefore, these strategies should always be implemented carefully and their effects investigated thoroughly. In this work, we will investigate the effect of crosslinkers and the incorporation of functional cargo on the self-assembly of a hydrazide-aldehyde LMWG system. By better understanding their effect on LMWG systems this knowledge can aid the fabrication of functional supramolecular hydrogel systems for a wide range of biomedical applications.

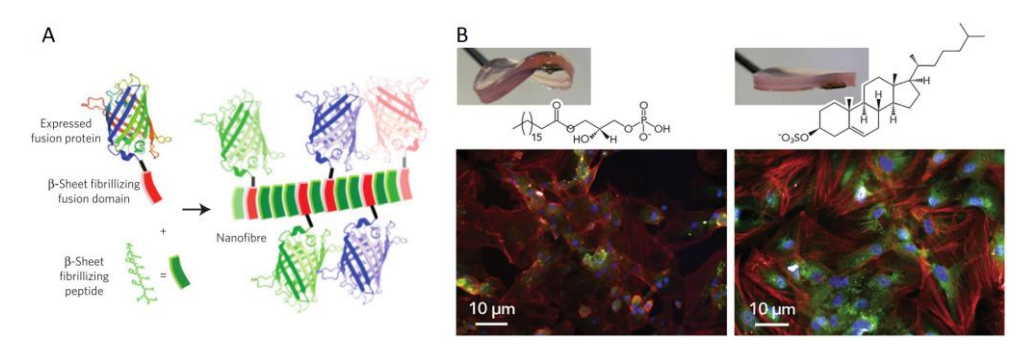
#### 1.7 Supramolecular hydrogels for biomedical applications

Over the past decades, biomaterials have evolved from wooden prosthetics to modern metal, ceramic and polymer based designs to repair and replace damaged tissue. The state of the art technologies in health care however, are constantly demanding higher performance and better control over function for these types of materials. Whereas traditional top-down designed biomedical materials offer good structural analogues to native tissue, they often do not have the capacity to fully mimic the natural structure and function of the replaced components. For this purpose, supramolecular self-assembling hydrogels have the potential to become the next-generation of biomaterials, as their structural properties can be modularly tuned, and can be made functional or even biomimetic in similar ways to these natural materials. This makes them excellent candidates for applications like three-dimensional cell culture, tissue engineering 80,81 and drug release 82-84.

Supramolecular hydrogels are eminently suitable for drug delivery applications as they can serve as a depot for drug administration, but simultaneously can degrade or erode over time to allow the gel material to clear the body. Many strategies exist to achieve drug delivery from supramolecular hydrogels like physical encapsulation of the drug or covalent tethering of the therapeutic compound to the gel network. The Xu group demonstrated the synthesis of a pre-gelator peptide covalently tethered to the antineoplastic drug Taxol motif with a phosphate group that inhibits self-assembly into hydrogel materials.<sup>24</sup> When enzymatic cleavage of the phosphate group occurs, gelation is enabled. This model work could lead to the formation of hydrogels initiated by specific enzymatic triggers that are present in disease-related conditions. On the other hand, the van Esch group has demonstrated synthesis of a gelator molecule that functions as a prodrug.<sup>85</sup> Based on the cyclohexane trisamide motif, a model drug was tethered to the core motif using an enzymatically cleavable linker. The prodrug molecule self-assembled into hydrogel structures and was largely protected from enzymatic degradation by the fibrous network. Upon increasing the temperature and in the presence of the enzyme, the model drug would be cleaved and released into the media.

Apart from drug release applications, supramolecular hydrogels can also be used to precisely present bioactive cues to cells. The Collier group has prepared supramolecular gels bearing multiple large protein cargos. By tethering different types of fluorescent proteins to self-assembling beta-sheet peptides, they formed colored supramolecular microgels. This system can be seen as a model system for immuno-

engineering applications where a controlled display of ligands is of interest (Scheme 1.7A). One of the most promising applications for supramolecular hydrogel materials can be in the field of tissue engineering and regenerative medicine, where supramolecular gel materials can be used to engineer dynamic scaffolds for cellular growth. Self-assembling peptide amphiphiles co-assembled with cell adhesion cues such as RGD were reported by Webber *et al.* to enhance the adhesion of bone-marrow mononuclear cells to these materials. Controlling the mechanical properties of a co-assembling peptide amphiphile – surfactant hydrogel system by tuning their concentration, Ulijn and Dalby demonstrated control over the differentiation of perivascular stem cells.<sup>87</sup> Growth of these stem cells on soft (1 kPa), stiff (13 kPa) and rigid (32 kPa) hydrogels led to neuronal, chondrogenic and osteogenic differentiation, respectively. Hence, control over the mechanical properties as well as incorporation and presentation of functional moieties in supramolecular hydrogels is of great importance for their application in biomedical relevant areas (Scheme 1.7B).



Scheme 1.7. A) Supramolecular self-assembly of protein fused to  $\beta$ -sheet forming peptides into microgels. B) Soft (left) and rigid (right) peptide amphiphile hydrogels for controlled differentiation of perivascular stem cells. Images adapted from references 86 and 87.

#### 1.8 DNA as a nanotechnology building block

As the genetic storage medium for all living organisms, DNA is an ever-evolving repository of Nature's diversity. Apart from its biological role, nucleic acids are also very interesting from a materials point of view. DNA has predictable dimensions; 2 nanometer thickness, a helical pitch of 3.4 nm and a large persistence length of 150 base pairs (50 nm). The highly specific interactions between adenine and thymine or guanine and cytosine facilitates their assembly over long distances with nearly flawless precision. Other than these simple linear Watson and Crick interaction rules, DNA can also assemble into more complex structures using unconventional base-pairing such as Hoogsteen interactions. Furthermore, oligonucleotides can adopt looped, branched and higher order structures, such as G-quadruplexes (G-rich motif) and i-motifs (C-rich motif).

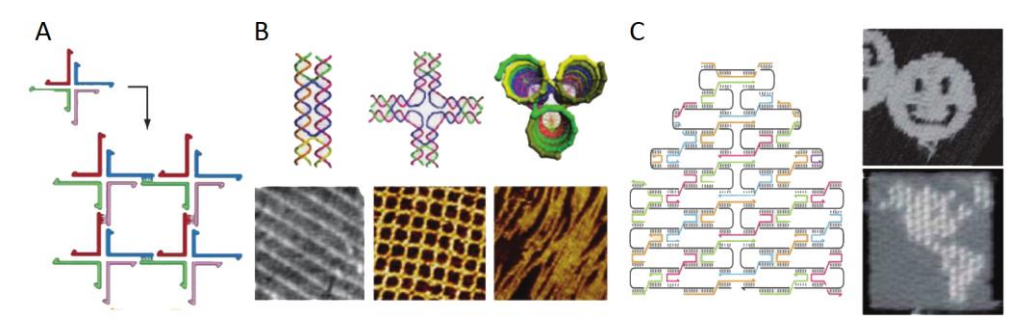
Advances in commercial availability, lowered production costs and synthetic scalability over the last years have opened up the ability of DNA as a nanoscale building block. Synthetic production of oligonucleotides has provided a large chemical library with a wide range of artificial and modified nucleotides. In turn, this has increased the complexity of oligonucleotide sequences from an already astonishing  $4^N$  for N-bases, to  $X^N$  where X is based on the amount of natural, artificial and modified nucleotides. This transition yields not only expansion of the standard code, but also its function and stability.

Oligonucleotides by design qualify as one of the oldest supramolecular polymers around. While their interactions are primarily driven by hydrophobicity, as the phosphate backbone is highly soluble and the bases hydrophobic, van der Waals forces and hydrogen bonding between the bases result in their specific self-assembly. These non-covalent interactions are responsive to a wide variety of stimuli like temperature, ionic strength, pH, solvents and enzymes. These features make oligonucleotides a perfect tool for developing programmable and predictable bottom-up supramolecular assemblies where complementary sticky ends between oligonucleotides can interact to form higher ordered species. Hany techniques have been designed to manipulate DNA in a biological context (like gene therapy, vaccination, PCR, antisense oligonucleotides), whereas tools and techniques to control DNA self-assembly have only been devised in the last decades. The field of DNA nanotechnology can be coarsely divided into structural and dynamic DNA nanotechnology, in which the former has a deeper focus on the formation of discrete DNA-based objects and the latter on what DNA can provide in terms dynamic and

responsive materials. <sup>95,96</sup> The combination of these subfields has the potential to give rise to DNA-based materials with highly defined structures and precisely controlled dynamic characteristics.

#### 1.9 Structural and supramolecular DNA nanotechnology

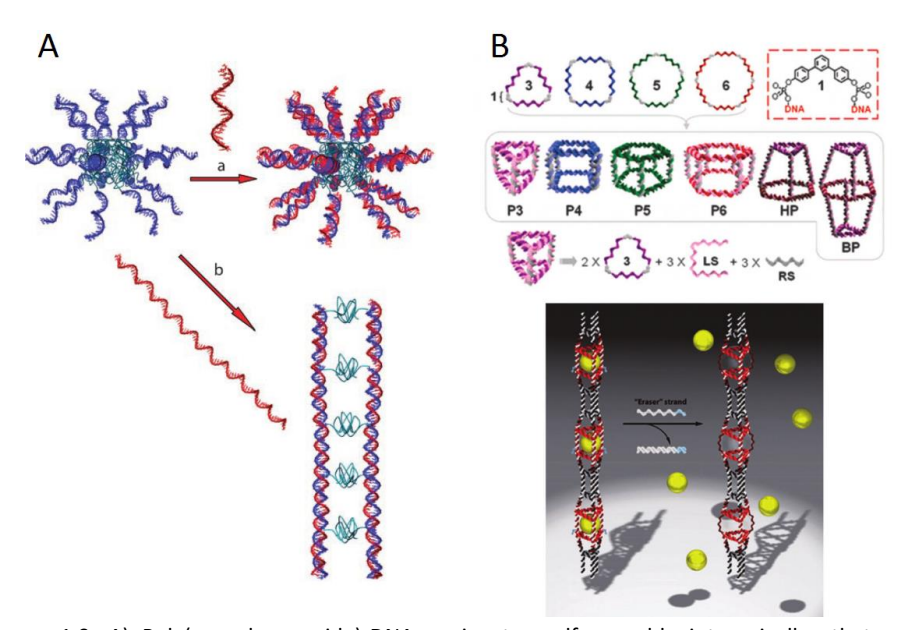
The field of structural DNA nanotechnology was pioneered by the Seeman group. Looking for a solution to obtain well-ordered protein lattices for X-ray crystallization Seeman aimed to make a DNA-based lattice to precisely position and suspend the proteins. 97 Inspired by the naturally occurring Holliday junctions, Seeman made both two and three-dimensional DNA structures by exclusively using the sticky end interactions of double stranded DNA to make artificial, immobile four-way junctions that on a larger scale could assemble into DNA tiles (Scheme 1.8A). 98 Their initial attempts later resulted in the formation of structurally rigid double and triple crossover motifs that could make well-defined two-dimensional lattices with periodic repeats (Scheme 1.8B).99 Since these initial reports, the field of structural DNA nanotechnology has developed accurate and controlled methods to self-assemble a multitude of architectures including DNA rectangles, ladders, cubes and tubes (Scheme 1.8C). 93,100 Nowadays, these discrete structures are even used in performing simple mathematical calculations using the principles of DNA-based self-assembly. 101 Another method to form self-assembled DNA-based superstructures is by DNA origami. A long scaffolding strand, typically a single stranded viral DNA, is folded with the help of staple strands into a specific superstructure with high precision. This technique has been applied for the assembly of two- and three-dimensional objects including the famous DNA smiley, stars, disks, <sup>102</sup> a box with a controllable lid, <sup>103</sup> and the patterning of molecular cargo<sup>104</sup> and devices<sup>105</sup> on the origami's themselves.



Scheme 1.8. Examples of structural DNA nanotechnology: A) DNA four-way junction, B) DNA-based tiles and junction motifs, C) a long DNA strand is folded into a DNA origami (smiley and map of the Western Hemisphere) using small DNA staple strands. Images adapted from reference 93.

The combination of organic molecules and DNA is a developing branch of research in DNA nanotechnology. Whereas in classical structural DNA nanotechnology the final materials are based solely on DNA, supramolecular DNA nanotechnology

combines the best of synthetic inorganic or organic chemistry with nucleic acids to form hybrid materials with unique properties. 106 Herrmann and coworkers synthesized poly(propylene oxide)-DNA conjugates that self-assemble in spherical micelles due to the hydrophobic character of the poly(propylene oxide) polymer and the hydrophilic character of the oligonucleotides. 107 Going one step further, they could align these micelles into higher-ordered ladder-like structures using additional DNA strands as templates (Scheme 1.9A). Organic molecules are also excellent candidates to define shapes and bends that oligonucleotides cannot encompass themselves. The Sleiman group has shown that organic molecules can guide the selfassembly of nucleic acids into triangles and squares by acting as vertices for these shapes. 108 these types of shapes can also be addressed with DNA-functionalized gold nanoparticles depending on their sequence design. <sup>109</sup> Moreover, by adding additional vertical support strands to a wide range of two-dimensional template shapes, they were converted into three-dimensional structures like prisms and boxes using the same design rules, which could even be polymerized into peapod-like nanotubes that could harbor gold nanoparticles in their interior (Scheme 1.9B). 110 Combining the best of both worlds, supramolecular DNA nanotechnology opens up the possibility to make both structurally defined functional materials with a dynamic character.

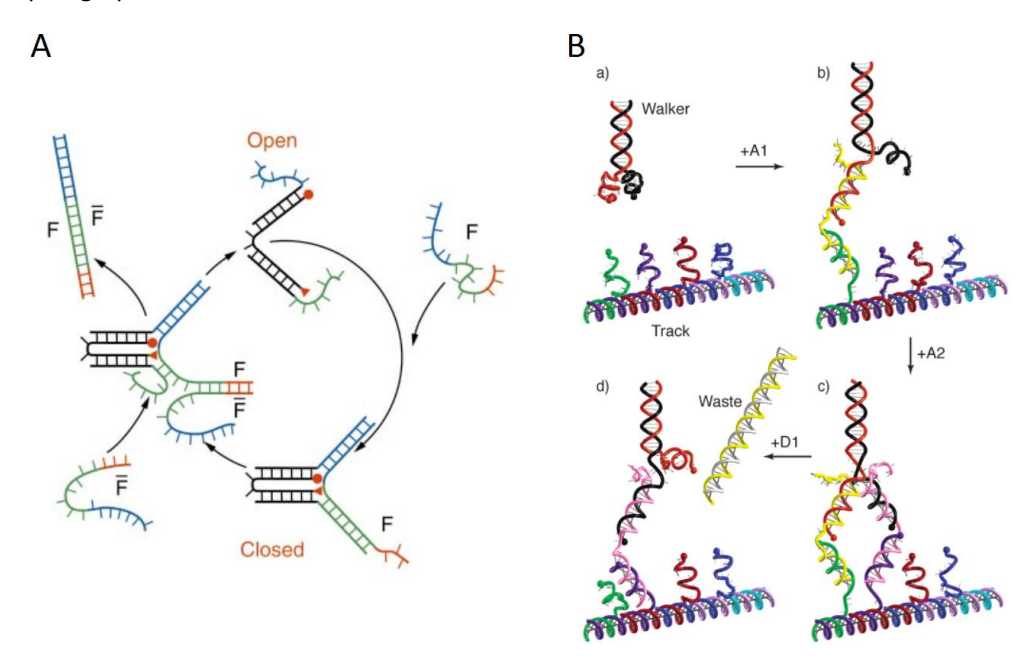


Scheme 1.9: A) Poly(propylene oxide)-DNA conjugates self-assemble into micelles that can be aligned into ladder like structures. B) Supramolecular DNA-organic molecule hybrids for the assembly of a multitude of geometrical shapes that can be polymerized and loaded with gold nanoparticles. Images adapted from references 107 and 110.

#### 1.10 Dynamic DNA nanotechnology

Compared to structural DNA nanotechnology where the aim is that structures are brought to their thermodynamic equilibrium end-state by various preparation protocols, dynamic DNA nanotechnology focuses on the design and fabrication of reconfigurable and autonomously operating devices that have an out-of-equilibrium and dynamic character. 96 Nucleic acids are readily addressable by stimuli like heat, pH, ionic strength, and so on. However, DNA-based assemblies can also be very powerfully controlled using nucleic acids themselves. Dynamic DNA nanotechnology is mostly based on DNA strand displacement events, in which two DNA strands partially or fully hybridize with each other at the expense of an earlier formed DNA duplex. Strand displacement events are initiated by hybridization at single-stranded toehold domains and through a random walk-like branch migration process that displaces the pre-existing duplexes to provide the most energetically favorable DNA duplex. As the rate of strand displacement is fully determined by toehold length and the DNA sequence of both the invading strand and the target duplex, the kinetics of the displacement events can be easily tuned by sequence design. 111,112 In Nature. enzymes like helicase and polymerase can do strand displacement reactions. Here the reactions are performed without the use of enzymes and are solely based on the biophysical properties of DNA itself.

The most basic strand displacement reactions were pioneered by Yurke and coworkers who showed the construction of DNA-based tweezers. 113 The DNA structure could be reversibly switched between an open and closed state by addition of two different DNA strands. The first strand binds the tweezers arms to close it, only leaving a short overhanging toehold. Addition of a second strand, fully complementary to the first closing strand, removes the closing strand by toeholdmediated strand displacement to provide an inactive double stranded waste product (Scheme 1.10A). This technique has also been used to make reprogrammable DNA nanostructures, such as in the control of a DNA-lock on a nanoscale box formed by DNA origami. 103 Using the same principles, Shin and Pierce made one of the first dynamic DNA machines: the DNA walker. 114 They fabricated a DNA track based on multiple DNA strands with four exposed single stranded positions for the twostranded walker to bind by attachment strands. Using a clever design, the DNA walker sequentially bound in a step-wise fashion to all four positions mimicking the natural movement and stride of kinesins on microtubules (Scheme 1.10B). Strand displacement reactions have also been used extensively to make simple Boolean logicgate systems, in which output information is stored within hybridized oligonucleotides. Addition of one or more input strands will cause the sequential displacement of pre-hybridized strands to reveal the output of the reaction. More complex computational systems exist, but generally rely on strand displacement cascading events and signal amplification. These will be discussed in the next paragraph.



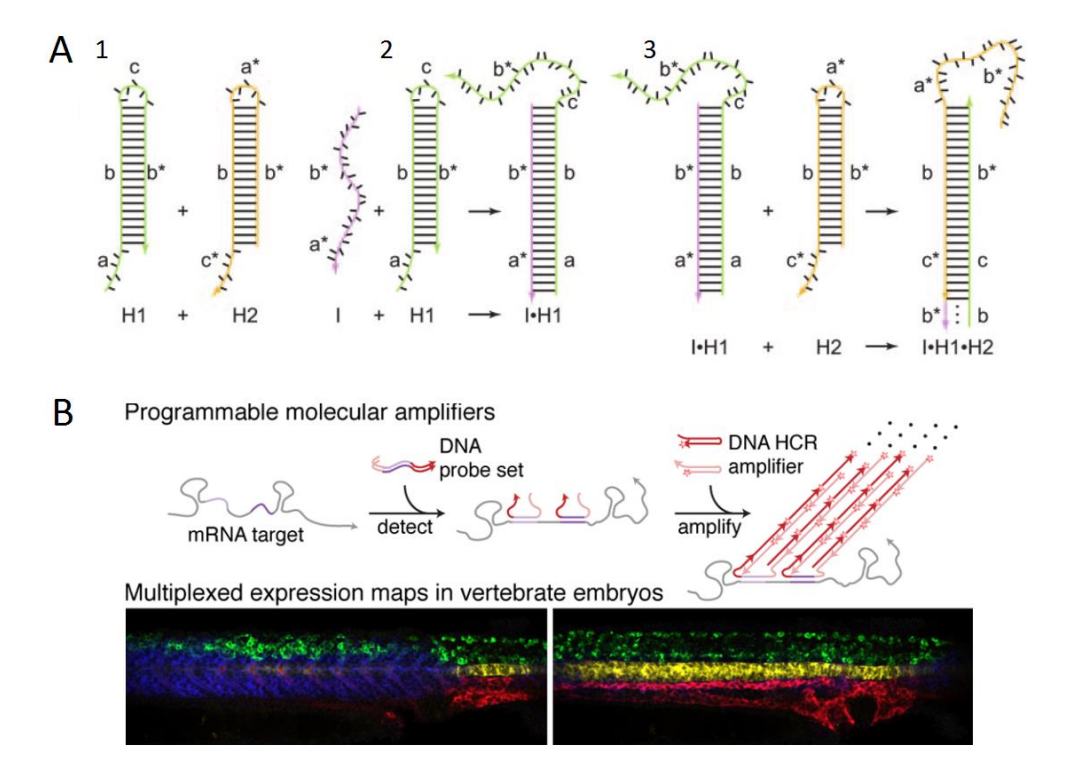
Scheme 1.10. A) DNA-based tweezers that can be reversibly opened and closed using strand displacement. B) DNA-walker that can autonomously walk over a track of DNA strands using sequential hybridization and strand displacement reactions. Images adapted from references 113 and 114.

DNA nanotechnology techniques based on strand displacement have exclusively relied on individual displacement events, where a continuous or sequential addition of one or more oligonucleotide strands is required to maintain the reaction sequence. However, an intriguing technique using dynamic DNA nanotechnology involves cascading reactions, in which complex autonomous systems can be developed by using the output of a first reaction as an input for the next reaction. Designing displacement reactions in this way eliminates the constant need for new external inputs for every step. <sup>96</sup> Advanced amplifying cascading reactions even allow for catalytic activity of the input strands, where they can be recycled during the reaction to achieve very high signal amplification from a single input. <sup>117,118</sup> Software packages like NUPACK<sup>119</sup> and visual DSD<sup>120</sup> have made it possible to test many of

these reactions in silico, thus providing much-needed tools to simplify the design of these systems. By far, the most used cascading displacement reaction is the hybridization chain reaction (HCR). Developed by Pierce, 121 the original HCR system involves the recognition of a single initiator strand by one of two metastable hairpin species to enable their cascading reaction (Scheme 1.11A). In absence of the DNA initiator strand, the two hairpins are locked in a kinetically trapped conformation and can coexist in a metastable state (Scheme 1.11A.1). Addition of the DNA initiator strand (containing domains A\* and B\*) to the hairpins triggers a toehold mediated strand displacement reaction on the first hairpin, which opens up the hairpin by hybridization (with domains A and B) and reveals the previously inaccessible loop and stem region (domains C and B\*)(Scheme 1.11A.2). The disclosure of this looped region can be seen as the output of the first reaction and the new input of the subsequent reaction, as this sequence can initiate a similar opening in the second hairpin by hybridization with complementary domains C\* and B. In turn, the opened up second hairpin displays the identical sequence as the DNA initiator strand (domains A\* and B\*) and thus allows the chain reaction to progress (Scheme 1.11A.3). In this way, a single DNA initiator strand is consumed in the process and theoretically enables the HCR reaction to continue until the supply of either of hairpins is exhausted. In terms of design, the most important parameters are the length of the toehold and loop size, which respectively majorly control both the rate of reaction and store the potential energy required for the chain reaction to continue cascading. Tuning the length of these domains allows for control over the kinetics of HCR. 122 Next to linear HCR, oligonucleotides can also be designed to allow branched and dendritic growth of the HCR arms, which drastically increases growth kinetics. 123

The classical way to visualize the hybridization chain reaction is by gel electrophoresis. However, due to the unique properties of both the DNA and the ability to chemically modify DNA with a wide range of dyes and label-attachment chemistries, a wide range of techniques including atomic force microscopy, surface plasmon resonance, fluorescence, luminescence, colorimetry and many more can be used. Based on its excellent specificity, sensitivity, and signal amplification properties, applications for HCR include: solution-phase and surface bound detection of simple DNA targets or small molecules and proteins using aptamers, the HCR-mediated gold aggregation for colorimetric detection of analytes, interaction with specific intra- and extracellular targets, point-of-care detection of cancer cells and markers, mapping and amplification of multiple miRNA targets *in vitro* in zebrafish (Scheme 1.11B), aptamer binding initiated-HCR for the detection of proteins or delivery of medicine and DNA-based hydrogel formation.

thesis, the hybridization chain reaction is a very powerful tool to create functional and dynamic DNA-based supramolecular materials.



Scheme 1.11: A) Schematic representation of the hybridization chain reaction. B) Hybridization chain reaction using fluorescently labeled hairpins to localize and visualize miRNA expression in zebrafish. Images adapted from references 121 and 130.

#### 1.11 DNA-functionalized polymer and hydrogel systems

As explained in the previous sections, DNA on its own can be used in a multitude of structurally static and responsive dynamic setups, but materials completely made from DNA can be expensive depending on the envisaged application. Combining DNA with covalent polymers can not only decrease the cost of the resulting materials, but also introduce a broad range of stimuli-responsive properties into covalent polymer materials. Therefore, the marriage between these two groups of building materials has tremendous potential to make assemblies that can benefit from both sets of molecular properties. From a synthetic point of view, the progress in synthesizing DNA oligomers with reactive modifications has significantly increased coupling efficiencies and the ease of making hybrid DNA-polymer conjugates. In addition, highly efficient solution-phase reactions such as Michael additions, and copper-catalyzed or strain promoted azide-alkyne cycloadditions allow for near quantitative coupling efficiencies rendering nucleic acids as attractive modules to be used in polymer materials.

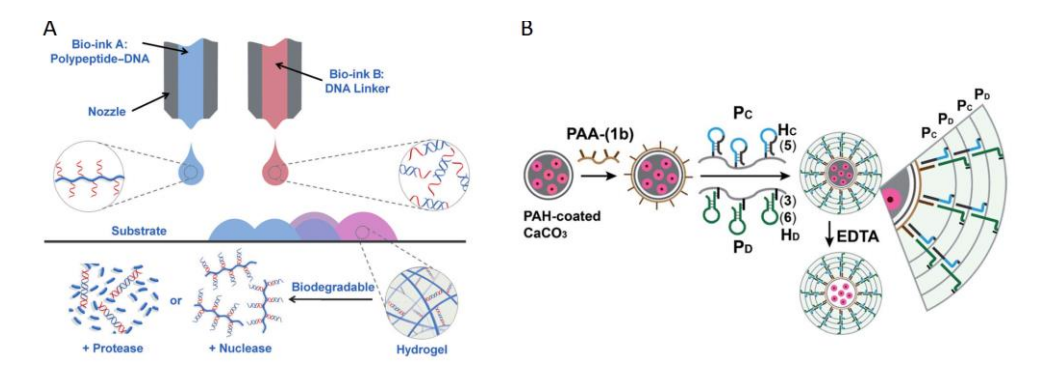
Earlier work on linear DNA-block copolymers have shown the construction of responsive micellar structures, where DNA typically serves as a highly charged hydrophilic block and the organic polymer fulfills the role of hydrophobic block. Changing the morphology from linear polymers to grafted polymers possibly allows for more complex architectures like worms, spheres and cylinders. Graft copolymers are made using one of the following three strategies: grafting onto, grafting from and grafting through. In the grafting onto approach, the organic polymer backbone is functionalized with chemical groups that can react with a functional group on the oligonucleotide. In this way, the grafts are directly conjugated to the polymer backbone using a single chemical reaction. Grafting from uses a similar approach, but the grafts are made by the successive polymerization of the monomers in situ. Lastly, the grafting though strategy relies on the polymer graft to be functionalized with a polymerizable group to synthesize the polymeric backbone in situ.

DNA grafted polymers are typically made using either grafting onto or grafting through methods. Grafting onto is typically used as an easy way to make lower grafting density polymers as DNA is a highly charged and typically bulky molecule and the high density grafting would not be achieved due to steric and electrostatic repulsions. Grafting though on the other hand enables more densely packed graft copolymers as the DNA is exclusively incorporated at the periphery of

the polymer and thus does not suffer as much from repulsive forces. One of the early strategies to make DNA grafted materials was by functionalizing DNA oligomers with acrydite groups. In this way, many research groups have shown the formation of DNA-functionalized poly(acrylamide) graft copolymers where a percentage of the acrylamide monomers is functionalized with DNA and incorporated using standard radical polymerization. Over the last decade, many different polymer backbones and a wide variety of coupling strategies have been successfully demonstrated to make DNA-functionalized polymers.

The combination of DNA and organic polymers can also be used to synthesize functional hydrogel materials. In these systems, the DNA often functions as the stimuli-responsive component of the material and the organic polymer functions as the bulk component. In this way, DNA-grafted covalent polymers have been used for stimuli-responsive control over mechanical properties of gel networks based on external triggers for instance including temperature, pH, light, enzymes and small molecules. 140,141 Some examples and applications are shown in the next part. A straightforward design involves complementary DNA strands tethered to a covalent polymer backbone resulting in the construction of hydrogel materials upon hybridization. The Maeda group was one of the first to demonstrate such an approach through the preparation of DNA-grafted poly(acrylamide) hydrogels that could shrink or swell in response to specific single stranded DNA sequences. <sup>138</sup> Tan and coworkers prepared an aptamer-crosslinker hydrogel for the detection of cocaine. 142 By competitive binding of the target molecule with the aptamers embedded in the crosslinker, the integrity of the DNA-grafted polymer network was compromised and dissolved. Using this method, as low as 20 ng of cocaine was detected, demonstrating the excellent sensitivity of the DNA-graft copolymer hydrogel system. Using a polypeptide-DNA graft copolymer, DNA-assembled hydrogel formation for threedimensional bioprinting was demonstrated. 143 By alternating the printing of the graft copolymer material and a DNA based crosslinker in a layer-by-layer fashion, the Liu group and collaborators could seed cells in controlled and biodegradable materials of various shapes (Scheme 1.12A). DNA-grafted polymers have also been used to make stimuli-responsive hydrogel microcapsules for drug release. 144 By loading calcium carbonate microcapsules with Doxorubicin and subsequently coating the capsules with HCR initiator bearing polymers, a small hydrogel layer can be made by adding graft copolymers functionalized with HCR hairpins. The hairpins in this system have a dual role as they also contained aptamer sequences for either ATP or cocaine detection. More specifically, addition of these molecules would disassemble the hydrogel corona coating the calcium carbonate microspheres and facilitate efflux of Doxorubicin from the spheres (Scheme 1.12B).

Currently, numerous examples of covalent polymer – DNA hybrid materials exist, however, the combination of supramolecular polymers consisting of amphiphiles combined with DNA is still in its infancy. As discussed in the functional supramolecular polymer section, the Häner group showed the loading of DNAfunctionalized gold nanoparticle cargo on pyrene-based supramolecular polymers. 145 Miller and coworkers have shown the synthesis of a self-assembling beta-sheet forming peptide hydrogel with immobilized DNA oligonucleotides for the detection of a fluorescently labeled target DNA. 146 In solution, the target DNA is in a quenched state but upon hybridization on the supramolecular fiber, its fluorescence is turned on as the proximal quencher becomes displaced. This proof-of-concept report demonstrates the ability of the peptide hydrogel to be used for the detection of biomolecules. Lastly, the Liu group has demonstrated the self-assembly of poly(benzyl ether) dendrons conjugated to short DNA oligonucleotides. 147 The DNA could be loaded by hybridization with a complementary mannose conjugated DNA oligomer. The mannose in turn could serve as a binding site for Escherichia coli bacteria. All these examples demonstrate the potential to assemble DNA-functionalized building blocks into organic supramolecular polymers and the possibility to use the DNA for orthogonal assembly.



Scheme 1.12: A) Polypeptide-DNA graft copolymer and DNA linker that can form a biodegradable hydrogel network for cell culture applications upon mixing by printing. B) Responsive hydrogel coated calcium carbonate microcapsules based on performing a hybridization chain reaction on the particles surface. Images adapted from references 143 and 144.

#### 1.12 Aim and outline

The literature study highlights the potential of functional supramolecular materials based on one-dimensionally stacked supramolecular and covalent polymers, as well as gels, with DNA, as both a static or dynamic component. To explore the scope of these hybrid materials, it is important to combine new organic supramolecular building blocks and with a range of DNAs to study mechanistic aspects of their self-assembly.

Thus, the focus of the experimental work contained in this dissertation involves the design, synthesis and study of functional supramolecular polymer materials for biomedical applications and diagnostics using both (supramolecular) polymers and DNA as building blocks.

In Chapter 2, we describe the synthesis of a DNA-dextran graft copolymer. Using the hybridization chain reaction, a dynamic DNA nanotechnology technique, a novel non-covalent grafting from technique is shown on the DNA-dextran graft copolymer. The effect of performing HCR on these graft copolymers will be first examined under dilute conditions using gel electrophoresis, spectroscopy (fluorescence), light scattering (DLS, SAXS) and imaging techniques (AFM). Afterwards, we will show the formation of hydrogels at higher concentrations using particle-tracking microrheology.

Chapter 3 focuses on the design and synthesis of DNA-functionalized multicomponent supramolecular polymers. By self-assembling DNA-functionalized bolaamphiphiles on a squaramide-based supramolecular polymer system, we demonstrate the reversible loading of differently sized DNA-functionalized gold nanoparticles using DNA strand displacement. The construction of these reversibly addressable functionalized fibers will be demonstrated using transmission electron microscopy, zeta-potential, gel electrophoresis, fluorescence and thermal denaturation experiments.

Chapter 4 aims to increase the mechanical properties of a reaction-coupled multicomponent low molecular weight hydrogelator system by using various (bio)polymeric crosslinkers. The effect of stiff, charged DNA- and soft, neutral poly(ethylene glycol) crosslinkers were examined on the formation of a reaction-coupled gelator material. Using rheology, SEM and confocal microscopy, we show the effect of both crosslinker types on the mechanical properties of the gelator networks and their influence on the gelation pathway.

Using the same LMWG system, chapter 5 describes the self-assembly of a controlled drug release platform. First, we show the capability to make stable biocompatible hydrogels using L-histidine methyl ester as a catalyst by rheology and SEM. Secondly, we show a time-controlled effect of the extent of Doxorubicin conjugation to the core gelator by differing incubation time of the drug with the core. Using variable pre-incubation times of the drug molecule with respect to the various components, the mechanical properties of the network and their drug release profiles are affected. Lastly, the potential of these hydrogels to deliver Doxorubicin to MCF-7 breast cancer cells is demonstrated *in vitro*.

# 1.13 References

- A. C. Mendes, E. T. Baran, R. L. Reis and H. S. Azevedo, *Wiley Interdiscip. Rev. Nanomedicine Nanobiotechnology*, 2013, **5**, 582–612.
- 2 E. Krieg, M. M. C. Bastings, P. Besenius and B. Rybtchinski, *Chem. Rev.*, 2016, **116**, 2414–2477.
- M. J. Webber, E. A. Appel, E. W. Meijer and R. Langer, *Nat. Mater.*, 2015, 15, 13–26.
- 4 L. Yang, X. Tan, Z. Wang and X. Zhang, *Chem. Rev.*, 2015, **115**, 7196–7239.
- 5 E. W. De Greef, F.A., Smulders, M.J., Wolffs, M., Schenning, A.P..H.J., Sijbesma, R.P., Meijers, *Chem. Rev.*, 2009, **109**, 5687–5754.
- 6 J. D. Hartgerink, E. Beniash and S. I. Stupp, *Science*, 2001, **294**, 1684–1688.
- 7 S. Sivakova and S. J. Rowan, *Chem. Soc. Rev.*, 2005, **34**, 9–21.
- 8 F. Wang, C. Han, C. He, Q. Zhou, J. Zhang, C. Wang, N. Li and F. Huang, *J. Am. Chem. Soc.*, 2008, **130**, 11254–11255.
- 9 U. S. Schubert and H. Hofmeier, Macromol. Rapid Commun., 2002, 23, 561–566.
- R. P. Sijbesma, F. H. Beijer, L. Brunsveld, B. J. B. Folmer, J. H. K. K. Hirschberg, R. F.
   M. Lange, J. K. L. Lowe and E. W. Meijer, *Science*, 1997, 278, 1601 LP-1604.
- 11 A. C. H. Pape, M. M. C. Bastings, R. E. Kieltyka, H. M. Wyss, I. K. Voets, E. W. Meijer and P. Y. W. Dankers, *Int. J. Mol. Sci.*, 2014, **15**, 1096–111.
- M. Fernandez-Castano Romera, R. P. M. Lafleur, C. Guibert, I. K. Voets, C. Storm and R. P. Sijbesma, *Angew. Chem. Int. Ed.*, , DOI:10.1002/anie.201704046.
- J. D. Hartgerink, E. Beniash and S. I. Stupp, *Proc. Natl. Acad. Sci. U. S. A.*, 2002, **99**, 5133–8.
- 14 J. Wu, J. Li, U. Kolb and K. Müllen, *Chem. Commun.*, 2006, **1**, 48–50.
- S. Cantekin, T. F. A. de Greef and A. R. A. Palmans, *Chem. Soc. Rev.*, 2012, 41, 6125–6137.
- M. B. Baker, L. Albertazzi, I. K. Voets, C. M. A. Leenders, A. R. A. Palmans, G. M. Pavan and E. W. Meijer, *Nat. Commun.*, 2015, **6**, 6234.
- A. Friggeri, C. Van Der Pol, K. J. C. Van Bommel, A. Heeres, M. C. A. Stuart, B. L. Feringa and J. Van Esch, *Chem. A Eur. J.*, 2005, **11**, 5353–5361.

- J. Boekhoven, A. M. Brizard, P. van Rijn, M. C. a Stuart, R. Eelkema and J. H. van Esch, *Angew. Chem. Int. Ed.*, 2011, **50**, 12285–9.
- J. Boekhoven, J. M. Poolman, C. Maity, F. Li, L. van der Mee, C. B. Minkenberg, E. Mendes, J. H. van Esch and R. Eelkema, *Nat. Chem.*, 2013, **5**, 433–437.
- V. Saez Talens, P. Englebienne, T. T. Trinh, W. E. M. Noteborn, I. K. Voets and R. E. Kieltyka, *Angew. Chem. Int. Ed.*, 2015, **54**, 10502–10506.
- Y. Yamamoto, T. Fukushima, Y. Suna, N. Ishii, A. Saeki, S. Seki, S. Tagawa, M. Taniguchi, T. Kawai and T. Aida, *Science*, 2006, **314**, 1761–1764.
- M. Kumar, P. Brocorens, C. Tonnelé, D. Beljonne, M. Surin and S. J. George, *Nat. Commun.*, 2014, **5**, 5793.
- 23 H. Su, J. M. Koo and H. Cui, *J. Control. Release*, 2015, **219**, 383–395.
- Y. Gao, Y. Kuang, Z. F. Guo, Z. Guo, I. J. Krauss and B. Xu, J. Am. Chem. Soc., 2009, 131, 13576–13577.
- 25 M. J. Webber, J. Tongers, M. A. Renault, J. G. Roncalli, D. W. Losordo and S. I. Stupp, *Acta Biomater.*, 2015, **23**, S42–S51.
- 26 T. Aida, E. W. Meijer and S. I. Stupp, *Science*, 2012, **335**, 813–7.
- J. P. Hill, W. Jin, A. Kosaka, T. Fukushima, H. Ichihara, T. Shimomura, K. Ito, T. Hashizume, N. Ishii and T. Aida, *Science*, 2004, **304**, 1481–3.
- A. Pal, M. Malakoutikhah, G. Leonetti, M. Tezcan, M. Colomb-Delsuc, V. D. Nguyen, J. van der Gucht and S. Otto, *Angew. Chem. Int. Ed.*, 2015, **54**, 7852–7856.
- L. Albertazzi, D. van der Zwaag, C. M. A. Leenders, R. Fitzner, R. W. van der Hofstad and E. W. Meijer, *Science*, 2014, **344**, 491–495.
- L. Albertazzi, F. J. Martinez-Veracoechea, C. M. a Leenders, I. K. Voets, D. Frenkel and E. W. Meijer, *Proc. Natl. Acad. Sci. U. S. A.*, 2013, **110**, 12203–8.
- 31 Y. Vyborna, M. Vybornyi, A. V Rudnev and R. Häner, *Angew. Chem. Int. Ed.*, 2015, **54**, 7934–7938.
- 32 Y. Vyborna, M. Vybornyi and R. Haner, *Chem. Commun.*, 2017, **53**, 5179–5181.
- 33 S. S. Lee, T. Fyrner, F. Chen, Z. Álvarez, E. Sleep, D. S. Chun, J. A. Weiner, R. W. Cook, R. D. Freshman, M. S. Schallmo, K. M. Katchko, A. D. Schneider, J. T. Smith, C. Yun, G. Singh, S. Z. Hashmi, M. T. McClendon, Z. Yu, S. R. Stock, W. K. Hsu, E. L. Hsu and S. I. Stupp, *Nat. Nanotechnol.*, DOI:10.1038/nnano.2017.109.
- R. E. Kieltyka, M. M. C. Bastings, G. C. van Almen, P. Besenius, E. W. L. Kemps and

- P. Y. W. Dankers, Chem. Commun., 2012, 48, 1452-4.
- 35 R. Lin, A. G. Cheetham, P. Zhang, Y. Lin and H. Cui, *Chem. Commun.*, 2013, **49**, 4968–70.
- 36 L. L. Lock, M. LaComb, K. Schwarz, A. G. Cheetham, Y. a Lin, P. C. Zhang and H. G. Cui, Faraday Discuss., 2013, 166, 285–301.
- 37 K. Y. Lee and D. J. Mooney, *Chem. Rev.*, 2001, **101**, 1869–1880.
- S. J. Buwalda, K. W. M. Boere, P. J. Dijkstra, J. Feijen, T. Vermonden and W. E. Hennink, *J. Control. Release*, 2014, **190**, 254–273.
- S. J. Buwalda, T. Vermonden and W. E. Hennink, Biomacromolecules, 2017, 18, 316-330.
- N. A. Peppas, P. Bures, W. Leobandung and H. Ichikawa, *Eur. J. Pharm. Biopharm.*, 2000, 50, 27–46.
- 41 E. Bakaic, N. M. B. Smeets and T. Hoare, RSC Adv., 2015, **5**, 35469–35486.
- 42 T. R. Hoare and D. S. Kohane, *Polymer (Guildf).*, 2008, **49**, 1993–2007.
- 43 N. M. Sangeetha and U. Maitra, *Chem. Soc. Rev.*, 2005, **34**, 821–836.
- 44 X. Du, J. Zhou, J. Shi and B. Xu, *Chem. Rev.*, 2015, **115**, 13165–13307.
- 45 E. A. Appel, J. del Barrio, X. J. Loh and O. A. Scherman, *Chem. Soc. Rev.*, 2012, **41**, 6195–214.
- D. B. Amabilino, D. K. Smith and J. W. Steed, Chem. Soc. Rev., 2017, 46, 2404-2420
- 47 D. K. Smith, *Chem. Commun.*, 2006, **1**, 34–44.
- 48 K. Skilling, B. Kellam, M. Ashford, T. D. Bradshaw and M. Marlow, *Soft Matter*, 2016, **12**, 8950–8957.
- 49 M.-O. M. Piepenbrock, G. O. Lloyd, N. Clarke and J. W. Steed, *Chem. Rev.*, 2009, 110, 1960–2004.
- 50 O. Gronwald and S. Shinkai, *Chemistry*, 2001, **7**, 4328–4334.
- L. Chen, J. Raeburn, S. Sutton, D. G. Spiller, J. Williams, J. S. Sharp, P. C. Griffiths, R. K. Heenan, S. M. King, A. Paul, S. Furzeland, D. Atkins and D. J. Adams, *Soft Matter*, 2011, **7**, 9721.
- 52 J. W. Steed, Chem. Commun., 2011, 47, 1379–1383.

- 53 L. E. Buerkle and S. J. Rowan, *Chem. Soc. Rev.*, 2012, **41**, 6089–102.
- 54 X. Yang, G. Zhang and D. Zhang, J. Mater. Chem., 2012, 22, 38.
- 55 M. D. Segarra-Maset, V. J. Nebot, J. F. Miravet and B. Escuder, *Chem. Soc. Rev.*, 2013, **42**, 7086–98.
- 56 T. Muraoka, C. Y. Koh, H. Cui and S. I. Stupp, *Angew. Chem. Int. Ed.*, 2009, **48**, 5946–5949.
- 57 Z. Huang, H. Lee, E. Lee, S.-K. Kang, J.-M. Nam and M. Lee, *Nat. Commun.*, 2011, **2**, 459.
- D. J. Adams, L. M. Mullen, M. Berta, L. Chen and W. J. Frith, Soft Matter, 2010, 6, 1971–1980.
- K. J. C. van Bommel, C. van der Pol, I. Muizebelt, A. Friggeri, A. Heeres, A. Meetsma, B. L. Feringa and J. van Esch, *Angew. Chem. Int. Ed. Engl.*, 2004, **43**, 1663–1667.
- 60 D. B. Rasale and A. K. Das, *Int. J. Mol. Sci.*, 2015, **16**, 10797–10820.
- 61 Y. Gao, Z. Yang, Y. Kuang, M. L. Ma, J. Li, F. Zhao and B. Xu, *Biopolymers*, 2010, **94**, 19–31.
- 62 M. E. Hahn and N. C. Gianneschi, *Chem. Commun.*, 2011, **47**, 11814.
- A. R. Hirst, S. Roy, M. Arora, A. K. Das, N. Hodson, P. Murray, S. Marshall, N. Javid, J. Sefcik, J. Boekhoven, J. H. van Esch, S. Santabarbara, N. T. Hunt and R. V Ulijn, *Nat. Chem.*, 2010, **2**, 1089–1094.
- Z. Yang, H. Gu, D. Fu, P. Gao, J. K. Lam and B. Xu, Adv. Mater., 2004, 16, 1440– 1444.
- J. Raeburn, A. Zamith Cardoso and D. J. Adams, *Chem. Soc. Rev.*, 2013, **42**, 5143–56.
- 66 J. Raeburn and D. J. Adams, *Chem. Commun.*, 2015, **51**, 5170–5180.
- 67 X. Y. Liu and P. D. Sawant, *Adv. Mater.*, 2002, **14**, 421–426.
- 68 X. Y. Liu and P. D. Sawant, *Appl. Phys. Lett.*, 2001, **79**, 3518–3520.
- 69 W. E. M. Noteborn, D. N. H. Zwagerman, V. S. Talens, C. Maity, L. van der Mee, J. M. Poolman, S. Mytnyk, J. H. van Esch, A. Kros, R. Eelkema and R. E. Kieltyka, Adv. Mater., 2017, 29, 2.
- A. E. Way, A. B. Korpusik, T. B. Dorsey, L. E. Buerkle, H. a. Von Recum and S. J. Rowan, *Macromolecules*, 2014, **47**, 1810–1818.

- 71 X. Zhang, X. Chu, L. Wang, H. Wang, G. Liang, J. Zhang, J. Long and Z. Yang, *Angew. Chem. Int. Ed. Engl.*, 2012, **51**, 4388–92.
- R. E. Kieltyka, a. C. H. Pape, L. Albertazzi, Y. Nakano, M. M. C. Bastings, I. K. Voets, P. Y. W. Dankers and E. W. Meijer, *J. Am. Chem. Soc.*, 2013, **135**, 11159–11164.
- 73 Y. Li, Y. Ding, M. Qin, Y. Cao and W. Wang, *Chem. Commun.*, 2013, **49**, 8653–5.
- M. M. E. Koenigs, A. Pal, H. Mortazavi, G. M. Pawar, C. Storm and R. P. Sijbesma, *Macromolecules*, 2014, **47**, 2712–2717.
- 75 M. A. Khalily, M. Goktas and M. O. Guler, *Org. Biomol. Chem.*, 2015, **13**, 1983–1987.
- V. D. Nguyen, A. Pal, F. Snijkers, M. Colomb-Delsuc, G. Leonetti, S. Otto and J. van der Gucht, *Soft Matter*, 2016, **12**, 432–440.
- 77 J. Maitra and V. K. Shukla, *Am. J. Polym. Sci.*, 2014, **4**, 25–31.
- 78 N. Huebsch and D. J. Mooney, *Nature*, 2009, **462**, 426–432.
- 79 S. Sur, C. J. Newcomb, M. J. Webber and S. I. Stupp, *Biomaterials*, 2013, **34**, 4749–57.
- 80 P. Y. W. Dankers, M. C. Harmsen, L. A. Brouwer, M. J. A. van Luyn and E. W. Meijer, *Nat. Mater.*, 2005, **4**, 568–74.
- H. Jung, J. S. Park, J. Yeom, N. Selvapalam, K. M. Park, K. Oh, J. A. Yang, K. H. Park, S. K. Hahn and K. Kim, *Biomacromolecules*, 2014, **15**, 707–714.
- 82 J. A. Sáez, B. Escuder and J. F. Miravet, *Tetrahedron*, 2010, **66**, 2614–2618.
- M. Rodrigues, A. C. Calpena, D. B. Amabilino, M. L. Garduño-Ramírez and L. Pérez-García, *J. Mater. Chem. B*, 2014, **2**, 5419.
- 84 G. Liang, Z. Yang, R. Zhang, L. Li, Y. Fan, Y. Kuang, Y. Gao, T. Wang, W. W. Lu and B. Xu, *Langmuir*, 2009, 25, 8419–8422.
- 85 K. J. C. van Bommel, M. C. a Stuart, B. L. Feringa and J. van Esch, *Org. Biomol. Chem.*, 2005, **3**, 2917–2920.
- 6 G. A. Hudalla, T. Sun, J. Z. Gasiorowski, H. Han, Y. F. Tian, A. S. Chong and J. H. Collier, *Nat. Mater.*, 2014, **13**, 829–836.
- 87 E. V. Alakpa, V. Jayawarna, A. Lampel, K. V. Burgess, C. C. West, S. C. J. Bakker, S. Roy, N. Javid, S. Fleming, D. A. Lamprou, J. Yang, A. Miller, A. J. Urquhart, P. W. J. M. Frederix, N. T. Hunt, B. Péault, R. V. Ulijn and M. J. Dalby, *Chem*, 2016, **1**, 512.
- 88 N. C. Seeman, *Nature*, 2003, **421**, 427–31.

- 89 Y. H. Roh, R. C. H. Ruiz, S. Peng, J. B. Lee and D. Luo, *Chem. Soc. Rev.*, 2011, **40**, 5730.
- 90 Y. Sannohe, M. Endo, Y. Katsuda, K. Hidaka and H. Sugiyama, *J. Am. Chem. Soc.*, 2010, **132**, 16311–16313.
- 91 Y. Dong, Z. Yang and D. Liu, Acc. Chem. Res., 2014, 47, 1853–1869
- 92 A. T. Phan and J.-L. Mergny, *Nucleic Acids Res.*, 2002, **30**, 4618–25.
- 93 F. A. Aldaye, A. L. Palmer and H. F. Sleiman, *Science*, 2008, **321**, 1795–1799.
- 94 R. Chhabra, J. Sharma, Y. Liu, S. Rinker and H. Yan, *Adv. Drug Deliv. Rev.*, 2010, 62, 617–625.
- 95 N. C. Seeman, Nano Lett., 2010, **10**, 1971–8.
- 96 D. Y. Zhang and G. Seelig, *Nat. Chem.*, 2011, **3**, 103–13.
- 97 N. C. Seeman, J. Theor. Biol., 1982, **99**, 237–247.
- D. Yang, M. J. Campolongo, T. N. Nhi Tran, R. C. H. Ruiz, J. S. Kahn and D. Luo, *Wiley Interdiscip. Rev. Nanomedicine Nanobiotechnology*, 2010, 2, 648–669.
- 99 N. C. Seeman, Annu. Rev. Biochem., 2010, **79**, 65–87.
- 100 A. V Pinheiro, D. Han, W. M. Shih and H. Yan, *Nat. Nanotechnol.*, 2011, **6**, 763–72.
- 101 R. D. Barish, R. Schulman, P. W. K. Rothemund and E. Winfree, *Proc. Natl. Acad. Sci. U. S. A.*, 2009, **106**, 6054–6059.
- 102 P. W. K. Rothemund, *Nature*, 2006, **440**, 297–302.
- E. S. Andersen, M. Dong, M. M. Nielsen, K. Jahn, R. Subramani, W. Mamdouh, M.
   M. Golas, B. Sander, H. Stark, C. L. P. Oliveira, J. S. Pedersen, V. Birkedal, F.
   Besenbacher, K. V Gothelf and J. Kjems, *Nature*, 2009, 459, 73–6.
- N. V Voigt, T. Tørring, A. Rotaru, M. F. Jacobsen, J. B. Ravnsbæk, R. Subramani, W. Mamdouh, J. Kjems, A. Mokhir, F. Besenbacher and K. V. Gothelf, *Nat. Nanotechnol.*, 2010, **5**, 200–203.
- 105 S. M. Douglas, I. Bachelet and G. M. Church, *Science*, 2012, **335**, 831–834.
- 106 F. a. Aldaye and H. F. Sleiman, *Pure Appl. Chem.*, 2009, **81**, 2157–2181.
- 107 K. Ding, F. E. Alemdaroglu, M. Börsch, R. Berger and A. Herrmann, *Angew. Chem. Int. Ed. Engl.*, 2007, **46**, 1172–5.
- 108 F. A. Aldaye and H. F. Sleiman, *J. Am. Chem. Soc.*, 2007, **129**, 13376–13377.

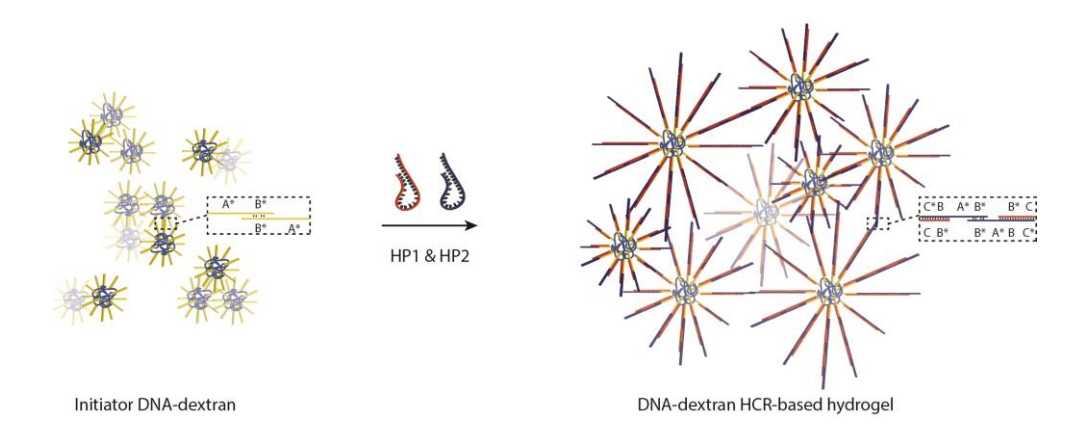
- 109 F. Aldaye, H. Yang, M. Slim and H. Sleiman, *Polymer (Guildf).*, 2007, **48**, 573–574.
- 110 P. K. Lo, P. Karam, F. a Aldaye, C. K. McLaughlin, G. D. Hamblin, G. Cosa and H. F. Sleiman, *Nat. Chem.*, 2010, **2**, 319–328.
- 111 D. Y. Zhang and E. Winfree, J. Am. Chem. Soc., 2009, **131**, 17303–14.
- N. Srinivas, T. E. Ouldridge, P. Šulc, J. M. Schaeffer, B. Yurke, A. A. Louis, J. P. K. Doye and E. Winfree, *Nucleic Acids Res.*, 2013, **41**, 10641–10658.
- B. Yurke, A. J. Turberfield, A. P. Mills, F. C. Simmel and J. L. Neumann, *Nature*, 2000, **406**, 605–608.
- J. Shin and N. A. Pierce, J. Am. Chem. Soc., 2004, **126**, 10834–10835.
- 115 G. Seelig, D. Soloveichik, D. Y. Zhang and E. Winfree, *Science*, 2006, **314**, 1585–1588.
- D. Han, Z. Zhu, C. Wu, L. Peng, L. Zhou, B. Gulbakan, G. Zhu, K. R. Williams and W. Tan, *J. Am. Chem. Soc.*, 2012, **134**, 20797–804.
- 117 D. Y. Zhang and E. Winfree, J. Am. Chem. Soc., 2008, **130**, 13921–13926.
- D. Y. Zhang, A. J. Turberfield, B. Yurke and E. Winfree, Science, 2007, 318, 1121–1125.
- J. N. Zadeh, C. D. Steenberg, J. S. Bois, B. R. Wolfe, M. B. Pierce, A. R. Khan, R. M. Dirks and N. A. Pierce, J. Comput. Chem., 2011, 32, 170–173.
- 120 M. R. Lakin, S. Youssef, F. Polo, S. Emmott and A. Phillips, *Bioinformatics*, 2011, **27**, 3211–3213.
- 121 R. M. Dirks and N. A. Pierce, *Proc. Natl. Acad. Sci. U. S. A.*, 2004, **101**, 15275–15278.
- 122 Y. S. Ang and L. L. Yung, *Chem. Commun.*, 2016, **52**, 4219–4222.
- 123 F. Xuan and I. M. Hsing, J. Am. Chem. Soc., 2014, **136**, 9810–9813.
- 124 S. Bi, S. Yue and S. Zhang, *Chem. Soc. Rev.*, 2017, **46**, 4281–4298.
- 125 J. S. Kahn, A. Trifonov, A. Cecconello, W. Guo, C. Fan and I. Willner, *Nano Lett.*, 2015, **15**, 7773–7778.
- 126 Q. Wang, X. Yang, X. Yang, K. Wang, H. Zhang and P. Liu, *Analyst*, 2015, **1**, 7657–7662.
- M. Rana, M. Balcioglu, M. Kovach, M. S. Hizir, N. M. Robertson, I. Khan and M. V Yigit, *Chem. Commun.*, 2016, **52**, 3524–3527.

- 128 G. Zhu, S. Zhang, E. Song, J. Zheng, R. Hu, X. Fang and W. Tan, *Angew. Chem. Int. Ed. Engl.*, 2013, **52**, 5490–6.
- 129 G. Zhou, M. Lin, P. Song, X. Chen, J. Chao, L. Wang, Q. Huang, W. Huang, C. Fan and X. Zuo, *Anal. Chem.*, 2014, **86**, 7843–7848.
- 130 H. M. T. Choi, V. a. Beck and N. a. Pierce, ACS Nano, 2014, 8, 4284–4294.
- 131 Y. M. Wang, Z. Wu, S. J. Liu and X. Chu, *Anal. Chem.*, 2015, **87**, 6470–6474.
- J. Wang, J. Chao, H. Liu, S. Su, L. Wang, W. Huang, I. Willner and C. Fan, *Angew. Chem. Int. Ed.*, 2017, 1–6.
- 133 X. Xiong, C. Wu, C. Zhou, G. Zhu, Z. Chen and W. Tan, *Macromol. Rapid Commun.*, 2013, **34**, 1271–1283.
- 134 F. E. Alemdaroglu and A. Herrmann, *Org. Biomol. Chem.*, 2007, **5**, 1311–20.
- F. E. Alemdaroglu, N. C. Alemdaroglu, P. Langguth and a. Herrmann, *Adv. Mater.*, 2008, **20**, 899–902.
- T. R. Wilks, J. Bath, J. W. de Vries, J. E. Raymond, A. Herrmann, A. J. Turberfield and R. K. O'Reilly, *ACS Nano*, 2013, **7**, 8561–72.
- 137 C. Feng, Y. Li, D. Yang, J. Hu, X. Zhang and X. Huang, *Chem. Soc. Rev.*, 2011, **40**, 1282–95.
- 138 Y. Murakami and M. Maeda, *Biomacromolecules*, 2005, **6**, 2927–9.
- 139 P. Chen, C. Li, D. Liu and Z. Li, *Macromolecules*, 2012, **45**, 9579–9584.
- 140 Y. Shao, H. Jia, T. Cao and D. Liu, Acc. Chem. Res., 2017, **50**, 659–668.
- 141 J. S. Kahn, Y. Hu and I. Willner, Acc. Chem. Res., 2017, **50**, 680–690.
- Z. Zhu, C. Wu, H. Liu, Y. Zou, X. Zhang, H. Kang, C. J. Yang and W. Tan, *Angew. Chem. Int. Ed. Engl.*, 2010, 49, 1052–6.
- C. Li, A. Faulkner-Jones, A. R. Dun, J. Jin, P. Chen, Y. Xing, Z. Yang, Z. Li, W. Shu, D. Liu and R. R. Duncan, *Angew. Chem. Int. Ed.*, 2015, 54, 3957–3961.
- 144 W.-C. Liao, S. Lilienthal, J. Kahn, M. Riutin, Y. S. Sohn, R. Nechushtai and I. Willner, *Chem. Sci.*, 2017, **8**, 3362–3373.
- 145 Y. Vyborna, M. Vybornyi and R. Haner, *Chem. Commun.*, 2017, 1–7.
- 146 P. J. S. King, A. Saiani, E. V. Bichenkova and A. F. Miller, *Chem. Commun.*, 2016, **52**, 6697–6700.

F. Wu, J. Jin, L. Wang, P. Sun, H. Yuan, Z. Yang, G. Chen, Q. H. Fan and D. Liu, *ACS Appl. Mater. Interfaces*, 2015, **7**, 7351–7356.

# **CHAPTER 2**

# Grafting from a hybrid DNA-dextran graft copolymer by the hybridization chain reaction



This chapter was prepared as an Original Research paper: W. E. M. Noteborn, J. A. J. Wondergem, A. Iurchenko, F. Chariyev-Prinz, D. Donato, I. K. Voets, D. Heinrich, R. E. Kieltyka

#### 2.1 Abstract

Nucleic acid-polymer conjugates are an attractive class of materials that are endowed with tuneable and responsive character. Herein, we exploit the dynamic character of nucleic acids by the hybridization chain reaction to prepare hybrid DNA grafted covalent polymers. The cascade of sequential strand displacement reactions results in growth of the DNA grafts on a dextran polymer backbone, leading to eventual hydrogel formation with increasing concentration. Because of the growth of the DNA grafts is in a dynamic fashion, applications are envisaged where the viscoelastic properties of the material can be exploited for drug delivery or detection using viscosity as readout.

Keywords: hybridization chain reaction, graft copolymer, hydrogel, DNA, dextran.

#### 2.2 Introduction

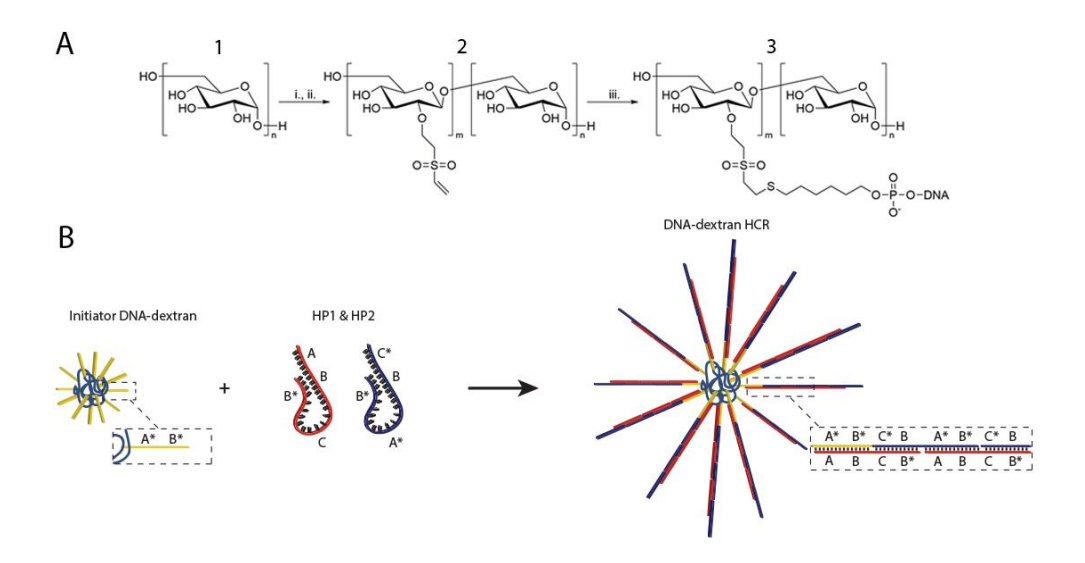
Nucleic acids are powerful tools for the construction of materials because of their sequence programmability and predictable dimensions.<sup>1–3</sup> Consequently, DNA nanotechnology has exploited its use as a structural unit for the bottom-up construction of numerous discrete two and three-dimensional architectures.<sup>4–7</sup> More recent developments within the field have centered on benefitting from the dynamic properties of DNA through the use of strand displacement reactions to provide reconfigurable and autonomous functions.<sup>8–10</sup> Strand displacement is a reaction that is fueled by the energy released in the hybridization of partial or fully complementary DNA strands through branch migration of a pre-hybridized DNA strand.<sup>11</sup> Catalyzed hairpin assembly (CHA),<sup>12</sup> entropy-driven catalysis (EDC)<sup>13</sup> and the hybridization chain reaction (HCR)<sup>14,15</sup> rely on strand displacement cascades to create multi-layered adaptable and reconfigurable DNA-based circuits,<sup>16</sup> autonomous DNA walkers<sup>17,18</sup> and amplifiers.<sup>19,20</sup> These techniques can be useful for a range of applications from smart therapeutics to diagnostics<sup>9,21,22</sup>, using gel electrophoresis, fluorescence and electrical detection as readouts.

Beyond DNA nanotechnology, the inherent structural and dynamic features of nucleic acids can be an invaluable means to tailor the morphology and responsiveness of polymer materials in a programmable and tuneable fashion. <sup>23–27</sup> Often DNA is introduced as the water-soluble domain of a block copolymer to provide responsive micellar structures and hydrogels. <sup>28–33</sup> Although numerous reports have demonstrated the use of a block copolymer approach, graft copolymer architectures can provide additional handles to modify the polymer architecture through variation of grafting densities, lengths and the choice of the backbone itself. <sup>34,35</sup> The consequence of these structural modifications can result in a broader range of morphologies, such as worms, spheres and cylinders. <sup>36,37</sup>

Classically, most synthetic strategies to prepare grafted copolymers involve covalent grafting from, to, and through the polymer backbone to permanently fix the side chains<sup>37</sup>. On the other hand, the more recent exploration into grafting strategies based on non-covalent interactions has opened the door to a whole new range of graft copolymer materials that can be tuneable, responsive, and dynamic.<sup>36</sup> Non-covalent molecular recognition motifs have been used to append organic molecules and biopolymers using a non-covalent "grafting onto" approach to enable structural transitions.<sup>38–41</sup> Therefore, combining graft copolymers with dynamic DNA nanotechnology can yield a new class of grafted polymer hybrids that respond

through highly specific molecular interactions in a programmable and dynamic fashion with important consequences over several length scales.

Herein, we report the use of dynamic DNA nanotechnology on a hybrid dextran-DNA graft copolymer employing the hybridization chain reaction. These particles enable the autonomous growth of nucleic acid polymers off a covalent polymer backbone when supplied with two metastable hairpins (HP1 and HP2) that undergo an energetically favorable cascade of kinetically controlled strand displacement reactions (Scheme 2.1). Of important note, these hairpins can coexist stably in solution and are triggered only by the presence of the initiator DNAs. We examine the self-assembly process of the initiator DNA-dextran graft copolymer and the DNA hairpins by several molecular techniques, as well as their potential to form hydrogel materials as an output.



Scheme 2.1. (A) Initiator DNA-dextran graft copolymer synthesis: dextran (1) (Mn: 10, kDa,  $n_{av}$ : 62) was reacted with divinyl sulfone to form dextran-vinyl sulfone (dextran-VS,  $m_{av}$  = 19) (2). Chemoselective ligation of a thiol-modified HCR initiator single stranded DNA by a Michael addition reaction on dextran-VS (3). Reaction conditions: (i) 0.1 M NaOH, divinyl sulfone, (ii) 5 M HCl, (iii) 0.1 M PBS pH 8.5, using a 1 to 3 ratio of 5'-thiol-modified HCR initiator DNA with respect to the present vinyl sulfone groups. (B) Schematic representation of HCR driven non-covalent grafting from an initiator DNA-dextran graft copolymer by HP1 and HP2.

#### 2.3 Results and discussion

To synthesize the grafted dextran copolymer with the initiator DNAs for HCR, vinyl sulfone groups were first introduced on dextran for subsequent bioconjugation with DNA. The reaction of dextran ( $M_n = 10 \text{ kDa}$ ) with divinyl sulfone (using 1.5 molar equivalents with respect to all hydroxyl groups) was performed under basic conditions (0.1M NaOH).<sup>42</sup> The sample was reacted for 0.5 minutes with thorough vortexing and immediate quenching by the addition of 5 M HCl and dialysis purification (75 % yield). By controlling the molar equivalents and reaction time, a reproducible degree of substitution of 31 % (19 hydroxyl groups functionalized per chain) was obtained as determined from  $^1$ H-NMR measurements (see supporting information). Additionally, size exclusion chromatography (SEC) showed no change in dispersity ( $\Phi$  ~ 1.05) or size of the vinyl sulfone substituted polymers.

In a subsequent step, dithiothreitol(DTT)-mediated deprotection of the 5'disulfide protected initiator DNA strand was pursued to enable its conjugation to the dextran polymer by vinyl sulfone thiol-Michael addition. Excess DTT was removed by an ethyl acetate extraction to prevent a competitive reaction with the vinyl sulfone groups on dextran and the deprotected 5'-thiol DNA. The conjugation reaction was carried out immediately by mixing the freshly reduced 5'-thiol DNA with dextran-vinyl sulfone in PBS at pH 8.5 overnight under inert conditions. The formation of the DNAdextran graft copolymer conjugate was assessed by agarose gel electrophoresis (Figure 2.1A). In comparison to the unreacted DNA (lane 1, bottom) observed as both free thiol-DNA (bottom diffuse DNA band) and dithiol species in which two thiol-DNAs reacted with each other (middle sharp DNA band), a large, slowly migrating and smeared band was observed indicative of the formation of the initiator DNA-dextran conjugate (lane 1, top). Analysis of the agarose gels by densitometry revealed that 74% of the added 5'-thiol DNAs were conjugated to dextran. Most likely, complete substitution of the vinyl sulfone groups on the polymer backbone is hindered by the high electrostatic charge and steric constraints of the DNA oligonucleotides. Gel electroelution was used to separate and remove the unreacted initiator DNA from the initiator DNA-dextran graft copolymer followed by dialysis to provide a final yield of 70 %. After purification, a 2 % agarose gel electrophoresis was performed, showing complete removal of the unreacted 5'-thiol DNA from the DNA-dextran graft copolymer (Figure 2.1A, Lane 2).

The capacity of the DNA initiator-dextran graft copolymer to trigger HCR from the polymer backbone was initially evaluated by gel electrophoresis and fluorescence

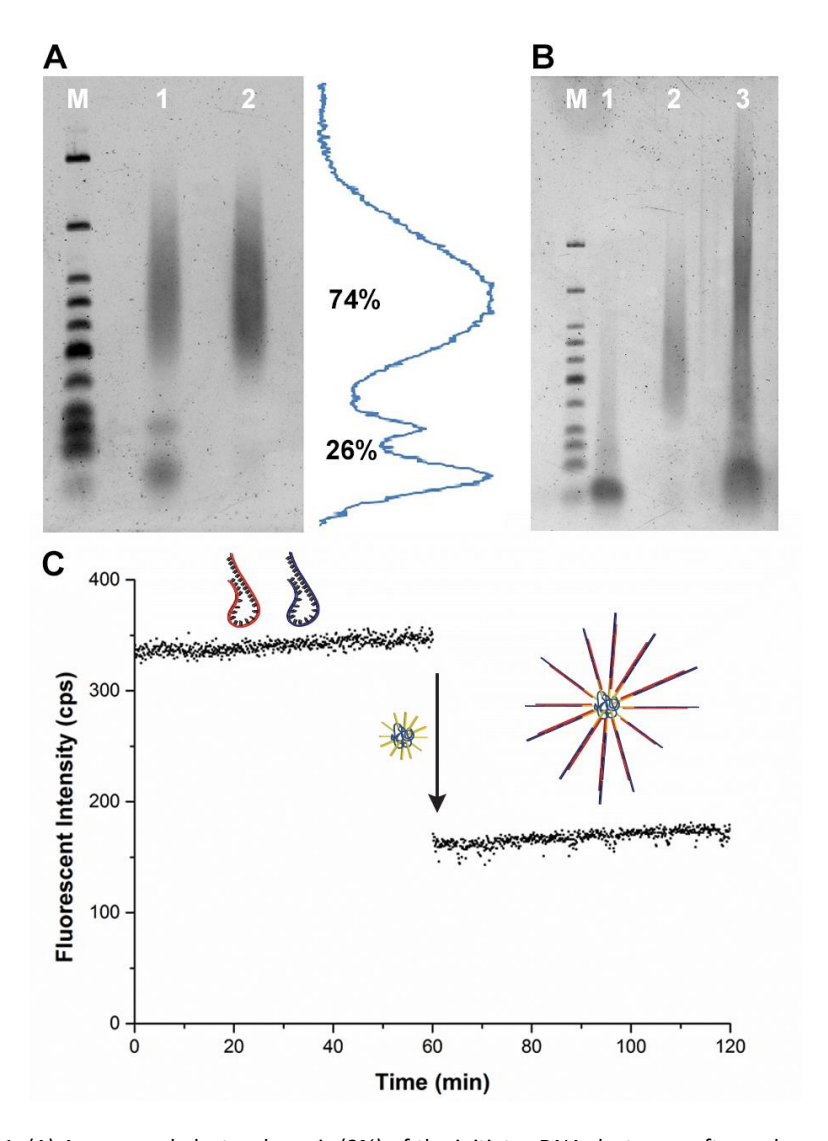


Figure 2.1. (A) Agarose gel electrophoresis (2%) of the initiator DNA-dextran graft copolymer before (Lane 1) and after purification (Lane 2). Lane M contains a low molecular weight DNA marker ranging from 25 to 766 bp. (B) Agarose gel electrophoresis (2%) showing the products of HCR after addition of the initiator DNA-dextran graft copolymer. Combination of HP1 and HP2 (Lane 1), initiator DNA-dextran graft copolymer (Lane 2), HCR of HP1 and HP2 on the initiator DNA-dextran graft copolymer (Lane 3). Lane M contains a low molecular weight DNA marker ranging from 25 to 766 bp. (C) Fluorescence time course measurement of HP1-2AP HP1 ( $\lambda_{\rm ex}$ = 303 nm,  $\lambda_{\rm em}$ = 365 nm) with HP2 and the addition at 60 minutes of the DNA-dextran initiator, triggering the hybridization chain reaction and fluorescence quenching.

spectroscopy on dilute solution phase samples to provide insight into the self-assembly process at the molecular scale. Pre-hybridized DNA hairpins (HP1, HP2) thermally annealed in 5X SSC buffer were mixed in equimolar quantities and added to the DNA initiator-dextran graft copolymer in the same buffer to start the reaction. Agarose gel electrophoresis (2%) one hour after the start of the reaction showed that addition of the folded HP1 and HP2 to the DNA-dextran graft copolymer resulted in increased retention of the polymer initiator (Figure 2.1B, Lane 3). This result would suggest growth of the DNA grafts by HCR through opening of the metastable DNA hairpins. In contrast, lower gel retention of the negative controls including the initiator DNA-dextran graft copolymer (Figure 2.1B, Lane 2) and the metastable HCR hairpins only (Figure 2.1B, Lane 1) was observed, underpinning the occurrence of the HCR reaction on the dextran polymer.

Nucleic acid fluorescence quenching experiments involving a 2-aminopurine functionalized hairpin 1 (HP1-2AP) for self-assembly further supported the findings by gel electrophoresis. 2-AP-labelled oligonucleotides are fluorescent in their single stranded form, but become rapidly quenched when hybridized. The decrease in fluorescence intensity can be directly related to hairpin polymerization in the HCR reaction. As a control, stability of the 2-AP hairpin and its polymerization without the copolymer were first examined by monitoring the fluorescence of HP1-2AP itself and when mixed with HP2, respectively. Initially, a stable fluorescence signal was recorded for both samples consistent with folded hairpins of HP1-2AP and HP2 (Figure 2.1C). After one hour, the addition of either the DNA initiator strand on its own or grafted to the dextran copolymer to the HP1-2AP and HP2 solution resulted in rapid quenching of the fluorescence signal of the 2-AP indicative of hairpin or initiator DNA-graft copolymers (Figure 2.1C) opening and polymerization of ssDNA (Figure S2.1). Collectively, these results show that DNA hairpin polymerization occurs by HCR on the DNA initiator-dextran graft copolymer.

Because of our interest in using the HCR reaction to modulate physicochemical properties of polymer materials, we examined the morphology of the DNA-graft copolymers self-assembly at the nanoscale by dynamic light scattering (DLS), small angle X-ray scattering (SAXS) and atomic force microscopy (AFM). Particle size measurements of the various components (HP1, HP2, HP1 and HP2, dextran-VS, initiator DNA-dextran and the HCR reaction mixture) as dilute solutions were examined by DLS. The individual hairpins and their combination displayed an average size of 6 nm and 8 nm, respectively (Figure 2.2A). The initiator DNA-dextran graft copolymer showed an average size on the order of 500 nm. Surprisingly, addition of

HP1 and HP2 to the initiator DNA-dextran graft copolymer resulted in the formation of micron-sized aggregates. The experimentally determined large size of the aggregates, even before addition of HP1 and HP2, suggests that clustering of the initiator DNA-polymer occurs and the resultant HCR products. A similar trend was observed by AFM for the samples prepared at room temperature except with a larger average diameter prior to the start of HCR on the initiator DNA-graft copolymer (Figure 2.2B, left,  $57 \pm 25$  nm), and afterwards (Figure 2.2B, right,  $183 \pm 53$  nm) with a networked structure. SAXS experiments in solution also showed aggregation of the

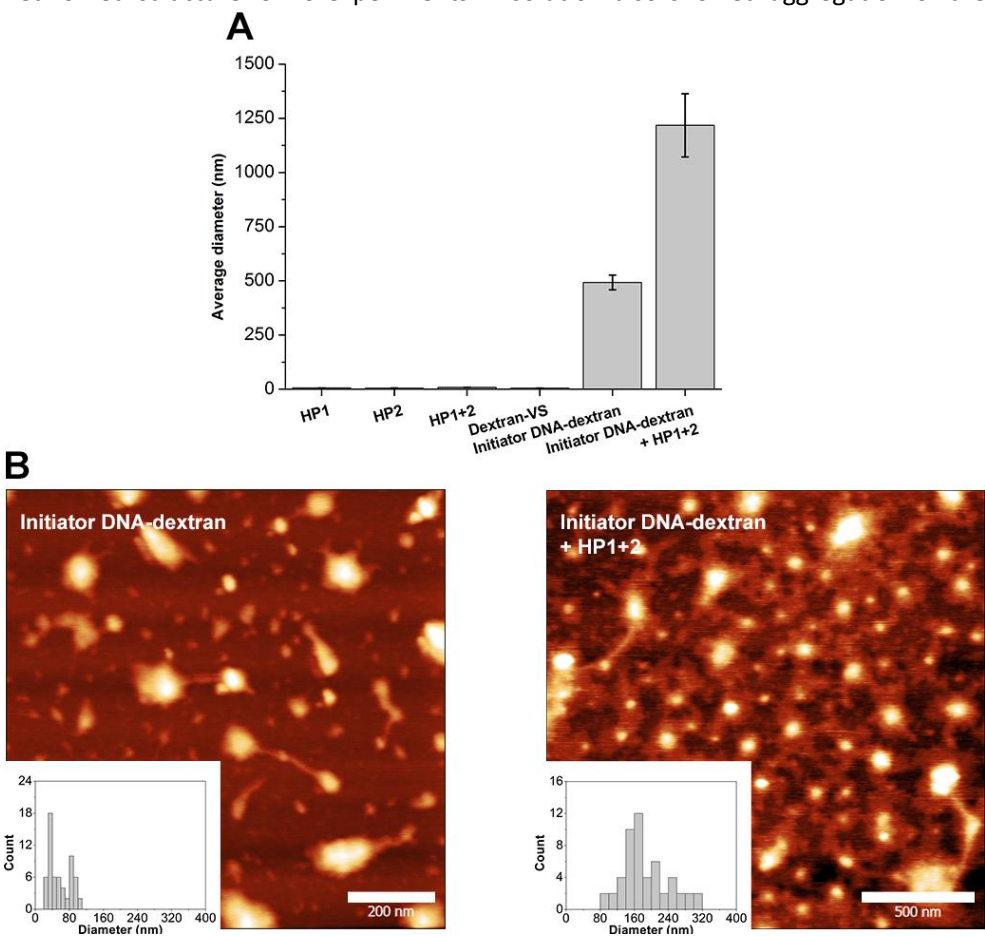


Figure 2.2. (A) Particle size distributions of native HP1, HP2, HP1 and HP2, dextran-VS, initiator DNA-dextran graft copolymer and the initiator DNA-dextran graft copolymer after HCR (left to right) by DLS. (B) Atomic force micrographs (AFM) of drop-casted native samples of initiator DNA-dextran graft copolymers before (above) and after executing HCR with HP1 and HP2 resulting in the formation of HCR DNA-dextran graft copolymers (below). Scale bars are 200 and 500 nm, respectively. Insets: histograms of DNA-dextran particle diameter.

DNA-dextran graft copolymer before and upon addition of both HP1 and HP2 at room temperature (Figure 2.3). Modeling of the HP1 and HP2 SAXS profiles with a form factor for Gaussian chains yielded a radius of gyration ( $R_{\rm g}$ ) of 2.5  $\pm$  0.3 nm for HP1 and 2.3  $\pm$  0.3 nm for HP2. Conversely, aggregates with sizes above the resolution of the instrument ( $\pi/q_{\rm min}$  = 31 nm) were observed for the initiator DNA-dextran graft copolymer before and after addition of both HP1 and HP2. The experimental SAXS profile of the initiator DNA-dextran, HP1 and HP2 mixture is distinct from the theoretical SAXS profile from the sum of the 3-component mixture (Figure 2.3). This difference proves that the hairpins interact with the initiator DNA-dextran aggregates triggering a conformational change when mixed.

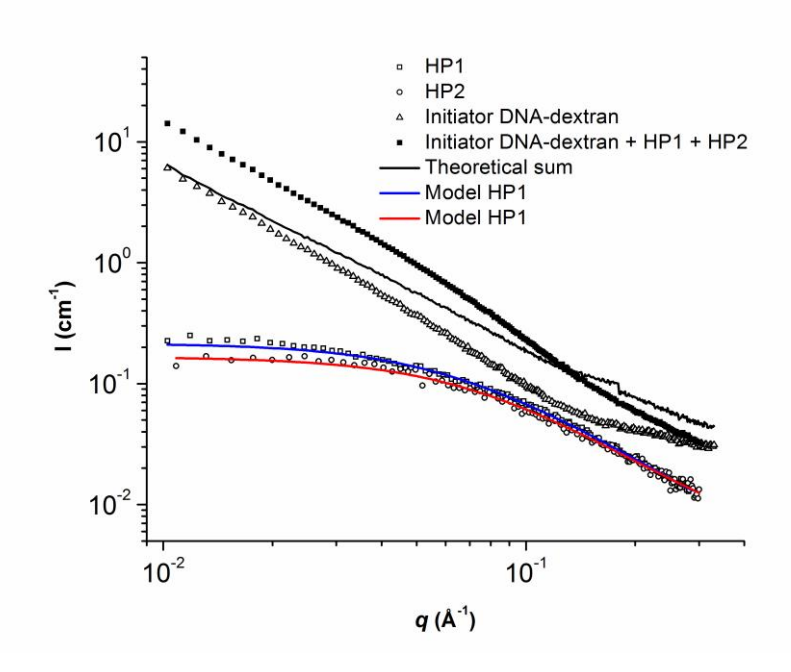


Figure 2.3. SAXS profiles of native HP1 (blue) and HP2 (red) modeled with a form factor for Gaussian chains, the initiator DNA-dextran before (black, open triangles) and after HCR (black, cubes) and a theoretical summated profile of the HCR components.

In an effort to disrupt the pre-aggregated initiator DNA-graft copolymers, the samples were heated to 60 °C before addition of HP1 and HP2 and their particle sizes were measured by DLS (Figure 2.4A). After heat treatment, initiator DNA-graft copolymers before and after subsequent hairpin addition revealed particle population with an average size of 14 nm and 66 nm, respectively, which are on par with theoretically estimated size predictions and points to the likely disruption of the

initiator DNA-graft polymer aggregates. The changes in particle diameter were further supported by AFM imaging on both  $60^{\circ}$ C and room temperature samples drop-casted on mica before and after HCR. Prior to the addition of HP1 and HP2, the  $60^{\circ}$ C sample of the initiator DNA-dextran graft copolymer showed small aggregates highly disperse in diameter (Figure 2.4B, left,  $14 \pm 10$  nm). These spherical aggregates grew in size after addition of HP1 and HP2 with the formation of hairy protrusions (Figure 2.4B, right,  $40 \pm 18$  nm).

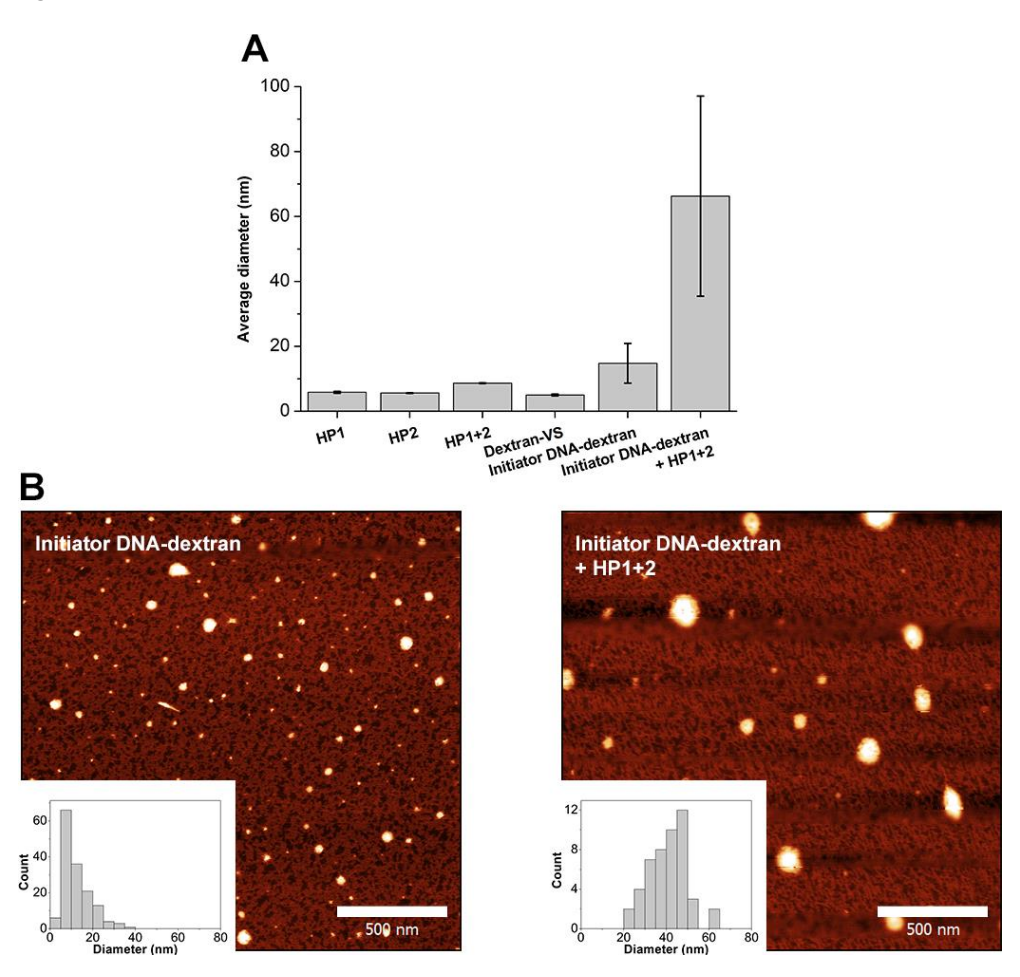
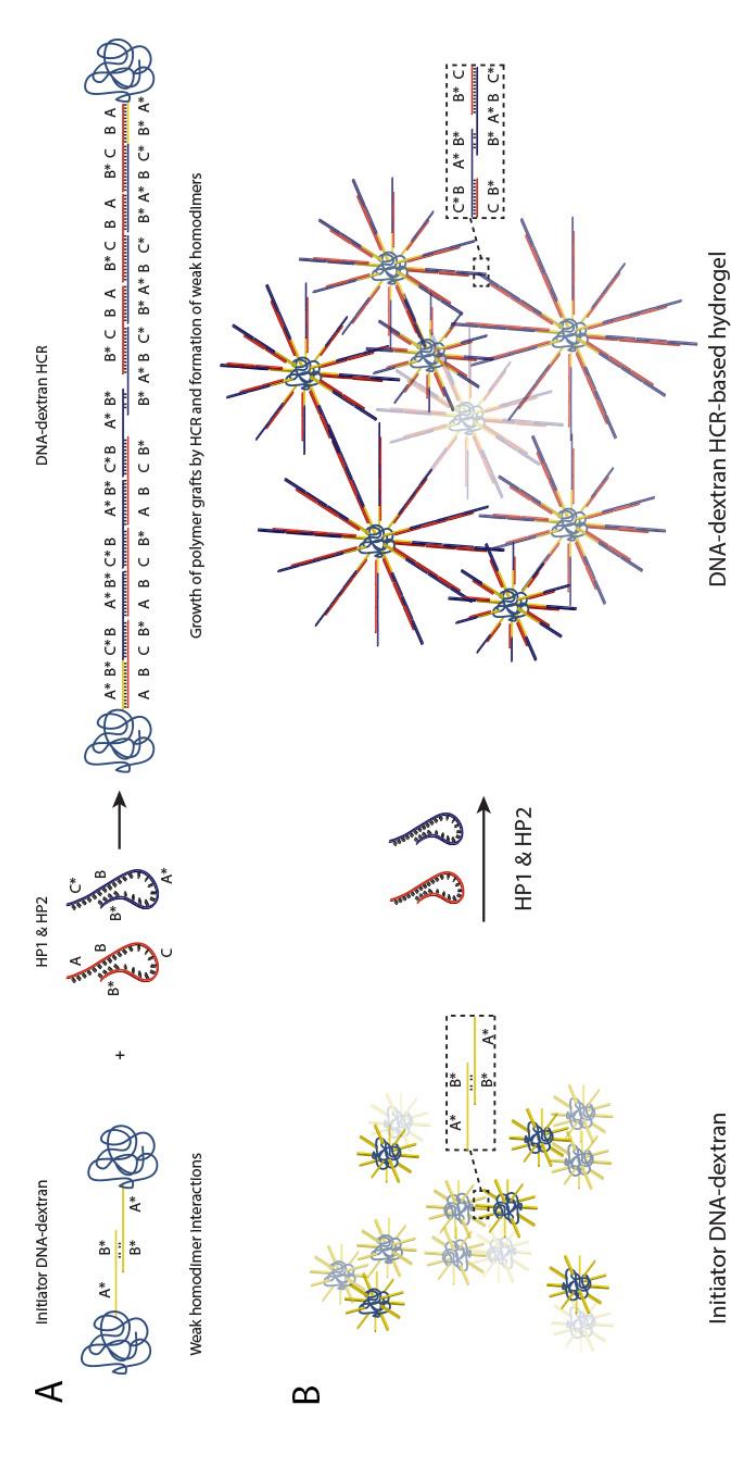


Figure 2.4. (A) Particle size distributions of heat treated HP1, HP2, HP1 and HP2, dextran-VS, initiator DNA-dextran graft copolymer and the initiator DNA-dextran graft copolymer after HCR (left to right) by DLS. (B) Atomic force micrographs (AFM) of drop-casted heat treated samples of initiator DNA-dextran graft copolymers before (above) and after executing HCR with HP1 and HP2 resulting in the formation of HCR DNA-dextran graft copolymers (below). Scale bar is 500 nm. Insets: histograms of DNA-dextran particle diameter.

To rationalize the increased aggregate sizes prior to HCR on the initiator DNA-dextran graft copolymer, in-depth analysis of the DNA sequences by NUPACK<sup>43</sup> was pursued. These investigations revealed weak homodimer interactions between four nucleotides in the initiator DNA strands (B\*), and HP1 and HP2 (B\*) once hybridized with a computed free energy of -11.09 kcal/mol. This value is in contrast to a computed free energy of -40.86 kcal/mol for each formed duplex during the HCR reaction. By careful DNA sequence evaluation, weak homodimer interactions are proposed to occur at the outset before HCR of the initiator DNA-grafted polymer and afterwards (Scheme 2.2). These computational results are in agreement with the large aggregate sizes observed solely for the initiator DNA-graft copolymer by experiment and may contribute to the greater aggregate sizes observed after HCR. However, it is unclear the extent to which each effect contributes to the final large aggregate sizes after polymerization, but it appears that both play a role in the formed products.

Finally, the potential of forming hybrid-DNA polymer materials by performing HCR on a grafted initiator DNA-polymer was probed at high polymer concentrations (1.25 - 5.0 wt%) using particle-tracking microrheology. This technique involves determining the mean squared displacement (MSD) of micrometer fluorescently labeled tracer particles subject to Brownian motion within the material over time. Whereas conventional oscillatory rheology requires large sample volumes, particletracking microrheology requires volumes as low as 10 µL, which is highly advantageous for the screening of physicochemical properties of DNA-based materials. Fluorescently-labeled polystyrene beads 1 µm in diameter were mixed within: a solution of HP1 and HP2 (Figure 2.5A, B, C, black tracks), initiator DNAdextran graft copolymer lacking the HCR hairpins (red tracks) various solutions of initiator DNA-dextran graft-copolymer, to which were added to the initiator DNAdextran copolymer (green tracks). In these experiments, a total polymer concentration of 1.25, 2.5 and 5 wt% of the DNA initiator-dextran copolymer and/or a 3-fold excess of both HP1 and HP2 were examined. For the various conditions, the bead tracks were followed over time to monitor the self-assembly process of the DNA-grafts (green tracks: 0-20 minutes, blue tracks: 20-40 minutes). The combination of the initiator DNA-dextran graft copolymer and both hairpins HP1 and HP2 showed significantly reduced Brownian motion-induced bead displacements over time in comparison to control samples. The strongest reduction of particle motion was



Scheme 2.2. Proposed mechanism of initiator DNA-graft copolymer self-assembly before and after HCR. (A): Initiator DNA-dextran graft copolymer bearing multiple initiator sequences can aggregate through weak homodimer interactions in domain B\*. Addition of HP1 and HP2 starts the energetically favorable HCR reaction on the initiator DNA-dextran graft copolymer results in the growth of the DNA grafts. Exposed single stranded B\* domains on HP1 and HP2 incorporated on the grafted supramolecular polymer can form weak homodimer interactions to form larger aggregated structures. (B) Growth mechanism of DNA grafts by HCR on the initiator DNA-dextran graft copolymer at the nanoscale. By HCR driven grafting from in a non-covalent manner using HP1 and HP2 the initial DNA-initiator graft copolymer aggregates grow in size with weak homodimer interactions facilitating further aggregation and eventual network percolation.

observed for the 5 wt% mixtures, such that axes with smaller increments for x and y displacements were required for better visualization. These particle tracks were converted into MSDs and plotted with respect to time by time-wise data segmentation (Figure 2.6A, B and C, respectively). Control samples containing only HP1 and 2 (black) or initiator DNA-dextran graft copolymer (red) displayed a linear increase in their MSDs over lag time consistent with the power law behavior of Newtonian fluids for all sample concentrations. Addition of HP1 and HP2 to the initiator DNA-dextran copolymer resulted in a decrease in the MSD values with respect to time (green: 0-20 minutes, blue: 20-40 minutes) for the 1.25 and 2.5 wt% solutions, indicative of increasingly viscous materials. For the 5.0 wt% sample, a decrease in both the MSD values as well as a slope of zero was observed on par with

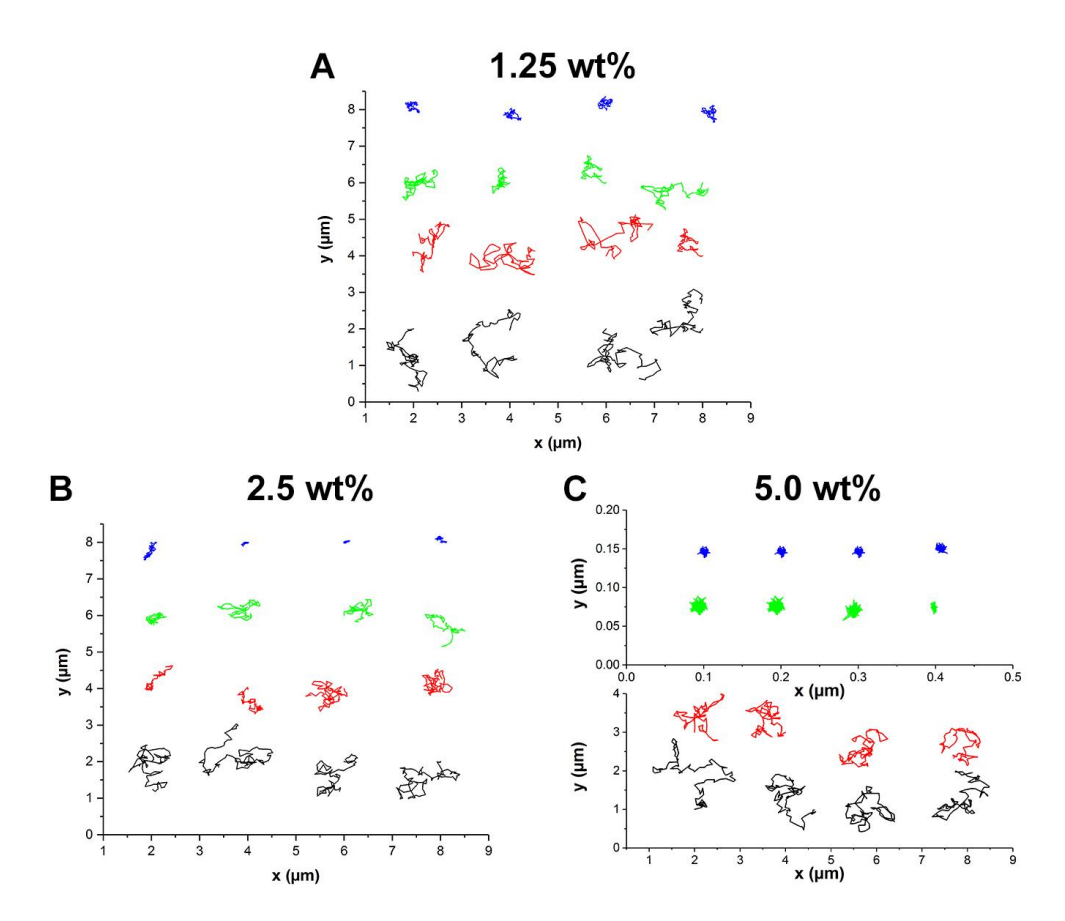


Figure 2.5. Particle tracking microrheology on 1.25, 2.5 and 5.0 wt% DNA-dextran HCR samples under various conditions. *Black*: HP1+2 only, *red*: initiator DNA-dextran only, *green*: HCR containing initiator DNA-dextran and HP1+2 0-20 minutes, *blue*: 20-40 minutes: A, B, C) Representative collections of displacement tracks for 4 beads per test condition for 1.25, 2.5 and 5.0 wt% samples, respectively.

the rapid formation of a viscoelastic solid material. As a control, performing the same HCR experiments on 2.5 wt% samples with an unconjugated initiator DNA did not result in the formation of equally viscous materials as seen in samples containing the initiator DNA-dextran graft copolymer (Figure S2.3).

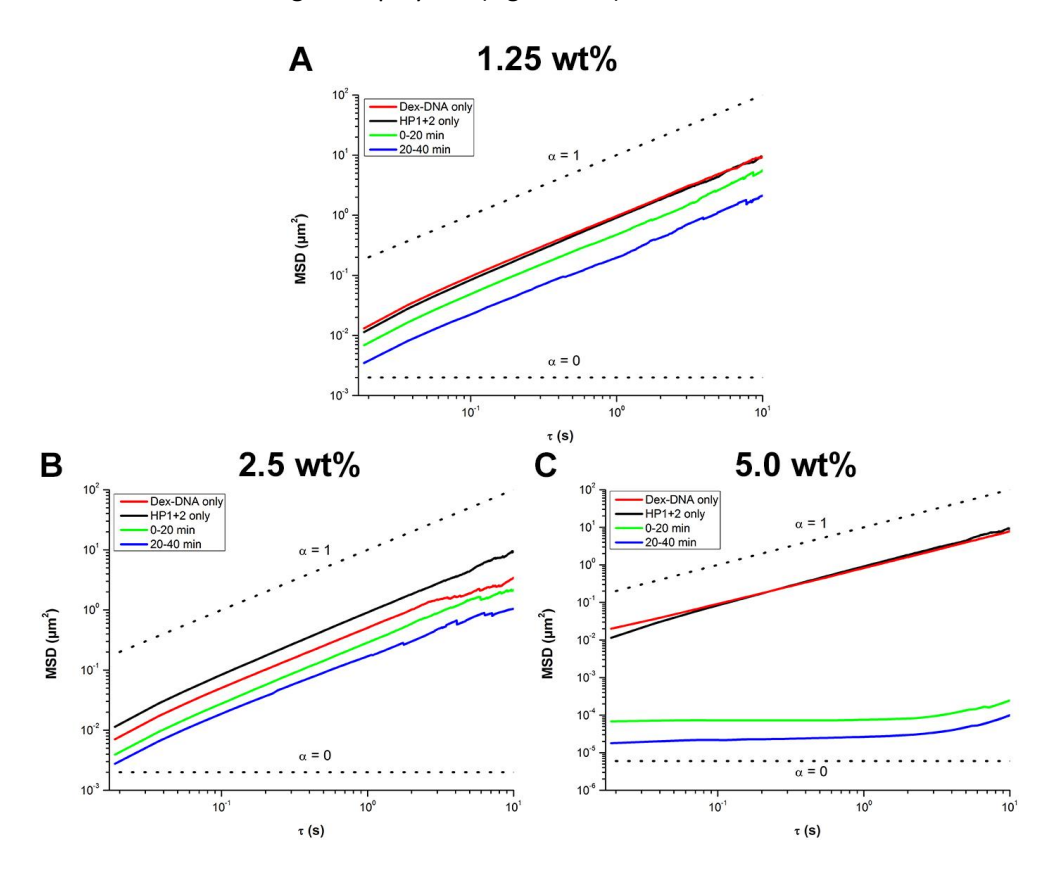


Figure 2.6. Particle tracking microrheology on 1.25, 2.5 and 5.0 wt% DNA-dextran HCR samples under various conditions. A, B, C) MSD versus lag time plots for 1.25, 2.5 and 5.0 wt% samples, respectively.

To gain further insight into the physicochemical properties of the materials, the storage (G') and loss (G'') moduli were extracted from the complex modulus obtained from a numerical approximation of the Laplace transform of the MSD data. G' and G'' of the various samples (1.25, 2.5 and 5 wt%, Figure 2.7A, B, C respectively) as a function of frequency were determined after 40 minutes of equilibration. As expected, for the 1.25 and 2.5 wt% samples G'' was greater than G' over the entire frequency range consistent with liquid-like behavior. Conversely, for the 5 wt% G' was greater than G'', synonymous with the formation of a viscoelastic material. Most likely, the growth of the DNA grafts by the HCR reaction and weak homodimer

interactions are involved in the macroscopic gel-like behavior recorded for the 5 wt% sample.

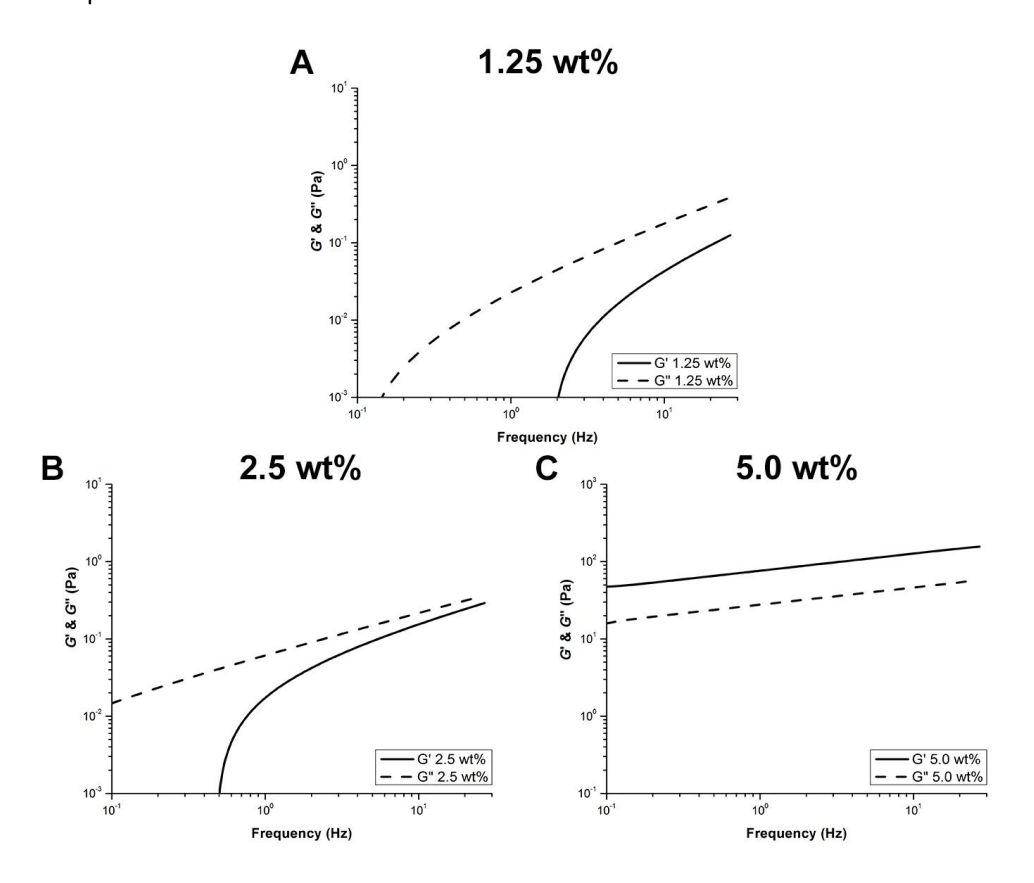


Figure 2.7. Particle tracking microrheology on 1.25, 2.5 and 5.0 wt% DNA-dextran HCR samples under various conditions. A, B, C) Rheological properties as a function of frequency for 1.25, 2.5 and 5.0 wt% samples, respectively (*solid lines*: G', *dashed lines*: G'').

#### 2.4 Conclusions

The DNA hybridization chain reaction is a hallmark example of dynamic DNA nanotechnology that can be used for sophisticated applications in detection with limits in the femtomolar range. We have shown that this technique based on DNA strand displacement can be applied on covalent polymers to drive on-demand growth of aggregate sizes with the potential to form macroscale materials depending on concentration. In combination with the advances in DNA solid phase synthesis and its continuously decreasing production costs, we envisage that implementing this technique on polymer materials opens up this area to a whole new level of structural abstraction, allowing for the future development of a wide range of responsive materials for applications in diagnostics and drug delivery, using viscosity-based changes as a readout.

### 2.5 References

- 1 McLaughlin, C. K.; Hamblin, G. D.; Sleiman, H. F. Chem. Soc. Rev. 2011, 40 (12), 5647.
- 2 Seeman, N. C. 2003, 421 (January), 1122.
- 3 Pinheiro, A. V; Han, D.; Shih, W. M.; Yan, H. Nat. Publ. Gr. 2011, 6 (12), 763.
- 4 Rothemund, P. W. K. Nature 2006, 440 (7082), 297.
- 5 Sobczak, J.-P. J.; Martin, T. G.; Gerling, T.; Dietz, H. Science 2012, 338 (6113), 1458.
- 6 Aldaye, F. A.; Palmer, A. L.; Sleiman, H. F. Science 2008, 321 (5897), 1795.
- 7 Douglas, S. M.; Bachelet, I.; Church, G. M. Science 2012, 335 (6070), 831.
- 8 Zhang, D. Y.; Seelig, G. Nat. Chem. 2011, 3 (2), 103.
- 9 Chen, Y. J.; Groves, B.; Muscat, R. A.; Seelig, G. Nat Nanotechnol 2015, 10 (9), 748.
- 10 Freeman, R.; Stephanopoulos, N.; Álvarez, Z.; Lewis, J. A.; Sur, S.; Serrano, C. M.; Boekhoven, J.; Lee, S. S.; Stupp, S. I. 2017, 8, 15982.
- 11 Zhang, D. Y.; Winfree, E. J. Am. Chem. Soc. 2009, 131 (47), 17303.
- 12 Li, B.; Ellington, A. D.; Chen, X. Nucleic Acids Res. 2011, 39 (16), e110.
- 13 Zhang, D. Y.; Turberfield, A. J.; Yurke, B.; Winfree, E. Science 2007, 318 (5853), 1121.
- 14 Dirks, R. M.; Pierce, N. A. Proc. Natl. Acad. Sci. U. S. A. 2004, 101 (43), 15275.
- 15 Choi, H. M. T.; Beck, V. a.; Pierce, N. a. ACS Nano 2014, 8, 4284.
- Seelig, G.; Soloveichik, D.; Zhang, D. Y.; Winfree, E. Science 2006, 314 (5805), 1585.
- 17 Shin, J.; Pierce, N. a. J. Am. Chem. Soc. 2004, 126 (35), 10834.
- 18 Sherman, W. B.; Seeman, N. C. Nano Lett. 2004, 4 (7), 1203.

- 19 Zhang, D. Y.; Winfree, E. J. Am. Chem. Soc. 2008, 130 (42), 13921.
- Zhang, D. Y.; Hariadi, R. F.; Choi, H. M. T.; Winfree, E. Nat. Commun. 2013, 4 (May), 1965.
- 21 Xu, Q.; Zhu, G.; Zhang, C. Y. Anal. Chem. 2013, 85 (14), 6915.
- Rudchenko, M.; Taylor, S.; Pallavi, P.; Dechkovskaia, A.; Khan, S.; Butler Jr, V. P.; Rudchenko, S.; Stojanovic, M. N. Nat. Nanotechnol. 2013, 8 (8), 580.
- 23 Shao, Y.; Jia, H.; Cao, T.; Liu, D. Acc. Chem. Res. 2017, 50 (4), 659.
- Serpell, C. J.; Edwardson, T. G. W.; Chidchob, P.; Carneiro, K. M. M.; Sleiman, H. F. J. Am. Chem. Soc. 2014, 136 (44), 15767.
- Noteborn, W. E. M.; Zwagerman, D. N. H.; Talens, V. S.; Maity, C.; van der Mee, L.; Poolman, J. M.; Mytnyk, S.; van Esch, J. H.; Kros, A.; Eelkema, R.; Kieltyka, R. E. Adv. Mater. 2017, 1603769.
- Vyborna, Y.; Vybornyi, M.; Haner, R. Chem. Commun. 2017.
- 27 Chen, P.; Li, C.; Liu, D.; Li, Z. Macromolecules 2012, 45 (24), 9579.
- Wilks, T. R.; Bath, J.; de Vries, J. W.; Raymond, J. E.; Herrmann, A.; Turberfield, A. J.; O'Reilly, R. K. ACS Nano 2013, 7 (10), 8561.
- 29 Rodríguez-Pulido, A.; Kondrachuk, A. I.; Prusty, D. K.; Gao, J.; Loi, M. A.; Herrmann, A. Angew. Chem. Int. Ed. 2013, 52 (3), 1008.
- 30 Soontornworajit, B.; Zhou, J.; Shaw, M. T.; Fan, T.-H.; Wang, Y. Chem. Commun. 2010, 46 (11), 1857.
- 31 Kahn, J. S.; Trifonov, A.; Cecconello, A.; Guo, W.; Fan, C.; Willner, I. Nano Lett. 2015, 15 (11), 7773.
- Liao, W.-C.; Lilienthal, S.; Kahn, J.; Riutin, M.; Sohn, Y. S.; Nechushtai, R.; Willner, I. Chem. Sci. 2017, 8, 3362.
- Tan, X.; Lu, X.; Jia, F.; Liu, X.; Sun, Y.; Logan, J. K.; Zhang, K. J. Am. Chem. Soc. 2016, 138 (34), 10834.
- Ohno, S.; Matyjaszewski, K. J. Polym. Sci. Part A Polym. Chem. 2006, 44 (19), 5454.

- Lee, H. II; Pietrasik, J.; Sheiko, S. S.; Matyjaszewski, K. Prog. Polym. Sci. 2010, 35 (1–2), 24.
- 36 Feng, C.; Li, Y.; Yang, D.; Hu, J.; Zhang, X.; Huang, X. Chem. Soc. Rev. 2011, 40 (3), 1282.
- 37 Sheiko, S. S.; Sumerlin, B. S.; Matyjaszewski, K. Progress in Polymer Science (Oxford). 2008, pp 759–785.
- Petersen, H.; Fechner, P. M.; Martin, A. L.; Kunath, K.; Stolnik, S.; Roberts, C. J.; Fischer, D.; Davies, M. C.; Kissel, T. Bioconjug. Chem. 2002, 13 (4), 845.
- 39 Schubert, U. S.; Hofmeier, H. Macromol. Rapid Commun. 2002, 23 (9), 561.
- 40 South, C. R.; Burd, C.; Weck, M. Acc. Chem. Res. 2007, 40 (1), 63.
- 41 Hammond, M. R.; Li, C.; Tsitsilianisb, C.; Mezzenga, R. Soft Matter 2009, 5, 2371.
- 42 Yu, Y.; Chau, Y. Biomacromolecules 2012, 13 (3), 937.
- Zadeh, J. N.; Steenberg, C. D.; Bois, J. S.; Wolfe, B. R.; Pierce, M. B.; Khan, A.
   R.; Dirks, R. M.; Pierce, N. A. J. Comput. Chem. 2011, 32 (1), 170.

## 2.6 Supporting Information

#### 2.6.1 Materials

Ethyl acetate, tris(hydroxymethyl)aminomethane (Tris base), boric acid, sodium chloride, sodium phosphate monobasic, sodium phosphate dibasic 3-hydroxypicolinic acid, divinyl sulfone, hydrochloric acid, sodium azide, 1,4-dithiothreitol (DTT), Agarose and Nile Red were obtained from Sigma Aldrich. Ammonium citrate dibasic, sodium hydroxide and ethylenediaminetetraacetic acid (EDTA) were purchased from Fluka. Dextran (Mn: 10kDa) was obtained from Pharmacosmos (Uppsala, Sweden). Dialysis membranes were purchased from Spectrum Laboratories (Rancho Dominguez, CA, USA). DNA loading buffer and 1.0 μm TetraSpeck<sup>™</sup> fluorescent polystyrene beads were purchased from Thermo Scientific and GelRed nucleic acid stain was obtained from Biotium. Oligonucleotides were commercially synthesized (IDT, Coralville, IA, USA). Micro-insert 4 well chambers were obtained from Ibidi. Water was deionized prior to use.

# 2.6.2 DNA sequences

5'-Thiol-C6 modified and unmodified oligonucleotides used in this study:

	Sequence (5' - 3')	MW (Da)
Initiator DNA-thiol	/5ThioMC6-D/AGTCTAGGATTCGGCGTGGGTTAA	7792.3
HP1	TTAACCCACGCCGAATCCTAGACTCAAAGTAGTCTAGGATTCGGCGTG	14736.6
HP2	AGTCTAGGATTCGGCGTGGGTTAACACGCCGAATCCTAGACTACTTTG	14798.6

#### 2.6.3 Instrumentation

DNA hybridization and heating of reactions were performed on an Eppendorf Thermomixer C. Gel electrophoresis studies were performed using a 20 x 20 cm standard horizontal electrophoresis unit and the resulting agarose gels were scanned using a Molecular Imager Gel Doc XR System. Measurement of DNA concentration was recorded on a Cary 300 UV-Vis spectrophotometer equipped with a Peltier

thermostatted cell holder, using 10 mm path length quartz cuvettes. Matrix-assisted laser desorption ionization-time-of-flight (MALDI-TOF)-MS spectra were acquired on a Bruker microflex LRF mass spectrometer in linear positive-ion mode using 3hydroxypicolinic acid as a matrix on a ground steel target plate. Nuclear magnetic resonance spectra (1HNMR, 300 MHz) were recorded on a Bruker DPX300 with chemical shifts reported to the residual solvent peak (D2O). Dynamic light scattering (DLS) experiments were performed on a Malvern Zetasizer Nano S using plastic cuvettes with a 10 mm path length and measurements were taken at an angle of 173°. Size exclusion chromatography experiments were performed with two detectors consisting of an interferometric RI-detector (Optilab DSP, Wyatt Technology) in line with a multi angle light scattering detector (Dawn-DSP-F, Wyatt Technology). Fluorescence data was obtained by using a fluorescent microplate reader TECAN infinite M100Pro (Switzerland). Excitation and emission wavelengths for 2-AP fluorescence quenching experiments were 303 nm and 365 nm, respectively, recorded with 4-nm bandwidths. Microrheology experiments were performed on a Nikon Eclipse Ti-E inverted microscope equipped with a confocal spinning disk unit (CSU-X1) operated at 10,000 rpm (Yokogawa, Japan) using a 100x Plan Fluor Lens (Nikon, Japan) and excited with a 488 solid state diode laser (Coherent, U.S.A.) by tracking 1.0 µm fluorescently labeled TetraSpeck polystyrene beads. Images were captured every 0.0186 seconds for 50000 frames by an Andor iXon Ultra 897 High Speed EM-CCD camera (Andor Technology, Northern Ireland). AFM micrographs were acquired in tapping mode imaging on a JPK Nanowizard Ultra AFM (JPK Instruments, Germany), using 70 kHz resonance frequency, 2 N/m force constant silicon cantilever tips. Small angle X-ray scattering measurements were performed on a SAXSLAB GANESHA 300 XL SAXS system, which comprises a GeniX 3D Cu Ultra Low Divergence micro focus sealed tube source producing X-rays with a wavelength  $\mathbb{Z} = 1.54$  Å at a flux of 1x108 ph/s and a Pilatus 300K silicon pixel detector with 487 x 619 pixels of 172 μm x 172 µm in size placed at two sample-to-detector distances of 713 and 1513 mm respectively to access a q-range of  $0.01 \le q \le 0.3 \text{ Å}-1 \text{ with } q = 42/2(\sin 2/2)$ . Silver behenate was used for calibration of the beam centre and the q range. The samples were filled at room temperature into the sample holder, being 2 mm quartz capillaries (Hilgenberg Gmbh, Germany) held in a metal block. The two-dimensional SAXS patterns were brought to an absolute intensity scale using the calibrated detector response function, known sample-to-detector distance, measured incident and transmitted beam intensities, and azimuthally averaged to obtain one dimensional SAXS profiles. The one-dimensional scattering curves were corrected for scattering of the solvent and quartz cell. Modeling of the scattering profiles was performed in the

software package SasView (http://www.sasview.org/) employing a form factor model for Gaussian polymer chains.

# 2.6.4 Synthetic routes

Scheme S1: Synthetic scheme for the preparation of dextran-VS and initiator DNA-dextran graft copolymer conjugates: i.) divinyl sulfone, 0.1 M NaOH, vortex, rt, 1 min, ii.) 5.0 M HCl, iii.) 5'-thiol initiator DNA, PBS 1X (pH 8.5), 37 °C, 24 h.

# 2.6.5 Synthesis of dextran-VS (1):

Dextran (M<sub>n</sub>: 10.0 kDa, 0.5 g, 0.05 mmol) was dissolved in 0.1 M NaOH (5.0 mL), and to this was added divinyl sulfone (3.27 mL, 32.6 mmol) while vigorously shaking on a vortex. After 1 minute, the reaction was quenched by adjusting the pH of the reaction to pH 5.0 using 5.0 M HCl. The reaction mixture was then dialyzed for 24 hours in a dialysis bag (MWCO: 1.0 kDa) to remove excess divinyl sulfone. Afterwards, the dialyzed reaction mixture was lyophilized to provide the product as a white solid.  $^1$ H-NMR ( $\delta_H$ [ppm], D<sub>2</sub>O, 300 MHz): 6.89-7.04 (m, 19H), 6.45-6.50 (d, 19H), 6.35-6.38 (d, 19H), 4.98-5.30 (m, 62H, anomeric proton), 3.30-4.10 (m, glucose units). The degree of substitution is defined using the ratio: (V / D \* 100%), in which V is the integral of the vinyl sulfone protons at 6.89-7.04 ppm and D the integral of the anomeric dextran protons at 4.98-5.30 ppm as obtained from the  $^1$ H-NMR spectra (19 out of 62 dextran monomers were functionalized, 31% substituted).

# 2.6.6 Synthesis of initiator DNA-dextran graft copolymer (2):

5'-Disulfide-protected initiator DNA oligonucleotide (1.0 mg, 130 nmol) was dissolved in phosphate buffer (200 µL, 0.1 M pH 8.0) and was reduced by adding DTT (12.0 mg, 78 µmol). The deprotection reaction was incubated for 1 hour under a nitrogen atmosphere to prevent re-oxidation at 37°C while shaking. Afterwards, DTT was removed from the reaction mixture by extraction with ethyl acetate 3 times (800 μL) and discarded. Completion of the oligonucleotide deprotection reaction was evaluated using MALDI-TOF-MS. The freshly deprotected 5'-thiol ssDNA initiator (200 µL, 130 nmol) was then added to a solution of dextran-VS (18.5 nmol, 0.19 mg) dissolved in phosphate buffer (50 µL, 0.5 M pH 8.5) and allowed to react for 24 hours while shaking at 37°C. DNA loading buffer (50 μL) was added to the crude reaction mixture. From this mixture, an aliquot with a DNA content of 500 ng was loaded in a 0.5 cm wide gel slot on a 3% agarose gel, serving as reference sample. The rest of the reaction mixture was loaded into a 10 cm wide gel slot of the same 3% agarose gel for purification. The reference band was then cut out of the gel, stained using GelRed and imaged to determine the location of the product on gel. The part of the gel containing the reaction product was then cut in pieces and loaded into a dialysis bag for electroelution of the product (1X TBE, 150 V, 3 h). The solution containing the product was the dialyzed overnight and lyophilized to obtain the initiator DNA-dextran graft copolymer conjugate as a white powder. Conjugation and purification were checked using 2% agarose gel electrophoresis.

# 2.6.7 Gel electrophoresis

Agarose gel electrophoresis (2 wt%) was carried out under non-denaturing conditions using 1X TBE buffer to monitor dextran functionalization with DNA and oligonucleotide hybridization to the DNA-grafts on the dextran copolymer. For all hydrogel and intermediate stage samples, gel aliquots containing 500 ng DNA (calculated from the concentration of DNA inside the reaction volume) were prepared by dilution of the gel in water and mixed with DNA-loading buffer. The corresponding electrophoretic mobility was analyzed on gel.

# 2.6.8 2-AP fluorescence quenching

Stock solutions of HP1-2AP and HP2 (both 600 nM) were prepared in 5×SSC buffer, and were heated to 95 °C for 2 minutes and allowed to cool to room temperature for 1 hour before use. For each experiment, HP1-2AP (250  $\mu$ L) was mixed with HP2 (250  $\mu$ L) or with 5×SSC buffer (250  $\mu$ L) in the case of the HP1-2AP only control sample. These prepared hairpin solutions were incubated at room temperature for 24 hours before the measurement. The initial fluorescence 2-AP signal was recorded after pipetting the sample into the well to obtain a stable fluorescence baseline (HP1-2AP only and HP1-2AP + HP2). After one hour, data acquisition was paused for 1 minute and Initiator DNA-dextran graft copolymer (20  $\mu$ L, 200 nM) or unconjugated initiator-DNA was added prior to continuing. In both cases, addition of the initiator DNA-dextran graft copolymer or unconjugated initiator-DNA resulted in equal fluorescent quenching suggesting the HCR reaction is working on both DNA-dextran graft copolymer and DNA only substrates in a similar fashion.

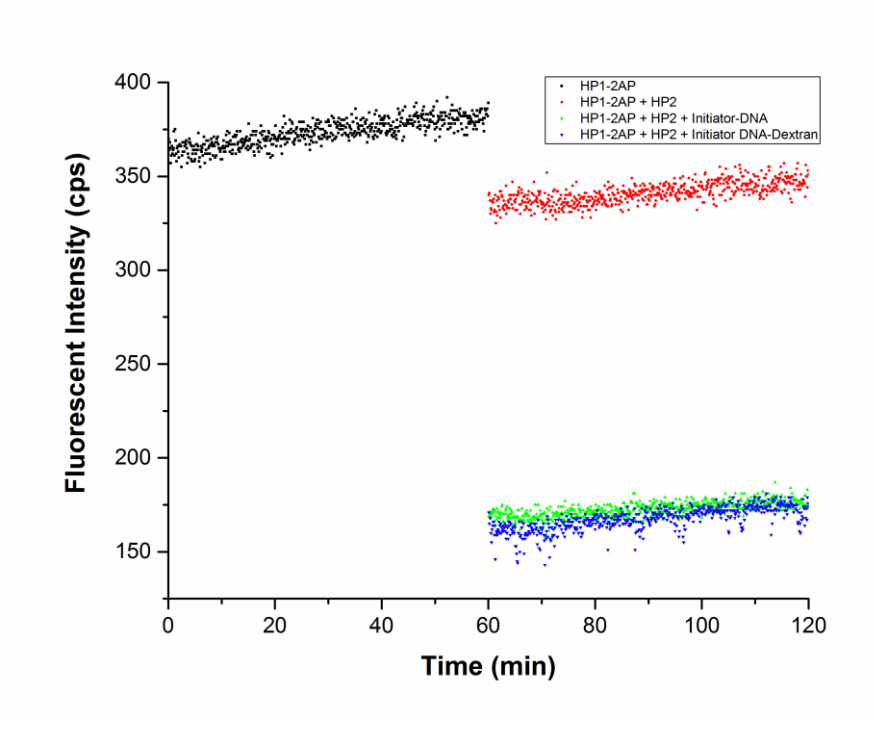


Figure S2.1. Control fluorescence quenching assays with a HP1-2AP with respect to time. Addition of HP2 (*red dots*) leads to a small drop in fluorescent intensity, suggestive of a minor interaction between the HP1and HP2. Addition of unconjugated initiator DNA (*green dots*) results in a similar drop in intensity as observed with initiator DNA-dextran graft copolymers (*blue dots*). This result suggests that the HCR reaction functions in a similar manner on both initiator DNA substrates (DNA and graft copolymer).

# 2.6.9 Dynamic light scattering

Dynamic light scattering (DLS) measurements were performed on 200  $\mu$ L solutions of HP1, HP2, HP1 and HP2, dextran-VS, initiator DNA-dextran and the initiator DNA-dextran graft copolymer with and without performing heat treatment (60 °C). Scattered light intensities and corresponding particle sizes of all samples were measured at a 173° angle in a polystyrene cuvette at 25°C. All samples were measured in triplicate.

# 2.6.10 Dynamic light scattering

Initiator DNA-dextran graft copolymer conjugates (stock solution concentration: 140  $\mu$ M), and HP1 and HP2 (stock solution concentration: 500  $\mu$ M each) were individually dissolved in 5x SSC buffer. The initiator DNA-dextran was either used directly from storage at room temperature or thermally denatured at 60 °C for 10 minutes before performing HCR. HP1 and HP2 were heated to 95 °C for 5 minutes, after which they were allowed to cool to room temperature over one hour. The Initiator DNA-dextran graft copolymer (2.5  $\mu$ L), HP1 (2.5 $\mu$ L) and HP2 (2.5  $\mu$ L) were taken from stock solutions and mixed in 5xSSC buffer (total volume 250  $\mu$ L) at room temperature for one hour. Freshly cleaved mica was incubated for 5 minutes with a 0.01 wt% solution of Poly-L-Lysine and rinsed with water two times. Afterwards, 25  $\mu$ L of the HCR reaction mixture was drop-casted on the freshly coated mica and incubated for 10 minutes. The excess sample was then blotted away using filter paper and the mica surface rinsed twice with water and the excess liquid was removed. The sample was allowed to dry overnight before imaging in tapping mode by AFM.

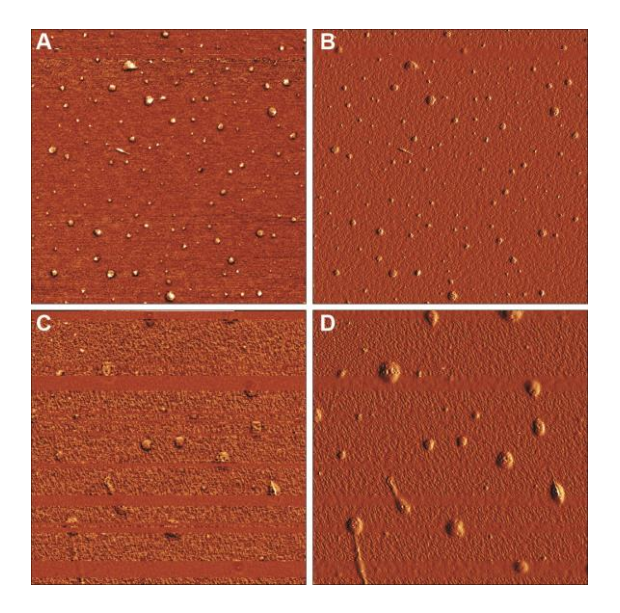


Figure S2.2. Atomic force micrographs of heat treated initiator DNA-dextran graft copolymer (A: phase, B: amplitude) and after the addition of HP1 and HP2 (C: phase, D: amplitude). Image size is 2 x 2  $\mu$ m.

# 2.6.11 Particle-tracking microrheology

Freshly prepared samples were made by mixing the initiator DNA-dextran graft copolymer with a 3-fold excess of HP1 and HP2 and fluorescently labeled beads (TetraSpeck 1 µm polystyrene beads) to result in a final concentrations of 1.25, 2.5 and 5.0 wt% in a total volume of 11 µL. The mixtures were pipetted into an Ibidi Micro-insert 4-well chamber for fluorescent microscopy imaging of particle displacement. After image acquisition, the fluorescence signals of the beads were tracked by a center-of-mass particle tracking algorithm. The algorithm is implemented in Python, named TrackPy and available online.<sup>2</sup> Bead trajectories were then manually checked for tracking errors and inconsistencies. Tracks for the 5.0 wt% DNA-hairpin experiment were drift corrected using a forward-rolling ensemble mean drift of 10 frames. Tracks in Figure 2 were randomly selected as an example for bead movement inside the gels. To compute the mean squared displacements (MSDs) and viscoelastic properties of the various samples, bead trajectories were processed using custom made MATLAB routines. MSDs were determined for individual trajectories and then averaged to determine the various ensemble average MSDs as a function of time and type of experiment. A cut-off of 100 data points per trajectory was used as a criterion for the inclusion of the trajectory MSD data into the ensemble average, and this criterion was re-evaluated per lag-time point. The viscoelastic curves, i.e. the storage (G') and loss (G'') modulus, were calculated using a well-established computational scheme.<sup>3,4</sup> First, the ensemble averaged MSDs are calculated. Then, a numerical approximation of the Laplace transform is used to compute the complex viscoelastic modulus.<sup>5</sup> The exact temperature used to calculate the viscoelastic modulus was estimated using water calibrations for appropriate durations of the measurement. The viscoelastic modulus is fit to a suitable functional form (fourthorder polynomial) and then analytically continued. Finally, G' and G'' are approximated by taking the real and imaginary parts of the analytical continuation.

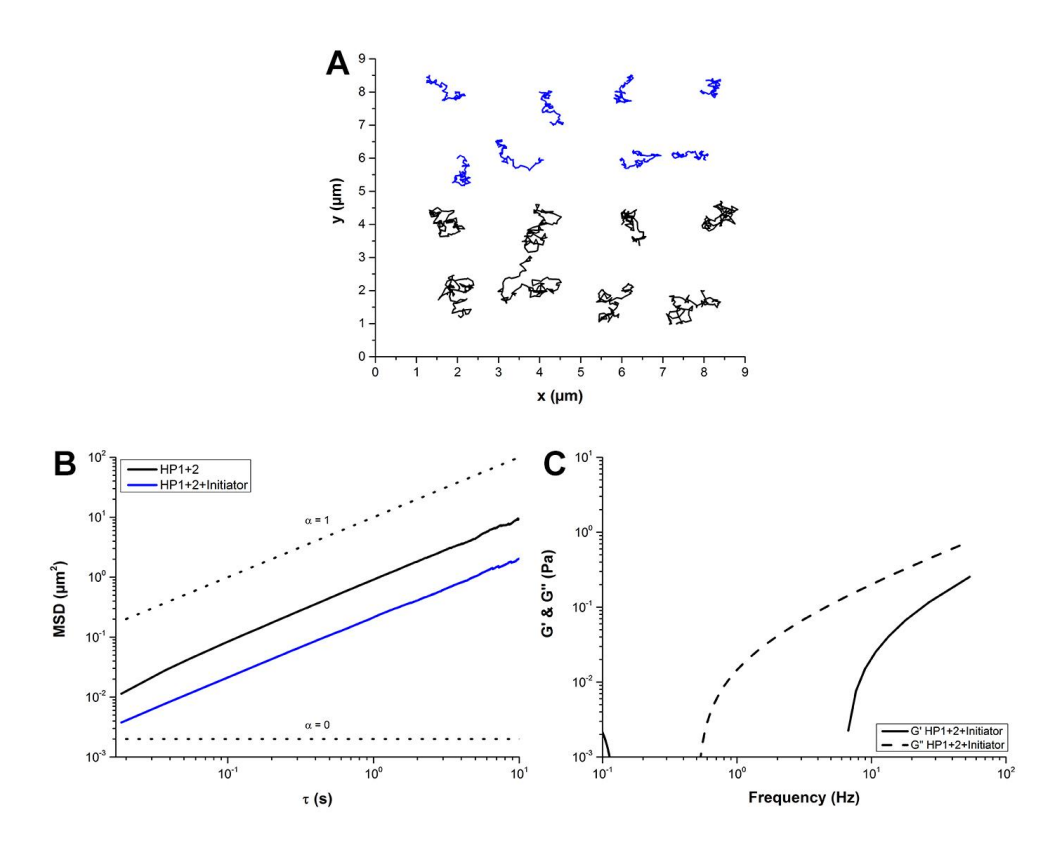


Figure S2.3. Particle tracking microrheology on 2.5 wt% unconjugated initiator DNA mixed with HP1 and HP2. A: representative collection of bead tracks (*black*: HP1+2 only, *blue*: HP1+2+initiator), B: Plot of MSD with respect to lag time, C: Rheological properties as a function of frequency.

# 2.6.12 References

- 1 Crocker, J.; Grier, D. J. Colloid Interface Sci. 1996, 179 (1), 298.
- Allan, D.; Caswell, T.; Keim, N.; van der Wel, C. August 2016,.
- 3 Mason, T. G.; Weitz, D. A. Phys. Rev. Lett. 1995, 74 (7), 1250.
- 4 Mason, T. G.; Gang, H.; Weitz, D. A. J. Mol. Struct. 1996, 383 (1–3), 81.
- 5 Hasnain, I. A.; Donald, A. M. *Phys. Rev. E* **2005**, *73* (3), 5.

# **CHAPTER 3**

# Reversible loading of nanoscale elements on a multicomponent supramolecular polymer system using DNA strand displacement

$$X_{1} \longrightarrow_{0} \stackrel{\text{I}}{\longrightarrow} \stackrel{\text{I}}{$$

This chapter was published as an Original Research paper: W. E. M. Noteborn, V. Saez Talens, R. E. Kieltyka, ChemBioChem. Accepted Author Manuscript. doi:10.1002/cbic.201700441

#### 3.1 Abstract

Nucleic acids are excellent building blocks to enable switchable character in supramolecular polymer materials because of their inherent dynamic character and potential for orthogonal self-assembly. Herein, we use DNA-grafted squaramide bolaamphiphiles in a multicomponent supramolecular polymer system and we show that they can be addressed by DNA-labeled gold nanoparticles (5 and 15 nm) through sequence complementarity. These nanoparticles can be selectively erased or rewritten on-demand using DNA-strand displacement.

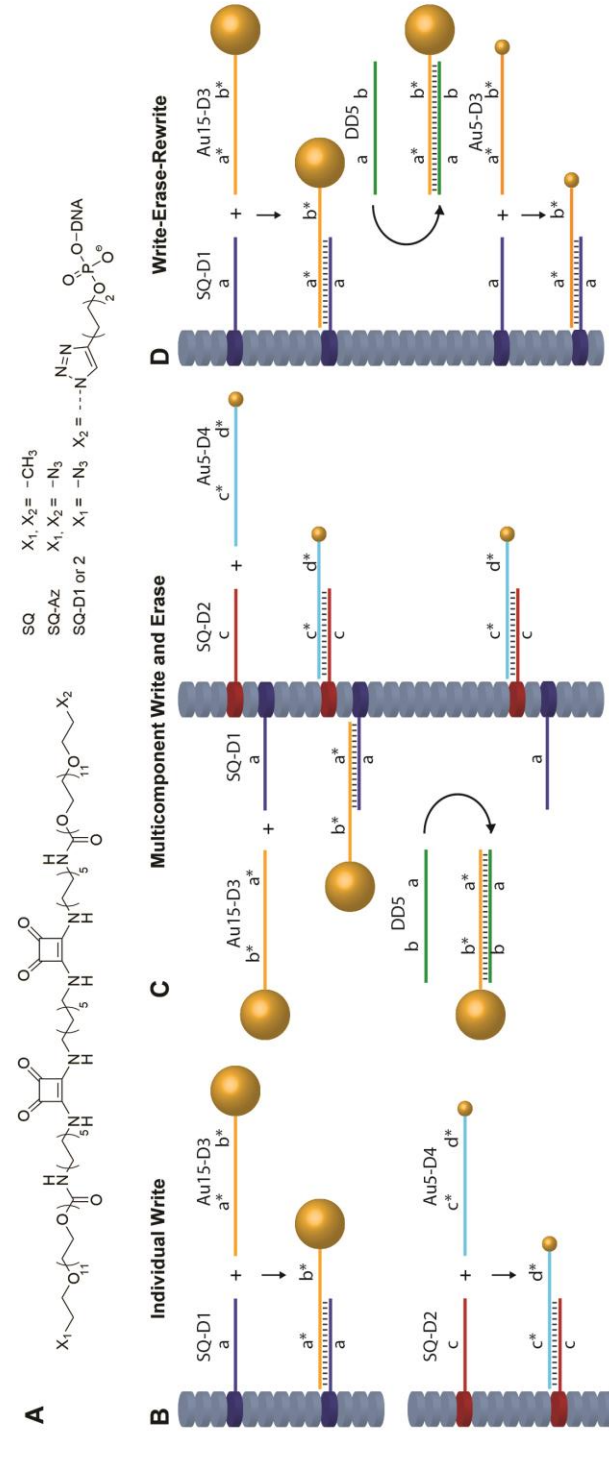
Keywords: supramolecular polymer, self-assembly, DNA strand displacement, multicomponent, gold nanoparticles

# 3.2 Introduction

Since their inception three decades ago, the interest in supramolecular polymer materials continues to rise with the field striving towards function. Supramolecular polymers consist of monomer units self-assembled through molecular recognition or stacking using a combination of non-covalent interactions such as hydrogen-bonding,  $\pi$ -stacking, charge and solvophobicity, to provide networked structures with dynamic character over several length scales.  $^{1-9}$  These features make supramolecular polymer materials excellent candidates for the construction of modular multicomponent systems, in which functional monomers can be introduced by simply matching the non-covalent interactions of the native and functional monomer units.  $^{10-12}$ 

Engineering of function within shape persistent one-dimensional supramolecular polymers consisting of amphiphiles can involve tethering<sup>13–17</sup> or embedding<sup>18–21</sup> of specific (bio)molecular or nanoscale components. For example, bioactive peptides<sup>12,14,22</sup> and drugs<sup>16,23</sup> have been incorporated into them using various covalent chemistries in order to prepare monomers that self-assemble into supramolecular polymers with a multivalent presentation of a given component for applications in the biomedical area. Taking this one step further, if non-covalent and orthogonally addressable tethers are grafted onto supramolecular polymers consisting of amphiphiles, reversible, potentially on-demand displays of application-specific components can be envisioned.

A particularly attractive class of molecules for the dynamic display of functional units are nucleic acids. DNA has been widely exploited as a nanotechnological building block because of its precise dimensions, sequence programmability and dynamic character. The recent use of DNA on its own or in combination with covalent polymers, amphiphiles or nanoparticles has resulted in stimuli-responsive scaffolds sensitive to specific nucleic acid inputs or to (bio)molecules through the introduction of aptamers. It is thus highly appealing to introduce these types of features into supramolecular polymer materials based on amphiphiles to exploit their potential for orthogonal self-assembly to tune both materials properties and function. However, only a few groups have examined this powerful combination thus far. The description of the dynamic display of the dynamic displ



Schematic of the reversible loading of squaramide-based supramolecular polymers with AuNPs by orthogonal self-assembly: B) The SQ and SQ-D2, both 0.5 mol%) are self-assembled with SQ, distinct DNA sequences can be labeled simultaneously by complementary AuNP-DNAs of 5 from the supramolecular polymer. D) The single 16-mer DNA tether (SQ-D1) can also be used to write-erase-rewrite AuNPs of various sizes. First, the Scheme 3.1. A) Bissquaramide bolaamphiphiles SQ, SQ-Az and SQ-D1 or SQ-D2 used in this study bearing methyl, azide or DNA-end groups B-C-D) supramolecular polymers are functionalized with a 16-mer DNA (SQ-D1 or SQ-D2, 1 mol%), which can be written on with a complementary 24-mer DNA-functionalized 15 nm (Au15-D3) or 5 nm (Au5-D4) AuNPs to form partial duplexes with a toehold. C) When DNA-containing monomers (SQ-D1 and 15 nm (Au15-D3 and Au5-D4). By a 24-mer DNA displacement strand (DD5) fully complementary to Au15-D3, an AuNP can be selectively erased 1 mol% SQ-D1 containing SQ supramolecular polymer is written with 24-mer DNA-labeled Au15-D3, which afterwards can be displaced using DD5, resulting in the regeneration of the **SQ-D1** tether. Introduction of **Au5-D3** then allows for its rewriting on the supramolecular polymer.

Previously, our group demonstrated the self-assembly of a squaramide-based bolaamphiphile (**SQ**) into supramolecular polymers in water.<sup>39</sup> The self-assembly of the monomer was driven by a combination of strong hydrogen-bonding interactions afforded by the ditopic squaramide unit<sup>40</sup> and the hydrophobic domain in which they are embedded relative to the peripheral oligo(ethylene glycol) chains. We herein report the synthesis of a squaramide bolaamphiphile that we decorate with DNA oligonucleotides and evaluate its incorporation into multicomponent supramolecular polymer for the reversible loading of ssDNA-labeled gold nanoparticles of distinct sizes with various presentations by orthogonal self-assembly (Scheme 3.1).

# 3.3 Results and discussion

DNA-coupled squaramide-based monomers were synthesized (see supporting information) by reacting **SQ-Az** with **5'-hexynyl** oligonucleotides by copper(I)-catalyzed alkyne-azide cycloaddition (CuAAC). The resulting mono-functionalized DNA-SQ bolaamphiphile conjugates (**SQ-D1**, **SQ-D2**) were purified by ultrafiltration, and quantified and characterized by UV-Vis spectroscopy and matrix assisted laser desorption/ionisation time-of-flight mass spectrometry (MALDI-TOF), respectively. Gel electrophoresis of the **SQ-D1/2** conjugates showed increased gel retention relative to the uncoupled DNA (Figure S3.1). Spherical gold nanoparticles (AuNPs) with 5 kDa maleimide-functionalized oligo(ethylene glycol) capping groups were conjugated to 5'-thiol DNA oligonucleotides (**Au15-D3**, **Au5-D3**, **Au5-D4**). By UV-Vis spectroscopy, 24 or 360 DNA strands per 5 or 15 nm AuNP were estimated on average (Figure 3.1).

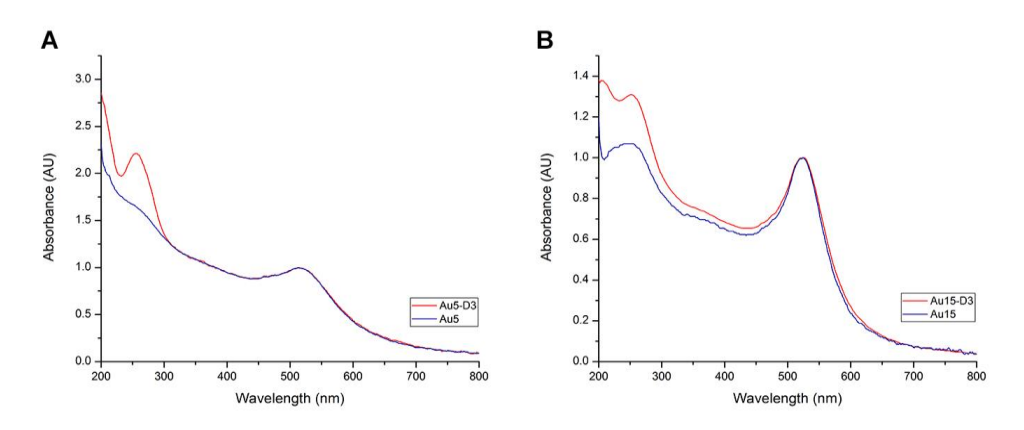


Figure 3.1. Quantification of DNA coupling on AuNPs (5 and 15 nm) by UV-Vis spectroscopy: A) DNA-AuNP conjugation on **Au5-D3**, B) DNA-AuNP conjugation on **Au15-D3**.

As a first approach, conventional transmission electron microscopy (TEM) was pursued to image the reversible loading and exchange of AuNPs by orthogonal self-assembly on the DNA-grafted SQ supramolecular polymers. The morphology was retained when the SQ polymer (50  $\mu$ M) was functionalized with 1 mol% SQ-D1 (Scheme 3.1A) by mixing in a 90% DMSO - 10%  $H_2O$  solution, lyophilization, and rehydration in 1X PBS. The mixing protocol was further supported by zeta potential measurements; where an increasingly negative value with the increase in DNA concentration (0-5 mol%) (Table S3.2 and Figure S3.2) was obtained. To validate the orthogonality of the DNA self-assembly approach on supramolecular polymers, several experiments were performed: individual writing of 5 (Au5-D4) and 15 nm (Au15-D3) AuNPs (Scheme 3.1B), writing of 5 and 15 nm (Au5-D4, Au15-D3) AuNPs simultaneously and erasing of the 15 nm AuNP (Scheme 3.1C), and writing of a 15 nm particle (Au15-D3), erasing it and rewriting with a 5 nm AuNP (Au5-D3) (Scheme 3.1D).

The writing of 5 (Au5-D4, 250 nM) or 15 nm (Au15-D3, 25 nM) AuNPs individually on the SQ supramolecular polymer (50 μM) with either SQ-D1 (0.5 μM) or **SQ-D2** (0.5 μM) resulted in their partial hybridization on the self-assembled aggregates (Scheme 3.1B and Figure 3.2A, B, C). Areas of low aggregate density showed clear labeling, but their width in several cases is roughly three times greater than the native **SQ** bolaamphiphile (average width ~ 7.5 nm), and is suggestive of their clustering when dried on the carbon grid (Figure 3.2 representative TEM micrographs of higher density can be found in Figure S3.3). Moreover, the addition of Au5-D4 or Au15-D3 to solely SQ supramolecular polymers without DNA tethers did not result in their writing on them (Figure S3.4). Further increasing the level of complexity, the potential for dual writing of both 5 and 15 nm AuNPs (Au5-D4 (540 nM), Au15-D3 (70 nM)) simultaneously on a SQ supramolecular polymer using grafted DNA tethers of distinct sequences (SQ-D1 and SQ-D2) was demonstrated (Scheme 3.1C and Figure 3.2D). To show the reversible labeling of the DNA-SQ supramolecular polymers, addition of an equimolar ratio of a fully complementary displacement DNA strand (DD5) to Au15-D3 resulted in its selective toehold-mediated removal (Figure 3.2E). Finally, a more complex sequence involving the writing of a 15 nm AuNP (Au15-D3, 25 nM), erasing it by adding the fully complementary DNA strand **DD5** and rewriting with a 5 nm AuNP (Au5-D3, 125 nM) was validated by the colocalization of the particles and supramolecular polymers in the first and last steps (Scheme 3.1D and Figure 3.2F, G, H). These experiments prove that DNA can be used as an orthogonal and reversible handle for self-assembly of nanoscale components on a multicomponent supramolecular polymer consisting of amphiphiles.

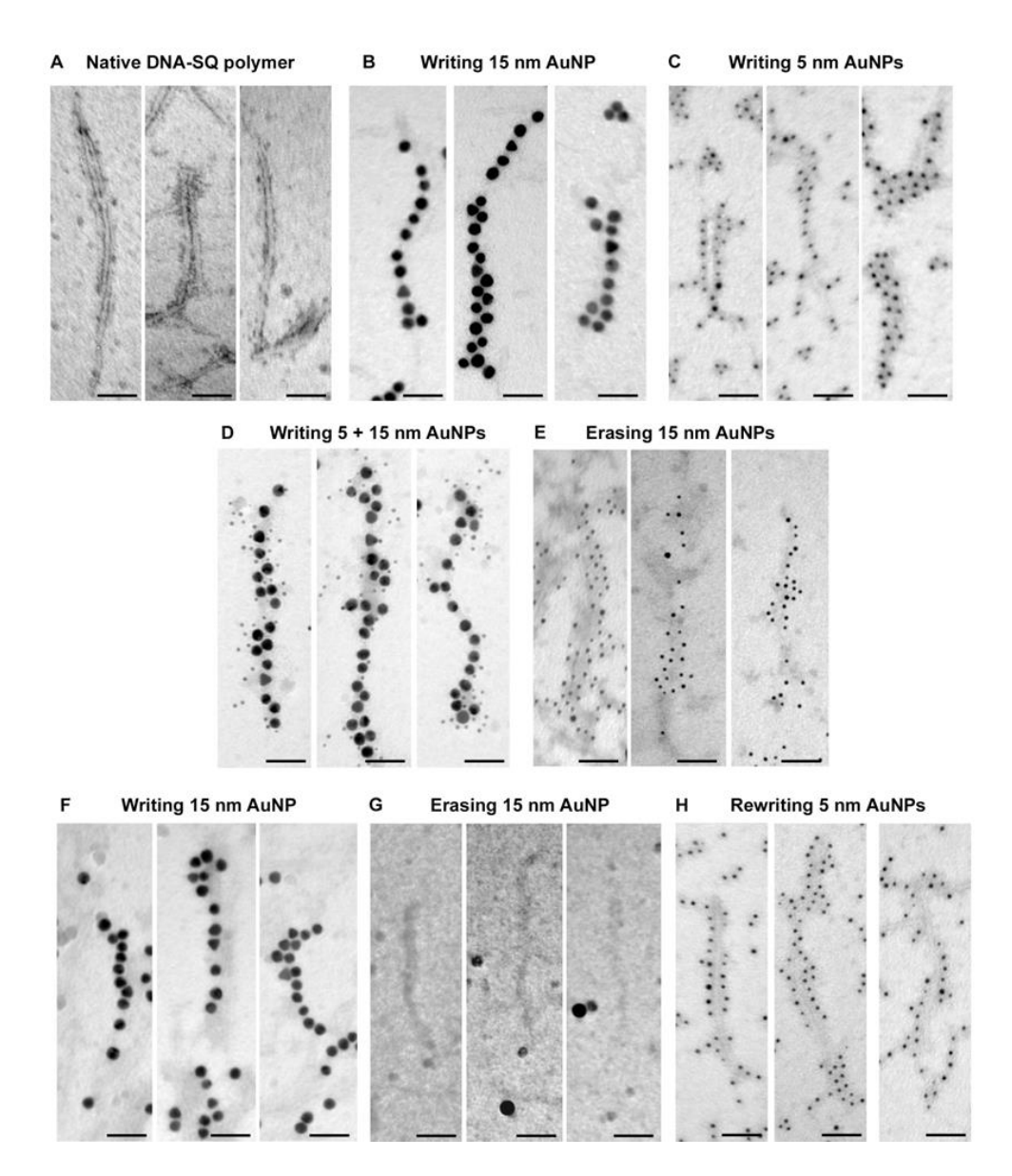


Figure 3.2. Conventional TEM images of **SQ/SQ-DX** multicomponent supramolecular polymers with and without AuNPs stained with uranyl acetate (0.8 %). A) **SQ** supramolecular polymers (50  $\mu$ M) bearing **SQ-D1** (0.5  $\mu$ M) or **SQ-D2** (0.5  $\mu$ M), B) **SQ** supramolecular polymer written on with 15 nm AuNPs (**Au15-D3**, 25 nM), C) and 5 nm AuNPs (**Au5-D4**, 250 nM). D) Dual writing of both 5 and 15 nm AuNPs (**Au15-D3**, 70 nM and **Au5-D4**, 540 nM) on independent DNA strands (**SQ-D1** and **SQ-D2**, both 0.25  $\mu$ M) E) and selective erasing of 15 nm AuNPs using **DD5**. F) SQ supramolecular polymers written on with 15 nm AuNPs (**Au15-D3**, 25 nM), G) which are erased using an equimolar amount of DNA displacement strand (**DD5**) H) and are rewritten on with 5 nm AuNPs (**Au5-D3**, 125 nM). Scale bars 50 nm.

To gain further insight into the orthogonal self-assembly process on SQ supramolecular polymers, namely the writing and erasing of AuNPs in the solutionphase, we used a combination of gel electrophoresis, fluorescence quenching, and thermal denaturation experiments. DNA hybridization (writing) and displacement (erasing) events on the DNA-grafted SQ supramolecular polymer were first probed by polyacrylamide gel electrophoresis (20%). Because of the small pore size of the acrylamide gel, an unconjugated 5'-disulfide DNA (disulfide-D3) was used instead of the corresponding AuNP-DNA to indirectly probe hybridization events. Thus, the SQ supramolecular polymer (50  $\mu$ M) with **SQ-D1** (0.5  $\mu$ M) was mixed with equimolar amounts of complementary unconjugated disulfide-D3 resulting in the appearance of a major band of higher gel retention, consistent with formation of a partially hybridized DNA duplex on the SQ supramolecular polymer (Figure 3.3A, Lane 4). As expected, a control sample based on combination of non-complementary SQ-D1 and DD5 did not yield a band of decreased mobility indicative of the lack of duplex formation (Lane 5). Mixing of DD5 and disulfide-D3 as performed in AuNP erasing experiments resulted in the formation of a complete duplex with an even higher retention (Lane 6). Moreover, premixing the **SQ** supramolecular polymer containing 1 mol% SQ-D1 and disulfide-D3 with the subsequent addition of DD5, as performed in the write-erase cascade, displayed three bands corresponding to the toeholdmediated displaced full duplex between DD5 and disulfide-D3, excess DD5 and SQ-D1 in order of increasing electrophoretic mobility (Lane 7).

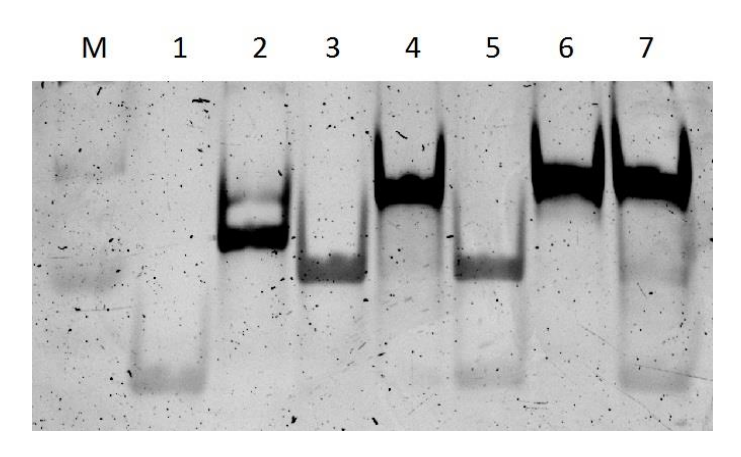


Figure 3.3. Polyacrylamide gel electrophoresis (20%) showing orthogonal self-assembly on **SQ** supramolecular polymers: **SQ-D1** (Lane 1), **disulfide-D3** (Lane 2) and **DD5** (Lane 3). The combination of **SQ-D1** and **disulfide-D3** forms a stable partial duplex (Lane 4), whereas the combination of **SQ-D1** and **DD5** does not (Lane 5). **DD5** mixed with the complementary **disulfide-D3** forms a full duplex (Lane 6). Premixed duplex of **SQ-D1** and **disulfide-D3** and subsequent addition of **DD5** shows the formation of the full duplex between **DD5** and **disulfide-D3**, excess **DD5** and **SQ-D1** (Lane 7).

Spectroscopic measurements involving UV-Vis and fluorescence spectroscopy were performed to further probe the coupling between AuNPs and the SQ supramolecular polymer through DNA. DNA-functionalized 5 nm AuNPs (Au5-D3) were combined in an equimolar quantity with complementary SQ supramolecular polymer with 1.0 mol% SQ-D1. By a thermal ramp by UV-Vis spectroscopy at 260 nm from 25 to 85 °C, a typical lower melting temperature of 58 °C (Figure 3.4) with a comparable profile to the unconjugated DNA strands (hexynyl-D1 and disulfide-D3) ( $T_m = 65$  °C) was recorded due to their less energetically favored hybridization on AuNPs relative to the solution phase.<sup>41</sup> These results are indicative of DNA hybridization between the DNA-grafted SQ supramolecular polymer and AuNPs.

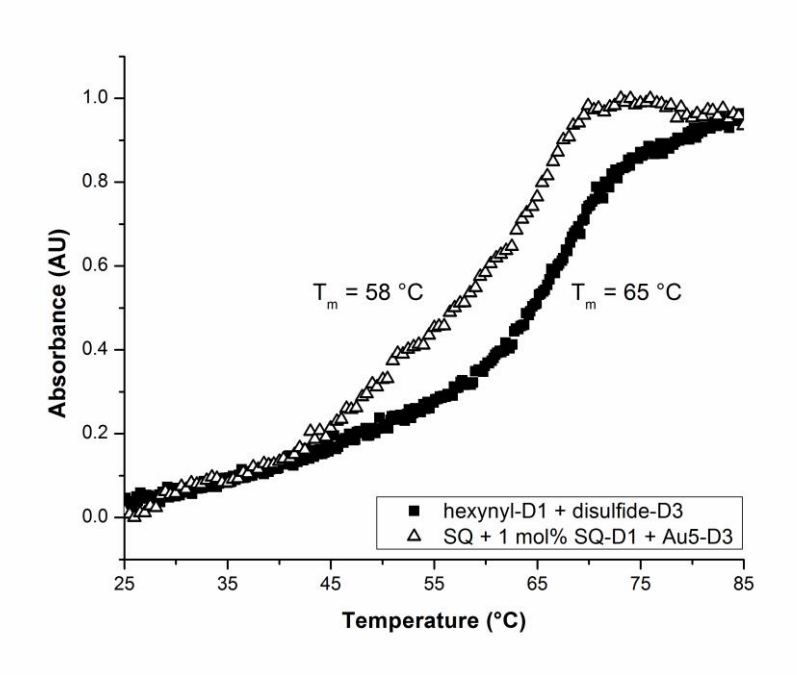


Figure 3.4. Normalized thermal denaturation profiles of **SQ** (50  $\mu$ M) with 1.0 mol% **SQ-D1** (0.5  $\mu$ M) and complementary **Au5-D3** (125 nM) and unconjugated **hexynyl-D1** and **disulfide-D3** 

Fluorescent quenching experiments using a 2-aminopurine (2-AP) labeled-DNA oligonucleotide was used to probe gold nanoparticle writing, erasing and rewriting by strand displacement. 2-AP oligonucleotides are fluorescent in their unhybridized state and become quenched upon duplex formation (Figure 3.5). First, the fluorescence intensity of the **SQ** supramolecular polymer (50  $\mu$ M) grafted with **SQ-D1-2AP** (0.5  $\mu$ M) is monitored for 10 minutes (black circles). Next, **Au5-D3**, (125 nM)

(white circles) was added to the fluorescently DNA-labeled supramolecular polymer. Mixing of the two solutions resulted in partial hybridization of the DNA-conjugated AuNPs on the supramolecular polymer and quenching of the 2-AP fluorescence signal. Addition of **DD5** (black triangles) to this mixture resulted in the recovery of fluorescence due toehold-mediated displacement of the **Au5-D3** DNA-conjugated 5 nm AuNP from the DNA-grafted **SQ** supramolecular polymer. Finally, addition of a second round of **Au5-D3** (125 nM) resulted in a second decrease in fluorescence and suggests partial hybridization and reloading of the **SQ** supramolecular polymer (white triangles). Taken together, gel electrophoresis, UV-Vis thermal denaturation and fluorescent quenching experiments show that ssDNA-labeled AuNPs can be orthogonally self-assembled on a multicomponent supramolecular polymer being written and erased from this scaffold.

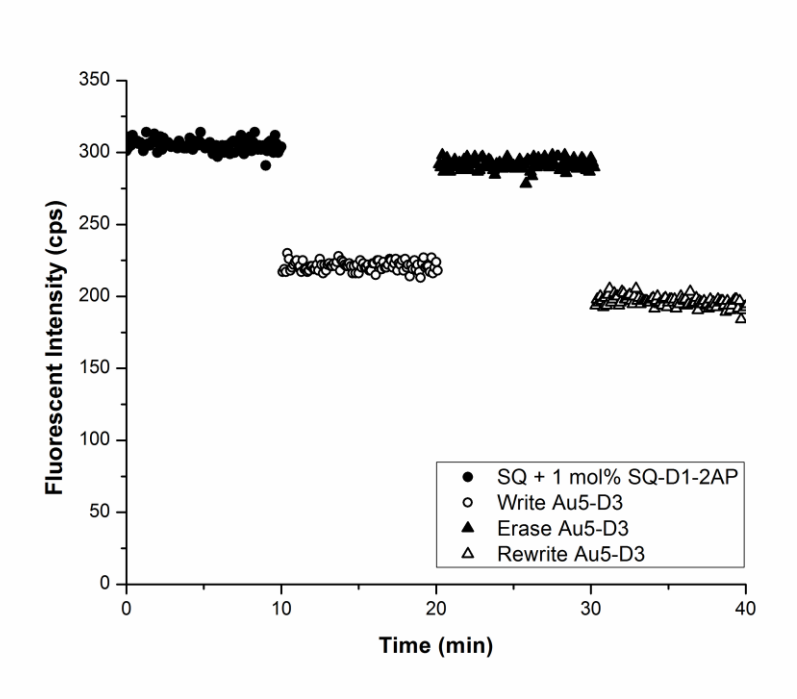


Figure 3.5. Fluorescent quenching experiment with 2-AP labeled DNAs on the SQ supramolecular polymer and a DNA-labeled 5 nm AuNP. SQ supramolecular polymer (50  $\mu$ M) with SQ-D1-2AP (0.5  $\mu$ M) is fluorescent (black circles) until Au5-D3 (125 nM) is added, resulting in quenching of the signal (white circles). Removal of Au5-D3 from the supramolecular polymer by addition of equimolar amounts of DD5, fully complementary SQ-D1 restores fluorescence signal (black triangles). Afterwards, addition of new Au5-D3 (125 nM) again results in fluorescence quenching (white triangles).

#### 3.4 Conclusions

In conclusion, we have shown that supramolecular polymers consisting of amphiphiles with DNA tethers can be addressed in a programmable and reversible way using orthogonal self-assembly of DNA. Moreover, because of the flexible azide-alkyne coupling chemistry and supramolecular mixing of the monomer components, multiple nanoscale elements can be tethered on the same DNA-labeled supramolecular polymer expeditiously, even simultaneously, through the introduction of several unique DNA sequences. This proof-of-concept study highlights the potential for the reversible labeling of these DNA-grafted supramolecular materials with several complex biological molecules (e.g. peptides, proteins), thus opening the door for the dynamic presentation of biochemical or biophysical signals.

# 3.5 References

- 1 E. Krieg, M. M. C. Bastings, P. Besenius, B. Rybtchinski, Chem. Rev. 2016, 116, 2414–2477.
- L. Albertazzi, D. van der Zwaag, C. M. A. Leenders, R. Fitzner, R. W. van der Hofstad, E. W. Meijer, Science 2014, 344, 491–495.
- 3 M. Fernandez-Castano Romera, R. P. M. Lafleur, C. Guibert, I. K. Voets, C. Storm, R. P. Sijbesma, Angew. Chem. Int. Ed. 2017, DOI 10.1002/anie.201704046.
- 4 E. A. Appel, F. Biedermann, U. Rauwald, S. T. Jones, J. M. Zayed, O. A. Scherman, J. Am. Chem. Soc. 2010, 132, 14251–60.
- H. Frisch, J. P. Unsleber, D. Lüdeker, M. Peterlechner, G. Brunklaus, M. Waller,
   P. Besenius, Angew. Chem. Int. Ed. 2013, 52, 10097–10101.
- A. Pal, M. Malakoutikhah, G. Leonetti, M. Tezcan, M. Colomb-Delsuc, V. D. Nguyen, J. van der Gucht, S. Otto, Angew. Chem. Int. Ed. 2015, 54, 7852–7856.
- A. Rödle, B. Ritschel, C. Mück-Lichtenfeld, V. Stepanenko, G. Fernández, Chem. A Eur. J. 2016, 22, 15772–15777.
- 8 S. Ogi, V. Stepanenko, K. Sugiyasu, M. Takeuchi, F. Würthner, J. Am. Chem. Soc. 2015, 137, 3300–3307.
- 9 E. Krieg, H. Weissman, E. Shimoni, A. Baris, B. Rybtchinski, J. Am. Chem. Soc. 2014, 136, 9443–9452.
- 10 T. Aida, E. W. Meijer, S. I. Stupp, Science 2012, 335, 813–7.
- 11 P. Besenius, J. Polym. Sci. Part A Polym. Chem. 2017, 55, 34–78.
- 12 J. Boekhoven, S. I. Stupp, Adv. Mater. 2014, 26, 1642–1659.
- 13 G. A. Hudalla, T. Sun, J. Z. Gasiorowski, H. Han, Y. F. Tian, A. S. Chong, J. H. Collier, Nat. Mater. 2014, 13, 829–836.

- 14 R. E. Kieltyka, M. M. C. Bastings, G. C. van Almen, P. Besenius, E. W. L. Kemps, P. Y. W. Dankers, Chem. Commun. 2012, 48, 1452–4.
- S. S. Lee, T. Fyrner, F. Chen, Z. Álvarez, E. Sleep, D. S. Chun, J. A. Weiner, R. W. Cook, R. D. Freshman, M. S. Schallmo, et al., Nat. Nanotechnol. 2017, DOI 10.1038/nnano.2017.109.
- L. L. Lock, M. LaComb, K. Schwarz, A. G. Cheetham, Y. Lin, P. Zhang, H. Cui, Faraday Discuss. 2013, 166, 285–301.
- 17 A. G. Cheetham, P. Zhang, Y. Lin, L. L. Lock, H. Cui, J. Am. Chem. Soc. 2013, 135, 2907–10.
- S. Prasanthkumar, S. Ghosh, V. C. Nair, A. Saeki, S. Seki, A. Ajayaghosh, Angew. Chem. Int. Ed. 2015, 54, 946–950.
- 19 W. Zhang, W. Jin, T. Fukushima, A. Saeki, S. Seki, T. Aida, Science 2011, 334, 340–343.
- 20 R. Marty, R. Nigon, D. Leite, H. Frauenrath, J. Am. Chem. Soc. 2014, 136, 3919–3927.
- 21 M. Kumar, P. Brocorens, C. Tonnelé, D. Beljonne, M. Surin, S. J. George, Nat. Commun. 2014, 5, 5793.
- 22 M. Zhou, A. M. Smith, A. K. Das, N. W. Hodson, R. F. Collins, R. V. Ulijn, J. E. Gough, Biomaterials 2009, 30, 2523–2530.
- 23 R. Lin, A. G. Cheetham, P. Zhang, Y. Lin, H. Cui, Chem. Commun. (Camb). 2013, 49, 4968–70.
- 24 F. A. Aldaye, A. L. Palmer, H. F. Sleiman, Science 2008, 321, 1795–1799.
- 25 N. C. Seeman, Nature 2003, 421, 427–31.
- 26 Y. J. Chen, B. Groves, R. A. Muscat, G. Seelig, Nat Nanotechnol 2015, 10, 748–760.
- A. Banerjee, D. Bhatia, A. Saminathan, S. Chakraborty, S. Kar, Y. Krishnan, Angew. Chem. Int. Ed. 2013, 52, 6854–6857.
- J. Fu, Y. R. Yang, A. Johnson-Buck, M. Liu, Y. Liu, N. G. Walter, N. W. Woodbury, H. Yan, Nat. Nanotechnol. 2014, 9, 531–536.

- 29 J. S. Kahn, Y. Hu, I. Willner, Acc. Chem. Res. 2017, 50, 680–690.
- A. Rodríguez-Pulido, A. I. Kondrachuk, D. K. Prusty, J. Gao, M. A. Loi, A. Herrmann, Angew. Chem. Int. Ed. 2013, 52, 1008–1012.
- 31 B. Soontornworajit, J. Zhou, M. T. Shaw, T.-H. Fan, Y. Wang, Chem. Commun. 2010, 46, 1857.
- 32 K. M. M. Carneiro, G. D. Hamblin, K. D. Hanni, J. Fakhoury, M. K. Nayak, G. Rizis, C. K. McLaughlin, H. S. Bazzi, H. F. Sleiman, Chem. Sci. 2012, 3, 1980–1986.
- 33 H. M. T. Choi, V. a. Beck, N. a. Pierce, ACS Nano 2014, 8, 4284–4294.
- P. Hazarika, B. Ceyhan, C. M. Niemeyer, Angew. Chem. Int. Ed. 2004, 43, 6469–6471.
- W. E. M. Noteborn, D. N. H. Zwagerman, V. S. Talens, C. Maity, L. van der Mee, J. M. Poolman, S. Mytnyk, J. H. van Esch, A. Kros, R. Eelkema, et al., Adv. Mater. 2017, 1603769.
- 36 Y. Vyborna, M. Vybornyi, R. Haner, Chem. Commun. 2017, 1–7.
- 37 P. J. S. King, A. Saiani, E. V Bichenkova, A. F. Miller, Chem. Commun. 2016, 52, 6697–6700.
- 38 F. Wu, J. Jin, L. Wang, P. Sun, H. Yuan, Z. Yang, G. Chen, Q. H. Fan, D. Liu, ACS Appl. Mater. Interfaces 2015, 7, 7351–7356.
- V. Saez Talens, P. Englebienne, T. T. Trinh, W. E. M. Noteborn, I. K. Voets, R. E. Kieltyka, Angew. Chem. Int. Ed. 2015, 54, 10502–10506.
- 40 F. R. Wurm, H.-A. Klok, Chem. Soc. Rev 2013, 42, 8179–8574.
- 41 C. Chen, W. Wang, J. Ge, X. S. Zhao, Nucleic Acids Res. 2009, 37, 3756–3765.

# 3.6 Supporting Information

#### 3.6.1 Materials

Methoxy-PEG11-alcohol and azido-PEG11-alcohol were obtained from Polypure (Norway). Carbonyldiimidazole (CDI), trityl chloride, diaminodecane, diaminoheptane, squaric acid dibutyl ester, DIPEA, CHCl<sub>3</sub>, DMSO, copper(II) sulfate, (+)-sodium L-ascorbate, acetic acid, tris(3-hydroxypropyltriazolylmethyl)amine (THPTA), 3-hydroxypicolinic acid, triethylamine, tris(hydroxymethyl)aminomethane (Tris base), boric acid, agarose, and Amicon Ultra 0.5 mL 3 kDa MWCO centrifugal filters were obtained from Sigma Aldrich. Ammonium citrate dibasic, sodium hydroxide and ethylenediaminetetraacetic acid (EDTA) were purchased from Fluka. 30% acrylamide/bis solution (19:1) and ammonium persulfate were obtained from Bio-Rad. N,N,N',N'-tetramethylethylenediamine (TEMED) and DNA loading buffer were purchased from Thermo Scientific. GelRed nucleic acid stain was obtained from Biotium. Single-stranded 5'-modified and unmodified oligonucleotides were purchased from Integrated DNA Technologies (IDT, Coralville, IA, USA). Carbon film coated 200 mesh copper TEM grids were obtained from Van Loenen Instruments (The Netherlands). Water was deionized prior to use.

# 3.6.2 DNA Sequences

Table S3.1. Modified and unmodified oligonucleotides used in this study.

	Sequence (5' - 3')	MW (Da)
hexynyl-D1	/5-Hexynyl/TTAACCCACGCCGAAT	4970.3
hexynyl-D2	/5-Hexynyl/TATACGTGCATACGAT	5040.3
disulfide-D3	/5-Disulfide/AGTCTAGGATTCGGCGTGGGTTAA	7792.3
disulfide-D4	/5-Disulfide/CTAGTCTAATCGTATGCACGTATA	7655.2
DD5	TTAACCCACGCCGAATCCTAGACT	7241.8
hexynyl-D1-2AP	TTAACCCACGCCG/i2AmPr/AT	4970.3

#### 3.6.3 Instrumentation

Reverse-phase chromatography was performed on a Grace Reveleris X1 flash chromatography system equipped with a C18 silica column. DNA containing reactions were heated on an Eppendorf Thermomixer C.  $^{1}$ H-NMR and  $^{13}$ C-NMR spectra were recorded on a Bruker AV-850 instrument with chemical shifts reported to the residual solvent peak (CHCl<sub>3</sub>). LC-MS analysis was performed on a Finnigan Surveyor HPLC system equipped with a Gemini  $C_{18}$  50 × 4.60 mm column (UV detection 200 - 600

nm), coupled to a Finnigan LCQ Advantage Max mass spectrometer with ESI. Matrix-assisted laser desorption ionization—time-of-flight (MALDI-TOF)-MS spectra were acquired on a Bruker microflex LRF mass spectrometer in linear positive-ion mode using 3-hydroxypicolinic acid as a matrix on a ground steel target plate. Measurement of DNA concentration and thermal denaturation studies were recorded on a Cary 300 UV-Vis spectrophotometer equipped with a Peltier thermostatted cell holder, using 10 mm path length quartz cuvettes. Gel electrophoresis studies were performed either using a 20 x 20 cm standard horizontal electrophoresis unit for agarose gels or on a 8.3 x 7.3 cm Mini-PROTEAN Tetra Cell electrophoresis unit for PAGE gel were scanned using a Molecular Imager Gel Doc XR System. Zeta potential measurements were performed on a Malvern Nano-ZS using a reusable dip cell. Fluorescence quenching experiments were carried out on a Tecan Plate Reader Infinite M1000 using 96 well plates (PP Microplate, solid F-bottom (flat), chimney well). TEM images were acquired on a JEOL 1010 with an accelerating voltage of 60 kV equipped with a CCD camera.

# 3.6.4 Synthetic routes

Scheme S3.1. i) CDI, 1 h, RT, neat, ii) CHCl<sub>3</sub>, 1 h, RT, iii) N-trityl decanediamine, DIPEA, CHCl<sub>3</sub>, reflux, overnight, iv) TFA, RT, 4 h, v) squaric acid dibutyl ester, DIPEA, CHCl<sub>3</sub>, RT, ON, vi) 1,7-diaminoheptane, DIPEA, CHCl<sub>3</sub>, reflux, overnight

Scheme S3.2. i) sodium L-ascorbate, Cu(II)-THPTA, 0.2 M triethylammonium acetate buffer pH 7, 50 v/v% DMSO, N<sub>2</sub>, 50 °C, 4 h

# 3.6.5 Synthesis of Azido-PEG11-C10-SQ (1)

Carbonyldiimidazole (CDI) (186 mg, 1.14 mmol) was added to azido-PEG11-alcohol (545 mg, 0.95 mmol) and reacted neat at room temperature for one hour. Afterwards, CHCl3 (1 mL) was added and the reaction was allowed to stir for another hour. N-trityl decanediamine  $^1$  (474 mg, 1.14 mmol), DIPEA (0.33 mL, 1.91 mmol) and CHCl $_3$  (10 mL) were added to the reaction mixture and refluxed overnight. Both solvent and base were then removed under vacuum, and TFA (5 mL) was added and stirred for four hours at room temperature to remove the trityl protection group. The TFA was subsequently removed and CHCl $_3$  (10 mL), squaric acid dibutyl ester (247  $\mu$ L, 1.15 mmol) and DIPEA (0.33 mL, 1.91 mmol) were added. This mixture was reacted overnight at room temperature and then purified using flash chromatography using a gradient of 10-90% ACN/H $_2$ O over 45 minutes on a  $C_{18}$  silica column. The product was concentrated by evaporation and lyophilized to obtain compound  $\bf 1$  as a white solid.

Yield: 66.3 % (583.4 mg)  $^{1}$ H-NMR ( $\delta_{H}[ppm]$ , CDCl $_{3}$ , 850 MHz): 6.56 (br, s, 1H), 5.07 (br, s, 1H), 4.48-4.70 (m, 2H), 4.04-4.20 (m, 2H), 3.40-3.90 (m, 43H), 3.22-3.34 (m, 3H), 2.96-3.05 (m, 2H), 2.71 (s, 2H), 1.60-1.71 (m, 2H), 1.43-1.53 (m, 2H), 1.27-1.40 (m, 4H), 1.00-1.27 (m, 12H), 0.82-0.87 (m, 3H).  $^{13}$ C-NMR ( $\delta_{C}[ppm]$ , CDCl3, 850 MHz): 189.46, 182.68, 177.09, 172.47, 156.43, 73.20, 70.40, 69.90, 69.52, 63.65, 50.57, 44.74, 40.89, 31.92, 30.54, 29.80, 29.29, 29.09, 28.98, 26.56, 26.26, 18.57, 13.59. LC-MS: 7.84 min, m/z: 922.60 [M+H] $^{+}$ . MALDI-TOF-MS: m/z calc: 922.12; found: 944.69 (M+Na) $^{+}$ .

# 3.6.6 Synthesis of Azido-SQ (SQ-Az)

Compound 1 (200 mg, 0.22 mmol) was dissolved in CHCl<sub>3</sub> (10 mL) and to this was added DIPEA (0.08 mL, 0.43 mmol) and diaminoheptane (14.1 mg, 0.11 mmol). The reaction was refluxed overnight while stirring and then purified using flash chromatography using a gradient of 10-90% ACN/ $H_2O$  over 45 minutes on a  $C_{18}$  silica

column. The product was concentrated by evaporation and lyophilized to obtain compound **2** as a white solid.

Yield: 58.7 % (116.4 mg)  $^{1}$ H-NMR ( $\delta_{H}[ppm]$ , CDCl $_{3}$ , 850 MHz): 7.85 (s, 2H), 7.60 (s, 2H), 5.02 (s, 2H), 4.17 (s, 4H), 3.65-3.73 (m, 90H), 3.37 (s, 4H), 3.11 (s, 4H), 2.52 (br, s, 2H), 1.63 (s, 8H), 1.14-1.48 (m, 38H).  $^{13}$ C-NMR ( $\delta_{C}[ppm]$ , CDCl $_{3}$ , 850 MHz): 182.58, 181.47, 168.96, 167.06, 156.46, 70.50, 69.99, 69.63, 63.73, 50.65, 44.78, 43.08, 41.04, 31.17, 29.95, 29.49, 29.27, 26.76, 26.43, 24.58. LC-MS: 7.62 min, m/z: 1826.93 [M+H] $^{\dagger}$ . MALDI-TOF-MS: m/z calc: 1826.24; found: 1849.29 (M + Na) $^{\dagger}$ .

# 3.6.7 Synthesis of SQ-DNA (SQ-D1, SQ-D2 and SQ-D1-2AP)

5'-functionalized hexynyl-D1, hexynyl-D2 or hexynyl-D1-2AP (20 nmol) was dissolved in deionized water (20 μL) and 2M triethylammonium acetate buffer at pH 7 (8.9 μL) was added. Compound SQ-Az (0.073 mg, 40 nmol) dissolved in DMSO (14.6 μL) and additional DMSO (54 μL) was added to the mixture. A mixture of THPTA (0.078 mg, 180 nmol) and CuSO<sub>4</sub> (0.026 mg, 160 nmol) dissolved in H<sub>2</sub>O (10.3 μL) was then added to the reaction mixture. Afterwards, sodium L-ascorbate (0.079 mg, 400 nmol) in H<sub>2</sub>O (20 μL) was added and the mixture was degassed with argon for 30 seconds. The reaction mixture was shaken at 50 °C for 4 hours and purified using Amicon Ultra 0.5 mL centrifugal filters with a MWCO of 3 kDa.

MALDI-TOF-MS: **SQ-D1** m/z calc: 6796.54, found: 6796.89  $[M+H]^{+}$ . **SQ-D2** m/z calc: 6866.54, found: 6867.03  $[M+H]^{+}$ .

# 3.6.8 Gel Electrophoresis

Polyacrylamide gel electrophoresis (PAGE) (20%) was carried out at room temperature under non-denaturing conditions to monitor oligonucleotide functionalization and displacement reactions. For all samples, aliquots containing 50 ng DNA (calculated by the concentration of DNA inside the sample volume) were prepared by sample dilution in water and mixing with DNA-loading buffer. Gels were run in 1X TBE buffer for 1.5 h at 150 V and then stained using GelRed before imaging.

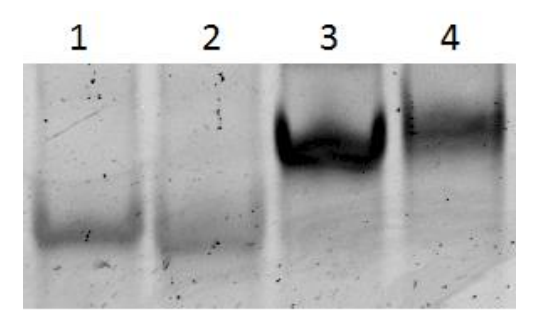


Figure S3.1. Polyacrylamide gel electrophoresis showing unmodified **hexynyl-D1** and **hexynyl-D2** (Lanes **1** and **2**) and **SQ** supramolecular polymer-DNA conjugates **SQ-D1** and **SQ-D2** (Lanes **3** and **4**).

# 3.6.9 UV-Vis characterization of AuNP-DNA conjugates

The extent of DNA coupling on AuNPs was quantified by measuring the absorbance at 520 and 260 nm. The UV-Vis spectra were normalized with respect to the peak at 520 nm. Subsequently, the difference in absorbance between unconjugated and DNA-conjugated AuNPs at 260 nm was used to calculate the extent of DNA coupling to the AuNPs. In this way, the extent of functionalization was determined to be 24 (5 nm AuNPs) or 360 (15 nm AuNPs) per particle on average.

# 3.6.10 Zeta potential measurements

Table S3.2 shows the different approaches tested for **SQ-D1** incorporation into **SQ** supramolecular polymers. Compared to heat or sonication treatment, mixing the components in DMSO (90%):  $H_2O$  (10%) and subsequent freeze drying before rehydration in 0.1X PBS and supramolecular polymer formation shows the most negative zeta potential, indicative of most efficient incorporation of **SQ-D1** into the fiber. DNA-**SQ** supramolecular polymers (containing 50  $\mu$ M **SQ**, 0-5 mol% **SQ-D1**) were then prepared accordingly and left to stand for 24 hours. **SQ** supramolecular polymers functionalized with increasing concentrations of **SQ-D1** show increasingly negative zeta potential, indicative of more incorporation of **SQ-D1** into the supramolecular fibers (Table S3.2). All zeta potential experiments were performed in triplicate.

Table S3.2. Zeta potential measurements of supramolecular polymers of **SQ** with and without DNA prepared by different mixing approaches

	Zeta potential (mV)
$\mathrm{H}_2\mathrm{O}$	-6.8 ± 1.71
<b>SQ</b> only	-10.9 ± 1.33
SQ + 0.5 mol% hexynyl-D1	-12.5 ± 1.55
<b>SQ</b> + 0.5 mol% <b>SQ-D1</b> + heat	-12.1 ± 0.81
<b>SQ</b> + 0.5 mol% <b>SQ-D1</b> + sonic	-11.2 ± 1.32
<b>SQ</b> + 0.5 mol% <b>SQ-D1</b> + DMSO	-17.8 ± 1.60

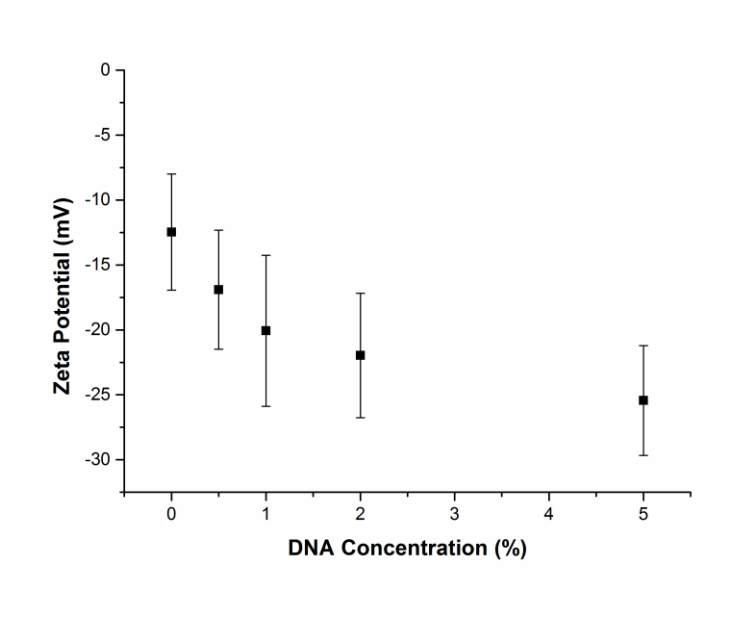


Figure S3.2. Zeta potential measurements show increasingly negative potentials for increasing concentrations of DNA mixed in the squaramide supramolecular polymer (50  $\mu$ M **SQ**, 0-5 mol% **SQ-D1**).

# 3.6.11 SQ and SQ-DX supramolecular polymer mixing protocol

In general, a stock solution of **SQ** (500  $\mu$ M, DMSO) was mixed with **SQ-D1** (5  $\mu$ M, H<sub>2</sub>O) or **SQ-D2** (5  $\mu$ M, H<sub>2</sub>O) and extra DMSO was added to obtain a DMSO / H<sub>2</sub>O ratio of 90 : 10. After 5 minutes, the samples were placed on the lyophilizer and once dried rehydrated in 1X PBS. The samples were then left to stand at room temperature for 24 hours to let the supramolecular polymers equilibrate before dilution into final experimental concentrations (typically 50  $\mu$ M **SQ**, 0.5  $\mu$ M **SQ-D1** or **SQ-D2**).

# 3.6.12 2-Aminopurine (2-AP) fluorescence quenching

A solution containing **SQ** supramolecular polymers (50  $\mu$ M) functionalized with 2-AP labeled DNA-functionalized monomer **SQ-D1-2AP** (1 mol%) in 1X PBS buffer was made according to the protocol outlined in Section 3.6.11. The fluorescence signal of the **SQ-D1-2AP** labeled supramolecular polymer was recorded for 10 minutes to obtain a stable fluorescence signal. **Au5-D3** (125 nM) in 1X PBS buffer was added to the **SQ-D1-2AP** supramolecular polymer solution, and the fluorescence signal was recorded for 10 minutes. An equimolar amount of DNA displacement strand, **DD5**, fully complementary to the DNA-AuNP was added and the fluorescence signal was also monitored for 10 minutes. Finally, additional **Au5-D3** (125 nM) was added and the fluorescence intensity was also recorded for 10 minutes.

#### 3.6.13 Thermal Denaturation Studies

Thermal denaturation of the formed DNA duplexes between **SQ-D1** (2 nmol) and complementary **Au5-D3** DNA-functionalized 5 nm AuNPs (125 nM) in 1X PBS was monitored using the absorbance at 260 nm on a Cary 300 UV-Vis spectrophotometer equipped with a thermal heating block. Samples were first annealed in a thermoshaker by heating to 85 °C and subsequently cooling down to room temperature over the course of 2 hours. Subsequently, the signal at 260 nm was followed in a heating ramp from 25 to 85°C at a rate of 0.20 °C/min.

# 3.6.14 Transmission Electron Microscopy (TEM)

TEM samples were prepared as described in Section 3.6.11 after 24 hours incubation. A 10  $\mu$ L supramolecular polymer solution containing **SQ** (50  $\mu$ M) and **SQ-D1** (0.5  $\mu$ M) or **SQ-D1** and **SQ-D2** (0.5  $\mu$ M each) with and without AuNPs was pipetted onto a sheet of Parafilm. A carbon film coated copper grid (200 mesh) was placed on top for one minute and removed, followed by blotting of the excess liquid by a filter paper. The grid was washed three times by placing it on a fresh drop of water and again blotting

away excess liquid. The samples were negatively stained using a 0.8% uranyl acetate solution for 15 minutes, followed by removal of the excess liquid by blotting and left to dry (30 minutes) before imaging. TEM images were acquired on a JEOL1010 with an accelerating voltage of 60 kV equipped with a CCD camera.

- For the 'Individual Write' experiments, **SQ** (50  $\mu$ M) and **SQ-D1** (0.5  $\mu$ M) were mixed with **Au15-D3** (25 nM) or **SQ-D2** (0.5  $\mu$ M) and were mixed with **Au5-D4** (250 nM).
- For the 'Multicomponent Write and Erase' experiments, **SQ** (50  $\mu$ M), **SQ-D1** (0.25  $\mu$ M) and **SQ-D2** (0.25  $\mu$ M) were mixed with **Au15-D3** (70 nM) and **Au5-D4** (540 nM). **DD5** was added in equimolar amounts to remove **Au15-D3**.
- For the 'Write-Erase-Rewrite' experiments, **SQ** (50  $\mu$ M) and **SQ-D1** (0.5  $\mu$ M) were mixed with **Au15-D3** (25 nM) to write on the supramolecular polymer. **DD5** was added in equimolar amounts to remove the 15nm AuNPs. Finally, **Au3-D3** (125 nM) was added to rewrite on the supramolecular polymer (concentration **SQ** after rewrite: 25  $\mu$ M).

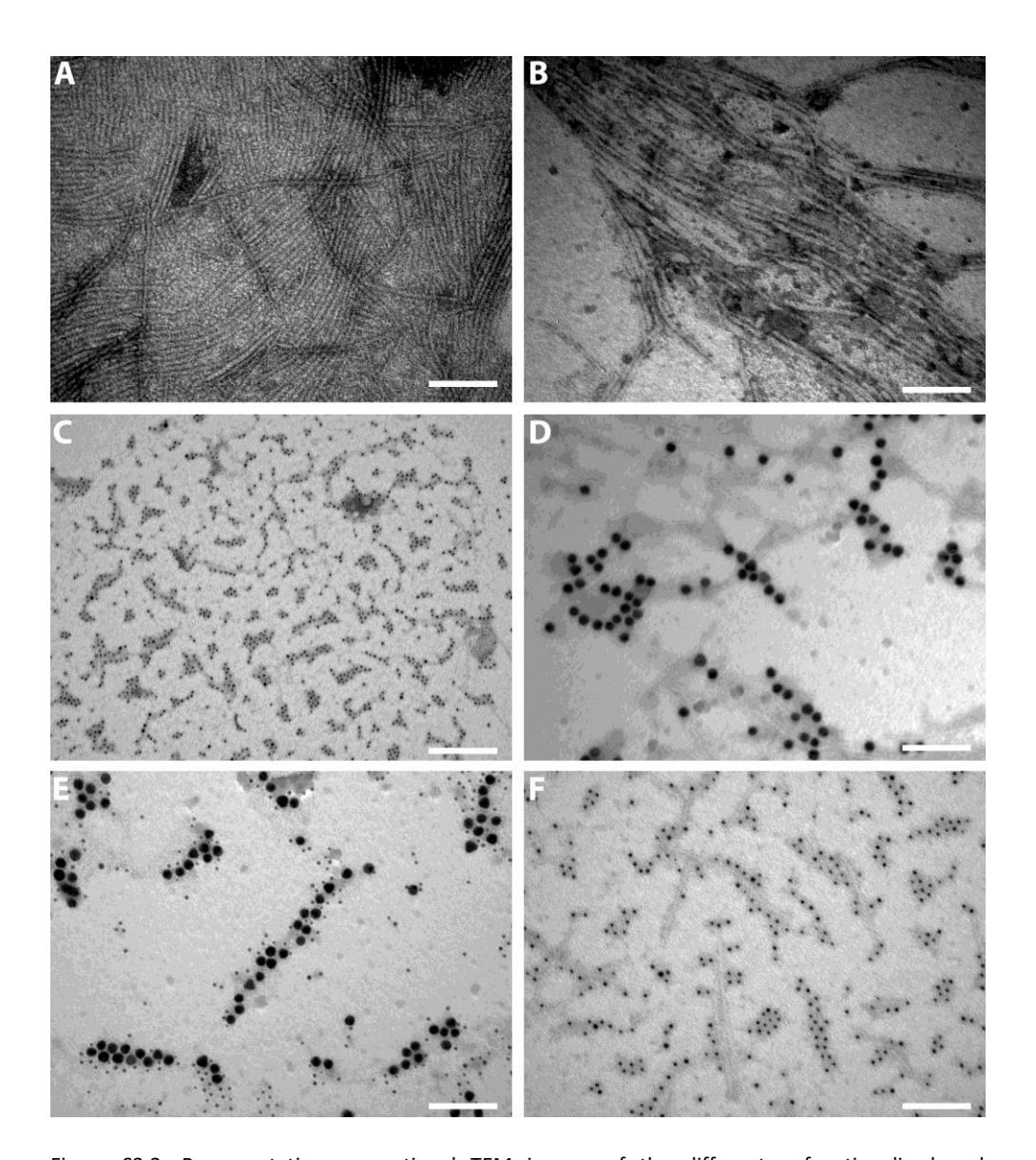


Figure S3.3. Representative conventional TEM images of the different unfunctionalized and functionalized SQ-based supramolecular polymers. A) SQ supramolecular polymers (50  $\mu$ M), B) SQ supramolecular polymers (50  $\mu$ M) mixed with SQ-D1 (0.5  $\mu$ M), C) "Individual Write" SQ supramolecular polymers (50  $\mu$ M) mixed with SQ-D1 (0.5  $\mu$ M) and Au5-D3 (250 nM), D) "Individual Write" SQ supramolecular polymers (50  $\mu$ M) mixed with SQ-D1 (0.5  $\mu$ M) and Au15-D3 (25 nM), E) "Multicomponent Write" SQ supramolecular polymers (50  $\mu$ M) mixed with SQ-D1, SQ-D2 (both 0.25  $\mu$ M), Au5-D4 (540 nM) and Au15-D3 (70 nM), F) "Write-Erase-Rewrite" SQ supramolecular polymers (25  $\mu$ M) rewritten with Au5-D3 (125 nM). Scale bars 100 nm.

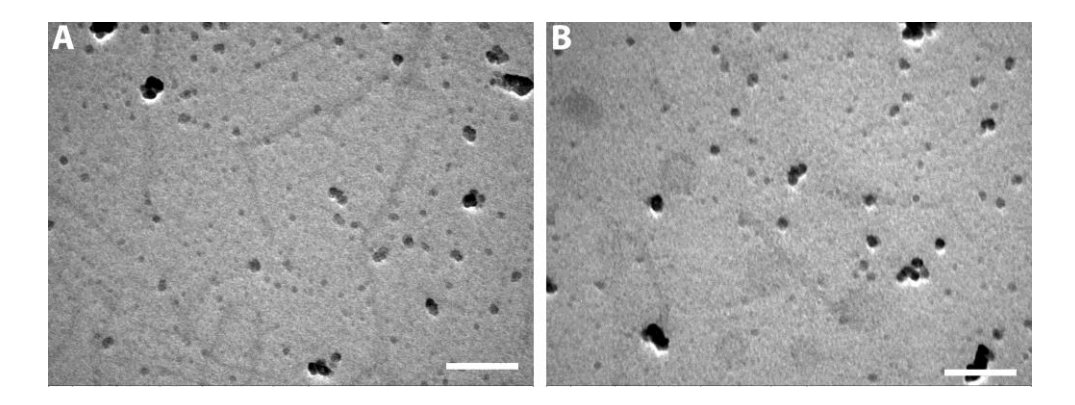


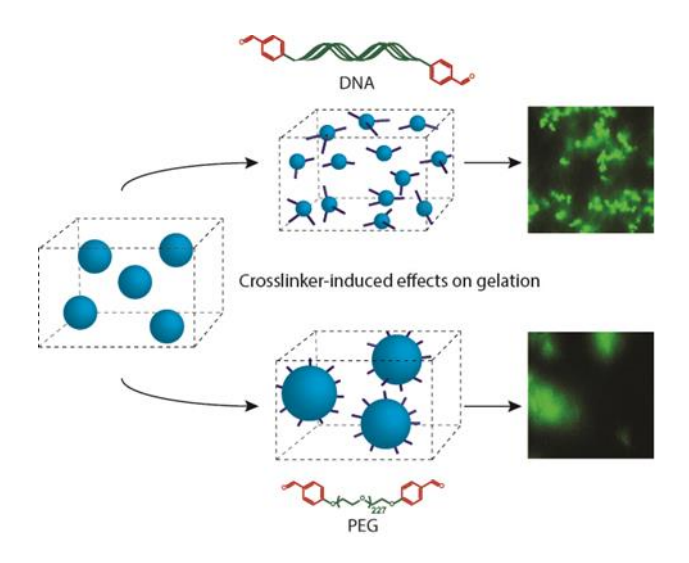
Figure S3.4. Conventional TEM images of unfunctionalized **SQ** supramolecular polymers (**SQ**, 50  $\mu$ M) mixed with A) **Au5-D3** (250 nM) or B) **Au15-D3** (25 nM), respectively, as a control. Scale bars 100 nm.

# 3.6.15 References

1 L. Zou, H. L. Pang, P. H. Chan, Z. S. Huang, L. Q. Gu and K. Y. Wong, Carbohydr. Res., 2008, 343, 2932–2938.

# **CHAPTER 4**

# Crosslinker-induced effects on the gelation pathway of a low molecular weight hydrogel



This chapter was published as an Original Research paper: W. E. M. Noteborn, D. N. H. Zwagerman, V. Saez Talens, C. Maity, L. van der Mee, J. M. Poolman, S. Mytnyk, J. H. van Esch, A. Kros, R. Eelkema, R. E. Kieltyka, Adv. Mater. 2017, 29, 1603769.

# 4.1 Abstract

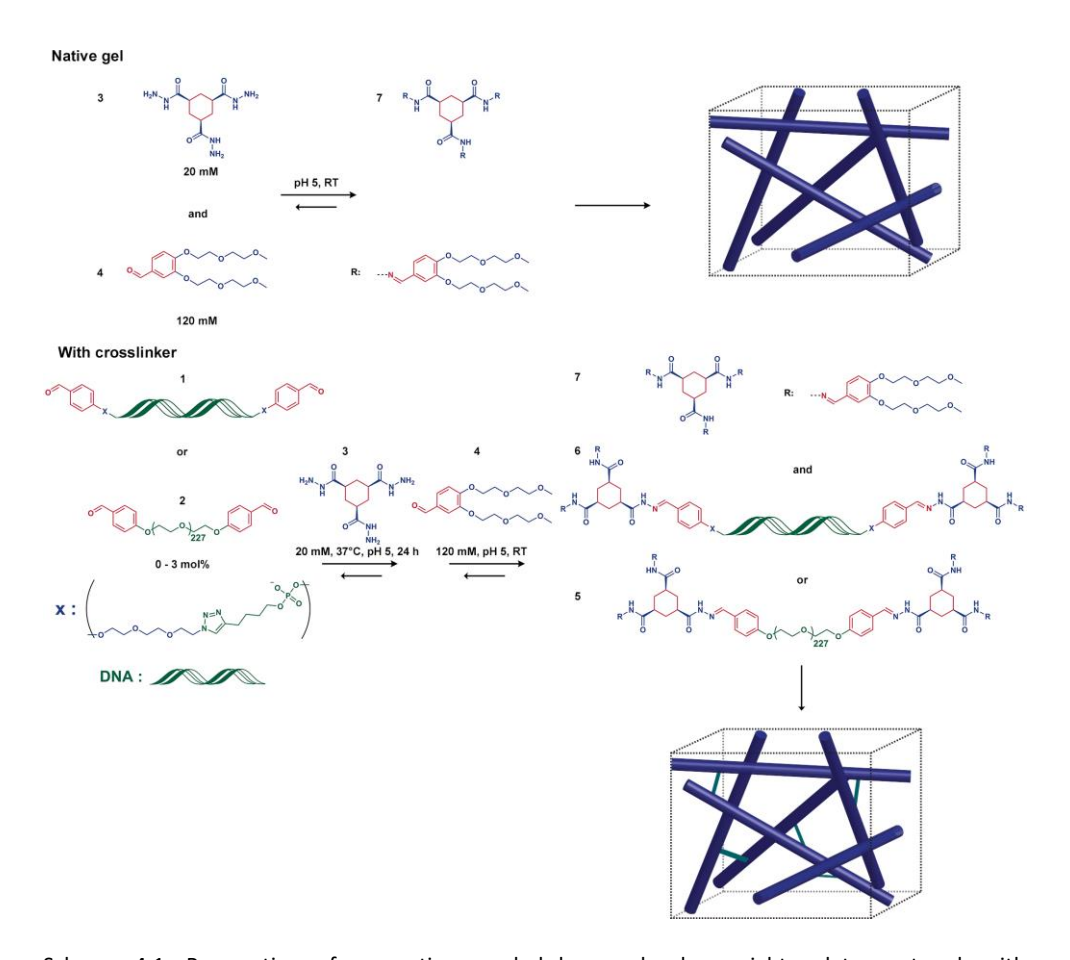
The use of polymeric crosslinkers is an attractive method to modify the mechanical properties of supramolecular materials, but their effects on the self-assembly of the underlying supramolecular polymer networks are poorly understood. Modulation of the gelation pathway of a reaction-coupled low molecular weight hydrogelator is demonstrated using (bio)polymeric crosslinkers of disparate physicochemical identities, providing a handle for control over materials properties.

Keywords: supramolecular materials, self-assembly, hydrogels, microstructures, crosslinkers

#### 4.2 Introduction

The field of supramolecular materials strives to prepare functional scaffolds for a range of applications from biomedicine to electronics. 1-4 Specific properties of these materials such as adaptiveness, responsiveness and recyclability can be ascribed to the supramolecular nature of their interactions over several length scales starting from monomers until the final self-assembled material. However, a caveat of their supramolecular nature is that they are often mechanically weak. 5-9 Several groups have recently disclosed the use of polymeric crosslinkers in supramolecular hydrogel materials composed of fibrillar aggregates to increase their mechanical properties by decoration with matched self-assembling units to the parent assembly or postmodification through covalent or non-covalent crosslinking strategies. 7,10-15 Commonly, the addition of polymeric crosslinkers results in an improvement of the material's mechanical properties, however competition between intra- and interfibrillar crosslinking can occur preventing them from reaching their full mechanical potential.<sup>13</sup> Nonetheless, it can also be envisaged that changes to the underlying supramolecular polymer network may occur when a crosslinker is added, greatly impacting the final material properties.

Supramolecular materials composed of low molecular weight gelators are of interest for use as biomedical materials, <sup>16–21</sup> biosensors, <sup>22,23</sup> optoelectronics <sup>24–26</sup> and personal care products, <sup>27</sup> due to their facile preparation and stimuli-responsive character. The rational design of these molecules remains still nontrivial due to a lack of understanding of how their self-assembly occurs over several length scales to provide a macroscopic material. 28,29 Numerous studies reveal the importance of nucleation and fiber branching events that occur during the self-assembly process on the final gel properties. 6,28,30,31 The primary rate of fiber nucleation determines the amount of nuclei formed and the degree of branching.<sup>30</sup> These processes can dictate both fiber segment length and individual fiber network compactness, in which more overlapping individual fiber networks result in their greater interpenetration to provide stiffer materials. Simple surfactants and polymers that interact with the growing fibers<sup>32</sup> or increase the solution viscosity<sup>33</sup> have been demonstrated to affect these processes variably, with the possibility to increase or decrease mechanical properties of the resultant gel material. Therefore, there is a need to examine the effect of complex functional supramolecular modules on the self-assembly pathways of multicomponent low molecular weight gelating systems to advance their use in numerous applications.



Scheme 4.1. Preparation of a reaction-coupled low molecular weight gelator network with (bio)polymeric crosslinkers under catalytic control. A) The native gel is synthesized in situ by reacting hydrazide (3) and aldehyde (4) at pH 5 at room temperature. B) The biopolymeric crosslinked hydrogel is synthesized in situ by reacting 5'-bisaldehyde functionalized dsDNA (20-mer) 1 or PEG 2 crosslinker (0-3 mol%), hydrazide 3 (20 mM) over 24 hours, and then aldehyde 4 (120 mM) at pH 5 leading to native or crosslinked gel networks.

Supramolecular materials formed by reaction-coupled self-assembly<sup>34–36</sup> provide an additional handle to control primary nucleation and fiber branching phenomena of low molecular weight hydrogelators by relying on reaction rate of the components. Van Esch and Eelkema reported the reaction-coupled self-assembly of a supramolecular hydrogel material by reacting a cyclohexane trishydrazide (hydrazide, compound 3) and three aldehyde-containing bis(diethylene glycol) benzaldehyde (aldehyde, compound 4) wedges to form 7, whose subsequent gelation pathway was affected by the nature of the catalyst used.<sup>36</sup> A comparison of the hydrazone-forming reaction between gelator components at pH 5 and 7 showed distinct changes in the

mechanical properties of the network consistent with differences in the hydrogel microstructure, thus demonstrating the importance of reaction rate on this process. In order to exploit such reaction-coupled materials for biomedical applications, control over mechanical properties and ligand presentation becomes important. We became thus interested in studying the effect of various (bio)polymeric crosslinkers on the self-assembly process of this reaction-coupled hydrazide-aldehyde gelator into hydrogel materials as a model system (Scheme 4.1). We selected duplex DNA (1), which acts as a stiff, negatively charged rigid rod below its persistence length (P = 50 nm, 150 bp)<sup>37</sup> ideal for the construction of (nano)materials,<sup>38–40</sup> and compared it against a soft, neutral poly(ethylene glycol) polymer (P = 0.37 nm<sup>41</sup>, 10 kDa) (2) of comparable size. Aldehyde moieties were specifically incorporated at the terminal ends of the (bio)polymers (1 and 2) to introduce them during the self-assembly of the reaction-coupled network composed of 3 and 4. We examined the effect of these two crosslinkers on the gelation of the reaction-coupled monomers into hydrogels over several length scales and compared their resultant materials properties.

#### 4.3 Results and discussion

To chemically ligate either DNA (20-mer, length  $\approx$  6 nm) or PEG (Mn = 10 kDa, Rh  $\approx$  3 nm)<sup>42</sup> crosslinkers to the hydrazide-aldehyde network, we first introduced aldehyde moieties synthetically at their terminal ends by polymer-specific approaches. Moreover, circular dichroism and thermal denaturation studies of the crosslinker 1 showed similar B-DNA characteristics to the unfunctionalized duplex (for detailed synthesis and characterization see Supporting Information). Originally, the hydrazide-aldehyde two-component hydrogel system was formed using a one-pot synthetic strategy by mixing hydrazide 3 and aldehyde 4 in a 1:6 molar ratio (20 mM 3: 120 mM 4) in 0.1 M phosphate buffer at pH 5 to yield a self-assembled network of 7 on the order of minutes.<sup>43</sup> Therefore, concentration and ratio of aldehyde and hydrazide were conserved to maintain their rate of reaction<sup>36</sup> and the effect of reaction time of crosslinkers 1 or 2 with 3 on the formation of the hydrogel network was probed in the present work.

Using oscillatory rheology, a self-assembly protocol was developed where crosslinkers **1** and **2** were required to be first individually reacted with **3** for 24 hours at 37 °C, and then mixed with **4** at room temperature. As a first attempt, a similar one-pot

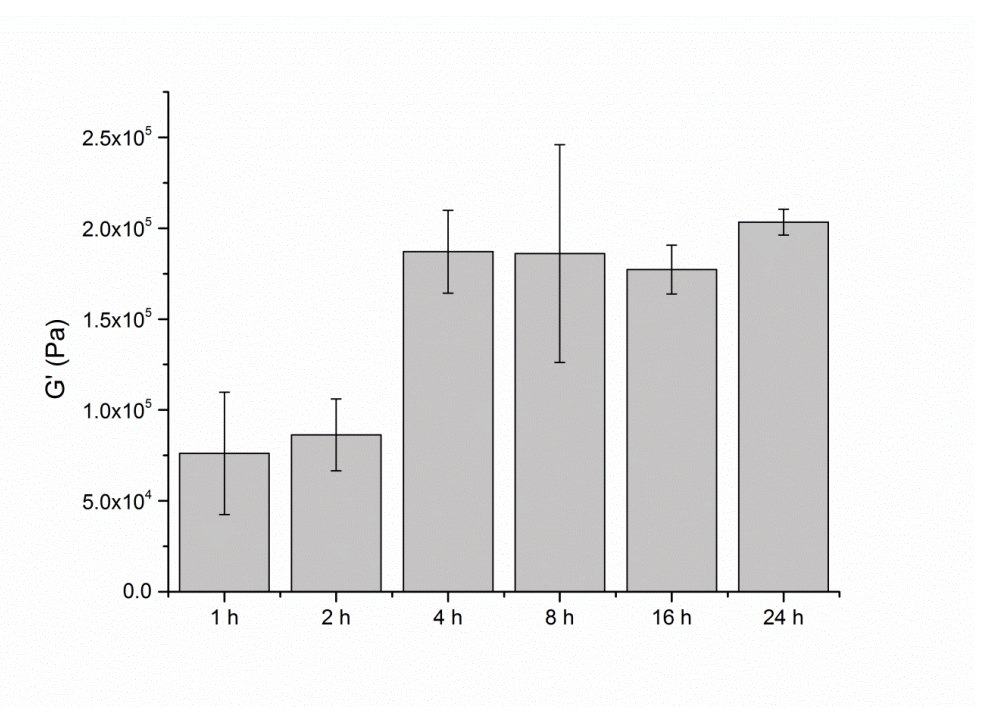


Figure 4.1. Oscillatory rheology measurements of reaction-coupled hydrogels containing 1 mol% DNA crosslinker 1 measured after different incubation times (1-24 hours) of 5'-bisaldehyde dsDNA 1 with 3, showing increased reaction times result in an increase in mechanical properties.

was used to prepare the self-assembled LMWG network with DNA where 1 mol% of 1 (relative to 3) was mixed with 3 (20 mM), and then immediately with 4 (120 mM) in 0.1 M phosphate buffer with 0.1 M NaCl. However, this mixing method did not result in an increase in mechanical properties or altered rheological kinetics after mixing with 4, suggestive of slower hydrazone formation. In order to facilitate multicomponent reaction-driven self-assembly with the biopolymeric crosslinker 1, it was required to be first reacted in an equimolar ratio with 3 at 37 °C to synthesize the labeled 5'-hydrazide duplex. The effect of reaction time on the incorporation of DNA into the self-assembled network was probed by oscillatory rheology (Figure 4.1). The relative storage (G') and loss (G") moduli of the final self-assembled material were followed as a function of the reaction time between the DNA crosslinker 1 and the hydrazide 3 at 37 °C, ranging from 1 to 48 hours. The addition of 4 to a mixture of 1 and 3 on the rheometer plate resulted in the rapid onset of rheological profiles synonymous with a viscoelastic material, where the storage (G') modulus was greater than the loss modulus (G''), in time sweep experiments. Whereas reaction times between 1 and 3 of up to two hours showed up to a two-fold increase in G' compared to the native LMW hydrogel, a 4-fold in-crease in storage modulus was observed for reaction times ranging from 4 to 16 hours. Furthermore, samples reacted for 24 hours repeatedly showed the highest mechanical stiffness with a 4.5-fold average increase. Therefore, a reaction time of 24 hours was used to first couple either crosslinker 1 or 2 with 3, and then 4 was added to start the reaction-coupled self-assembly process for all subsequent experiments. This protocol was further supported by a combination of MALDI-TOF-MS (Figure 4.2), gel electrophoresis (crosslinker 1) (Figure 4.3) and NMR (crosslinker 2) (Figure 4.4) studies over the various reaction steps to form the low molecular weight gelator material showcasing the potential for incorporation of the (bio)polymeric crosslinkers into the reaction-coupled network.

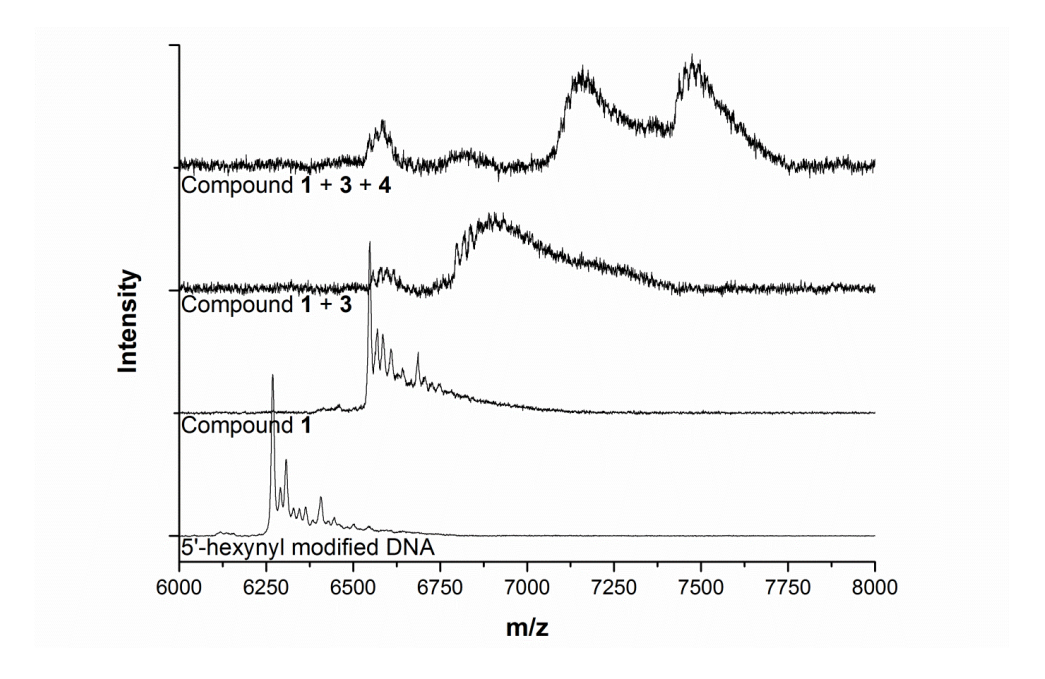


Figure 4.2. MALDI-TOF-MS characterization following the stepwise chemical ligation of all components to form decorated DNA crosslinker 5: unmodified 5'-hexynyl ssDNA is coupled with a heterobifunctional oligo(ethylene glycol) with benzaldehyde and azide moieties by copper catalyzed 1,3-dipolar cycloaddition providing 5'-aldehyde functionalized ssDNA, which is then reacted with 3 for 24 hours at 37° C providing 5'-hydrazide functionalized ssDNA, and further reaction with 4 at 37°C yields a ssDNA version of crosslinker 5.

The electrophoretic mobility of the unpurified dsDNA after each consecutive reaction step and centrifugal ultrafiltration was compared at the various concentrations based on those used in subsequent gel experiments. Samples based on 1.0, 2.0 and 3.0 mol% 5'-bisaldehyde dsDNA (Figure 4.3, lanes 5, 7, 9) after a 24-hour reaction period with **3** all showed the presence of two higher molecular weight species, suggestive of the formation of the 5'-mono- and bishydrazide functionalized

dsDNA. Further retardation of these bands is observed when aldehyde **4** is added to the 5'-hydrazide dsDNA to form crosslinker **5** and various intermediate products (Figure 4.3, lanes 6, 8, 10).

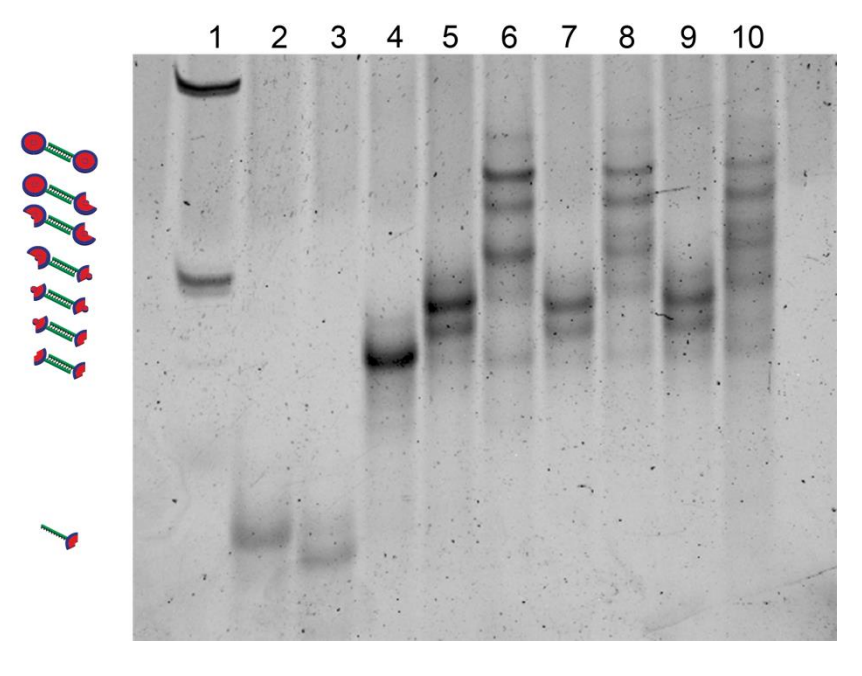


Figure 4.3. Polyacrylamide gel electrophoresis (20%) shows the stepwise formation of the DNA-LMWG **5** by hydrazone formation of **1** with **3**, and then **4** at pH 5. Individual 5'-benzaldehyde ssDNA conjugates (lanes 2 and 3, respectively) are hybridized to form dsDNA crosslinker **1** (lane 4). Addition of 20 mM **3** results in decreased gel mobility for 1.0 mol% (lane 5), 2.0 mol% (lane 7) and 3.0 mol% (lane 9) upon reaction with **1**. Compound **4** is then added to form the DNA crosslinker **5** (lane 6, 8, and 10).

Once the reaction conditions were optimized for hydrazone formation of the various components (DNA 1 or PEG 2 crosslinkers combined with hydrazide 3, and then aldehyde 4) at pH 5, the effect of reacting physicochemically distinct (bio)polymeric crosslinkers into the reaction-coupled supramolecular materials was explored. Oscillatory rheology was employed as a first approach to probe mechanical differences in the variably crosslinked materials, by examining time sweep profiles and comparing their final gel properties. Reaction of 3 (20 mM) and 4 (120 mM) in a 1:6 molar ratio without any added crosslinker provided a hydrogel material, which started to gelate with a steep increase after 7 minutes and showed a maximum storage modulus (48 ± 8 kPa) after 50 minutes. Gelation using the 5'-bisaldehyde dsDNA crosslinker 1 resulted in variable changes in mechanical properties of the LMWG network, relative to the native network, depending on the amount of DNA

added (Figure 4.6A). When 1 mol% of crosslinker  ${\bf 1}$  was added to the reaction-coupled assembly, a maximum in the mechanical properties was recorded with a striking 4.5-fold increase in storage modulus (209  $\pm$  8 kPa). In this case, gelation started earlier, after 5 minutes, with an initial steep increase followed by a slower increase in the later stages and reaching a maximum in its storage modulus after 90 minutes. However, using a larger relative amount of DNA crosslinker  ${\bf 1}$  (3 mol%), the onset of gelation was strongly retarded, only starting after 20 minutes and showing a shallow increase in mechanical stiffness over the measuring range. A plateau was not detected, however the maximum storage modulus (36  $\pm$  6 kPa) attained after 100 minutes was slightly below the native hydrazide-aldehyde hydrogel (48  $\pm$  8 kPa).

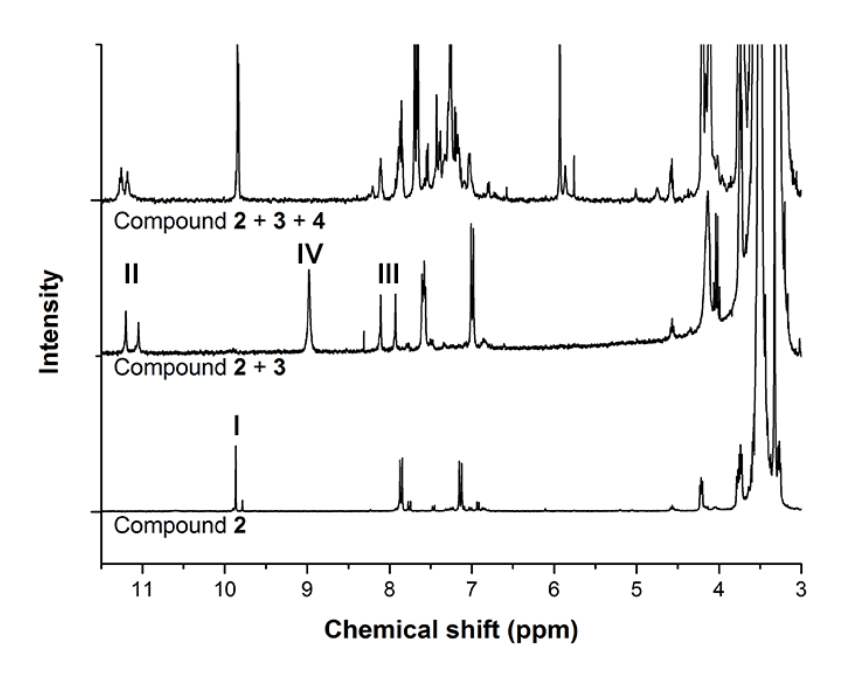


Figure 4.4. NMR characterization of the stepwise hydrazone reactions of PEG bisbenzaldehyde crosslinker 2. Reaction of aldehyde functionalized PEG-based crosslinker 2 by 24 hour incubation at 37 °C with **3** shows the disappearance of the aldehyde peak I (9.87 ppm) and appearance of characteristic hydrazone bond peaks at II (11.20 ppm) and III (7.93 ppm). Subsequent addition of **4** at 37° C results in the formation of crosslinker **6** as evidenced by the disappearance of the hydrazide protons at IV (8.98 ppm).

As a control, a 5'-aldehyde functionalized ssDNA was hybridized with its complementary sequence bearing no reactive group at its 5'-end to compare its effect on the reaction-coupled self-assembly of the hydrazide-aldehyde gelator system

relative to crosslinker **1**. The asymmetrically functionalized dsDNA when added at 1 mol% to **3**, and then reacted with **4** to form the hydrazide-aldehyde hydrogel resulted in materials of lower mechanical stiffness ( $120 \pm 20 \text{ kPa}$ ). When 5'-aldehyde ssDNA was reacted with **3**, and then **4**, materials of even lower mechanical stiffness (ssDNA:  $60 \pm 12 \text{ kPa}$ ) were synthesized relative to those with crosslinker **1**, but the storage modulus was still greater than the native gel (Figure 4.5). To better understand the effect of DNA on the network, an endonuclease operative at pH 5, DNasell, was added to the 5'-bisaldehyde dsDNA crosslinker **1** with **3** for 24 hours prior to the addition of **4** to form the hydrogel network. The storage modulus of the obtained hydrogel with 1 mol% of **1** was reduced by half, indicative of enzymatic degradation of the DNA crosslinks (Figure 4.6C). However, the storage modulus after enzyme addition was still greater than that of a native gel.

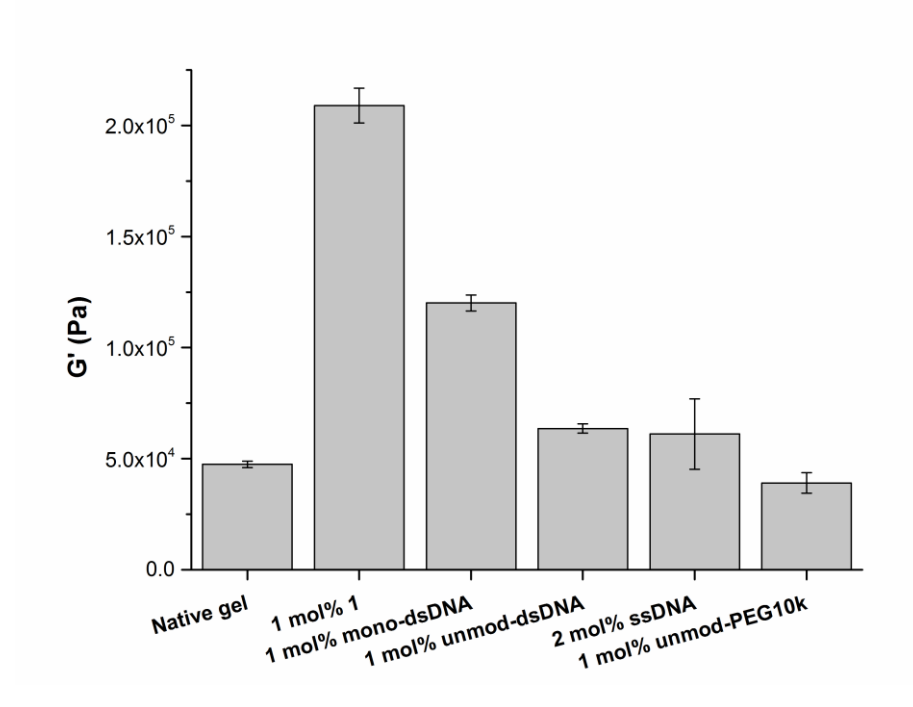


Figure 4.5. Oscillatory rheology measurements of **3** (20 mM) and **4** (120 mM) gels with various DNA and PEG crosslinkers as controls.

Much to our surprise, based on earlier reports of PEG-based crosslinkers<sup>11,13,15</sup> enhancing properties of supramolecular hydrogels, crosslinker **2** showed a decrease in mechanical (Figure 4.7B) properties over the entire concentration range as examined for DNA with an even greater negative impact on the modulus of the material when increasing its concentration. For example, addition

of 1 mol%  $\bf 2$  directly resulted in weaker materials in comparison to the native gel with a storage modulus of 29  $\pm$  9 kPa (Figure 4.6B), despite a slightly earlier onset of gelation at 6 minutes with a sigmoidal profile. Overall, these results indicate that the physicochemical characteristics of the crosslinker and its concentration can have important consequences on the rate of low molecular weight hydrogel formation, and its final mechanical properties. However, based on evidence from control samples and enzymatic degradation, the incorporation of the various crosslinkers into the network does not entirely account for the changes observed in the mechanical properties. Therefore, insight into the effect of the crosslinkers on the reaction-coupled self-assembly process needs to be considered.

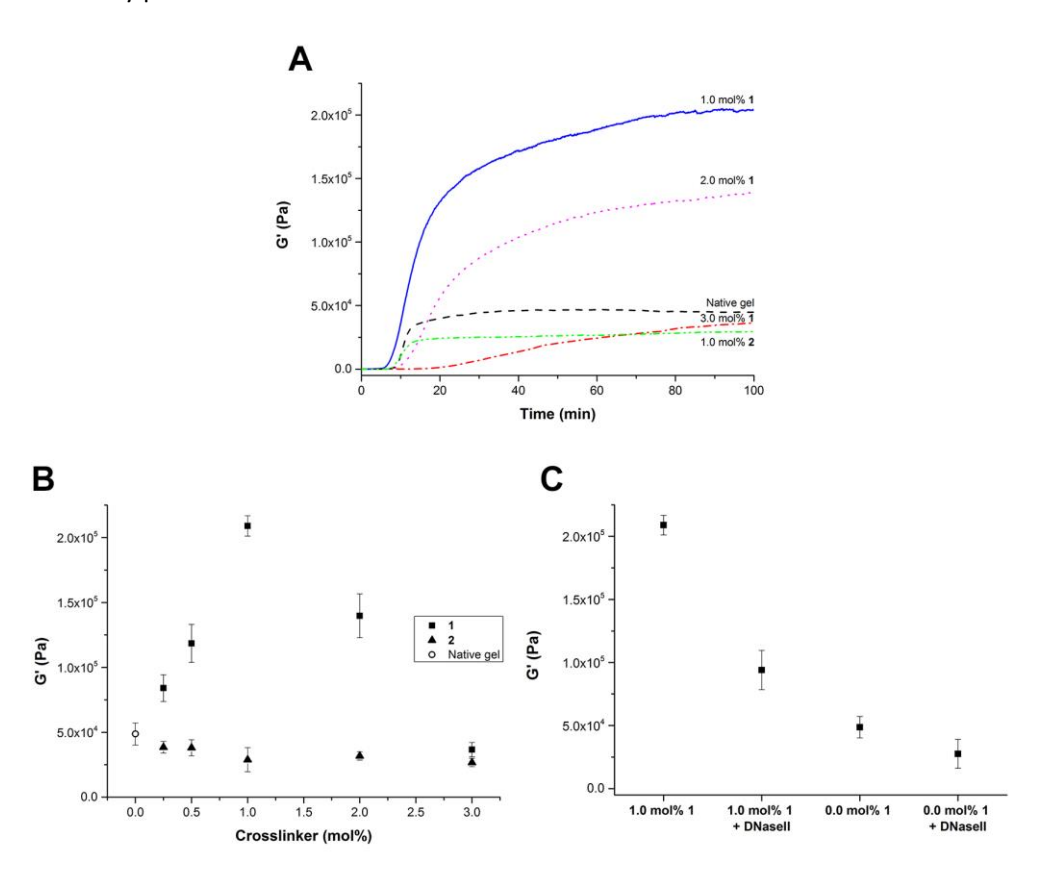


Figure 4.6. Oscillatory rheology data of reaction-coupled hydrogels with various crosslinkers at pH 5. (A) Time sweep measurements with **1** (native gel: black dashed, 1 mol%: blue continuous, 2 mol%: pink dotted, 3 mol%: red dash-dot) and **2** (1 mol%: green dash-dot-dot) at 0.05% strain, 1 Hz frequency. (B) Comparison of maximum measured storage moduli (*G'*) of hydrogels containing DNA **1** (squares) and PEG **2** (triangles)-based crosslinkers as a function of concentration. (C) Comparison of mechanical properties after degradation of 5'-bisaldehyde dsDNA crosslinks with DNasell prior to the start of reaction-coupled assembly with **3**.

Low molecular weight hydrogel formation is majorly governed by the kinetic rate of fiber formation and percolation, which is dictated by nucleation, branching and growth.<sup>30</sup> The dimensionality of fiber growth and branching in the presence of various crosslinkers using the Avrami equation before the onset of network percolation can be measured using the complex modulus, G\*, in the early stages of the rheological profile with respect to time (see supporting information Figure S4.5). The dimensionality of growth can then be assessed by solving for the Avrami coefficient. 44 Fitting the Avrami equation for the native hydrogel system lacking any crosslinker resulted in n = 1.31, suggestive of branched fibrillar growth. Addition of 1.0 mol% stiff DNA crosslinker 1 yields n = 1.70, indicating a higher degree of fiber branching. Conversely, the use of 3.0 mol% 1 results in a value of n = 0.76, which suggests one-dimensional or even growth that is hindered by the elimination of branching events. Analysis of the addition of 1.0 mol% 2 provides an n = 1.02, also suggestive of one-dimensional unbranched growth. Collectively, the Avrami coefficients suggest a strong influence of the crosslinker identity on the nucleation and fiber formation processes.

Scanning electron (SEM, Figure 4.7), confocal laser scanning (CLSM, Figure 4.7) and cryogenic-transmission electron (cryo-TEM, Figure 4.8) microscopies were used to gain insight into the hydrogel micro- and nanostructure with the various crosslinker concentrations to better understand the origin of the observed mechanical properties of the crosslinked materials. In the case of the native (compound 3 and 4 only) and 1.0 mol% DNA gels, dense, thin, highly branched fiber networks were observed by SEM (Figure 4.7 A,B) and CLSM in the hydrated state, albeit at a lower magnification (Figure 4.7 E,F). CLSM samples were stained with Nile Red (6.25 μM), a lipophilic dye to visualize the hydrophobic interior of the aggregates. Conversely, less dense, thicker fibrils alongside spherical aggregates were found upon increasing the DNA content to 3 mol% (Figure 4.7 C,G), whereas the addition of 1.0 mol% PEG-based crosslinker 2 resulted in a lack of well-defined fibrillar features with a larger surface in comparison to the native and 1.0 mol% DNA gel (Figure 4.7 D,H). These images suggest that low concentrations of 1 (≈ 1 mol%) support growth of long interpenetrating fiber networks, while higher concentrations of 1 or the addition of 2 trigger the formation of smaller, spherical or collapsed networks respectively, with either scenario abolishing the rheological properties of the material. Subsequently, cryo-TEM images were made of the various crosslinked gels to examine the effect of the added polymer on the fibrillar architecture after self-assembly (Figure 4.8). Near micron-long fibers were imaged in all samples. These results suggest that formation of

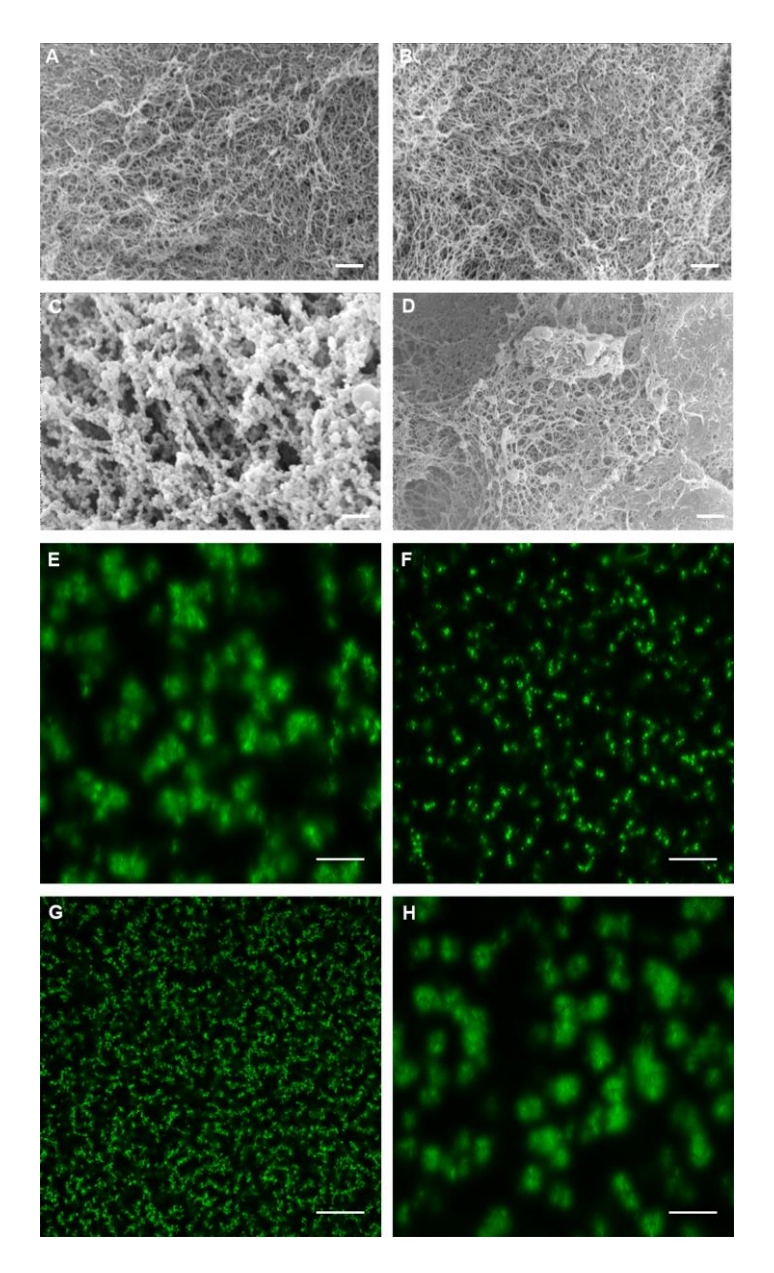


Figure 4.7. Visualization of the effect crosslinkers  ${\bf 1}$  and  ${\bf 2}$  on the reaction-coupled aldehydehydrazide hydrogel microstructure by scanning electron (SEM) and confocal laser scanning (CLSM) microscopies. A-D: Scanning electron micrographs of hydrogels (A) without crosslinker, (B)  ${\bf 1}$  mol%  ${\bf 1}$ , (C)  ${\bf 3}$  mol%  ${\bf 1}$  and (D)  ${\bf 1}$  mol%  ${\bf 2}$ . All SEM samples were prepared by critical point drying. Scale bar is  ${\bf 1}$   ${\bf 1}$   ${\bf 1}$  mol. E-H: Confocal laser scanning micrographs of hydrogels (E) without crosslinker, (F)  ${\bf 1}$  mol%  ${\bf 1}$  (G)  ${\bf 3}$  mol%  ${\bf 1}$  and (H)  ${\bf 1}$  mol%  ${\bf 2}$ . All CLSM samples were prepared in the presence of Nile Red (6.25  ${\bf \mu}$ M) as a fluorescent probe.  $\lambda_{\rm ex}$  = 488 nm, scale bar is 50  ${\bf \mu}$ m.

fibers at the nanoscale remains unaffected regardless of the crosslinker used, but highlights the importance of the assembly processes that occur at larger length scales. Therefore, both SEM and CLSM images of the supramolecular hydrogel microstructure with the various crosslinkers support the mechanical data obtained by oscillatory rheology.

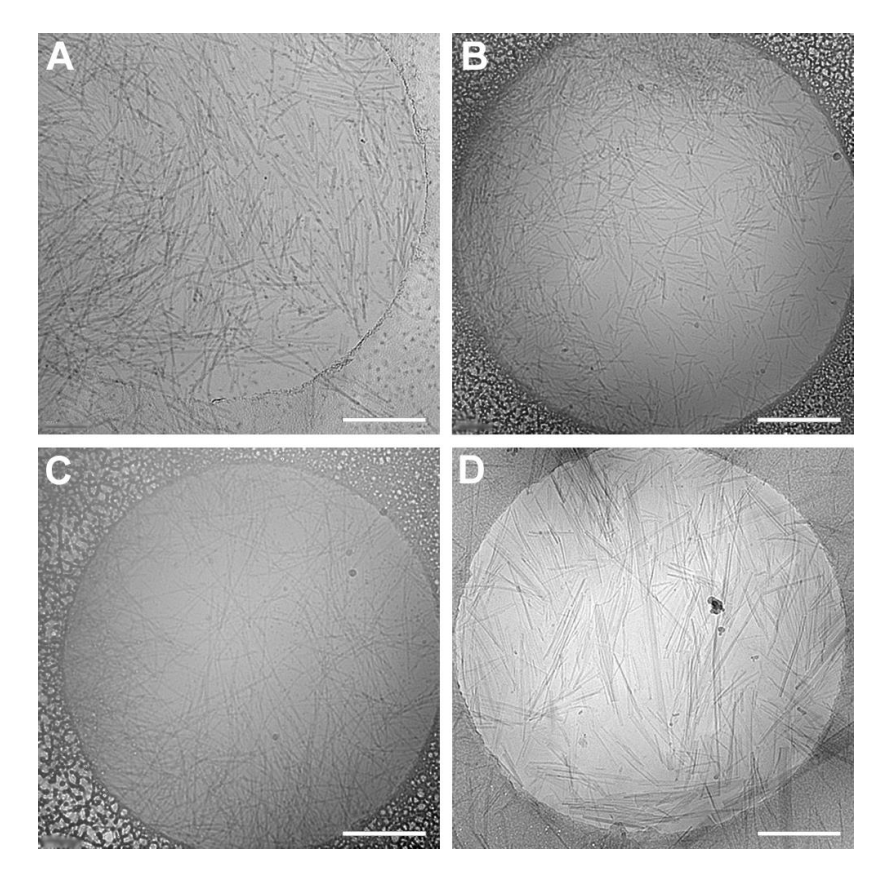


Figure 4.8. Cryo-TEM images of various hydrogel suspensions showing fiber formation under all conditions: a) hydrogel without any crosslinker, b) 1.0 mol% 1, c) 3.0 mol% 1, d) 1.0 mol% 2. Scale bars are 500 nm.

Intrigued by the influence of the various crosslinkers on the hydrogel microstructure, their unique gelation profiles and mechanical properties measured by oscillatory rheology, we sought to investigate the process of network formation in real-time by confocal laser scanning microscopy (CLSM, Figure 4.9). In the case of the native gel, addition of compound **4** (120 mM) to **3** (20 mM) with Nile Red displayed the initial formation of an emulsion with droplets of an average size of 2.87  $\pm$  0.42  $\mu$ m after 5 minutes (Figure 4.9A, 5 min), whereas no observable aggregate structures for **3** 

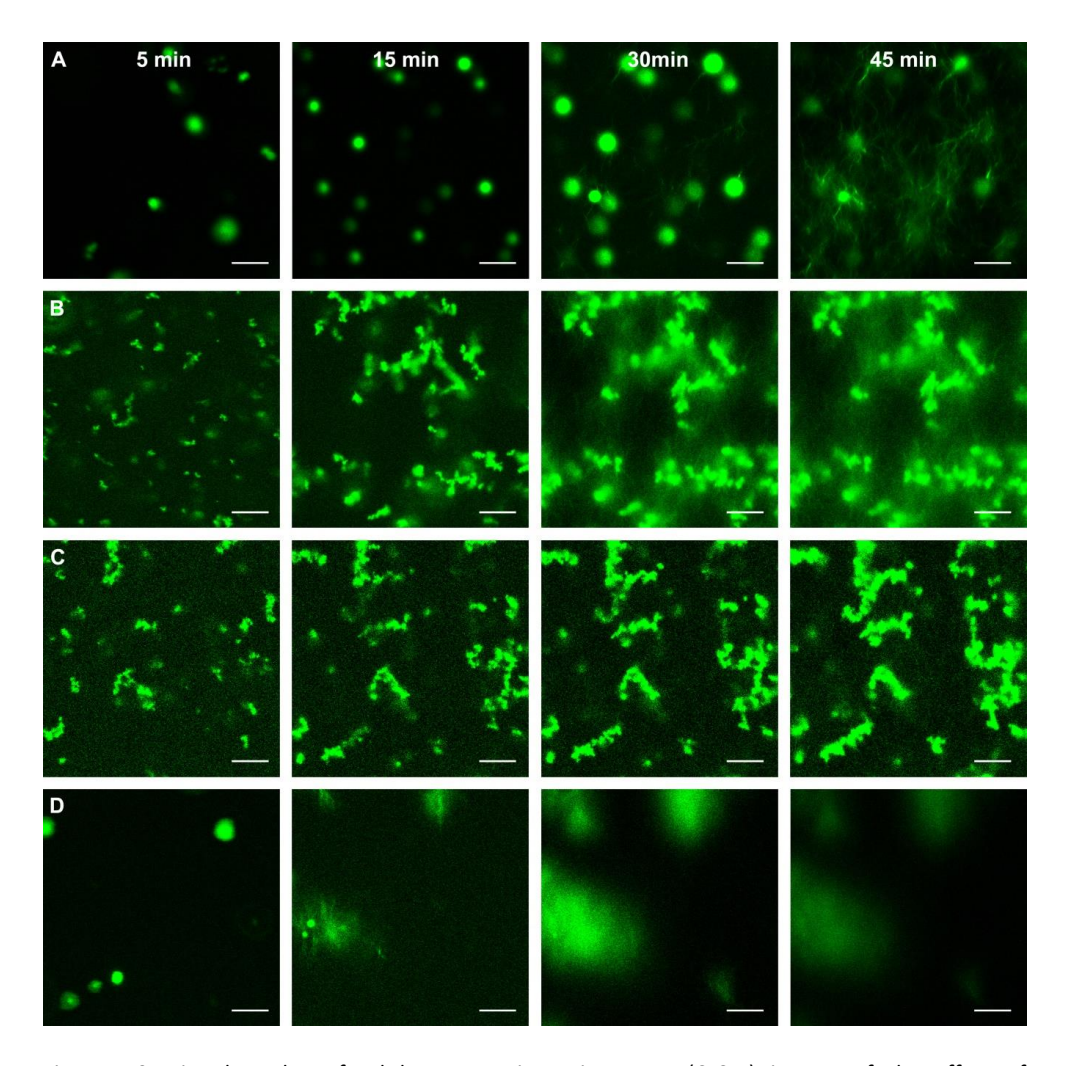


Figure 4.9. Time-lapsed confocal laser scanning microscopy (CLSM) images of the effect of crosslinkers  $\bf 1$  and  $\bf 2$  on the reaction-coupled self-assembly of the aldehyde-hydrazide hydrogel. Images of the various hydrogels were taken at various time points (5, 15, 30 and 45 minutes) after 24 hour incubation of  $\bf 1$  or  $\bf 2$  with  $\bf 3$ , and subsequent addition of  $\bf 4$  in the presence of Nile Red (6.25  $\mu$ M): (A) bare gel (B),  $\bf 1$  mol%  $\bf 1$  (C),  $\bf 3$  mol%  $\bf 1$  or (D)  $\bf 1$  mol%  $\bf 2$ . Scale bar is 10  $\mu$ m. Full videos can be found in supporting information (Movies S1-4).

were found by CLSM under the same conditions. Subsequently, depletion of the droplets was observed with the onset of fluorescent protrusions suggestive of fiber bundles evolving into a densely connected network, as observed previously in fully gelated samples by SEM (Figure 4.9A, 15-45 min, Movie S1). By acquiring images every 10 s by confocal microscopy, it became clear that these droplets served as nucleation centers for the subsequent growth of the network, and the addition of a particular

crosslinker affected their size and surface properties biasing the outcome of the gelation pathway of the reaction-coupled gelator. The addition of 1 mol% of 1 resulted in a decrease in the size of the individual droplets to 1.19 ± 0.26 µm, but an increase in their number after 5 min, and eventually flocculating prior to evolution of the fibrillar network based on the diffuse fluorescence emanating from the individual droplets (Figure 4.9B, Movie S2). When the concentration of 1 was increased to 3 mol%, the number of droplets increased to a greater extent with a decrease in size to 0.65 ± 0.15 µm after 5 min (Figure 4.9C, 5 min). The aggregates then clustered together becoming brighter and slightly larger in appearance, yet lacked the presumed formation of an extensive network similar to the connected spherical structures observed by SEM (Figure 4.9C, 15-45 min, Movie S3). As a control, the addition of 1 mol% asymmetrically modified crosslinker 1 did result in small droplets similar to those observed with the fully functionalized crosslinker 1. However, droplets functionalized with asymmetrically modified 1 did not show flocculation (Movie S5), suggesting that a doubly functionalized DNA crosslinker is required to induce their bridging. In contrast, the addition of 1 mol% 2 resulted in the appearance of larger spheres with a size of  $4.05 \pm 0.78 \, \mu m$  after 5 min, that became less regular and dense during the self-assembly process and eventually forming a discontinuous network in comparison to the native gel (Figure 4.9D, Movie S4). Dynamic light scattering (DLS) measurements supported the observed changes in size by CLSM when crosslinker 1 or 2 is added to 4 (Figure 4.10). Moreover, concentrationdependent DLS measurements of4 supported the presence of large aggregates with emulsion-like behavior (Figure 4.11). In all cases, the droplets were stable over the course of an hour as long as the hydrazide pre-monomer 3 was absent.

Most likely, the addition of the negatively charged DNA crosslinker to the droplet surface of pre-monomer 4 increases its charge and thereby reduces its size in parallel with increasing the concentration of the DNA crosslinker. However, the electrostatic stabilization of the droplets is short-lived with the addition of 3 resulting in flocculation occurring during the formation and crosslinking of the network. In the case of 1 mol% DNA, the crosslinker exerts a positive effect on network formation through increased nucleation sites, extensive fibrillization and formation of a robust crosslinked network due to its stiff and charged character, whereas its addition up to 3 mol% seems to prevent extensive fibrillar growth due to smaller droplet sizes. In the case of the PEG crosslinker 2, larger stable spherical aggregates are formed with steric stabilization of the pre-monomer droplets of 4 by the soft and neutral polymer, but they are fewer in number relative to the native gel. This decrease in nucleation centers increases their distance, therefore decreasing the potential for the clusters of

self-assembling fiber bundles to interpenetrate to form a strong network. Taken together, these results highlight that the crosslinker not only serves to reinforce the gelator network, but also its physicochemical properties can influence the early stages of the reaction-coupled gelation pathway; with both phenomena impacting the final network microstructure.

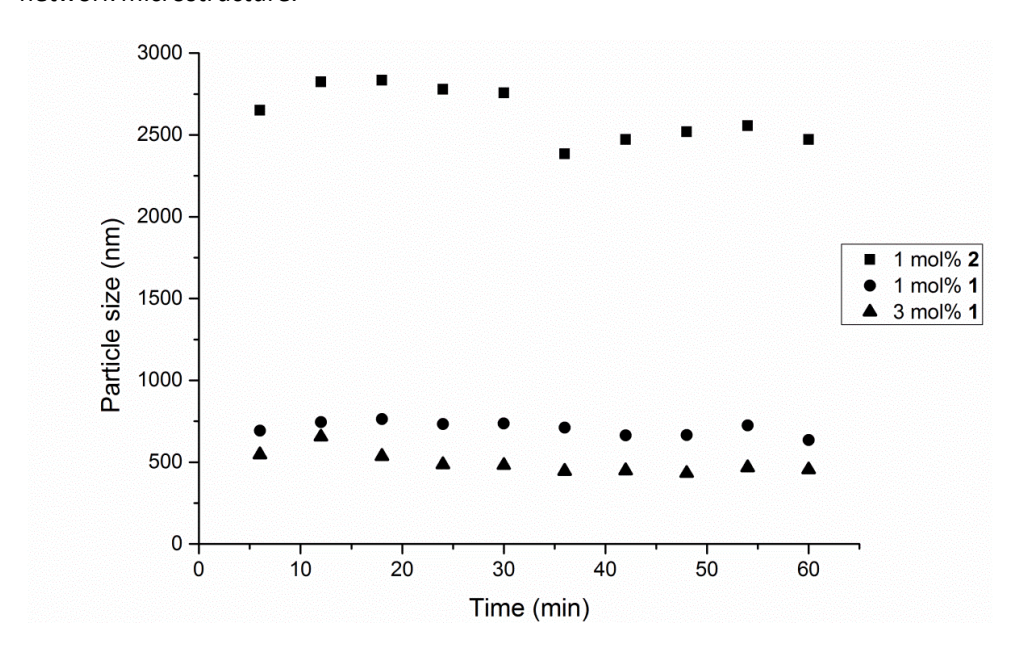


Figure .4.10. Time dependent particle size stability of various mole percentages of 1 or 2 with 4.

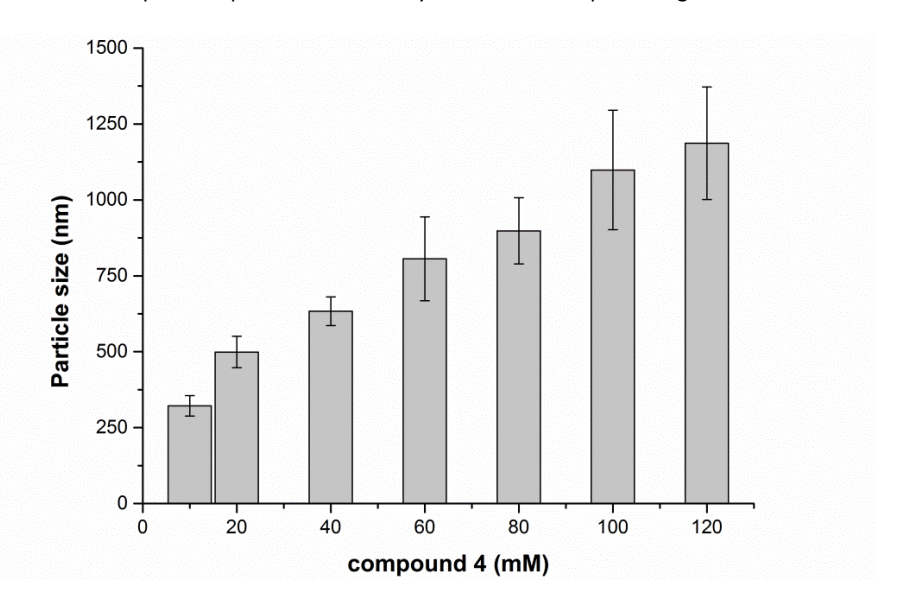
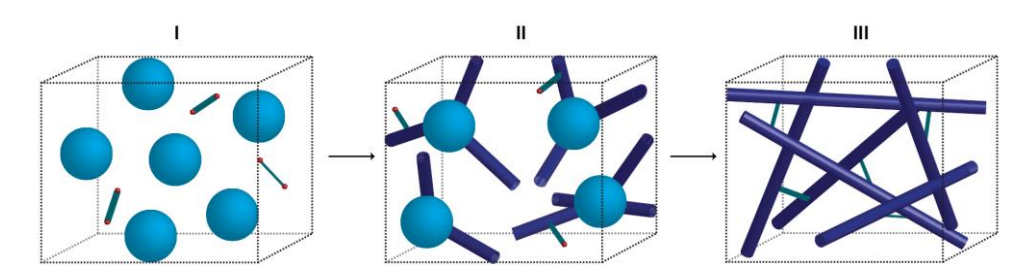


Figure 4.11. Particle size determination of **4** at various concentrations.

#### 4.4 Conclusions

The use of polymeric crosslinkers is an attractive strategy to control the properties of supramolecular polymer networks because of its facile nature. However, this method of modulating the materials properties can prove more complex as not all crosslinkers are equivalent in how they can interact with the scaffold monomers during their selfassembly process. We have shown that the incorporation of a stiff negatively charged DNA crosslinker results in the tunable increase of mechanical properties at low crosslinker concentrations (1 mol%) by oscillatory rheology. Importantly, a two-fold increase was observed for the 5'-bisaldehyde DNA crosslinker over the 5'monoaldehyde DNA crosslinker, suggestive of its incorporation into the hydrogel material as a crosslinking moiety. Alternatively, the addition of a soft and neutral PEGbased crosslinker at the same concentration or DNA at a greater concentration than 1 mol% results in samples that show decreased mechanical stiffness relative to the native material when added at the start of the self-assembly process. We used realtime imaging by CLSM (Movies S1-4) to gain insight into the formation of the reactioncoupled low molecular weight hydrogels in the presence of a given crosslinker due to the recent interest in the early stages of the self-assembly process on various supramolecular polymers and hydrogelators. 45-48 Importantly, we found that in addition to functioning as a crosslinker of the network, adding a crosslinker also modulates the size and surface chemistry of the spherical aggregates that act as depots of unreacted building block 4, dictating the self-assembly pathway of the low molecular weight gelator material over the various stages of nucleation, fiber growth and bundling (Scheme 4.2).



Scheme 4.2. Schematic representation of network formation of 1 or 2 with 3 and 4 over time, in which spherical aggregates of 4 (light blue) act as nucleation centers (I) for fibrillar growth (dark blue) incorporating the physicochemically distinct crosslinker moieties (green/red) (II) to form an interpenetrated network (III) and macroscopic hydrogel material.

The overarching goal to prepare modular, functional supramolecular materials for a broad range of applications requires the incorporation of tethered (bio)molecules or polymers with a wide variety of chemical and physical properties. Based on our results, careful consideration of the physicochemical features of the functional cargo becomes critical due to its potential for interaction with the early stage assemblies during the self-assembly process and its effect on the mechanical properties of the final material. Although caution must be exercised to provide an adequate balance between functionality and scaffold integrity in these reaction-coupled non-covalent materials for their widespread application, this work reveals new opportunities for control over their properties.

#### 4.5 References

- 1 T. Aida, E. W. Meijer, S. I. Stupp, Science 2012, 335, 813.
- 2 X. Du, J. Zhou, J. Shi, B. Xu, Chem. Rev. 2015, 115, 13165.
- E. Krieg, M. M. C. Bastings, P. Besenius, B. Rybtchinski, Chem. Rev. 2016, 116, 2414.
- 4 E. Appel, J. del Barrio, X. J. Loh, O. A. Scherman, Chem. Soc. Rev. 2012, 41, 6195.
- 5 C. H. Pape, M. M. C. Bastings, R. E. Kieltyka, H. M. Wyss, I. K. Voets, E. W. Meijer, P. Y. W. Dankers, Int. J. Mol. Sci. 2014, 15, 1096.
- 6 D. J. Cornwell, D. K. Smith, Mater. Horiz. 2015, 2, 279.
- A. E. Way, A. B. Korpusik, T. B. Dorsey, L. E. Buerkle, H. A. Von Recum, S. J. Rowan, Macromolecules 2014, 47, 1810.
- 8 C. Yan, D. J. Pochan, Chem. Soc. Rev. 2010, 39, 3528.
- 9 E. T. Pashuck, H. Cui, S. I. Stupp, J. Am. Chem. Soc. 2010, 132, 6041.
- 10 X. Zhang, X. Chu, L. Wang, H. Wang, G. Liang, J. Zhang, J. Long, Z. Yang, Angew. Chem. Int. Ed. 2012, 51, 4388.
- 11 R. E. Kieltyka, a. C. H. Pape, L. Albertazzi, Y. Nakano, M. M. C. Bastings, I. K. Voets, P. Y. W. Dankers, E. W. Meijer, J. Am. Chem. Soc. 2013, 135, 11159.
- 12 Y. Li, Y. Ding, M. Qin, Y. Cao, W. Wang, Chem. Commun. 2013, 49, 8653.
- 13 M. M. E. Koenigs, A. Pal, H. Mortazavi, G. M. Pawar, C. Storm, R. P. Sijbesma, Macromolecules 2014, 47, 2712.
- 14 M. A. Khalily, M. Goktas, M. O. Guler, Org. Biomol. Chem. 2015, 13, 1983.
- 15 V. D. Nguyen, A. Pal, F. Snijkers, M. Colomb-Delsuc, G. Leonetti, S. Otto, J. van der Gucht, Soft Matter 2016, 12, 432.
- 16 R. N. Shah, N. A. Shah, M. M. Del Rosario Lim, C. Hsieh, G. Nuber, S. I. Stupp, Proc. Natl. Acad. Sci.USA 2010, 107, 3293.

- A. Baral, S. Roy, A. Dehsorkhi, I. W. Hamley, S. Mohapatra, S. Ghosh, A. Banerjee, Langmuir 2014, 30, 929.
- 18 V. Jayawarna, M. Ali, T. A. Jowitt, A. F. Miller, A. Saiani, J. E. Gough, R. V. Ulijn, Adv. Mater. 2006, 18, 611.
- 19 J. P. Jung, J. Z. Gasiorowski, J. H. Collier, Biopolymers 2010, 94, 49.
- 20 Z. Yang, G. Liang, L. Wang, B. Xu, J. Am. Chem. Soc. 2006, 128, 3038.
- 21 J. A. Sáez, B. Escuder, J. F. Miravet, Tetrahedron 2010, 66, 2614.
- 22 Z. Yang, B. Xu, Chem. Commun. 2004, 2424.
- 23 M. Ikeda, T. Tanida, T. Yoshii, K. Kurotani, S. Onogi, K. Urayama, I. Hamachi, Nat. Chem. 2014, 6, 511.
- 24 J. D. Tovar, Acc. Chem. Res. 2013, 46, 1527.
- 25 S. R. Diegelmann, J. M. Gorham, J. D. Tovar, J. Am. Chem. Soc. 2008, 130, 13840.
- 26 J. Raeburn, D. J. Adams, Chem. Commun. 2015, 51, 5170.
- 27 Y. Ohsedo, Gels 2016, 2, 13.
- 28 J. Raeburn, A. Zamith Cardoso, D. J. Adams, Chem. Soc. Rev. 2013, 42, 5143.
- 29 J. H. Van Esch, Langmuir 2009, 25, 8392.
- 30 J. L. Li, X. Y. Liu, Adv. Funct. Mater. 2010, 20, 3196.
- 31 R. Wang, X.-Y. Liu, J. Xiong, J. Li, J. Phys. Chem. B. 2006, 110, 7275.
- 32 L. E. Buerkle, S. J. Rowan, Chem. Soc. Rev. 2012, 41, 6089.
- 33 G. Pont, L. Chen, D. G. Spiller, D. J. Adams, Soft Matter 2012, 8, 7797.
- 34 Z. Yang, B. Xu, Adv. Mater. 2006, 18, 3043.
- 35 S. Toledano, R. J. Williams, V. Jayawarna, R. V Ulijn, J. Am. Chem. Soc. 2006, 128, 1070.

- J. Boekhoven, J. M. Poolman, C. Maity, F. Li, L. van der Mee, C. B. Minkenberg, E. Mendes, J. H. van Esch, R. Eelkema, Nat. Chem. 2013, 5, 433.
- 37 Y. H. Roh, R. C. H. Ruiz, S. Peng, J. B. Lee, D. Luo, Chem. Soc. Rev. 2011, 40, 5730.
- 38 N. C. Seeman, Nature 2003, 421, 427.
- T. R. Wilks, J. Bath, J. W. de Vries, J. E. Raymond, A. Herrmann, A. J. Turberfield, R. K. O'Reilly, ACS Nano 2013, 7, 8561.
- 40 L. Peng, C. Wu, M. You, D. Han, Y. Chen, T. Fu, M. Ye, W. Tan, Chem. Sci. 2013, 4, 1928.
- 41 H. Lee, R. M. Venable, A. D. Mackerell, R. W. Pastor, Biophys. J. 2008, 95, 1590.
- J. K. Armstrong, R. B. Wenby, H. J. Meiselman, T. C. Fisher, Biophys. J. 2004, 87, 4259.
- J. M. Poolman, J. Boekhoven, A. Besselink, A. G. L. Olive, J. H. van Esch, R. Eelkema, Nat. Protoc. 2014, 9, 977.
- 44 X. Y. Liu, P. D. Sawant, Adv. Mater. 2002, 14, 421.
- A. Z. Cardoso, L. L. E. Mears, B. N. Cattoz, P. C. Griffiths, R. Schweins, D. J. Adams, Soft Matter 2016, 12, 3612.
- A. Levin, T. O. Mason, L. Adler-Abramovich, A. K. Buell, G. Meisl, C. Galvagnion, Y. Bram, S. a Stratford, C. M. Dobson, T. P. J. Knowles, E. Gazit, Nat. Commun. 2014, 5, 5219.
- 47 G. Fichman, T. Guterman, J. Damron, L. Adler-Abramovich, J. Schmidt, E. Kesselman, L. J. W. Shimon, A. Ramamoorthy, Y. Talmon, E. Gazit, Sci. Adv. 2016, 2, e1500827.
- 48 Y. M. Abul-Haija, S. Roy, P. W. J. M. Frederix, N. Javid, V. Jayawarna, R. V Ulijn, Small 2014, 10, 973.

## 4.6 Supporting Information

#### 4.6.1 Materials

Copper(II) sulfate. (+)-sodium L-ascorbate. acetic tris(3acid. hydroxypropyltriazlylmethyl)amine (THPTA), 3-hydroxypicolinic acid, triethylamine, potassium phosphate monobasic, tris(hydroxymethyl)aminomethane (Tris base), boric acid, sodium chloride, potassium carbonate, tosyl chloride, 4-hydroxybenzaldehyde, triethylamine, poly(ethylene glycol) (MW = 10 kDa), hydrochloric acid, dimethyl sulfoxide, dimethyl formamide (DMF), chloroform, Nile Red and Amicon Ultra 0.5 mL 3 kDa MWCO centrifugal filters were obtained from Sigma Aldrich. Ammonium citrate sodium phosphate dibasic dihydrate, sodium hydroxide 30% ethylenediaminetetraacetic acid (EDTA) were purchased from Fluka. acrylamide/bis solution (19:1) and ammonium persulfate were obtained from Bio-Rad. N,N,N',N'-tetramethylethylenediamine (TEMED) and DNA loading buffer were purchased from Thermo Scientific and GelRed nucleic acid stain was obtained from Biotium. Single-stranded 5'-hexynyl-modified oligonucleotides were commercially synthesized (IDT, Coralville, IA, USA). Water was deionized prior to use.

#### 4.6.2 DNA Sequences

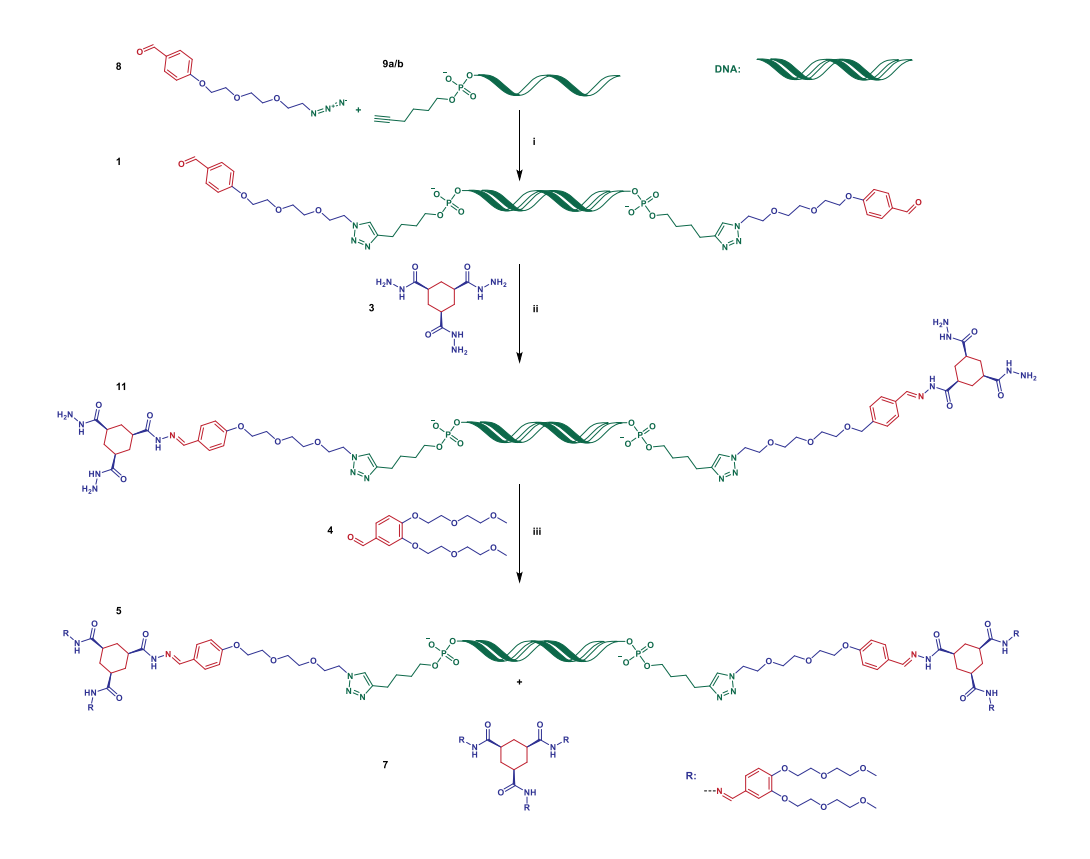
5'-hexynyl modified oligonucleotides used in this study:

	Sequence (5' - 3')	MW (Da)
9a	/Hexynyl/-TTCGGATCGCATAGTCGCAT	6268
9b	/Hexynyl/-ATGCGACTATGCGATCCGAA	6286

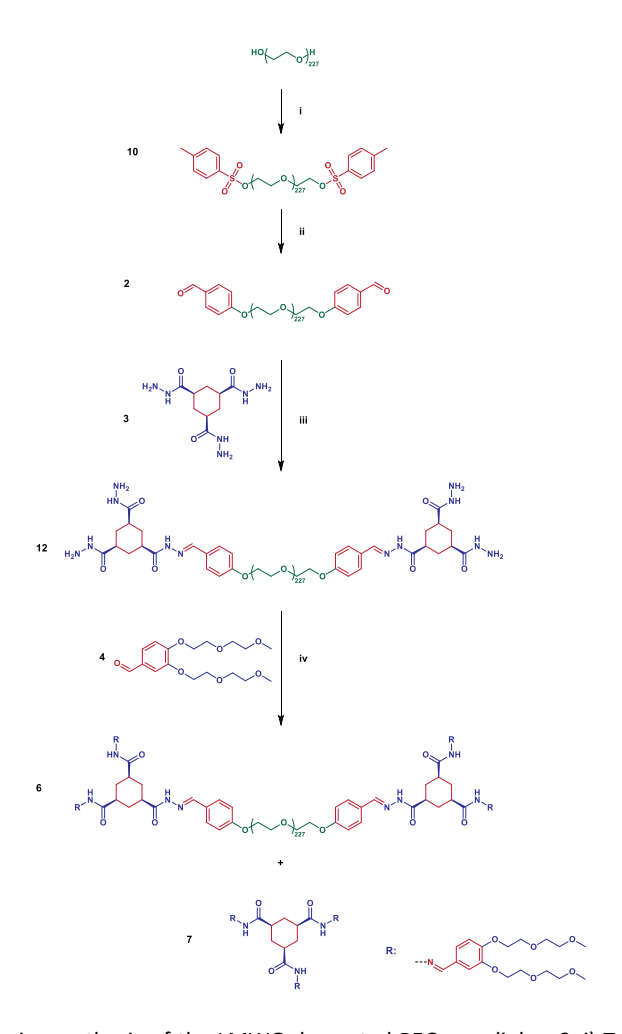
#### 4.6.3 Instrumentation

DNA hybridization and heating of reactions were performed on an Eppendorf Thermomixer C. Sample sonication was executed on a Branson 2510 ultra-sonicator. Reverse phase chromatography was performed on a Grace Reveleris X1 flash chromatography system equipped with a C18 silica column. Gel electrophoresis studies were performed using an 18 x 16 cm Hoefer SE600 standard vertical electrophoresis unit and the resulting PAGE gels were scanned using a Molecular Imager Gel Doc XR System. Measurement of DNA concentration and thermal denaturation studies were recorded on a Cary 300 UV-Vis spectrophotometer equipped with a Peltier thermostatted cell holder, using 10 mm path length quartz cuvettes. Circular dichroism studies were performed on a JASCO J-815 CD spectrophotometer using a 1.0 mm path length quartz cuvette. Matrix-assisted laser desorption ionization-time-of-flight (MALDI-TOF)-MS spectra were acquired on a Brucker microflex LRF mass spectrometer in linear positive-ion mode using 3hydroxypicolinic acid as a matrix on a ground steel target plate. Oscillatory rheology experiments were performed on a Discovery HR-2 hybrid rheometer using parallel plate geometry (20 mm), Peltier-based temperature control and a solvent trap. Samples were dehydrated for scanning electron microscopy measurements using a Bal-Tec CPD 030 critical point dryer. Scanning electron microscopy images were taken on a JEOL JSM-6400. Nuclear magnetic resonance spectra (<sup>1</sup>HNMR, 300 or 500 MHz) were recorded on a Bruker DPX300 or AV-500 instrument with chemical shifts reported to the residual solvent peak (CHCl<sub>3</sub> or DMSO). Dynamic light scattering (DLS) experiments were performed on a Malvern Zetasizer Nano S using plastic cuvettes with a 10 mm path length and measurements were taken at an angle of 173 °. Confocal laser scanning micrographs were acquired on a Zeiss LSM 710 confocal laser scanning microscope equipped with a Zeiss 40x/1.3 oil immersion objective. CryoEM micrographs were acquired on a Tecnai F20 equipped with a field emission gun (FEI company, The Netherlands) using a Gatan UltraScan camera (Gatan company, Germany).

## 4.6.4 Synthetic routes



Scheme S4.1: Stepwise synthesis of the LMWG-decorated DNA crosslinker 5: i) Sodium L-ascorbate, Cu(II)-THPTA, 0.2 M Triethylammonium Acetate buffer pH 7, 50 v/v% DMSO, N<sub>2</sub>, 37 °C, 3 h, ii) 0.1 M Phosphate buffer pH5 + 0.1 M NaCl, 37 °C, 24h, iii) 0.1 M Phosphate buffer pH5 + 0.1 M NaCl, 25 °C



Scheme S4.2: Stepwise synthesis of the LMWG-decorated PEG crosslinker 6: i) TsCl, Et<sub>3</sub>N, CHCl<sub>3</sub>, rt, 24 h, ii) 4-hydroxybenzaldehyde,  $K_2CO_3$ , dry DMF, 90 °C, 24 h, iii) 0.1 M Phosphate buffer pH 5 + 0.1 M NaCl, 37 °C, 24 h, iv) 0.1 M Phosphate buffer pH 5 + 0.1 M NaCl, 25 °C

#### 4.6.5 Synthesis of compounds 3, 4 and 8:

Compounds 3, 4 and 8 were synthesized as reported previously. 1-3

#### 4.6.6 Synthesis of 5'-aldehyde ssDNA (1a and 1b):

5′-hexynyl modified ssDNAs **9a** or **9b** (1.25 mg, 200 nmol) were separately dissolved in  $H_2O$  (200 μL) and 2M triethylammonium acetate buffer at pH 7 (100 μL) was added. Azido-diethylene glycol benzaldehyde compound 8 (0.08 mg, 300 nmol) in 50:50  $H_2O$ :DMSO (20 μL) and DMSO (450 μL) was added to the reaction mixture. Sodium L-ascorbate (0.036 mg, 180 nmol) in  $H_2O$  (200 μL) was added and the mixture degassed with argon for 30 seconds. A solution of THPTA (0.075 mg, 172 nmol) and CuSO<sub>4</sub> (0.025 mg, 156 nmol) in  $H_2O$  (50 μL) was added and flushed again for 30 seconds with argon. The reaction mixture was shaken at 37 °C for 3 hours and afterwards purified using Amicon Ultra 0.5 mL centrifugal filters with a MWCO of 3 kDa. MALDI-TOF MS: **1a** m/z calc: 6547.1, found: 6547.9 [M+H]<sup>+</sup>, **1b** m/z calc: 6565.1, found: 6566.1 [M+H]<sup>+</sup>.

#### 4.6.7 Synthesis of 5'-bishydrazide dsDNA (11):

5'-aldehyde ssDNA **1a** (20 nmol) and 1b (20 nmol) were mixed together in 20 μL of deionized water to form the hybridized dsDNA **1a+b**. Subsequently, hydrazide compound **3** (1.03 mg, 4.00 μmol) in 0.1 M phosphate buffer pH 5 and 100 mM NaCl (80 μL) was added to the reaction mixture so as to provide a ratio of 100:1 (3 to 1) and shaken (750 rpm) for 24 hours at 37 °C. The crude reaction mixture was purified using Amicon Ultra 0.5 mL centrifugal filters with a 3 kDa MWCO in order to remove excess compound **3** and for desalting. For MALDI-TOF MS characterization, the same procedure was followed but only using single strands **11a** to enable detection of the conjugate. MALDI-TOF-MS: **11a** m/z calc: 6787.2, found: 6787.3 [M+H] $^+$ .

#### 4.6.8 Synthesis of dsDNA low molecular weight gelator crosslinker (5):

Aldehyde compound **4** (8.21 mg, 24.00  $\mu$ mol) was dissolved in 0.1 M phosphate buffer and 100 mM NaCl at pH 5 (100  $\mu$ L) and mixed with the purified reaction mixture (100  $\mu$ L) of bishydrazide functionalized dsDNA compound **11**, in order to form the dsDNA-crosslinker **5**. The crude reaction mixture was purified using Amicon Ultra 0.5 mL centrifugal filters with a 3 kDa MWCO in order to remove excess compound **4** and for desalting. For MALDI-TOF MS characterization the same procedure was followed but only using single strands **5a** to enable detection of the conjugate MALDI-TOF-MS: **5a** m/z calc: 7435.5, found: 7111.8 [M+H] $^+$  (mono-substituted) and 7435.9 [M+H] $^+$ .

## 4.6.9 Synthesis of poly(ethylene glycol) bistosylate (10)

Compound **10** was synthesized by dissolving poly(ethylene glycol) (MW = 10 kDa) (2.0 g, 0.2 mmol), tosyl chloride (0.23 g, 1.2 mmol) and triethylamine (0.13 g, 0.1 mmol) in chloroform (25 mL) and reacted for 16 hours at room temperature. Afterwards, the reaction mixture was concentrated by rotary evaporation, precipitated from cold ether three times and used without further purification. Yield: 90% MALDI-TOF-MS: 10 m/z calc: 10980.3, found: 10980.4 [M+H]<sup>+ 1</sup>H-NMR ( $\delta_{H}$ [ppm], CDCl<sub>3</sub>, 300 MHz): 7.73 (d, 4H), 7.46 (d, 4H), 3.2-4.2 (m, 900H), 2.44 (s, 6H)

## 4.6.10 Synthesis of poly(ethylene glycol) bisaldehyde (2)

Compound **2** was synthesized by dissolving compound **10** (0.5 g, 0.5 mmol), 4-hydroxybenzaldehyde (0.024 g, 2.0 mmol) and potassium carbonate (0.034 g, 2.5 mmol) in dry DMF and was reacted for 24 hours at 90 °C. Afterwards, the reaction mixture was concentrated by rotary evaporation and neutralized by adding 1 M HCl. The aqueous layer was extracted three times with ethyl acetate, and the combined organic fractions were concentrated by rotary evaporation. Finally, the product was washed three times with cold ether, dried, and used without any further purification. Yield: 70%. MALDI-TOF MS: 2 m/z calc: 10880.4, found: 10880.3 [M+H]<sup>+ 1</sup>H-NMR ( $\delta_{\rm H}[{\rm ppm}]$ , DMSO-d6, 300 MHz): 9.87 (s, 2H), 7.85-7.88 (d, 4H), 7.13-7.15 (d, 4H), 3.2-4.2 (m, 900H)

### 4.6.11 Synthesis of poly(ethylene glycol) bishydrazide (12)

Compound **2** (20 nmol) was dissolved in deionized water (20  $\mu$ L) and compound **3** (1.03 mg, 4.00  $\mu$ mol) in 0.1 M phosphate buffer pH 5 and 100 mM NaCl (80  $\mu$ L) was added in a 100:1 molar ratio of compound **3** to **2** and shaken (750 rpm) for 24 hours at 37 °C. For MALDI-TOF-MS and NMR characterization the crude reaction mixture was purified using flash column chromatography using a 10-90% CH3CN/H2O gradient over 30 minutes using a C18 silica column. MALDI-TOF-MS: 12 m/z calc: 11360.7, found: 11360.8 [M+H]<sup>+</sup>. <sup>1</sup>H-NMR ( $\delta_{H}$ [ppm], DMSO-d6, 300 MHz): 11.05-11.20 (d, 2H), 8.98 (br s, 4H), 7.93-8.10 (d, 2H), 7.58 (m, 4H), 7.01 (d, 4H), 4.14 (br s, 8H), 3.20-4.20 (m, 900H), 2.08-2.19 (t, 6H), 1.37-1.74 (m, 12H)

# 4.6.12 Synthesis of poly(ethylene glycol) low molecular weight gelator crosslinker (6)

Compound **4** (8.21 mg, 24.00 µmol) was added to the purified reaction mixture (100 µL) of compound **12** in 0.1 M phosphate buffer with 100 mM NaCl at pH 5 (100 µL). This mixture was allowed to react in order to form compound **6**. For MALDI-TOF-MS and NMR characterization the crude reaction mixture was purified using flash column chromatography using a 10-90% CH<sub>3</sub>CN/H<sub>2</sub>O gradient over 30 minutes using a C18 silica column.  $^1$ H-NMR ( $\delta_H$ [ppm], DMSO-d6, 300 MHz): 11.20-11.30 (d, 6H), 8.10 (br t, 3H), 7.90-7.95 (br t, 3H), 7.53-7.55 (d, 4H), 7.43 (d, 4H), 7.38-7.40 (d, 4H), 7.21-7.24 (d, 6H), 7.03-7.15 (d, 4H), 3.20-4.20 (m, 890H)

#### 4.6.13 Thermal Denaturation studies

Thermal denaturation of complementary oligonucleotides **1** and **9** was followed by monitoring the absorbance at 260 nm on a Cary 300 UV-Vis spectrophotometer equipped with a thermal heating block using the following time program: Annealing at 85 °C and subsequent cooling to 10 °C at 0.71 °C/min, heating to 85 °C at 0.20 °C/min and finally cooling down to 10 °C at 0.20 °C/min. Using this method, 4.0 nmol of **9a** and **9b**, or **1a** and **1b** in 0.1 M phosphate buffer with 100 mM NaCl at pH 5 were prepared. The thermal denaturation studies showed cooperative and reversible

transitions with a melting temperature difference of 0.6 °C relative to the unfunctionalized duplex DNA.

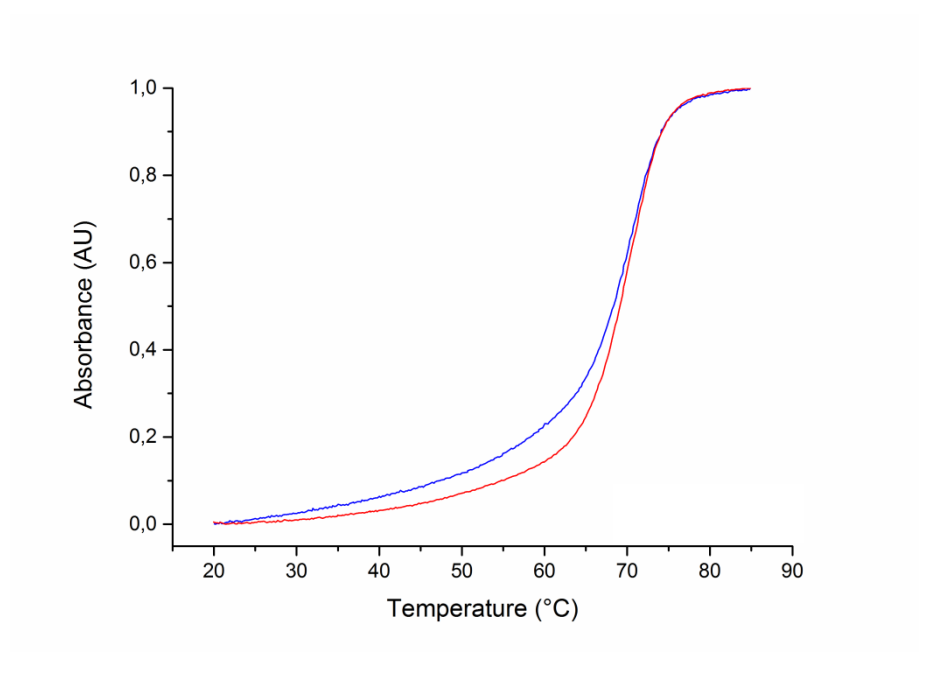


Figure S4.3. Normalized thermal denaturation profiles of **9a+b** (blue) and **1a+b** (red) in 0.1 M phosphate buffer with 100 mM NaCl at pH 5, indicating an increase in melting temperature from 68.9 °C (**9a+b**) to 69.5 °C (**1a+b**) upon conjugation of **8**.

#### 4.6.14 Circular Dichroism

Circular dichroism (CD) studies were performed to observe the effect of conjugation of **8** to **9a** or **9b** on the hybridized dsDNA secondary structure. CD studies were performed on a JASCO J-815 CD spectrophotometer with a 1.0 mm path length quartz cuvette. Scans were taken from 320-220 nm at a scan speed of 100 nm/min with 3 consecutive acquisitions. Solutions of 4.0 nmol of **9a** and **9b**, or **1a** and **1b** in 0.1 M phosphate buffer with 100 mM NaCl at pH 5 (250  $\mu$ L) were prepared and heated to 95 °C for 5 minutes and subsequently, allowed to cool to room temperature. CD spectroscopy of both samples (**9a+b** blue, **1a+b** red) showed no apparent changes to the dsDNA secondary structure following the characteristic bands for B-DNA (negative band around 245 nm and a positive band between 260-280 nm).

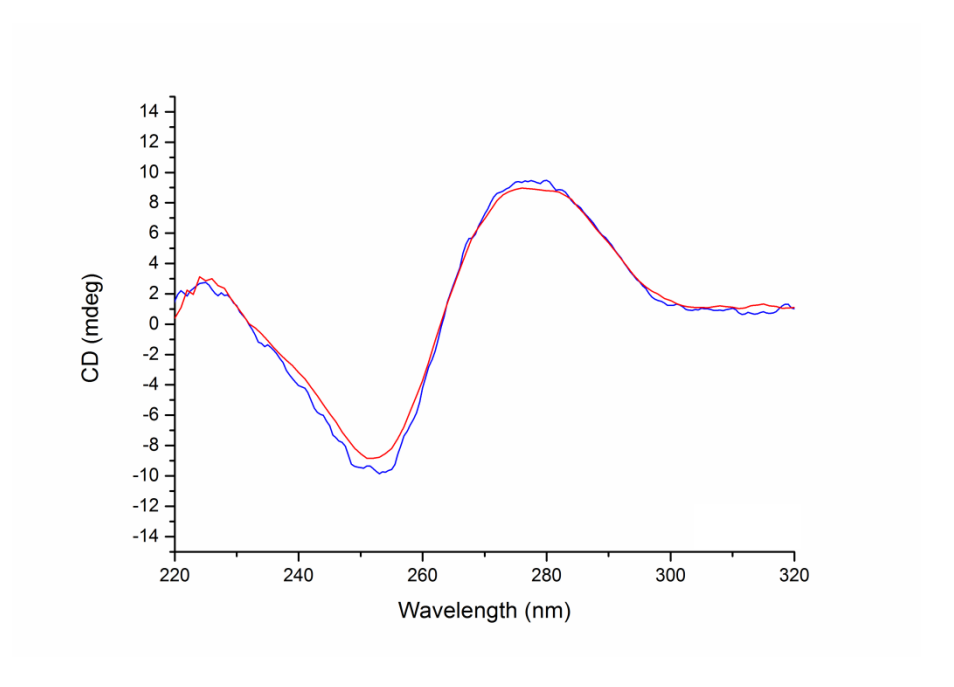


Figure S4.4. CD spectra of **9a+b** (blue) and **1a+b** (red) in 0.1 M phosphate buffer with 100 mM NaCl at pH 5.

## 4.6.15 General gelation protocol

Hydrogels (final concentrations: 20 mM **3**, 120 mM **4**), unless otherwise indicated, were made using the following protocol: Stock solutions of **3** (50 mM, using brief sonication and heating) and **4** (240 mM, turbid yellow solution) were in prepared in 0.1 M phosphate buffer pH 5 containing 100 mM NaCl. Crosslinker **1** or **2** in a 0-3 mol% ratio (with respect to **3**) dissolved in the aforementioned buffer (20  $\mu$ L) was transferred to an appropriate reaction vessel. Compound **3** (80  $\mu$ L, 1.03 mg) was added, and then the reaction was shaken (750 rpm) for 24 hours at 37 °C. Afterwards compound **4** (100  $\mu$ L, 8.21 mg) was added to the reaction mixture at room temperature, to trigger formation of the hydrogel.

#### 4.6.16 Gel Electrophoresis

Polyacrylamide gel electrophoresis (PAGE) (20%) was carried out under non-denaturing conditions to monitor oligonucleotide hybridization and functionalization in the multicomponent reaction-coupled assembly. For all hydrogel and intermediate stage samples, gel aliquots containing 100 ng DNA (calculated by the concentration of DNA inside the gel volume) were prepared by gel dilution in water and mixed with DNA-loading buffer.

## 4.6.17 Oscillatory rheology

Freshly prepared hydrogel samples were gently pipetted directly between the lower and upper plate of the rheometer (gap size:  $500~\mu m$ ). All time sweep measurements were conducted at a frequency of 1.0 Hz and 0.05% strain at 25 °C ± 0.2 °C.

## 4.6.18 Avrami analysis

The dimensionality of fiber growth was assessed by plotting  $\ln(-\ln(1-X))$  against  $\ln(t-t0)$  using the complex modulus,  $G^*$ , from rheological data in which  $X = (G^*_t - G^*_0)/(G^*_{max} - G^*_0)$ . The Avrami coefficient n was determined by calculating the slope of the first transition where nucleation and growth of the fibers takes place.<sup>4</sup>

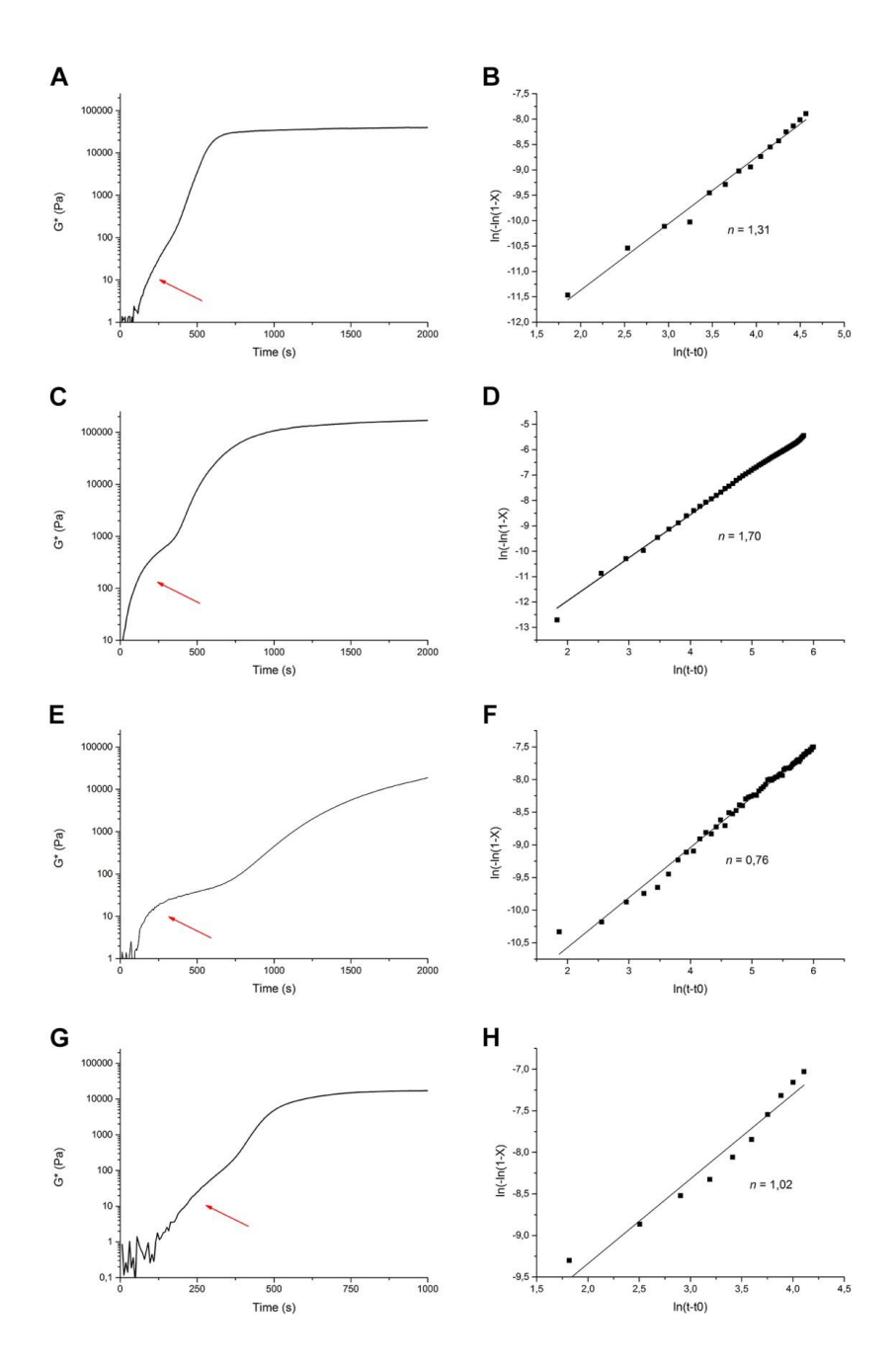


Figure S4.5. Avrami analysis of complex moduli ( $G^*$ ) obtained from oscillatory rheology profiles of the various hydrogel samples (3 (20 mM) and 4 (120 mM)). Arrows were used to indicate the region of the curve fitted for subsequent analysis. Time sweep data: a) without crosslinker, c) 1.0 mol% 1, e) 3.0 mol% 1, g) 1.0 mol% 2. Avrami plots and corresponding coefficients (n): b) without crosslinker, d) 1.0 mol% 1, f) 3.0 mol% 1, h) 1.0 mol% 2.

#### 4.6.19 Scanning Electron Microscopy

Hydrogel samples, 4 hours after preparation, were fixed overnight using a solution of 2 % glutaraldehyde in 0.1 M sodium cacodylate (pH 7.2). The hydrogels were dehydrated by immersion in increasingly higher concentrations of ethanol (70 - 100 % ethanol, in 10 % steps for 15 minutes each) and finally 100 % ethanol was exchanged by 100 % acetone. Samples containing acetone were subsequently dried by means of critical point drying. Dried samples were then glued on SEM stubs and coated with gold using a gold sputter coater. Finally, scanning electron micrographs were recorded on a JEOL JSM-6400, equipped with a tungsten filament gun operating at 10 kV with an 8 mm WD.

## 4.6.20 Enzymatic digestion

Enzymatic degradation of DNA-based crosslinks was performed prior to gel formation by adding 100 units of DNaseII in a 0.1 M phosphate buffer with 0.1 M NaCl at pH 5 to a mixture of 1 mol% 1 (20  $\mu$ L, 20.0 nmol final concentration) and 3 (80  $\mu$ L, 20 mM final concentration) in the same buffer. The reaction mixture was shaken (750 rpm) for 24 hours at 37 °C. Afterwards, a turbid solution of 4 (100  $\mu$ L, 120 mM final concentration) was added to facilitate hydrogelation and mechanical properties were measured by oscillatory rheology as described in section 9.

#### 4.6.21 Dynamic Light Scattering

Concentration dependent dynamic light scattering (DLS) measurements were performed on 200  $\mu$ L solutions of compound 4 in 0.1 M phosphate buffer with 0.1 M NaCl at pH 5. Samples ranging in concentration from 10-120 mM were prepared individually prior to measurement and their scattered light intensities and corresponding particle sizes were measured at a 173 ° angle in a polystyrene cuvette at 25 °C. In a second experiment, crosslinkers 1 or 2 (ranging from 0-3 mol%) were mixed with 200  $\mu$ L of buffered solutions of 4 (120 mM) and their effect on the particle size was recorded. All samples were measured in triplicate.

Table S1: Particle size determination for spherical particles of 4 with crosslinker 1 or 2

Particle size (µm)

120 mM **4** only 1.19 ± 0.12

1 mol% **1** + **4** 0.70 ± 0.05

3 mol% 1 + 4 0.46  $\pm$  0.02

1 mol% 2 + 4 2.19  $\pm$  0.09

## 4.6.22 Confocal laser scanning microscopy

Confocal laser scanning micrographs were acquired on a Zeiss LSM 710 confocal laser scanning microscope equipped with a Zeiss 40x, 1.3 oil immersion objective and using an excitation wavelength of 488 nm and an emission filter of 510-570 nm. Still images were acquired at 2956 x 2956 pixels (354 x 354  $\mu$ m) and time-lapse movies were acquired at 536 x 536 pixels (64 x 64  $\mu$ m) at an interval of 10 seconds per frame. Samples were prepared as described in the general gelation protocol with the addition of 0.5  $\mu$ L of a Nile Red solution (2.5 mM) dissolved in ethanol prior to adding a turbid solution of **4**. Samples were briefly mixed by gentle pipetting before deposition into Ibidi 8-well slides for live imaging in a climate controlled room (18 °C). Samples for still images were taken 4 hours after the onset of gel formation. Droplets were sized by manually taking the average size of 30 individual droplets per sample using the ImageJ software.

### 4.6.23 Cryogenic TEM

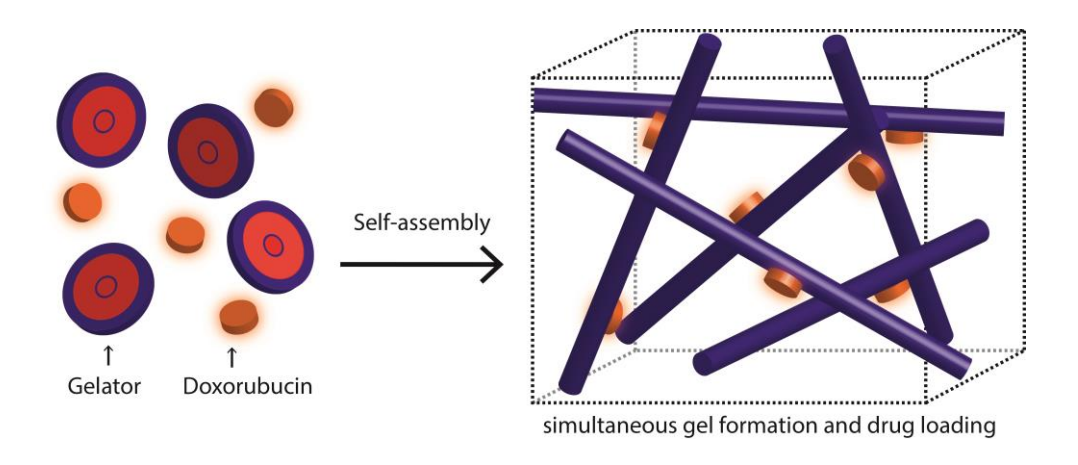
Cryogenic TEM samples were prepared as described in the general gelation protocol and 4 hours after the onset of gelation. A 3  $\mu$ L gel was pipetted onto a freshly glow-discharged Quantifoil R2/2 holey carbon coated grid (300 mesh Cu grids), blotting for 1 second and plunge-freezing in liquid ethane at -183 °C using a Leica EM GP (95 % humidity, RT, Whatman No.4 blotting paper). The vitrified grids were imaged with a Tecnai F20 equipped with a field emission gun (FEI company, The Netherlands) at 120 keV using a Gatan UltraScan camera (Gatan company, Germany) with a defocus between -5 and -8  $\mu$ m.

## 4.6.24 References

- Boekhoven, J.; Poolman, J. M.; Maity, C.; Li, F.; van der Mee, L.; Minkenberg, C. B.; Mendes, E.; van Esch, J. H.; Eelkema, R. Nat. Chem. 2013, 5, 433.
- Poolman, J. M.; Boekhoven, J.; Besselink, A.; Olive, A. G. L.; van Esch, J. H.; Eelkema, R. Nat. Protoc. 2014, 9, 977.
- Poolman, J. M.; Maity, C.; Boekhoven, J.; van der Mee, L.; le Sage, V. A. A.; Groenewold, G. J. M.; van Kasteren, S. I.; Versluis, F.; van Esch, J. H.; Eelkema, R. J. Mater. Chem. B 2016, 4, 852.
- 4 Liu, X. Y.; Sawant, P. D. Adv. Mater. 2002, 14, 421.

# **CHAPTER 5**

Tuning drug release from a reaction-coupled low molecular weight gelator system by modulating its reaction pathway



This chapter was prepared as an Original Research paper: Willem E. M. Noteborn, Maria Broto Torredemer, Chandan Maity, Frank Versluis, Rienk Eelkema and Roxanne E. Kieltyka

## 5.1 Abstract

Here we report the ability to control the release properties of a chemotherapeutic drug in a reaction-coupled low molecular weight gelating system. By modulating its reaction time, we gain control over the extent of covalently bound and physically encapsulated drug. This approach can be used to expeditiously synthesize a broad range of drug-laden hydrogel materials with varied release profiles in situ, with numerous applications in the biomedical sector.

Keywords: reaction coupled self-assembly, low molecular weight gelator, drug release, reaction time control

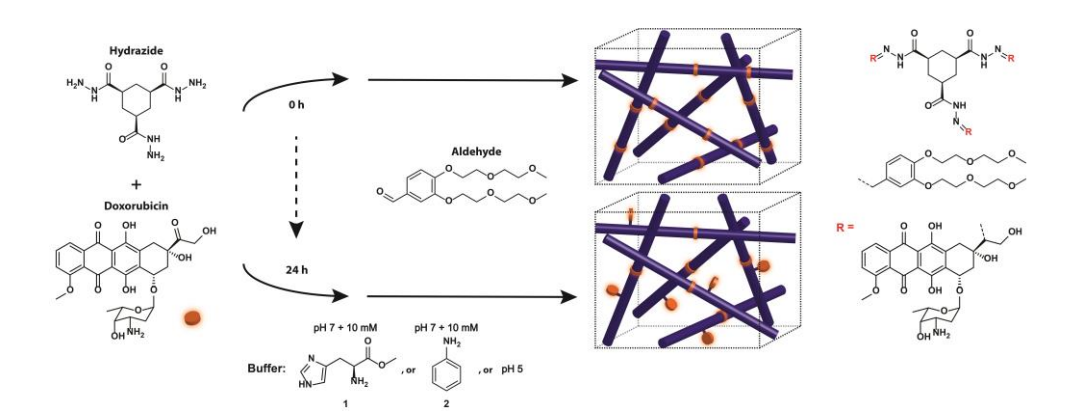
## 5.2 Introduction

Low molecular weight gelators (LMWG) are eminently suitable scaffolds for biomaterials due to their capacity to self-assemble into soft, three-dimensional matrices in water.<sup>1–6</sup> Nowadays, the field of supramolecular chemistry is striving towards gaining control over the physical properties of self-assembled structures and their function. A unique handle to tune these materials is by using reaction-coupled self-assembly, in which the formation, change, or disruption of a chemical bond initiates the self-assembly process.<sup>4,7–13</sup> More specifically, a range of photochemical, catalytic, bioconjugation and enzymatic reactions have been used to achieve kinetic control in these systems.<sup>10,14–17</sup> Thus, the reaction-coupled method has been demonstrated to be a powerful way to tune the hierarchical structure and mechanical properties of supramolecular materials with exciting applications in the biomedical domain.<sup>7,18,19</sup>

Functional modules, such as bioactive peptides or drugs, can be easily incorporated in self-assembling systems by exclusively physical<sup>3,20–23</sup> or covalent<sup>24–26</sup> means. They are commonly incorporated as preformed functional monomers or mixed in with the unfunctionalized bulk material to prepare biomaterial for three-dimensional cell culture and drug release.<sup>24,27–30</sup> Another way to introduce functionality can be achieved using reaction-coupled self-assembly, in which both functional and unfunctionalized LMWG monomers can be synthesized in situ simultaneously. This can enable the expeditious formation of and control over various material attributes, such as stiffness and porosity. Consequently, this approach can be highly attractive for applications in drug delivery to provide user-defined control over drug release in a synthetically facile manner, without prior complex chemical modifications of the drug molecules to be delivered.

Previously, a self-assembling LMWG system driven by hydrazone formation between cyclohexane trishydrazide (hydrazide) and three oligo(ethylene glycol)-functionalized benzaldehyde (aldehyde) wedges was reported by Eelkema and van Esch. The use of a nucleophilic (aniline) or acid (pH 5) catalyst increased the rate of formation of the LMWG, enhancing the mechanical stiffness of the network and lowering the porosity. This work demonstrated the potential of using the reaction rate as a handle to control the final properties of the self-assembled material. Herein, we explore the potential for using this methodology to introduce drug molecules in a tuneable and facile manner into the network by modulating the reaction pathway of the various components (Scheme 5.1). We exploit the use of the hydrazone bond in

this reaction-coupled system to ligate a model drug, Doxorubicin, by its ketone moiety<sup>32,33</sup> and control its release from the resulting hydrogel network.



Scheme 5.1. Doxorubicin-induced pathway selection for the formation of a reaction-coupled low molecular weight gelator. Pre-incubation of Doxorubicin with hydrazide leads to drug-conjugated networks that affect the physicochemical properties of the formed hydrogel and its subsequent drug release profile.

### 5.3 Results and discussion

To first adapt the system to self-assemble under physiological conditions, we introduce the use of a nucleophilic and biocompatible catalyst L-histidine methyl ester 1 and compare its performance to the previously used catalysts, aniline 2 or pH 5. To quantify the effect of the different catalysts on the self-assembly process and the mechanical properties of the resultant materials, we employed oscillatory rheology. Time sweep measurements were recorded to monitor the gelation process measuring the increase of the storage (G') and loss moduli (G'') as a function of time. The hydrazide-aldehyde hydrogels were made by dissolving all gel constituents in phosphate buffer (10 mM 1 or 2 at pH 7 or a buffer at pH 5). The mixed hydrazidealdehyde samples showed a two-stage growth profile, most notably at pH 7, likely arising from fibril nucleation and growth, and their subsequent entanglement. Through comparison of the storage moduli (G') with respect to the various catalysts at the plateau of the various curves,  $\mathbf{1}$  (G' = 60 kPa) provided a stronger material at pH 7 in comparison to 2 (G' = 35 kPa). On the other hand, an even stiffer material was formed at pH 5 (G' = 95 kPa) (Figure 5.1). Interestingly, the measured storage moduli for the catalysts at pH 7 reflected trends reported for a model acylhydrazone reaction, where 1 was a more active catalyst thus further emphasizing the effect of catalytic rate on mechanical properties of the resultant network.<sup>34</sup> In an attempt to increase the gelation kinetics using catalyst 1, the amount of aldehyde that was added was increased from 1 eq (16 h) to 3 eq (1.5 h), showing a clear dependence of the speed of network formation on the amount of aldehyde gelator present. Moreover, the samples containing 3 eq of aldehyde formed substantially stiffer hydrogel networks (Figure 5.2).

To provide insight into the origin of the distinct rheological profiles, we imaged the hydrogel microstructures by scanning electron microscopy (SEM) of the self-assembled gels. Gels consisting of a 1:1 ratio of hydrazide (40 mM) and aldehyde (120 mM) with catalyst 1 resulted in an open, interconnected network structure (Figure 5.3A). An increase to 3 equivalents of aldehyde (360 mM) resulted in a densely packed architecture consistent with a stronger gel (Figure 5.3B). Compared to 1, catalyst 2 resulted in a more open network of fibrils in line with oscillatory rheology data showing a weaker gel (Figure 5.3C). In contrast, a highly dense network of fibrils is observed for gels formed in pH 5 buffer solutions (Figure 5.3D).

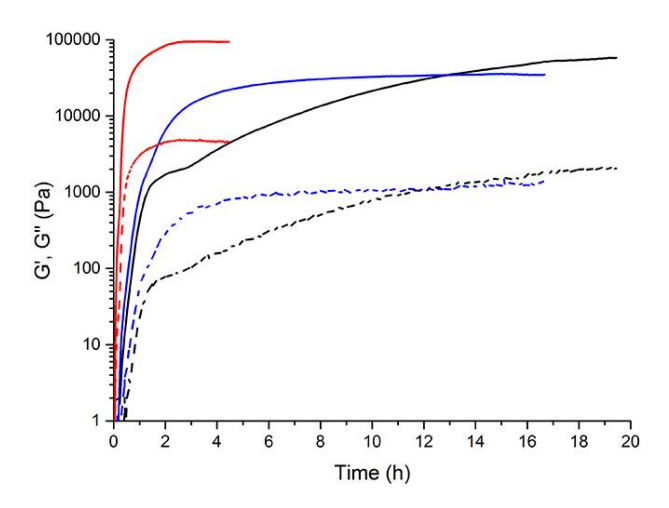


Figure 5.1. Time sweep measurements (0.05 strain%, 1.0 Hz) monitoring hydrogel formation by catalysts using oscillatory rheology: **1** (black: G' solid, G" dotted), **2** (blue: G' solid, G" dotted), pH 5 (red: G' solid, G" dotted).

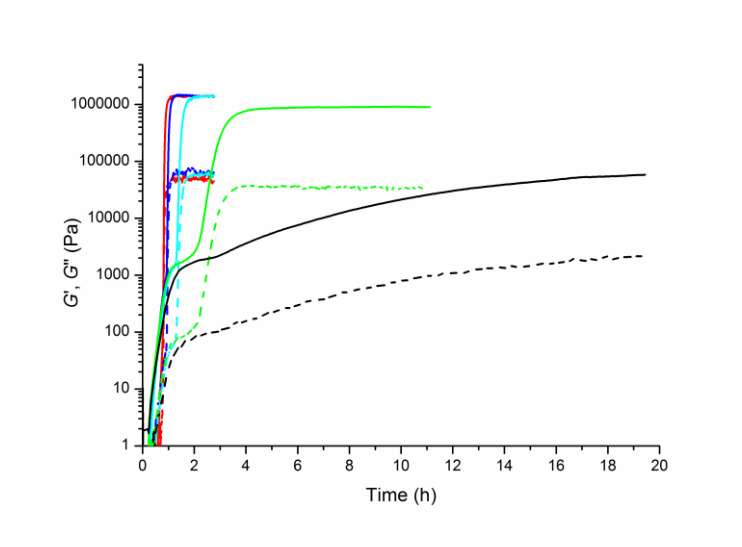


Figure 5.2. Oscillatory rheology on 40 mM hydrogels of hydrazide catalyzed by **1** with decreasing equivalents of aldehyde (G' solid lines, G" dashed lines). hydrazide:aldehyde 1:3 (red), hydrazide:aldehyde 1:2 (blue), hydrazide:aldehyde 1:1.5 (cyan), hydrazide:aldehyde 1:25 (green), hydrazide:aldehyde 1:1 (black).

Hence, scanning electron micrographs corroborate the strong relationship between the catalytic rate gel formation and the mechanical stiffness of the hydrogel materials. As unreacted aldehydes have previously been shown to exert cellular toxicity, <sup>35,36</sup> only gel mixtures based on the equimolar ratio of hydrazide and aldehyde were pursued to study the potential of this hydrogel system for applications in drug delivery.

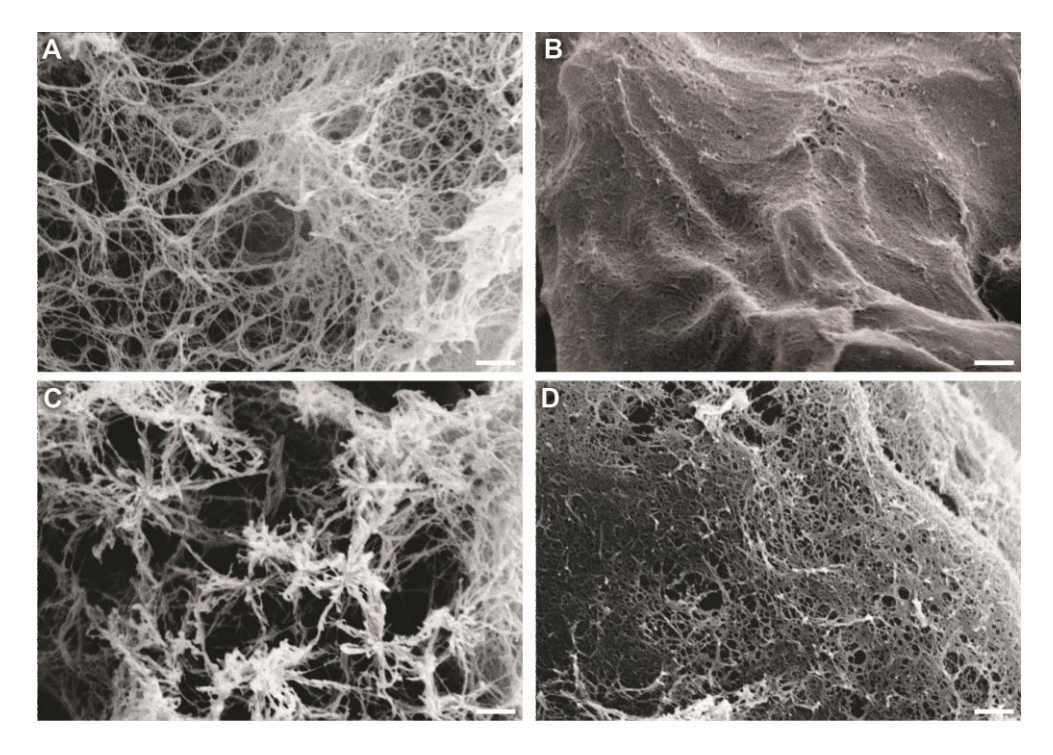


Figure 5.3. Scanning electron micrographs of gels with a 1:1 ratio (A,C,D) of hydrazide (40 mM) and BzPEG (120 mM) catalyzed by A) 1, C) 2, or D) pH 5. B) Scanning electron micrograph of a gel with a 1:3 ratio hydrazide (40 mM) and aldehyde (360 mM) catalyzed by 1 at pH 7. Scale bars are 1.0 µm.

Once the two-component hydrogel system consisting of hydrazide (40 mM) and aldehyde (120 mM) was established at pH 7 with catalyst 1, modulation of their reaction pathway was explored to incorporate a model drug, Doxorubicin, by its ketone moiety. By increasing the reaction time between Doxorubicin with the hydrazide core prior to addition of the aldehyde wedge, it is anticipated that its conjugation to the core will occur. However, if all components are mixed simultaneously, exclusive hydrophobic encapsulation of the drug molecule is expected due to the lower reactivity of ketones compared to aldehydes. We therefore examined the reaction rate between Doxorubicin and the hydrazide core by LC-MS with respect to time. This study showed that after 24 h 55% of the Doxorubicin was conjugated, and a maximum of 80% was achieved after 7 days (Figure 5.4). The

remainder of the reaction mixture consisted of a peak that is twice the mass of Doxorubicin, consistent with its dimerized form (Doxorubicin Dimer Impurity 3).

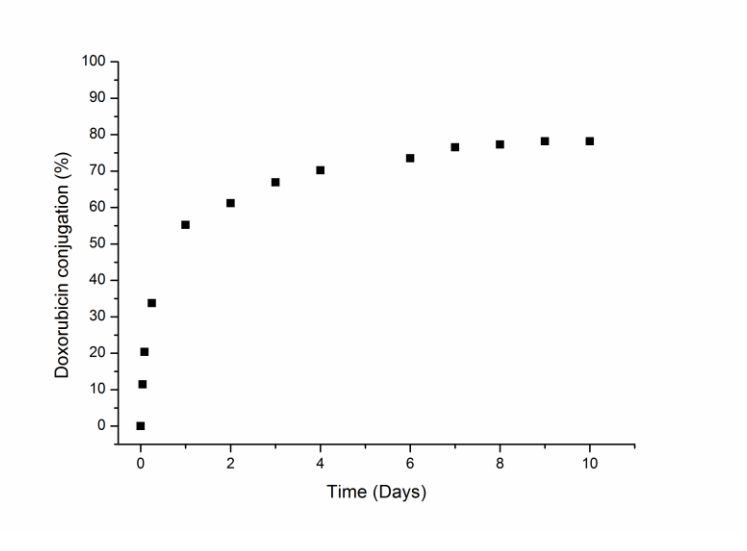


Figure 5.4. Extent of Doxorubicin – hydrazide conjugation measured by peak integration of LCMS spectra and the ratio of unconjugated and conjugated Doxorubicin species ( $\lambda_{abs}$ : 480 nm, unconjugated Doxorubicin t = 4'55" – 5'00", conjugated Doxorubicin t = 3'30" – 4'45").

The effect of Doxorubicin conjugation on the microstructure, mechanical and release properties of the hydrazide - aldehyde hydrogel was subsequently investigated. The influence of the Doxorubicin and hydrazide pre-incubation step before the addition of aldehyde on the mechanical properties of the self-assembled hydrogel was probed by oscillatory rheology. Comparison of the native and Doxorubicin-loaded hydrogel scaffolds (1.0 mg/mL) showed that pre-incubation of the hydrazide with Doxorubicin had a significant influence on their mechanical stiffness (Figure 2A). Whereas the native hydrogel had a maximum storage modulus (G') of 60 kPa, hydrogels prepared with Doxorubicin (1.0 mg/mL) without any incubation step prior to the addition of the aldehyde showed a decrease in mechanical stiffness to 26 kPa. Pre-incubation of Doxorubicin with the hydrazide before the addition of the aldehyde, at various time points up to 24 h, showed an increasingly detrimental effect on network stiffness (24 h incubation, 2 kPa) (Figure 5.5). Hydrazide samples prepared using a 7 day pre-incubation time with Doxorubicin were abandoned for further study due to the formation of a film, which could not be redissolved after the addition of the aldehyde. Directly adding the Doxorubicin without pre-incubation time but

varying the drug concentration from 0.5 to 2.0 mg/mL did not result in a variation in mechanical properties between the different concentrations of Doxorubicin (Figure 5.6), supporting the effect of the reaction pathway on the physicochemical properties reaction-coupled hydrogels.

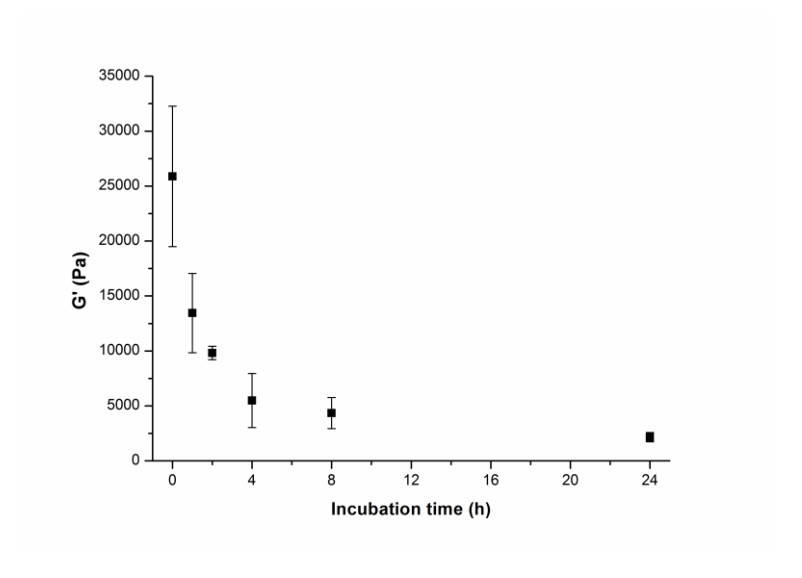


Figure 5.5. Comparison of maximum mechanical stiffness (G') of hydrogels catalyzed by **1** and incubated with 1.0 mg/mL Doxorubicin incubated for different amounts of time (0.05 strain%, 1.0 Hz).

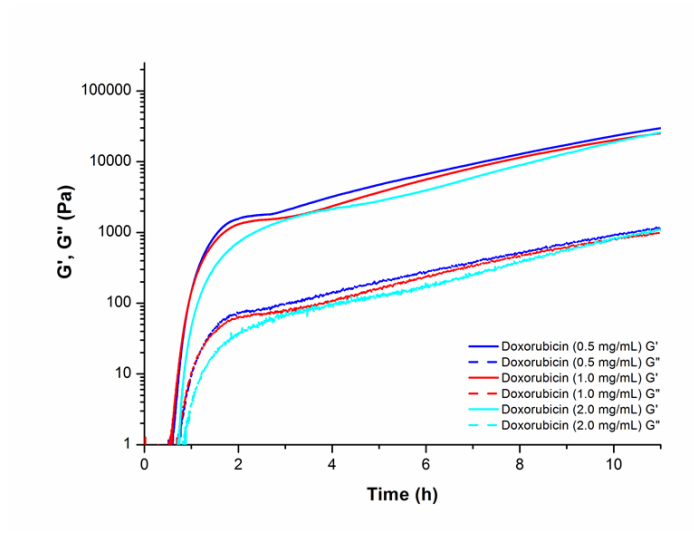


Figure 5.6. Oscillatory rheology on hydrazide - aldehyde (40 mM, 120 mM) hydrogels catalyzed by 1 loaded with 0.5 - 2.0 mg/mL Doxorubicin without pre-incubation.

To probe the effect of Doxorubicin on the nucleation and growth of the network, Avrami analysis was applied to the first stage of rheological data to assess the dimensionality of growth. The Avrami coefficients (n) were approximately 2 for all pre-incubation time points, suggesting a two-dimensional fiber branching growth mechanism with marginal differences between the various incubation times as expected (Figure S5.1). The most significant differences between the hydrazide and aldehyde samples of varied drug incubation times occurred in the second stage of the rheological profiles with the onset of network percolation. Increased pre-incubation times of the hydrazide with Doxorubicin showed increased delays in the profiles to reach a maximum in network stiffness, suggesting that the conjugated drug has a negative effect on network percolation (Figure 5.7).<sup>7,37</sup>

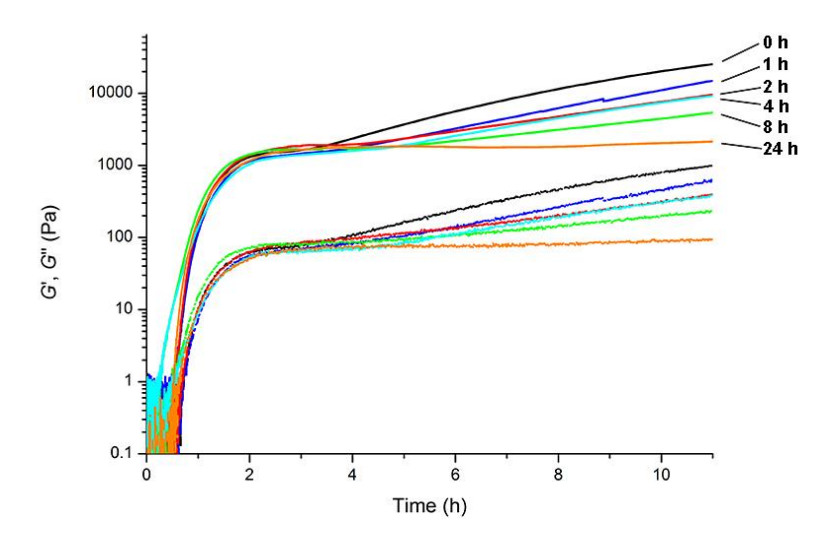


Figure 5.7. Oscillatory rheology on hydrazide - aldehyde (40 mM, 120 mM) hydrogels catalyzed by 1 loaded with 1.0 mg/mL Doxorubicin and pre-incubated for different amounts of time before the addition of aldehyde: 0 h (black), 1 h (blue), 2 h (red), 4 h (cyan), 8 h (green), 24 h (orange) (G' solid lines, G" dashed lines).

Previously, we observed that the hydrazide-aldehyde reaction-coupled hydrogel network starts with the initial formation of emulsion-like droplets of aldehyde that serve as nucleation centers from which the network grows. These droplets are depleted over time as the reaction between the various components proceeds and their perturbation can affect various physical attributes of the final hydrogel. Dynamic light scattering (DLS) measurements showed that the hydrophobic Doxorubicin reduces the aldehyde droplets in size by 20% (Figure 5.8). SEM images after self-assembly of the Doxorubicin-loaded hydrogels displayed a densely fibrous network for directly mixed (0 h incubation) and pre-incubated (24 h incubation)

samples (Figure 5.9). Both of these gels were indistinguishable from the native gel formed by 1 at pH 7. Moreover, confocal laser scanning microscopy (CLSM) visualization of the network formation process was aided by the fluorescent properties of Doxorubicin. Doxorubicin interacts with the aldehyde droplets due to their fluorescence, as earlier suggested by DLS measurements, and colocalizes within the fibrous network afterwards (Figure 5.10). From these results, it can be concluded that Doxorubicin interacts with the hydrogel network in a conjugation-dependent manner due to modifying the reaction pathway of the hydrogel components, but the resultant microstructural differences that give rise to the observed mechanical profiles are subtle

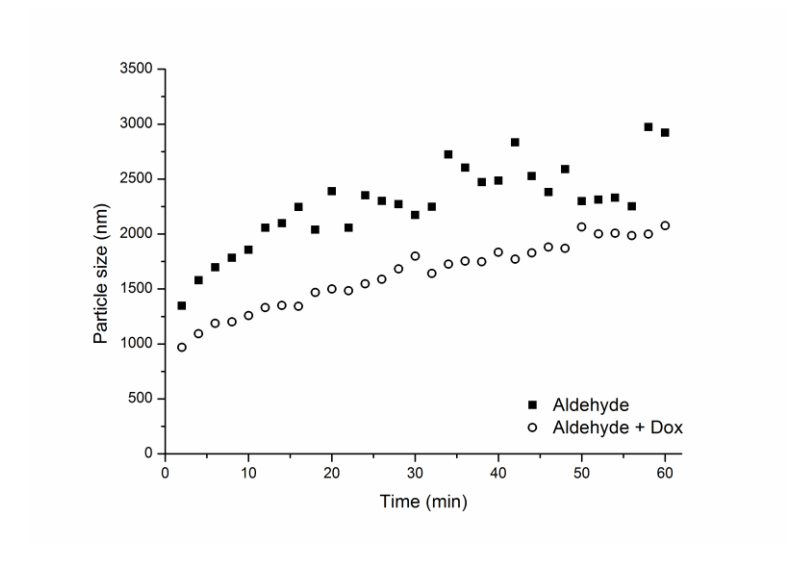


Figure 5.8. Time dependent aldehyde particle size stability with (open circles) and without (closed squares) 1.0 mg/mL Doxorubicin.

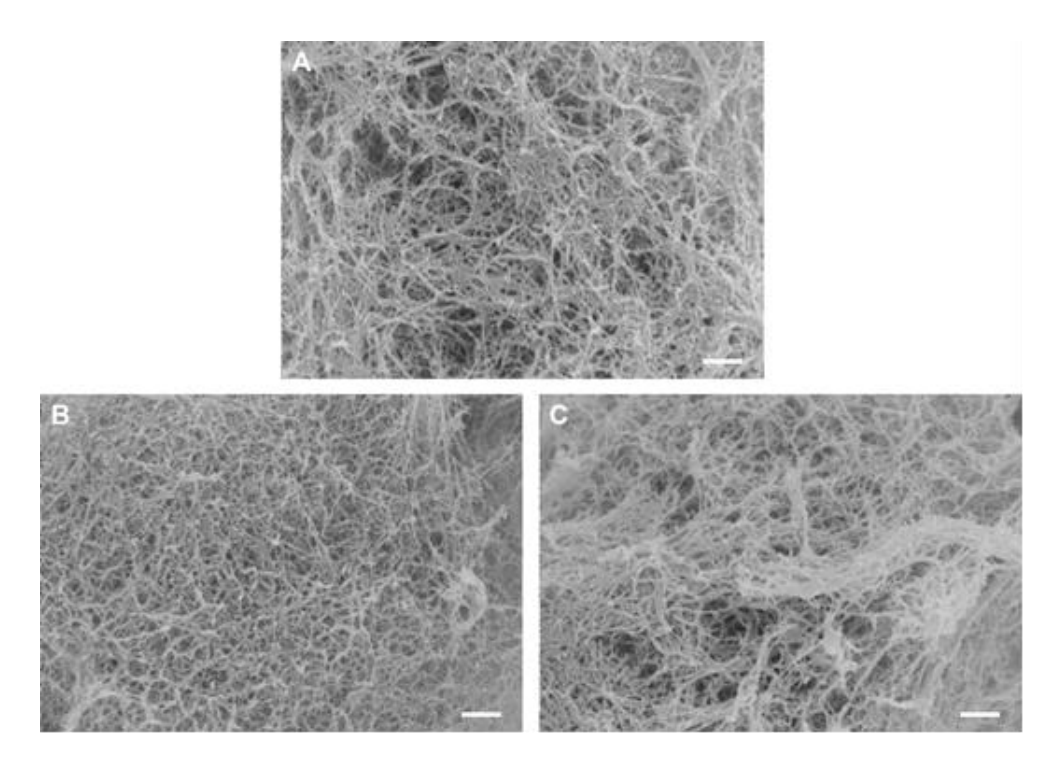


Figure 5.9. Scanning electron micrographs of 40 mM hydrazide, 120 mM aldehyde hydrogels catalyzed by  $\bf 1$  at pH 7 (A) without Doxorubicin, (B) with 1.0 mg/mL Doxorubicin (without preincubation) and (C) with 1.0 mg/mL Doxorubicin pre-incubated for 24 hours. Scale bars 1  $\mu$ m.

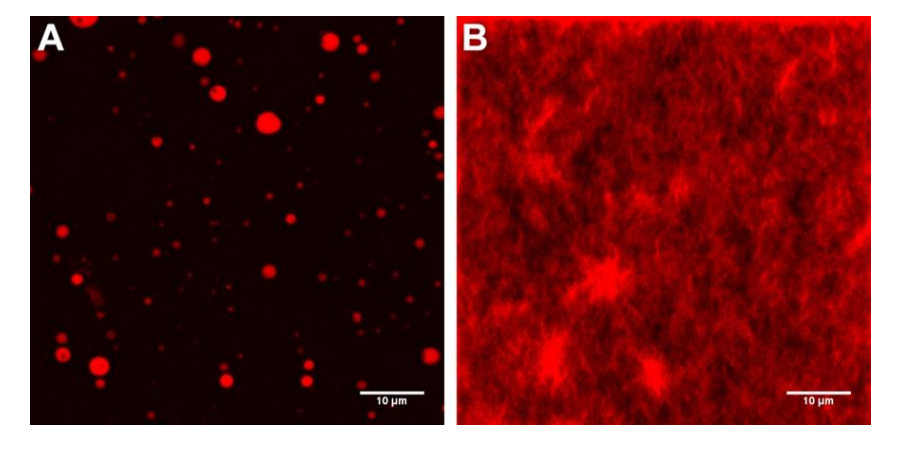


Figure 5.10. CLSM micrographs of Doxorubicin loaded hydrogel formation (40 mM hydrazide, 120 mM aldehyde catalyzed by 1 at pH 7, 1.0 mg/mL Doxorubicin, 24 h Doxorubicin - hydrazide preincubation) using the fluorescent properties of Doxorubicin for visualization. (A) Aldehyde droplets loaded with Doxorubicin at the beginning of the gelation process and (B) volume spanning hydrogel network showing the colocalization of Doxorubicin with the fiber network.

The effect of the Doxorubicin-hydrazide incubation time on the release of Doxorubicin from the reaction-coupled hydrogels was probed by a drug release experiment for a period of 28 days. In a typical experiment, Doxorubicin-loaded gels were allowed to gelate for 24 hours after which a buffer (5x the gel volume) was placed on top to facilitate drug release. These release buffers were exchanged on a daily basis and amount of Doxorubicin present within the solution was quantified by measuring its absorbance at 480 nm (Figure 5.11). Incubation times of 0 and 24 h of Doxorubicin and hydrazide-aldehyde resulted in sustained albeit distinct release profiles. During the first 7 d of the drug release experiment, Doxorubicin gels synthesized with a 24 h pre-incubation step involving hydrazide showed a steeper release curve relative to the 0 h sample. This result may be due to the weaker stiffness of the self-assembled network with the longer Doxorubicin incubation time. In general, complete release of Doxorubicin from the hydrogels was not observed due to the lack of material swelling and its slow degradation over the measuring period (Table 5.1). After 28 d, a 20 % lower release of Doxorubicin from the 24 hour preincubation strategy with hydrazide (55 % conjugated drug, 69 µg released) compared to those synthesized without pre-incubation step (0 % conjugated drug, 86 µg released) was observed, demonstrating the effect of altering the reaction pathway of the components on the release profile.

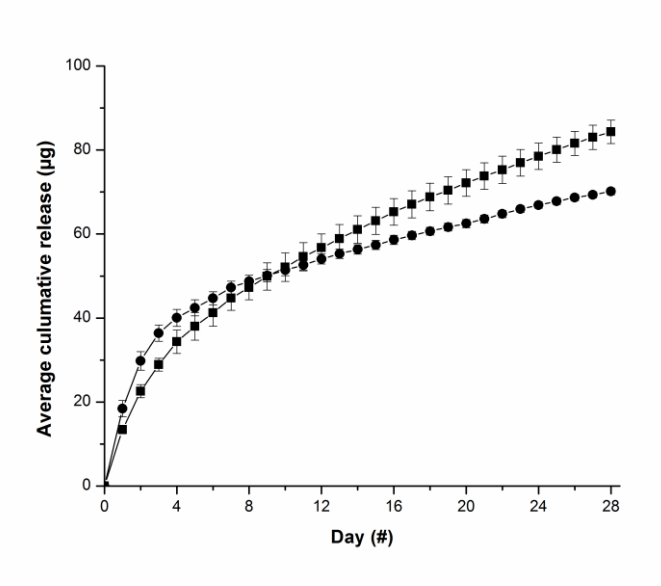


Figure 5.11. Doxorubicin drug release from hydrogels formed by 1 at pH 7 with 24 hour pre-incubation (circles) and without incubation (squares).

Table 5.1. Hydrogel degradation and swelling assay on hydrazide-aldehyde hydrogels catalyzed by 1 using different drug loading strategies. The change in weight of the material is expressed in percent.

Drug loading strategy	Weight change (%)
Native (no drug)	102.3 ± 3.1 %
0 h pre-incubation	97.5 ± 1.2 %
24 h pre-incubation	95.2 ± 0.9 %

Finally, a cell viability assay with MCF-7 human breast cancer cells was performed to evaluate the efficacy of cargo delivery from the scaffold and its toxicity. Hydrogels loaded with Doxorubicin (0.5 mg/mL) synthesized with the 0h preincubation strategy and hydrogels without Doxorubicin were suspended within a Transwell® set-up above seeded MCF-7 breast cancer cells. Only the hydrogels with a 0 h Doxorubicin incubation step were evaluated because of the amount of Doxorubicin released from both the pre-incubated and directly loaded gels used in this study would lead to concentrations far above the requirement to inhibit the cancer cell growth. The inhibition of cell growth was measured daily over a three-day period using a tetrazolium dye (MTT). The bare hydrogel showed viability on par with the control sample (108.2 +/- 1.4%), whereas the drug loaded gel showed significant cell death (49.9 +/- 3.1%) after three days (Figure 5.12). Phase contrast images of the wells containing Doxorubicin-loaded gels further support this finding, presenting cells of a rounded morphology (Figure 5.13). Moreover, cell death due to Doxorubicin was confirmed by CLSM, which showed localization of red fluorescence primarily at the nucleus showing the effective delivery of the drug (Figure 5.14). These results show both the biocompatibility of the LMWG platform as well as its capacity for drug delivery as established by Doxorubicin-induced cell death.

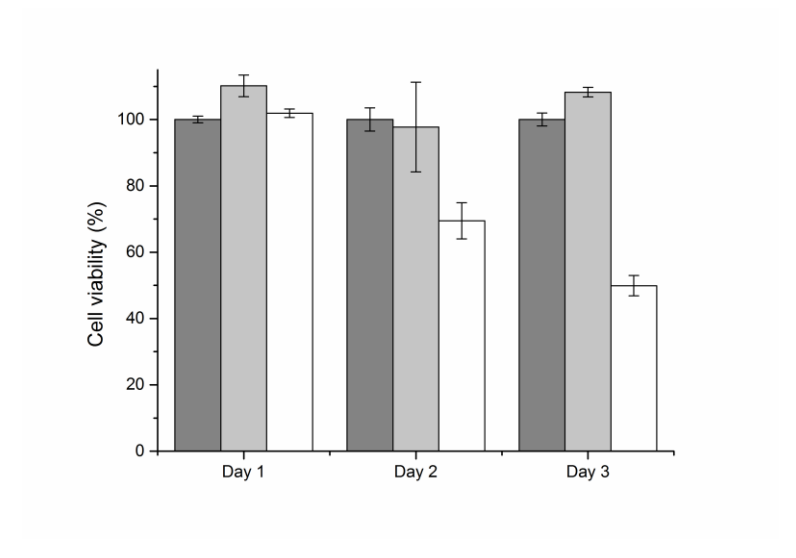


Figure 5.12. MTT-cell viability essay showing the effect of Doxorubicin release (0.5 mg/mL) from hydrogels catalyzed by **1** on MCF-7 cells. Conditions: untreated cells (d*ark grey*); cells treated with bare hydrogel (*light grey*); cells treated with drug-loaded hydrogels (*white*).

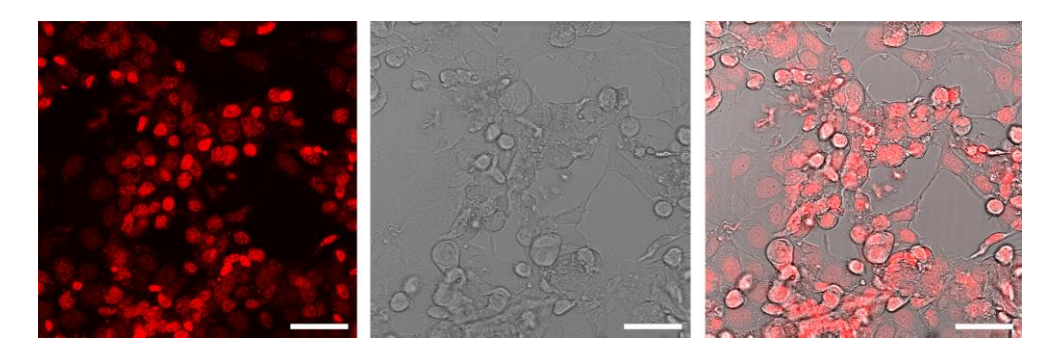


Figure 5.13. CLSM micrographs of MCF-7 cells subjected to hydrogels with Doxorubicin (0.5 mg/mL). Left: fluorescent image (Doxorubicin,  $\lambda_{ex}$  480 nm), middle: transmission image, right: merged image. Scale bar 50  $\mu$ m.



Figure 5.14. Phase contrast images of MCF-7 cells taken on day 3 of a hydrogel drug release assay with doxorubicin (0.5 mg/mL). A) untreated cells, B) cells treated with hydrogel without doxorubicin and C) cells treated with hydrogel containing doxorubicin. Scale bar size 30  $\mu$ m.

### 5.4 Conclusion

In conclusion, we demonstrate control over the drug release properties of a reaction-coupled low molecular weight gelator by modifying its reaction pathway. Using this strategy, the Doxorubicin can be easily incorporated into the self-assembled network by encapsulation or conjugation depending on the incubation time with hydrazide. Furthermore, we show the biocompatibility of the reaction-coupled material by lowering the equivalents of aldehyde and using a biocompatible catalyst, L-histidine methyl ester at pH 7, and demonstrated its capacity to release Doxorubicin by exerting its toxicity on MCF-7 breast cancer cells. This study thus highlights the immense potential of adapting the reaction-coupled gelation strategy to expeditiously formulate drug-laden materials in situ with tuneable release profiles for a broad range of therapeutic applications.

## 5.5 References

- 1 E. Krieg, M. M. C. Bastings, P. Besenius and B. Rybtchinski, Chem. Rev., 2016, 116, 2414–2477.
- 2 X. Du, J. Zhou, J. Shi and B. Xu, Chem. Rev., 2015, 115, 13165–13307.
- A. Baral, S. Roy, A. Dehsorkhi, I. W. Hamley, S. Mohapatra, S. Ghosh and A. Banerjee, Langmuir, 2014, 30, 929–36.
- 4 M. Ikeda, T. Tanida, T. Yoshii, K. Kurotani, S. Onogi, K. Urayama and I. Hamachi, Nat. Chem., 2014, 6, 511–8.
- 5 J. Raeburn and D. J. Adams, Chem. Commun., 2015, 51, 5170–5180.
- 6 S. R. Diegelmann, J. M. Gorham and J. D. Tovar, J. Am. Chem. Soc., 2008, 130, 13840–13841.
- J. Boekhoven, J. M. Poolman, C. Maity, F. Li, L. van der Mee, C. B. Minkenberg, E. Mendes, J. H. van Esch and R. Eelkema, Nat. Chem., 2013, 5, 433–7.
- 8 Z. Yang and B. Xu, Adv. Mater., 2006, 18, 3043–3046.
- 9 Z. Yang, H. Gu, D. Fu, P. Gao, J. K. Lam and B. Xu, Adv. Mater., , DOI:10.1002/adma.200400340.
- 10 S. Toledano, R. J. Williams, V. Jayawarna and R. V Ulijn, J. Am. Chem. Soc., 2006, 128, 1070–1071.
- 11 F. Zhao, C. S. Weitzel, Y. Gao, H. M. Browdy, J. Shi, H.-C. Lin, S. T. Lovett and B. Xu, Nanoscale, 2011, 3, 2859–61.
- 12 M. E. Hahn and N. C. Gianneschi, Chem. Commun., 2011, 47, 11814.
- 13 M. A. Azagarsamy, P. Sokkalingam and S. Thayumanavan, J. Am. Chem. Soc., 2009, 131, 14184–14185.
- 14 P. K. Vemula, J. Li and G. John, J. Am. Chem. Soc., 2006, 128, 8932–8938.
- 15 X. Li, J. Li, Y. Gao, Y. Kuang, J. Shi and B. Xu, J. Am. Chem. Soc., 2010, 132, 17707–17709.

- 16 L. Frkanec, M. Joki, J. Makarevi, K. Wolsperger and M. Ž. Ini, J. Am. Chem. Soc, 2002, 124, 9716–9717.
- 17 D. B. Rasale and A. K. Das, Int. J. Mol. Sci., 2015, 16, 10797–10820.
- A. R. Hirst, S. Roy, M. Arora, A. K. Das, N. Hodson, P. Murray, S. Marshall, N. Javid, J. Sefcik, J. Boekhoven, J. H. van Esch, S. Santabarbara, N. T. Hunt and R. V Ulijn, Nat. Chem., 2010, 2, 1089–94.
- J. S. Foster, J. M. Zurek, N. M. S. Almeida, W. E. Hendriksen, V. A. A. Le Sage, V. Lakshminarayanan, A. L. Thompson, R. Banerjee, R. Eelkema, H. Mulvana, M. J. Paterson, J. H. Van Esch and G. O. Lloyd, J. Am. Chem. Soc., 2015, 137, 14236–14239.
- S. Sutton, N. L. Campbell, A. I. Cooper, M. Kirkland, W. J. Frith and D. J. Adams, Langmuir, 2009, 25, 1365–1370.
- N.Ashwanikuma, N. A. Kumar, S. A. Nair and G. S. V. Kuma, RDC Adv., 2014, 29157–29164.
- A. Friggeri, B. L. Feringa and J. Van Esch, J. Control. Release, 2004, 97, 241–248.
- A. Altunbas, S. J. Lee, S. a. Rajasekaran, J. P. Schneider and D. J. Pochan, Biomaterials, 2011, 32, 5906–5914.
- 24 K. J. C. van Bommel, M. C. a Stuart, B. L. Feringa and J. van Esch, Org. Biomol. Chem., 2005, 3, 2917–2920.
- 25 J. A. Sáez, B. Escuder and J. F. Miravet, Tetrahedron, 2010, 66, 2614–2618.
- 26 J. B. Matson and S. I. Stupp, Chem. Commun., 2011, 47, 7962–4.
- 27 M. Zhou, A. M. Smith, A. K. Das, N. W. Hodson, R. F. Collins, R. V. Ulijn and J. E. Gough, Biomaterials, 2009, 30, 2523–2530.
- 28 A. G. Cheetham, P. Zhang, Y. Lin, L. L. Lock and H. Cui, J. Am. Chem. Soc., 2013, 135, 2907–10.
- J. Boekhoven, M. Koot, T. a Wezendonk, R. Eelkema and J. H. van Esch, J. Am. Chem. Soc., 2012, 134, 12908–11.

- P. K. Vemula, G. A. Cruikshank, J. M. Karp and G. John, Biomaterials, 2009, 30, 383–393.
- J. M. Poolman, J. Boekhoven, A. Besselink, A. G. L. Olive, J. H. van Esch and R. Eelkema, Nat. Protoc., 2014, 9, 977–88.
- B. Buchs, W. Fieber, F. Vigouroux-Elie, N. Sreenivasachary, J.-M. Lehn and A. Herrmann, Org. Biomol. Chem., 2011, 9, 2906–2919.
- 33 J. B. Matson, C. J. Newcomb, R. Bitton and S. I. Stupp, Soft Matter, 2012, 8, 3586–3595.
- D. Larsen, M. Pittelkow, S. Karmakar and E. T. Kool, Org. Lett., 2014, 17, 274–277.
- Y. Cheng, A. A. Nada, C. M. Valmikinathan, P. Lee, D. Liang, X. Yu and S. G. Kumbar, J. Appl. Polym. Sci., 2014, 131, 1–11.
- 36 R. M. Lopachin and T. Gavin, Chem. Res. Toxicol., 2014, 27, 1081–1091.
- L. Chen, K. Morris, A. Laybourn, D. Elias, M. R. Hicks, A. Rodger, L. Serpell and D. J. Adams, Langmuir, 2010, 26, 5232–5242.
- W. E. M. Noteborn, D. N. H. Zwagerman, V. S. Talens, C. Maity, L. van der Mee, J. M. Poolman, S. Mytnyk, J. H. van Esch, A. Kros, R. Eelkema and R. E. Kieltyka, Adv. Mater., 2017, 29, 2.

# **5.6 Supporting Information**

#### 5.6.1 Materials

L-Histidine methyl ester (1), aniline (2), doxorubicin dihydrochloride, dimethylsulfoxide (DMSO), thiazolyl blue tetrazolium bromide (MTT) and Corning Transwell® membrane culture inserts (6.5 mm, 0.4 µm pore size) were obtained from Sigma Aldrich. Dulbecco's modified eagle cell culture medium (DMEM), Fetal Calf Serum (FCS), Penicillin, Streptomycin and GlutaMAX were obtained from Thermo Fisher Scientific. Hydrazide and aldehyde gelator molecules were synthesized as previously reported.¹ Water was deionized before use.

### 5.6.2 General methods

Oscillatory rheological measurements were obtained on a Discovery Hybrid Rheometer-2 (DHR-2) equipped with 20 mm diameter parallel plate geometry, Peltierbased temperature control and a solvent trap. Samples for scanning electron microscopy were prepared on a Ball-Tec CPD 030 critical point dryer. Scanning electron microscopy (SEM) imaging was performed using a JEOL JSM-6400. UV-Vis spectroscopy was executed on a BioDrop µLite using quartz cuvettes of a 1 cm path length. LC-MS analysis was performed on a Finnigan Surveyor HPLC system equipped with a Gemini C18 50×4.60 mm column (UV detection at 200-600 nm), coupled to a Finnigan LCQ Advantage Max mass spectrometer with ESI. The mobile phase consisted of H<sub>2</sub>O and CH<sub>3</sub>CN with 0.1% trifluoroacetic acid. Dynamic light scattering (DLS) experiments were performed on a Malvern Zetasizer Nano S using plastic cuvettes with a 10 mm path length and measurements were taken at an angle of 173°. Confocal laser scanning micrographs for hydrogel imaging were acquired on a Zeiss LSM 710 confocal laser scanning microscope equipped with a Zeiss 40x/1.3 oil immersion objective. Fluorescence and transmittance MCF-7 cell imaging was acquired on a LEICA SPE confocal system equipped with a DMI4000B-CS microscope and a HCX APO L U-V-I water immersion objective (40x/NA 0.80). Phase contrast images were acquired on an Olympus IX 81 microscope. MCF-7 human melanoma cells were cultured (37 °C, 5 % CO<sub>2</sub>) in DMEM with 10 % Fetal Calf Serum, 0.02% GlutaMAX and Penicillin (100 U/mL) and Streptomycin (100 µg/mL).

# 5.6.3 General gelation methods

Hydrogels were prepared by separately dissolving the desired concentration of hydrazide (50 - 100 mM) in 80  $\mu$ L and aldehyde (80 - 160 mM) in 100 $\mu$ L of a given buffer as stated below. The same buffer (20  $\mu$ L) with or without doxorubicin (200  $\mu$ g) was then pre-incubated with hydrazide (0 – 24 hours) before addition of aldehyde and used according to the protocol for the given experiment (*vide infra*). Buffers at pH 7 consisted of 0.1 M phosphate with 0.1 M NaCl and of either 10 mM catalyst 1 or 2, and the buffer pH 5 contained 0.1 M phosphate with 0.1 M NaCl.

# 5.6.4 Rheology

Oscillatory rheology samples (final concentration hydrazide: 40 mM) were prepared according to the general gelation protocol with and without doxorubicin (0 - 2.0 mg/mL). The components were mixed by pipetting three times and the sample was loaded on a parallel plate with a 500  $\mu$ m gap. All time sweep measurements were performed at 25 °C ± 0.2 °C using 0.05 % strain and a frequency of 1.0 Hz. All rheological measurements were performed in triplicate.

## 5.6.5 Scanning electron microscopy

Hydrogel samples (200  $\mu$ L) were prepared overnight and dehydrated step-wise in ethanol (increasing in ethanol volume; 70-80-90-95-100%, 15 minutes for each step) and then in acetone. The dehydrated hydrogel was then dried using a critical point dryer. The dried hydrogel was mounted on a SEM stub and sputter coated with gold. Scanning electron micrographs were acquired on a JEOL JSM-6400, equipped with a tungsten filament gun operating at 10 kV and 8 mm working distance.

# 5.6.6 Avrami analysis

The dimensionality of fiber growth was assessed by plotting  $\ln(-\ln(1-X))$  against  $\ln(t-t_0)$  using the complex modulus,  $G^*$ , from rheological data in which  $X = (G^*_t-G^*_0)/(G^*_{max}-G^*_0)$ . The Avrami coefficient n was determined by calculating the slope of the first transition where nucleation and growth of the fibers takes place.<sup>2</sup>

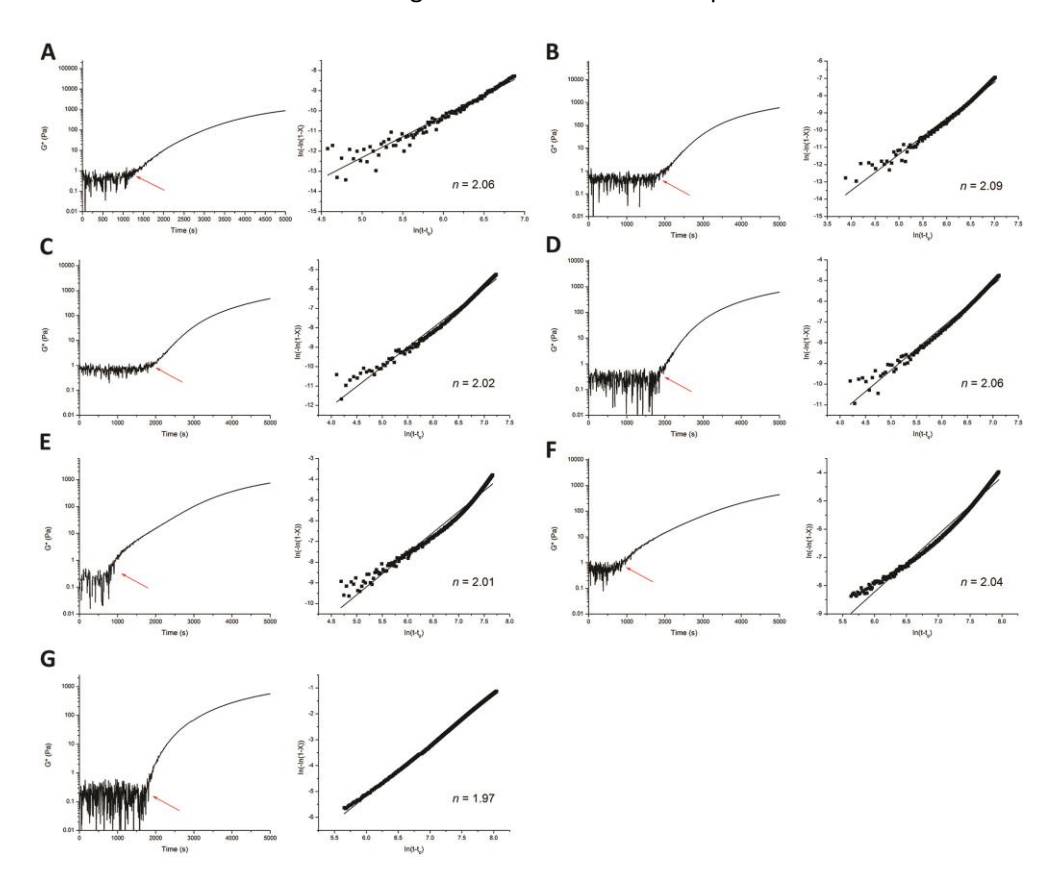


Figure S5.1. Avrami analysis of complex moduli (G\*) obtained from oscillatory rheology profiles of the various hydrogel samples with (1.0 mg/mL) and without Doxorubicin and with different incubation times. Arrows were used to indicate the region of the curve fitted for subsequent analysis. Time sweep data and Avrami plots of: A) gel without Doxorubicin, B) 0 h incubation, C) 1 h incubation, D) 2 h incubation, E) 4 h incubation, F) 8 h incubation, G) 24 h incubation.

# 5.6.7 Confocal laser scanning microscopy

Confocal laser scanning micrographs were acquired on a Zeiss LSM 710 confocal laser scanning microscope equipped with a Zeiss 40x, 1.3 oil immersion objective and using an excitation wavelength of 488 nm and an emission filter of 510-570 nm for both imaging Doxorubicin only and NileRed stained hydrogels. Still images were acquired at 536 x 536 pixels (64 x 64  $\mu$ m). Samples were prepared as described in the general gelation protocol with the addition of 0.5  $\mu$ L of a Nile Red solution (2.5 mM) dissolved in ethanol prior to adding a solution of aldehyde. Gelation samples were mixed by pipetting before deposition into Ibidi 8-well slides for imaging. Images were taken directly after mixing and 24 hours after the onset of gel formation.

# 5.6.8 Dynamic light scattering

Dynamic light scattering (DLS) measurements were performed on 200  $\mu$ L solutions of aldehyde (120 mM) mixed with and without 1.0 mg/mL Doxorubicin in pH 7 buffer containing 10 mM L-histidine methyl ester (1). Their resulting scattered light intensities and corresponding particle sizes were measured at a 173° angle in a polystyrene cuvette at 25°C. All samples were measured in triplicate.

# 5.6.9 Hydrogel degradation and swelling assay

Hydrogel samples (200  $\mu$ L) were prepared according to the gelation protocol above using the various catalysts and were allowed to gelate for 24 hours, at which point the wet weight of the hydrogel was determined. Afterwards, 0.1 M pH 7 phosphate buffer with 0.1 M NaCl (1 mL) was added on top and left to stand overnight. On the following day, a portion of the supernatant (800  $\mu$ L) was carefully removed and replaced with an equal amount of fresh buffer over a 28-day period. The final weight of the hydrogel was determined by removing all of the supernatant. The percentage of hydrogel degradation or swelling by weight was determined by the following equation: Weight change (%) = [Weight (hydrogel after degradation or swelling)] x 100%.

# 5.6.10 Vial drug release studies

Hydrogel samples (200  $\mu$ L) were prepared according to the general gelation protocol with doxorubicin (1.0 mg/mL) using the various buffers at pH 7 with catalyst **1**. Samples were made using either the no pre-incubation or 24 hour pre-incubation time strategy, in which the doxorubicin is pre-incubated with hydrazide before the addition of aldehyde, and afterwards allowed to stand for 24 hours. A 0.1 M phosphate buffer with 0.1 M NaCl (1 mL) was added on top of the hydrogel and left to stand for 24 hours. Afterwards, a fraction of the supernatant (800  $\mu$ L) was replaced daily with the appropriate fresh buffer. The removed fraction was analyzed by UV-Vis spectroscopy following the absorbance 480 nm to quantify the amount of doxorubicin released from the hydrogel. This experiment was also repeated for a hydrogel catalyzed by **1** at pH 7 with doxorubicin using a release buffer at pH 5 consisting of 0.1 M phosphate buffer with 0.1 M NaCl.

# 5.6.11 Cell viability studies

MCF-7 cells were seeded at a density of 25,000 cells/well (24 well plate) in medium (500  $\mu$ L) for 24 hours before hydrogel application. Hydrogels catalyzed by **1** with and without doxorubicin were prepared in Transwell® inserts and were suspended following day in the well plate. The viability of the cells was determined using the MTT assay at 24 hour intervals. An MTT stock solution (5 mg/mL) was prepared in 1x PBS and filter sterilized. The MTT stock solution (20  $\mu$ L) was added to each well and incubated for 4 hours to enable the formation of purple formazan crystals. The medium was aspirated and the formazan crystals were re-dissolved in DMSO (500  $\mu$ L). The extent of formazan production was quantified by UV-Vis spectroscopy using the absorbance band at 570 nm. Results were reported in % viability = [A570 (cells treated with hydrogel) / A570 (cells untreated)] x 100%. All conditions were tested in triplicate. For images taken by confocal laser scanning microscopy, cells were seeded on top of a glass coverslip within the well and removed prior to imaging on microscope slide.

# 5.6.12 References

- J. M. Poolman, J. Boekhoven, A. Besselink, A. G. L. Olive, J. H. van Esch, R. Eelkema, Nat. Protoc. 2014, 9, 977–88.
- 2 X. Y. Liu, P. D. Sawant, Adv. Mater. 2002, 14, 421–426.

# **CHAPTER 6**

**Summary and Perspectives** 

Self-assembly is an abundant process in nature and is vital to many processes in living organisms. During the last decade the fields of supramolecular chemistry and polymer science have made an integrated effort in the design, synthesis and application of supramolecular polymers. Supramolecular polymers rely on relatively weak noncovalent interactions such as hydrogen bonding, solvophobicity and  $\pi$ -stacking to selfassemble using a wide array of natural and artificially designed interaction motifs. Using these principles, both end-functionalized polymers interacting via molecular recognition and stacked monomers self-assembling into one-dimensional structures have been demonstrated. These supramolecular polymers have the ability to form gel-phase materials at high concentrations because physical or covalent interactions between the overlapping polymers promote stopping the solvent flow. The possibility to perform self-assembly in water and their stimuli-responsive nature to stimuli like heat, light, pH, ionic strength and catalysis opened up the possibility to make functional supramolecular materials with many applications ranging from sensors to drug delivery platforms and biomaterials. A uniquely naturally-occurring supramolecular polymer is DNA which, apart from its role in genetics, can be used as a building block for both structural and dynamic applications such as making wellorganized three-dimensional lattices or reconfigurable and autonomously operating DNA-based devices. One particular reaction of note is the hybridization chain reaction, a toehold-mediated strand displacement reaction that has great potential for the detection and amplification of nucleic acid signals. As every class of materials has their own advantages, designing multicomponent materials from multiple types of building blocks such as DNA, and supramolecular and covalent polymers, has the potential to create highly advanced, organized and responsive materials both from structural and functional points of view. This dissertation has focused on designing such multicomponent functional supramolecular materials for biomedical applications and diagnostics.

In chapter 2, the synthesis of a DNA-dextran graft copolymer is shown. A novel grafting from strategy using the hybridization chain reaction as a driving force for graft growth is reported (Figure 6.1). The design encompasses the immobilization of thiolated HCR initiator sequences on a dextran-vinyl sulfone polymer using a Michael addition. The initiator-DNA polymer mixed with the two HCR hairpins similar to the native unconjugated HCR system triggers growth of the DNA grafts Interestingly, homodimer interactions between the initiator sequences results in the formation of aggregated initiator DNA-dextran clusters prior to graft growth by HCR. These aggregates are still capable of initiating HCR and afterwards form bigger clusters due to similar homodimer interactions between HCR-extended DNA grafts.

These clusters can be readily broken by heating at 60 °C to reveal the expected monomeric graft copolymer sizes. The morphological changes of these polymers have been shown using gel electrophoresis, fluorescence, light scattering (DLS, SAXS) and atomic force microscopy. At higher concentrations, performing the hybridization chain reaction on the aggregated polymers results in the formation of hydrogel materials, as demonstrated by particle tracking microrheology. By the same approach and a catalytic amplification strategy, this model system can be turned into a detection system for specific oligonucleotide-based targets, such as microRNAs. Consequently, this approach would yield a simple and robust, instrument-free method to detect the presence of disease biomarkers in the future.

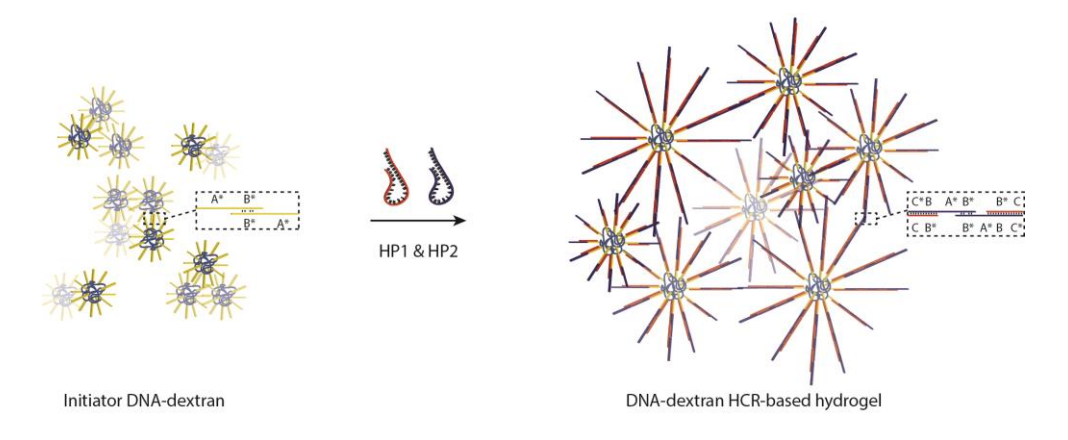


Figure 6.1. Grafting from a hybrid DNA-dextran graft copolymer by the hybridization chain reaction

Chapter 3 showcases the design and synthesis of a functional multicomponent squaramide-based supramolecular polymer for the reversible loading of gold cargo (Figure 6.2). First, the synthesis of DNA-functionalized supramolecular monomers by performing CuAAC reactions with hexynylfunctionalized DNA and azide-functionalized bola-amphiphilic supramolecular monomers was shown. Next, the incorporation of the DNA-functionalized monomers into native supramolecular polymers was demonstrated using zeta potential measurements. Lastly, the reversible loading of DNA-functionalized gold nanoparticles with different sizes (5 and 15 nm) was shown in both a multicomponent and write-erase-rewrite fashion. For this, DNA strand displacement techniques were used in which toehold mediated strand displacement could selectively address sequence specific targets and thus selectively remove specific gold nanoparticles. The formation of these reversibly addressable functionalized fibers and the strand displacement

reactions have been demonstrated using extensive transmission electron microscopy studies combined with gel-electrophoresis and fluorescence experiments. Having made a supramolecular platform for controlled cargo loading, erasing and rewriting, this opens up possibilities to decorate supramolecular fibers with specific cell signaling molecules, which could be used for guiding of cellular differentiation. In this way, multiple signaling molecules could be sequentially presented and removed to allow specific control over signaling cues. Another application of this system would be in the specific release of cargo if the system would be designed in such a way that the presence of naturally occurring sequences like miRNAs can trigger cargo release.

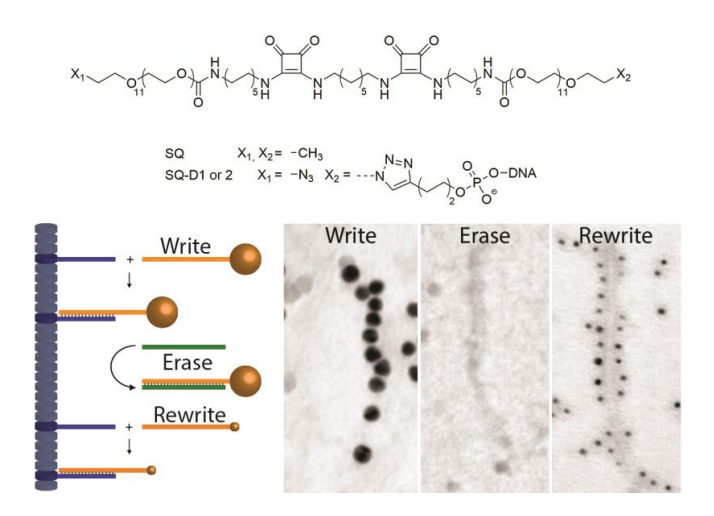


Figure 6.2. Reversible loading of nanoscale elements on a multicomponent supramolecular polymer system using DNA strand displacement

Chapter 4 demonstrates the effect of crosslinkers on the gelation pathway of a reaction-coupled multicomponent low molecular weight hydrogelator system, with the goal to improve the mechanical properties of the resulting networks. In this LMWG system, a hydrazone bond is formed between a cyclohexane trishydrazide core and three di(ethylene glycol) benzaldehyde wedges to drive the formation of a hydrogel. Two distinct crosslinkers, a stiff charged DNA- and soft neutral polyethylene glycol-modified crosslinker, both end-functionalized with benzaldehyde motifs were synthesized for incorporation into the fibrous hydrogel network (Figure 6.3). Surprisingly, rheological measurements showed that addition of up to 1.0 mol% of a stiff DNA crosslinker resulted in the increase of the storage modulus, G', of the gel up to 4.5 fold, but the PEG-based crosslinker did not yield any increase in mechanical

properties. Fluorescent confocal laser scanning microscopy revealed the nucleation and growth phenomena present in this system and showed the either positive or negative effects of the different crosslinkers on network formation resulted in distinct mechanical properties. This study revealed the effect of crosslinkers of varied stiffness on the mechanical properties of the network, but also the effects that additives can have on the gelation process. As the incorporation of crosslinkers and other (bio)molecules is required to make functional materials for biological applications, this work has shown that their incorporation needs to be taken into consideration in the design of such systems. Finally, this work saliently demonstrates the potential for another level of control over the self-assembly of reaction coupled LMWG systems, which can be exploited for use broadly in the low molecular weight gelator field.

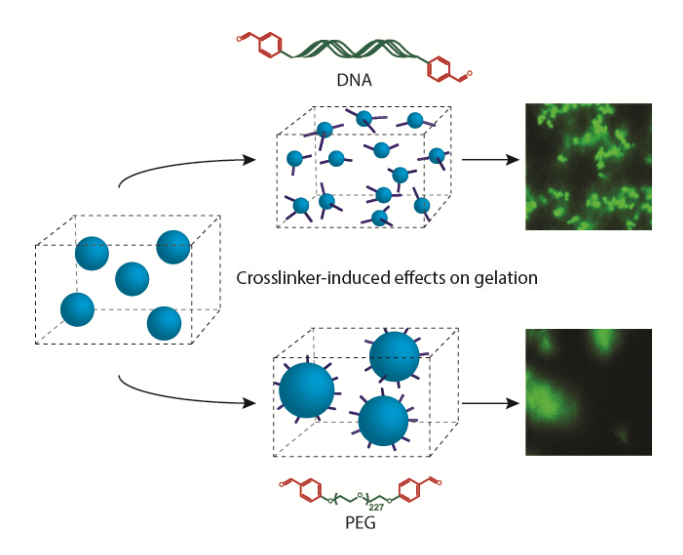


Figure 6.3. Crosslinker-induced effects on the gelation pathway of a low molecular weight hydrogel

Chapter 5 describes the synthesis of a controlled drug release platform using the same LMWG system as the previous chapter. First, the formation the hydrogels at pH 7.0 was demonstrated using a nucleophilic and biocompatible catalyst L-histidine methyl ester by rheology and SEM. Next, the anticancer drug Doxorubicin was incorporated by a reactive ketone moiety in the acetyl side chain of the drug molecule. The extent of Doxorubicin conjugation could be controlled in a time-dependent fashion by changing the incubation time of the ketone bearing drug to the hydrazine core gelator with the hydrazide core. Modulating the incubation time of the Doxorubicin drug and gelator core before addition of the second peripheral gelator not only influenced the extent of drug conjugation, but also drastically influenced

both the mechanical properties of the hydrogel network and the drug release profiles. Lastly, the LMWG system loaded with Doxorubicin delivered Doxorubicin in an effective manner to MCF-7 breast cancer cells *in vitro*, showing its potential as a tunable multicomponent drug delivery platform. The potential of reaction time coupled cargo loading and its effect on the release properties and mechanical performance of the material allows for further development of user-defined control over supramolecular materials for applications in the biomedical domain.

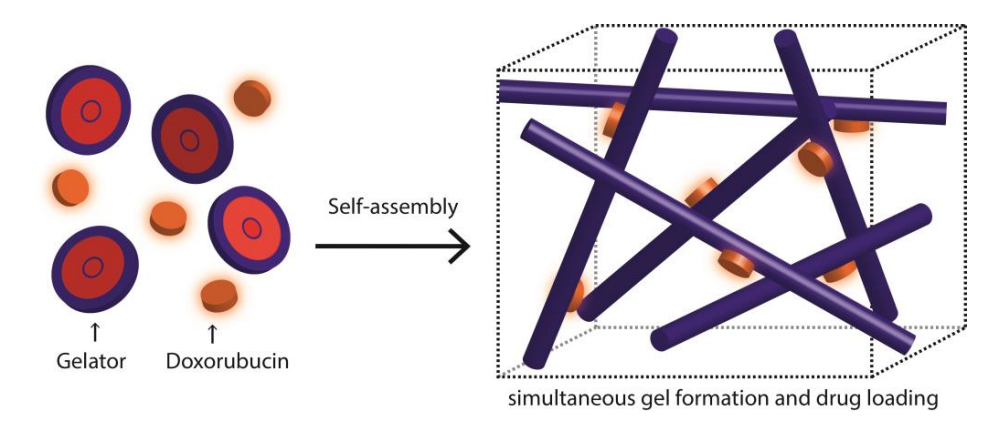


Figure 6.4. Tuning drug release from a reaction-coupled low molecular weight gelator system by modulating its reaction pathway

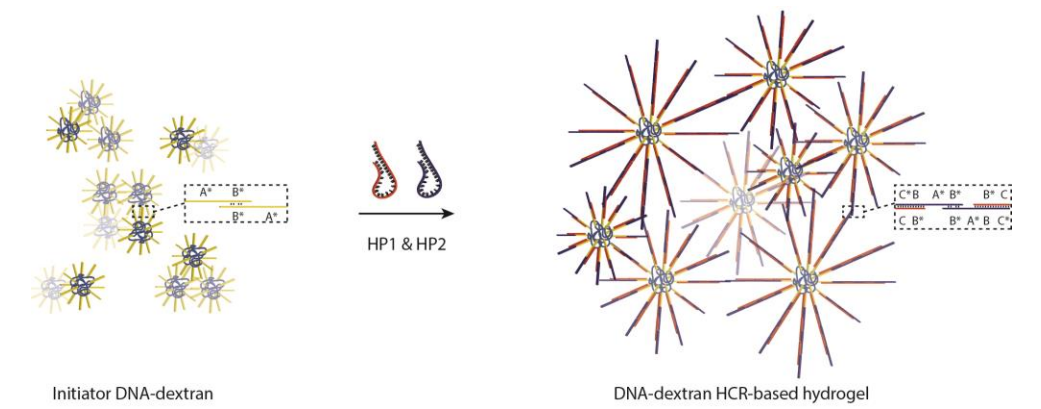
# **CHAPTER 7**

Nederlandse Samenvatting en Perspectieven

Zelf-assemblage is een zeer veel voorkomend proces in de natuur dat vitaal is voor vele processen in levende organismen. De laatste decenia hebben de wetenschapsvelden van de supramoleculaire- en polymeerchemie een geïntegreerde inspanning gedaan om supramoleculaire polymeren te ontwerpen, synthetiseren en toe te passen. Supramoleculaire polymeren maken gebruik van relatief zwakke nietcovalente interacties zoals waterstofbrug formatie, hydrofobe/hydrofiele scheiding en  $\pi$ -interacties om de zelf-assemblage van een breed scala aan zowel natuurlijke als artificieel ontwikkelde moleculaire bouwstenen te programmeren. Door toepassing van deze principes zijn eind-gefunctionalizeerde polymeren gemaakt die interacteren via moleculaire herkenning en gestapelde monomeren die zelf-assembleren in ééndimensionale structuren. Deze supramoleculaire polymeren hebben de mogelijkheid om bij hoge concentratie hydrogel materialen te maken door fysische of covalente interacties tussen de overlappende polymeren en daardoor de stroom van oplosmiddelen te minimalizeren. De mogelijkheid van deze materialen om te zelfassembleren in water en te reageren op externe stimuli zoals warmte, licht, pH, ion sterkte en katalyse het mogelijk gemaakt om functionele supramoleculaire materialen te creëren met applicaties variërend van sensoren tot medicijn afgifte platformen en biomaterialen. Een uniek en natuurlijk voorkomend supramoleculair polymeer is DNA, dat los van zijn rol in genetica ook gebruikt kan worden als een bouwsteen voor zowel structurele als dynamische toepassingen zoals het maken van goed georganiseerde drie-dimensionale roosters of reconfigureerbare en autonoom werkende op DNA gebaseerde apparaten. Een bijzondere en noemenswaardige reactie is de hydridisatie ketting reactie, een DNA overhang gedreven streng verdringingsreactie die veel potentie heeft in de detectie en amplificatie van nucleïnezuur gebaseerde signalen. Elke klasse van materialen heeft zijn eigen voordelen heeft en daarom is het ontwerpen van uit meerdere componenten bestaande materialen een mogelijkheid om zeer geavanceerde, georganiseerde en responsieve materialen te maken. Door gebruik te maken meerdere type bouwstenen zoals DNA, supramoleculaire- en covalente polymeren kunnen materialen gecreërd worden vanuit zowel het oogpunt van hun structuur en functie. Deze dissertatie is toegespitst op het ontwerp van dergelijke uit meerdere componenten bestaande functionele supramoleculaire materialen voor toepassingen in de biomedische wereld en diagnostiek.

In hoofdstuk 2 is de synthese van een dextraan copolymeer met DNA zijtakken beschreven. Ik heb een nieuwe strategie ontwikkeld om DNA zijtakken te vormen op de dextraan polymeren door gebruik te maken van de hybridisatie ketting reactie (HCR) als drijvingskracht voor zijtak groei vanaf het copolymeer (Figuur 7.1). Het ontwerp omvat de immobilizatie van gethioleerde HCR initiator sequenties via

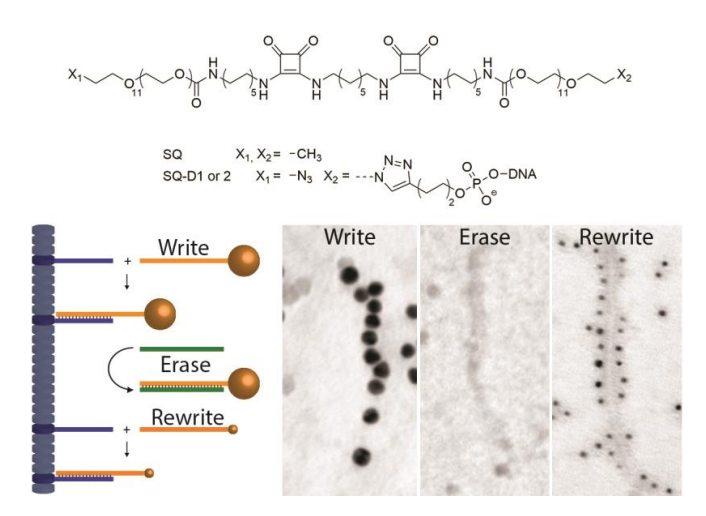
een Michael additie met een met vinyl sulfon gefunctionaliseerde dextraan. Het initiator-DNA polymeer is net zoals het ongeconjugeerde initiator DNA in staat om de groei van de zijtakken te starten wanneer het samengevoegd wordt met twee complementaire HCR hairpin DNAs. Opvallend is dat homodimeer interacties tussen de initiator sequenties resulteert in de formatie van geaggregeerde initiator DNAdextraan clusters voordat de groei van de zijtakken door HCR start. Deze aggregaten hebben nog steeds de mogelijkheid om de HCR te initializeren en vormen de gegroeide zijtakken op de copolymeren vormen nog grotere geaggregeerde clusters door vergelijkbare homodimeer interacties. Na verhitting van de aggregaten tot 60 °C worden de monomeren terug verkregen. Met behulp van gel electroforese, fluorescentie, licht verstrooing (DLS, SAXS) en atoomkrachtmicroscopie werden de morfologische veranderingen van deze polymeren te bestudeerd. Bij hogere concentraties kan de uitvoering van de hybridisatie ketting reactie op de copolymeren resulteren in de formatie van hydrogel materialen, zoals gedemonstreerd is met behulp van microreologie. Door kleine aanpassingen in dit systeem en de toevoeging van een katalytische amplificatie strategie kan er een detectie systeem voor specifieke oligonucleotide-gebaseerde doelwit moleculen, zoals microRNAs, gerealiseerd worden. Hierdoor zou deze aanpak in de toekomst een simpele en robuuste methode kunnen opleveren om biomarkers van specifieke ziektes te detecteren zonder gebruik te maken van gespecialiseerde apparatuur.



Figuur 7.1. Groei van DNA zijtakken vanaf een hybride DNA-dextraan copolymeer door gebruik te maken van de hybridisatie ketting reactie

Hoofdstuk 3 beschrijft het ontwerp en de synthese van een op squaramides gebaseerd functioneel supramoleculair polymeer. Dit supramoleculaire polymeer kan gebruikt worden voor het reversibel binden van goud deeltjes (Figuur 7.2). De synthese van DNA-gefunctionaliseerde supramoleculaire monomeren is beschreven waarbij koper gekatalyseerde azide-alkyn ringaddities tussen hexynyl-

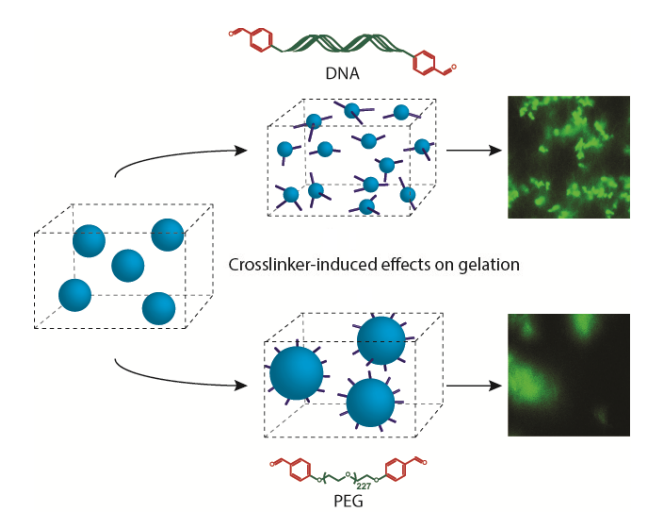
gefunctionaliseerd DNA en azide gefunctionaliseerde bolaamfifiele supramoleculaire monomeren gebruikt werden om de doelmoleculen te synthetiseren. Vervolgens werd de incorporatie van de DNA-gefunctionaliseerde monomeren in nietgefunctionaliseerde supramoleculaire polymeren gedemonstreerd door gebruik te maken van zeta potentiaal metingen. Als laatste is het tegelijktijdige laden en lossen van verschillende groottes DNA-gefunctionaliseerde goud nanodeeltjes (5 en 15 nm) gedemonstreerd. Hiervoor werd gebruik gemaakt DNA streng verdringingsreacties, waarin selectief sequentie specifieke doelwitten geadresseerd werden, resulterend in het selectief verwijderen van goud nanodeeltjes. De vorming van deze reversibel adresseerbare gefunctionaliseerde fibers en de streng verdringingsreacties werd gekarakteriseerd behulp van transmissie electron microscopie studies in combinatie met gel electroforese en fluorescentie experimenten. Met dit nieuwe supramoleculaire platform is het dan mogelijk om op een gecontroleerde manier lading (goud nanodeeltjes) te schrijven, wissen en Hierdoor kan dit systeem mogelijk gebruikt worden supramoleculaire fibers te maken waarop specifieke cellulaire signaal moleculen geladen kunnen worden. Deze zouden gebruikt kunnen worden voor bijvoorbeeld differentiatie van cellen aan te sturen. Op deze manier zouden meerdere en verschillende signaal moleculen op een opeenvolgende manier gepresenteerd en verwijderd kunnen worden, hetgeen specifieke controle over cellulaire signalering op kan leveren. Als het systeem responsief gemaakt wordt voor bijvoorbeeld de aanwezigheid en detectie van specifieke miRNA sequenties dan zou een andere



Figuur 7.2. Reversibel laden van nanogrootte elementen op een uit meerdere componenten bestaand supramoleculair polymeer door middel van DNA streng verdringingsreacties

mogelijk toepassing van dit systeem het specifiek afgeven van medicinale lading kunnen zijn.

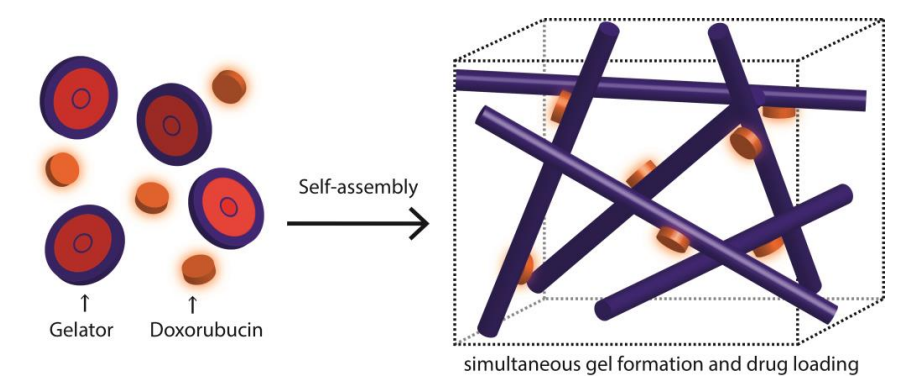
Hoofdstuk 4 laat het effect van crosslinkers zien op de vorming van een reactie gekoppelde laag moleculair gewicht hydrogelator (LMWG) systeem dat uit meerdere componenten bestaat. Het doel hiervan is de mechanische eigenschappen van het resulterende netwerk te verbeteren. In dit LMWG systeem wordt een hydrazon verbinding gemaakt tussen een hydrofobe cyclohexaan trishydrazide binnenkant en drie hydrofiele di(ethyleen glycol) benzaldehyde moleculen om zo de formatie van een hydrogel te bewerkstelligen. Twee verschillende crosslinkers werden gesynthetiseerd om ze vervolgens in het uit fibers bestaande hydrogel netwerk te incorporeren: een stijf en geladen DNA- en een zachte neutrale polyethyleen glycol (PEG) gemodificeerde crosslinker, beide met eind-gefunctionaliseerde benzaldehyde motieven (Figuur 7.3). Reologische metingen toonden aan dat de toevoeging van tot 1.0 mol% DNA crosslinker resulteerde in een tot maximaal 4.5 voudig verbeterde mechanische sterkte, terwijl de PEG crosslinker bij geen enkele concentratie een positief effect had op de sterkte van de hydrogel. Met behulp van fluorescente confocale laser scanning microscopie wordt het mechanisme van nucleatie en groei bestudeert. Hierdoor konden de positieve en negatieve effecten van de verschillende crosslinkers (DNA, PEG) op de netwerk formatie en de mechanische eigenschappen verklaard worden.



Figuur 7.3. Crosslinker-geïnduceerde effecten op het gelatie process van een laag moleculair gewicht hydrogelator systeem

Deze studie liet dus niet alleen het effect van de crosslinkers met verschillende stijfheid op de mechanische eigenschappen van het netwerk zien, maar ook het effect dat additieven kunnen hebben op de vorming van hydrogelen. Aangezien de incorporatie van crosslinkers en andere (bio)moleculen noodzakelijk is om functionele materialen te maken voor biologische applicaties, heeft dit werk laten zien dat het mogelijke effect van de incorporatie van functionaliteit in ogenschouw genomen moet worden het ontwerp. Tenslotte toont dit werk de mogelijkheid om extra controle over de zelf-assemblage van reactie gekoppelde LMWG-systemen te krijgen, wat van belang is om toepassingen te ontwikkelen voor deze laag molecuul gewicht gelators.

Hoofdstuk 5 beschrijft de synthese van een medicijn afgifte platform door gebruik te maken van hetzelfde LMWG systeem zoals beschreven in hoofdstuk 4 (Figuur 7.4). Als eerste zijn er hydrogels bij pH 7.0 gemaakt door gebruik te maken van een nucleofiele en biocompatabile katalysator, L-histidine methyl ester. Deze hydrogels zijn vervolgens met behulp van reologie en rasterelectronenmicroscopie bestudeerd. Vervolgens is het anti-kanker medicijn Doxorubicine geïncorporeerd door gebruik te maken van de reactieve keton groep in de acetyl zijketen van het molecuul. Uit deze experimenten bleek dat de mate van Doxorubicine conjugatie beïnvloed kan worden op een tijdafhankelijke manier door de incubatietijd van het keton bevattende medicijn met de hydrazine bevattende gelator kern te veranderen. Door de incubatietijd van Doxorubicine en de gelator kern te variëren vóór de toevoeging van de aldehyde gelator werd niet alleen de mate van medicijn conjugatie bepaald maar werden ook de mechanische eigenschappen van het netwerk en de



Figuur 7.4. Gecontroleerde medicijn afgifte door reactie tijd veranderingen in een reactie gekoppeld laag moleculair gewicht hydrogel systeen.

medicijn afgifte profielen significant beïnvloed. Tenslotte kon de Doxorubicine-hydrogel het medicijn op een effectieve manier *in vitro* aan MCF-7 borstkanker cellen afgeven. Hiermee werd bewezen dat dit afstembare uit meerdere componenten bestaande hydrogel systeem effectief gebruikt kan worden als medicijn afgifte platform. De mogelijkheid om reactietijd te koppelen aan de hoeveelheid conjugatie en het effect ervan op de zowel de afgifte- als de mechanische eigenschappen van hydrogel materialen kan gebruikt worden voor verdere ontwikkeling van de gebruiker gedefinieerde controle over supramoleculaire materialen voor toepassingen in het biomedische domein.

# **Curriculum Vitae**

Willem Noteborn was born on June 24, 1988 in Leiden, The Netherlands. He graduated from Stedelijk Gymnasium Leiden in 2006. In 2010, he obtained a Bachelor of Science degree in Life Science and Technology at the Universiteit Leiden and Technische Universiteit Delft. During the BSc program, he did a 5-month internship in the Soft Matter Chemistry group of Prof. dr. Alexander Kros on the synthesis of covalent hydrogel materials for applications in drug release and wrote his BSc thesis titled: "In situ forming Dex-mal and Human serum albumin crosslinked hydrogel for the purpose of drug carrying". In 2013, he obtained a Master of Science degree in Life Science and Technology, with the specialization "Research in Life Science and Technology" at the Universiteit Leiden. During his MSc program, he did a 1.5-year internship in the Moleculaire Biotechnology group of Prof. dr. Gilles van Wezel where he did research on the role of cytoskeleton proteins in cell division and the possible existence of kinesins in *Streptomyces coelicolor*. On this topic, he wrote his MSc thesis titled: "Racing fluorophores: a dynamics study of cytoskeleton proteins in *Streptomyces coelicolor*".

In June 2013, he started his PhD research under Prof. dr. Alexander Kros and Dr. Roxanne Kieltyka at the Supramolecular and Biomaterials Chemistry group of the Leiden Institute of Chemistry, Universiteit Leiden. During his PhD studies, he collaborated with Prof. dr. Jan van Esch and Dr. Rienk Eelkema (Technische Universiteit Delft), Prof. dr. Doris Heinrich (Universiteit Leiden) and Dr. Ilja Voets (Technische Universiteit Eindhoven). He presented the research described in this dissertation at the following meetings and conferences:

- Cell Observatory Lectures 2014 (Oral presentation)
- CHAINS 2015, Veldhoven, The Netherlands (Poster presentation)
- Reedijk Symposium 2015, Universiteit Leiden, The Netherlands (Poster presentation, first prize winner)
- Dutch Polymer Days 2016, Lunteren, The Netherlands (Poster presentation)
- CHAINS 2016, Veldhoven, The Netherlands (Oral presentation)
- Dutch Polymer Days 2017, Lunteren, The Netherlands (Oral Presentation)
- GRC and GRS conferences "Self-Assembly and Supramolecular Chemistry"
   2017, Geneva, Switzerland (Poster presentations)

# **List of Publications**

- 1. V. Saez Talens, P. Englebienne, T. T. Trinh, <u>W. E. M. Noteborn</u>, I. K. Voets and R. E. Kieltyka, Aromatic Gain in a Supramolecular Polymer. Angew. Chem. Int. Ed., 2015, 54: 10502. doi:10.1002/anie.201503905
- 2. <u>W. E. M. Noteborn</u>, D. N. H. Zwagerman, V. Saez Talens, C. Maity, L. van der Mee, J. M. Poolman, S. Mytnyk, J. H. van Esch, A. Kros, R. Eelkema, R. E. Kieltyka, Crosslinker-Induced Effects on the Gelation Pathway of a Low Molecular Weight Hydrogel. Adv. Mater. 2017, 29, 1603769. doi:10.1002/adma.201603769
- 3. <u>W. E. M. Noteborn</u>, Y. Gao, W. Jesse, A. Kros, R. E. Kieltyka, Dual-Crosslinked Human Serum Albumin-Polymer Hydrogels for Affinity-Based Drug Delivery. Macromol. Mater. Eng. 2017, 302, 1700243. https://doi.org/10.1002/mame.201700243
- 4. <u>W. E. M. Noteborn</u>, V. Saez Talens, R. E. Kieltyka, Reversible loading of nanoscale elements on a multicomponent supramolecular polymer system using DNA strand displacement. ChemBioChem. 2017, 18, 1995. doi:10.1002/cbic.201700441
- 5. <u>W. E.M. Noteborn</u>, J. A. J. Wondergem, A. Iurchenko, F. Chariyev-Prinz, D. Donato, I. K. Voets, D. Heinrich, R. E. Kieltyka, Grafting from a hybrid DNA-dextran graft copolymer by the hybridization chain reaction, submitted
- 6. <u>W. E. M. Noteborn</u>, M. Broto Torredemer, C. Maity, F. Versluis, R. Eelkema, R. E. Kieltyka, Tuning drug release from a reaction-coupled low molecular weight gelator system by modulating its reaction pathway, submitted
- 7. C. Tong, T. Liu, V. Saez Talens, <u>W. E. M. Noteborn</u>, T. H. Sharp, M. Hendrix, I. K. Voets, C. L. Mummery, V. Orlova, R. E. Kieltyka, Application of a low molecular weight gelator for 3D cell culture of human induced pluripotent stem cells and their derivatives, submitted
- 8. V. Saez Talens, D. M. M. Makurat, T. Liu, <u>W. E. M. Noteborn</u>, D. Wei, C. L. Guibert, I. K. Voets, R. E. Kieltyka, Morphological control over a squaramide-based supramolecular polymer in water by modulating its monomer structure, submitted